Universidad del País Vasco Euskal Herriko Unibertsitatea

NAZIOARTEKO BIKAINTASUN CAMPUSA
CAMPUS DE EXCELENCIA INTERNACIONAL

DEPARTAMENTO DE INGENIERÍA QUÍMICA

IMPLEMENTATION OF PRIMARY STRATEGIES FOR THE IMPROVEMENT OF BIOMASS STEAM GASIFICATION IN A SPOUTED BED REACTOR

TESIS DOCTORAL

María Cortázar Dueñas

Marzo, 2022

Universidad del País Vasco Euskal Herriko Unibertsitatea

NAZIOARTEKO BIKAINTASUN CAMPUSA
CAMPUS DE EXCELENCIA INTERNACIONAL

DEPARTAMENTO DE INGENIERÍA QUÍMICA

IMPLEMENTATION OF PRIMARY STRATEGIES FOR THE IMPROVEMENT OF BIOMASS STEAM GASIFICATION IN A SPOUTED BED REACTOR

MEMORIA

Que para optar al grado de Doctor en Ingeniería Química

Presenta

Doña María CortázarDueñas

Marzo, 2022

Esta Tesis es el resultado del trabajo de muchas personas y no sería justo no agradecerselo. Es por esto que en las siguientes líneas me gustaría agradecer toda la ayuda y el apoyo recibido durante todos estos años que han hecho posible que este trabajo se haya realizado con éxito.

Para empezar me gustaría dar las gracias a mis directores Martin Olazar y Gartzen López por confiar en mí para la realización de esta Tesis y como no, por toda vuestra ayuda, trabajo y dedicación. Gracias Martín por tu experiencia, visión general y todo el trabajo realizado y, a ti Gartzen, por proporcionarme todo el conocimiento necesario para alcanzar los objetivos de propuestos. Nunca olvidaré tus valiosos consejos, gran paciencia, apoyo incondicional y todo el tiempo dedicado. A su vez, me gustaría daros las gracias Maite, Maider y Jon, ya que aunque estéis hasta arriba de trabajo, no habéis dudado en implicaros en este proyecto y aportar vuestro granito de arena. Asimismo, me gustaría agradecer a Andrés Aguayo su ayuda a la hora de resolver las diversas dudas que me iban surgiendo y a Javier Bilbao por sus ánimos durante todos estos años.

También me gustaría acordarme de mis compañeros de laboratorio, Laura, Enara, Aitor, Itsaso, Santi, Irati, Mayra, Leire y Pablo, por hacer que el día y a día haya sido llevadero y por esas charlas en momentos de crisis. ¡Viva el trabajo en equipo!

Además, me gustaría agradecer al Prof. Bi por haberme acogido en el grupo RNG y ofrecerme la posibilidad de trabajar en sus instalaciones del Pulp and Paper Center en la Universidad de British Columbia, así como a todas las personas con las que he compartido esta experiencia: Xabi, Rachel, Jing, Lei, Roger, Jiantao, Yang y Alex.

Por último, me gustaría agradecer a mis aitas su apoyo. A mis "Txikitas", gracias por devolverme al mundo real, y, especialmente, a ti Eneko, por aguantarme y escucharme en los momentos menos dulces.

Bihotzez MILA ESKER,

María

INDEX

OBJECTIVES

This doctoral thesis is framed within an extensive research line, which covers the development of thermal and catalytic processes for the valorization of biomass and plastic wastes to obtain liquid fuels, raw materials (olefins and aromatics) and hydrogen. The knowledge acquired in biomass and plastic gasification on conventional spouted bed reactor has encouraged this thesis. Thus, the main objective of this thesis is to make progress in the biomass steam gasification process for synthesys gas production and tar removal. In this thesis, a novel reaction system based on spouted bed techonlogy is proposed, which sets out the incoporation of certain devices, such as a fountain confiner and a draft tube. This combination aims to solve the limitiations of the conventional conical spouted beds on gasification processes, according to the following specific goals:

- The development of a novel gas-solid contact regime based on a conical spouted bed reactor to promote tar elimination and impove process efficiency. This regime combines the advantages of fountain confined spouted beds with those of draft tubes. This goal entails the following sub-objectives:

- Characterization and definition of the fountain enhanced regime. This regime makes the spouted bed reactor with fountain confiner and draft tube highly efficient for biomass gasification.
- Assessment of the influence operating parameters, such as temperature, gas flow rate, particle size, bed mass and draft tube design (tube diameter and entrainment zone height) have on the reactor's hydrodynamics. These parameters will determine the gasification performance.
- Analysis of the effect fountain confiner has on residence time distribution, particle entrainment and bed stability when the fountain zone is enlarged.
- Evaluation of the effect fountain height has on the temparture profiles inside the fountain confiner. The effective volume in the fountain available for tar cracking reactions increases as the high temperature zone is increased.

- Knowledge of the fountain voidage in the fountain enhanced spouting regime, since the gas-solid contact between the tar compounds and the solid particles is essential for an efficient tar cracking.

- Process optimization from the design, operating conditions and primary catalysts point of view. A detailed evaluation of all these aspects will lead to the determination of the optimum conditions for removing tar in the biomass steam gasification. This goal involves the following secondary objectives:

- Assessment of the primary catalysts properties by their detailed characterization. These properties will determine their capability to remove tar and improve the overall gasification efficiency.
- Experimental evaluation of the regime, reaction temperature, primary catalysts and iron addition to olivine in the bench-scale plant, with the permanent gases (H_2, CO_2, CO, CH_4 and C_2-C_4) and tars being analyzed in-line by gas chromatography. Although the thesis was focused on reducing tar content in the product gas, other process parameters had also been taken into account.
- Determination of the most suitable reactor configuration and hydrodynamic regime for reducing tar formation.
- Analysis of the temperature effect on gasification performance and tar composition.
- Primary catalysts discrimination according to their capability to remove tar and improve the composition of the product gas.
- Evaluation of the potential to improve the overall process efficiency by loading iron to olivine by monitoring its activity and stability.
- Identification of the main causes of catalyst deactivation by characterizing the spent catalysts thoroughly to understand the relationship between their features and performance.

1

INTRODUCTION

This introduction analyzes H_2 and syngas production from biomass (Section 1.1), with special emphasis on steam biomass gasification (Section 1.2). Since the avoidance of tar formation is a key challenge in biomass gasification, a comprehensive overview on the tar produced is provided, covering its formation and growth, and reduction strategies. Thus, Section 1.3 describes in detail all the aspects related to tars, which particularly include the definition and complementary classifications of tars, as well as possible tar formation and growth mechanisms. Moreover, tar drawbacks on downstream application and human health and environment, as well as tar sampling techniques (online and off-line) are thoroughly discussed. Finally, the primary tar removal strategies are addressed in Section 1.4 by analyzing the effect operating conditions (temperature, ER and S/B), primary catalysts utilization (natural and supported metal catalysts) and reactor design modifications and improvements have on tar concentration.

1. 1. HYDROGEN AND SYNGAS PRODUCTION FROM BIOMASS

Since the Industrial Revolution, the worldwide energy mix became dependent on fossil fuels, which has strongly contributed to climate change. Nowadays, three-quarters of the greenhouse gas emissions emerge from the combustion of fossil fuels for power generation. Renewable energies come to the fore with the aim to reduce CO_2 emissions. EU's 2030 climate target plan proposes to reduce greenhouse gas emissions from energy, industry and transport sectors by at least 55 % by 2023 and become climate neutral by 2050 (WBA, 2020; Hafner and Raimondi, 2021; Pietzcker et al., 2021; Skjærseth, 2021).

Achieving net-zero emissions by 2050 will entail the transformation of the energy system, in which a wide range of technologies will play a crucial role. Hydrogen is one of the cleanest energy carriers, as it only produces water after combustion. However, up to now it is far from being the key pillar of the global energy system decarbonisation (IEA, 2021). It only represents a modest fraction of the worldwide energy mix and is almost fully produced from non-renewable resources, such as natural

gas (48 %), oil (30 %) or coal (18 %) (Figure 1.1). In fact, hydrogen production was responsible for the emission of 830 Mt CO_2 in the year 2020. Therefore, the future prospect of the H_2 market is driven by the need to cut down on CO_2 emissions, which demands its production from cleaner technologies (electrolysis, fossil fuels with carbon capture, utilization and storage, and bioenergy). In this scenario, the development of hydrogen production from biomass or wastes has been considered as a vital strategy to achieve the European Green Deal (IEA, 2021; Kakoulaki et al., 2021; Kovač et al., 2021; Santamaria et al., 2021; Zore et al., 2021).

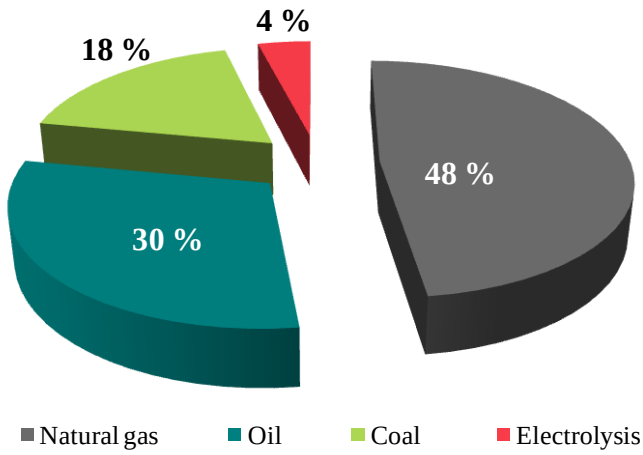

Figure 1.1. Worldwide H_2 production sources.

Hydrogen demand has strongly grown since 2000, particularly in refining and chemical industry. In 2020, global hydrogen consumption was of 90 Mt, 50 % more than that in 2000. Figure 1.2 shows the distribution of global H_2 consumption. Every year the major H_2 consumer is the industry sector with more than 50 Mt H_2 demand, mainly for feedstock. Chemical synthesis accounts for around 90 % of the industrial demand, with three-quarters approximately being directed to ammonia production (for urea and other fertilizers) and one-quarter to methanol and derivatives. The remaining H_2 is consumed in the direct reduced iron process for steelmaking. The H_2 consumption is slightly lower (close to 40 Mt H_2) in the refining sector, which is mainly used in hydrocracking, hydrotreating (e.g., fuel desulfurization) and biorefinery.

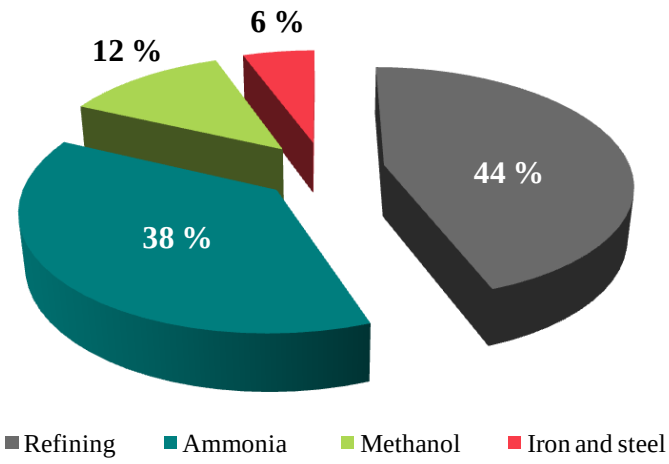

Figure 1.2. Global H_2 consumption by sector in 2020.

Renewable energy will be the key in the decarbonisation of our energy systems in the next decades. In 2018, around 14 % of the global primary energy came from renewable technologies, with the share of biomass-based sources including municipal and industrial waste, solid biomass, liquid biofuels and biogas being of around 67 % (WBA, 2020). Thus, biomass stands out as one of the best alternative energy candidates to produce heat, power and biofuels without contributing to a net rise in CO_2 level; that is, the CO_2 emitted during its use is compensated by the carbon stock accumulated during its growing stage (Claude et al., 2016; Ong et al., 2019).

According to the Directive 2009/28/EC from the European Parliament, published on 23 April 2009, on the promotion of the use of energy from renewable sources (European Parliament, 2009), biomass is defined as the biodegradable fraction of products, wastes and residues from biological origin from agriculture (including vegetal and animal substances), forestry and related industries including fisheries and aquaculture, as well as the biodegradable fraction of industrial and municipal wastes.

Biomass can be converted into H_2 or syngas through themochemical and biological processes. Thermochemical processes use heat to release hydrogen from biomass, whereas biological processes use several microorganisms, such as bacteria and algae in

the presence of sunlight or organic matter. Figure 1.3 gives a general outline of the direct and indirect routes for H_2 and syngas production. Indirect routes are those involving intermediate products for their subsequent transformation.

Overall, biochemical methods can only treat starch or sugar rich feedstocks and they are very selective about the produced products. The biochemical processes are highly developed, but they still work in batch and are time-consuming (Parthasarathy and Narayanan, 2014). The main biological methods for converting biomass into H_2 and syngas are fermentation and biophotolysis. All biological processes are controlled by the hydrogen-producing enzymes, such as hydrogenase and nitrogenase (Ni et al., 2006). Fermentation is a multi-enzyme process in which a great variety of bacterial populations are used in order to transform organic matter into hydrogen. Two types of fermentation may be distinguished: dark fermentation and photofermentation, with their main difference being (as their names suggest) the amount of light used in the process. Dark fermentation does not use light so microbes or microalgae are needed, whereas photofermentation uses sunlight as energy source instead of sugars (Cao et al., 2020; Ahmed et al., 2021). According to Zhang et al. (2020) who compared photo fermentation and dark fermentation processes, photofermentation is the most effective route, as it leads to the highest hydrogen content (58.90 %) and highest efficiency in energy conversion (10.12 %). Regarding biophotolysisis, this process is unique to photo autotrophic organisms, such as green algae and cyanobacteria. This microalgaes contain hydrogenase, and therefore they exhibit a great propensity for hydrogen production under sunlight. Compared to dark fermentation, which leads to H_2 and CO_2 combined with other gases, such as CH_4, biophotolysis process only produces H_2 (Ni et al., 2006; Mahidhara et al., 2019).

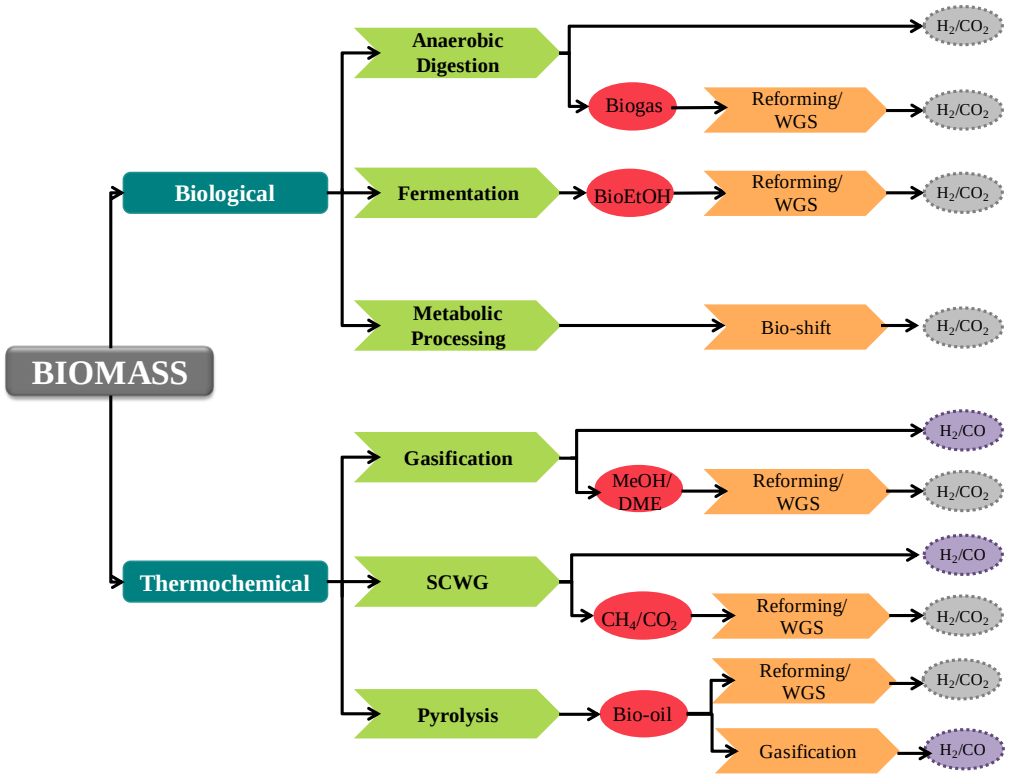

Figure 1.3. Biological and thermochemical strategies for H_2 and syngas production from biomass.

However, thermochemical methods can treat any kind of feedstock and the processes are much faster, although they produce a wide variety of products. Even so, they are interesting processes, as high concentrations of the desired intermediates and products are obtained (National Research Council, 2012). In terms of efficiency and production costs, thermochemical routes are more efficient (52 %) and cheaper than biochemical ones (Parthasarathy and Narayanan, 2014). The main thermochemical routes for biomass conversion into H_2 or syngas are pyrolysis, gasification and supercritical water gasification (SCWG). These technologies have been extensively studied by several authors (Lu et al., 2006; Alvarez et al., 2014; Amutio et al., 2015; Rapagnà et al., 2018; Ahlström et al., 2019; Kuba et al., 2021). Moreover, some other indirect routes, such as bio-oil steam reforming, bio-oil gasification and pyrolysis and in-line steam reforming are very promising to produce a H_2 rich gas (Remiro et al., 2013; Xiao et al., 2013; Ma

et al., 2014; Latifi et al., 2017; Quan et al., 2017; Zheng et al., 2018; Santamaria et al., 2020a). The main thermochemical processes for H_2 production from biomass sources are briefly described below, except biomass gasification process, which is described in detail in Section 1.2.

Super critical water gasification is a thermochemical process in which wet biomass (moisture content above 30 wt%) is converted into syngas. This process operates at temperatures ranging from 350 to 700 ºC and under conditions above the critical point of water (374.12 ºC ad 221.2 bar), wherein water has no distinct liquid or gaseous phase. The product distribution of this process varies hugely depending on operating temperature, pressure, residence time, feed, biomass particle size, reactor configuration and presence of catalyst (Rodriguez Correa and Kruse, 2018; Okolie et al., 2019). SCWG has several advantages over conventional gasification: i) biomass with high moisture content can be treated without an energy intensive drying step, which reduces the cost associated with feedstock drying and ii) high reaction rates are employed, leading to high H_2 and low CO yields, and low char and tar formation (Gemechu and Kumar, 2021) . However, it faces some challenges for its large scale implementation: i) feedstock pumping, as biomass must be resuspended into a pumpable liquid, ii) plugging by char, tar or salt precipitation and iii) high energy consumption, as water needs to be maintained at critical conditions (Lamb et al., 2020; Lee et al., 2021). According to Lamb et al. (2020), these drawbacks have hindered the measurability of the SCWG performance, leading to the use of laboratory scale reactors for critical studies of biomass chemical processing, with most of the runs being undertaken in batch reactors and, to a minor extent, in continuous mode.

In comparison with solid biomass gasification, bio-oil gasification is a relatively new and promising thermochemical route to produce H_2 rich gas (Zheng et al., 2019). Overall, bio-oil is better than biomass in terms of storage and transportation, as it has higher energy density. Accordingly, bio-oil gasification is potentially a more viable route than biomass gasification in large-scale plants (Braimakis et al., 2014). Thus, bio-oil gasification has the advantage of lower transportation costs when the dense bio-oil

is produced in small sized decentralized pyrolysis plants, and then stored and transported to a central biorefinery unit for gasification (Latifi et al., 2017b; Hwang et al., 2021). Moreover, the char produced in the pyrolysis step could also enhance H_2 production, as it may be mixed with the bio-oil to form a bioslurry, which could be fed into a reforming unit (Chen et al., 2015). In the literature, the distinction between bio-oil gasification and bio-oil reforming process is misleading. Usually bio-oil gasification processes are carried out at higher temperatures than reforming ones (around 800-1400 ºC) with no catalyst or primary natural catalysts (Arregi et al., 2018; Santamaria et al., 2021). However, bio-oil reforming takes place at milder temperatures (around 600-800 ºC) and in the presence of an active metallic reforming catalyst.

An alternative thermochemical route for biomass conversion into H_2 is the direct strategy of biomass pyrolysis and in-line steam reforming of the volatiles. It is noteworthy that this technology is focused on H_2 production whereas gasification processes lead to syngas as main product. Since both reactors are integrated together in the same unit, the operating conditions of both steps can be separately optimized (Han et al., 2018). In this process, intermediate temperatures are used: the pyrolysis step is carried out at 500º C, whereas the reforming one is performed in the 600-800 ºC temperature range on highly active reforming catalysts. Among its advantages, it is noteworthy that the reforming catalysts are not in direct contact with the biomass-derived impurities, as the latter remain in the pyrolysis reactor, which improves catalyst stability (Wu and Williams, 2010). Compared to bio-oil reforming, this two-step strategy has also some other benefits: i) the problems related to bio-oil handling, storage and vaporization are avoided by the in-line valorization of pyrolysis volatiles and ii) the scale up of the continuous process turns out to be easier (Santamaria et al., 2021).

The selection of a suitable technology involves a detailed assessment of the economic aspects, biomass availability and feasibility for treating the intermediate products in large catalytic conversion units (Santamaria, 2019).

1.2. BIOMASS GASIFICATION

Amongst all the thermochemical routes, gasification is a key technology for the large-scale exploitation of biomass, as it may allow a more effective conversion of biomass compared to pyrolysis. Generally, biomass gasification takes place at high temperatures (in 700- 1200 ºC temperature range) and in the presence of a gasifying agent (air, O_2, steam, CO_2 or their mixtures). The main product of the process is a gaseous mixture, mainly formed by H_2, CO, CO_2 and CH_4, although a solid residue (the organic unconverted fraction) and other undesired products such, as tars, are also formed. The obtained syngas could be used as fuel for heating and power generation or as an intermediate in the production of other fuels and chemicals, such as methanol, dymethyl ether and ammonia. Moreover, hydrogen of high purity may be obtained by further conversion of CO in syngas (Arregi et al., 2018; Ren et al., 2019b; Cao et al., 2020; Patuzzi et al., 2021). Figure 1.4 shows a scheme for the biomass gasification process.

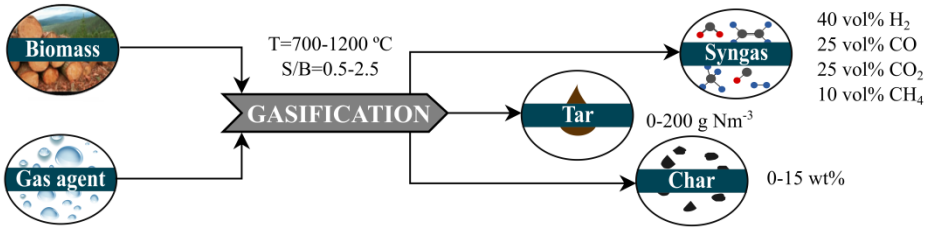

Figure 1.4. Schematic representation of the biomass gasification.

As mentioned above, biomass gasification requires a medium for reaction to form a synthesis gas that may be further employed in the production of valuable chemicals and biofuels. The use of one or another gasifying agent leads to a different product gas, so the choice among them is made based on a balance between the final product gas specification (for downstream application) and process costs (Mishra and Upadhyay, 2021).

Air is the most used gasifying agent due to its availability and low cost. Moreover, it promotes combustion and partial oxidation reactions, supplying the energy required for the gasification process. An average composition of the air gasification syngas is made up of 15 % H_2, 20 % CO, 2 % CH_4, 15 % CO_2 and 48 % N_2, which accounts for a low heating value gas (4-6 MJ Nm^{-3}) and moderate char and tar content. The obtained syngas is only suitable for conventional combustion engines, since it is very poor for using it in methanol synthesis (Asadullah, 2014b; Sansaniwal et al., 2017a). O_2 may be used in order to overcome the N_2 dilution of the syngas obtained in air gasification. The use of O_2 yields a high quality gas composed of 40 % H_2, 40 % CO and 20 % CO_2 and negligible tar and char content, which leads to a heating value in the 10-15 MJ Nm^{-3} range. However, the operating costs are high due to those involved by O_2 production (Parthasarathy and Narayanan, 2014; Mishra and Upadhyay, 2021). Use of steam rather than air produces a syngas with high H_2 concentration (of around 40 %) and improves the high heating value of the gas to 15-20 MJ m^{-3}, range, with the amount of tar generated being moderate. The average product gas composition obtained in biomass steam gasification is as follows: 40 % H_2, 25 % CO, 25 % CO_2 and 8 % CH_4. Nevertheless, the endothermic nature of steam gasification reactions entails an increase in the energy requirements of this process thereby increasing the process costs (Sansaniwal et al., 2017a; Cao et al., 2020). According to Karl and Pröll (2018), the high H_2 concentration and high heating value syngas obtained in the steam gasification make this technology interesting for the conversion of biomass into second generation fuels, such as Fischer-Tropsch diesel, methanol, dimethyl ether (DME) or substitute natural gas (SNG).

1.2.1. Stages and chemistry

Biomass gasification is a complex process, which involves several elementary gas-solid (heterogeneous reactions) and gas-phase reactions (homogeneous reactions) and heat and mass transfer processes. Independent of the gasifier configuration, the gasification process consists of the following stages: drying, pyrolysis, oxidation and reduction (Baruah and Baruah, 2014; Susastriawan et al., 2017; Motta et al., 2018). In a

typical gasifier, drying occurs at temperatures below 150 ºC. In this stage, the moisture of the biomass is evaporated, and consequently steam is released. The effect of the drying step on the gasification process is rather limited. The pyrolysis step corresponds to the thermal decomposition (devolatilization) of the dry biomass in the absence of oxygen, generating volatile compounds (mainly CO, H_2, CO_2, light hydrocarbons and tar) and char. Biomass pyrolysis reaction is shown by Eq (1.1).

$$\text{Biomass} \rightarrow \text{gas } (H_2, CO, CO_2, CH_4, \ldots) + \text{tar} + \text{char} \quad (1.1)$$

In the pyrolysis step products are diffused from the biomass pores to the gas phase in a series of reactions taking place at temperatures between 150 and 700 ºC. This step highly depends on temperature, heating rate, biomass composition and particle size. At temperatures below 600 ºC, biomass is initially decomposed into tar, char and gas, whereas at higher temperatures tars are cracked (Eq. (1.2)) or reformed into light hydrocarbons (Eq. (1.3)), or evolve towards more stable aromatic structures.

$$\text{Tar} \rightarrow CH_4 + CO + CO_2 + C \quad (1.2)$$

$$\text{Tar} + H_2O \rightarrow CO + H_2 \quad (1.3)$$

Given that oxidation stage is exothermic, it provides thermal energy to the endothermic reactions. The products of the pyrolysis steps react with the externally supplied oxidating agent (air, steam, CO_2 or their mixture). The exothermic nature of the oxidation reactions make the temperature rise in the gasifier to 800-1000 ºC range. In this step, oxygen contents below the stoichiometric one are needed for partial biomass oxidation. Char and hydrogen are usually the principal reactants, converting rapidly into CO_2 and H_2O as shown in Eqs. (1.4-1.6).

$$C(s) + \tfrac{1}{2}\, O_2 \rightarrow CO \quad (1.4)$$

$$CO + \tfrac{1}{2}\, O_2 \rightarrow CO_2 \quad (1.5)$$

$$H_2 + \tfrac{1}{2}\, O_2 \rightarrow H_2O \quad (1.6)$$

Finally, in the reduction stage, the pyrolysis and oxidation products (gas and char) react to produce the final product stream. Reduction yields to H_2, CO and CH_4 through a series of water gas shift (Eq. (1.7)), methane reforming (Eq. (1.8)), Boudouard (Eq. (1.9)), char gasification (Eq. (1.10)) and methanation (Eq.(1.11)) reactions.

$$CO + H_2O \leftrightarrow CO_2 + H_2 \quad (1.7)$$

$$CH_4 + H_2O \leftrightarrow CO + 3H_2 \quad (1.8)$$

$$C + CO_2 \rightarrow 2CO \quad (1.9)$$

$$C + H_2O \rightarrow CO + H_2 \quad (1.10)$$

$$C + 2\,H_2 \rightarrow CH_4 \quad (1.11)$$

Char gasification reactions are very slow, even at standard gasification temperatures. This is especially true for CO_2 gasification, which is between 2 and 5 times slower that steam gasification. Thus, char gasification is the controlling step in biomass gasification, since its reaction rate is much lower than the other reactions involved in biomass gasification (Di Blasi, 2009; Arregi et al., 2018; Cortazar et al., 2020).

1.2.2. Technologies

The gasifier, as the main element of a gasification plant, provides the space for biomass and gasification agent to be mixed to a certain extent, in some cases in the presence of primary catalysts and/or additives. According to Sansaniwal et al. (2017a), the design of a biomass gasifier depends on the fuel availability, particle shape, size and moisture content, ash content and end user applications. Thus, a large number of gasifiers have been used, as are fixed beds (updraft and downdraft), fluidized beds (bubbling, circulating and dual), entrained flow ones, spouted beds or plasma reactors, with the most commonly used being the first three (Sikarwar and Zhao, 2017). Figure 1.5 illustrates a schematic representation of the reactors used in biomass steam gasification.

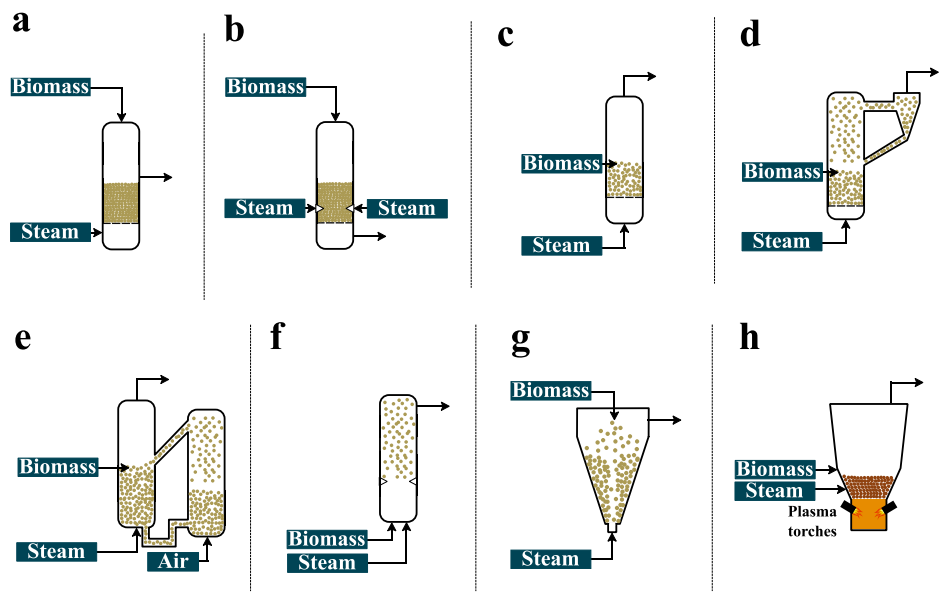

Figure 1.5. Reactor configurations for biomass steam gasification: (a) updraft fixed bed; (b) downdraft fixed bed; (c) bubbling fluidized bed; (d) circulating fluidized bed; (e) dual fluidized bed; (f) entrained flow; (g) spouted bed and (h) plasma.

Fixed bed gasifiers are the traditional ones for biomass gasification and they could be classified as updraft and downdraft, depending on the upward or downward flow of the gasifying agent. These gasifiers have a simple and robust design, lead to high carbon conversion rates and long residence times, and operate at low gas velocities, which make them suitable for small-scale heat and power generation applications (Sansaniwal et al., 2017a; Sikarwar and Zhao, 2017). In the updraft gasifiers, the gasifying agent enters from the bottom, whereas biomass is fed from the top, and therefore the interaction between the biomass and produced volatiles with the gasifying agent is in a counter current mode. Among their strengths, those worth mentioning are high thermal efficiency, small pressure drop and low tendency to form slag. However, they are very sensitive to the biomass moisture content and lead to high amounts of tar and low syngas yields. In the downdraft gasifiers, both gasifying agent and biomass flow

downwards, which results in a co-current flow. In comparison with updraft gasifiers, these ones produce less tar, and therefore a syngas of much better quality. Nevertheless, they cannot process biomasses with low density and high moisture and ash content, and the thermal efficiency is lower than in the updraft gasifiers (Molino et al., 2016; Pereira and Martins, 2017; Ren et al., 2019a). Although fixed bed reactors involve simple technology and, furthermore, the downdraft gasifiers lead to low tar contents due to the catalytic effect of the char, they have obvious drawbacks, such as low and non-uniform heat and mass transfer between the solid biomass and gasifying agent within the reactor, which hinders their scaling up, and so applications on large scale (Alauddin et al., 2010; Zeng et al., 2016; Mishra and Upadhyay, 2021).

Fluidized beds are based on the fluidization principle, so the bed particles bring into dynamic "fluid-like" state when the fluidization medium is forced to pass through the bed. This feature provides high mixing and gas-solid contact between phases, increasing the reaction rates and conversion efficiencies. Moreover, heat and mass transfer are enhanced, which enables a high operational flexibility (biomass with different features and wide particle size distributions may be treated) and bed isothermicity (Motta et al., 2018; Hoang et al., 2022). Thus, this technology is more attractive and economical for large-scale application. Fluidized beds are categorized into two types depending on the fluidization degree and the bed height: bubbling fluidized beds and circulating fluidized beds. Bubbling fluidized beds operate at low gas velocities (1-3 m s^{-1}), which is usually slightly greater than the minimum fluidization velocity, whereas circulating fluidized bed are design to operate at higher gas velocities (between 3 and 10 m s^{-1}), which means that the bed material is vigorously fluidized. Thus, the high fluidization gas velocity makes some of the bed material entrained from the reactor, which is recycled back to the reactor by a cyclone located at the gas outlet. Although higher conversion efficiencies have been achieved in circulating fluidized beds than in bubbling ones, both reactors undergo tar and dust related problems due to the short residence time of the volatiles in the reactor (Sansaniwal et al., 2017a; Ren et al., 2019a).

Entrained flow reactors operate at temperatures above 1000 ºC and high pressures (20-70 bar). They are highly efficient as they enhance carbon conversion, producing a low tar content gas. However, they require a very low particle size (< 0.4 mm) and almost fully dried biomass, which involves high capital and maintenance costs, and so restrictions for their scaling (Sikarwar et al., 2016; Zeng et al., 2016; Niu et al., 2019).

Regarding plasma reactors, they consists of two electrodes, usually Cu or carbon electrodes, through which an electrical energy is coupled to the gas These reactors generate an arc of electric discharge at temperatures of up to 10,000 ºC, creating atomic decomposition of the biomass. Although a good tar removal efficiency might be obtained, especially for heavy compounds, this technology involves high capital investment and maintenance (lifetime of pulse power supplier is limited), as well as high operational costs (high energy demand) (Ren et al., 2019a; Gao et al., 2022).

Conical spouted bed reactors stand out as an alternative to conventional fluidized bed. This technology allows handling larger particles sizes than those used in fluidized beds, including those with irregular texture, fine materials, and sticky solids, with no agglomeration or segregation problems (Aguado et al., 2005). Moreover, the countercurrent displacement of the solids in the annulus and the gas in the spout zone leads to high heat and mass transfer rates between phases (Makibar et al., 2011). It is noteworthy that this reactor has also a simple design (no distributor plate) and requires lower volumes than fluidized beds for the same capacity (a lower sand/biomass ratio is required). However, this technology is characterized by short gas residence times, which hinder tar conversion, and therefore overall process efficiency (Erkiaga et al., 2014).

Biomass gasification scale up has been successfully accomplished by the dual fluidized bed (DFB) reactor configuration due to its main features (wide particle size ranges, versatility for using different type of biomasses, high heat and mass transfer rates between phases, and bed isothermicity). It consists of two interconnected fluidized bed reactors: one reactor is used for gasification, whereas the second one is used to produce the heat required for the gasification process through char combustion. The heat

generated is transported to the gasification chamber by the circulation of the bed material. Up to now, the vast majority of the current biomass steam gasification demonstration or industrial scale plants are based on this technology (Karl and Pröll, 2018; Larsson et al., 2021). The research status of the DFB system was recently reviewed by Hanchate et al. (2021). Thus, Güssing (8 MWth) plant is running successfully since the year 2001 along with industrial scale operations in Oberwart (8.5 MWth) and Ulm (15 MWth). Moreover, GoBiGas plant in Sweden has been recently commissioned.

Although the steps of the gasification process are independent of the gasifier configuration, the location of the zones described in Section 1.2.1 is clearly identified in a fixed bed reactor (Figure 1.6), as there are no mixing effects in this type or reactor. However, given the intense mixing in a fluidized bed, which leads to high heat and mass transfer rates between the reactants, the locations of the reaction zones depend on the geometry of the reactor and the distribution of the feeding points. Typically, reactor designs aim to optimize the char combustion zone close to the oxidant feed point(s) in order to enhance carbon conversion efficiency and produce the heat required to carry out the gasification reactions, as well as the negative impact of partial oxidation on the cold gas efficiency (Siedlecki et al., 2011). Thus, the development of biomass gasification is conditioned by the efficient conversion of the feed and the avoidance of troublesome by-products (Claude et al., 2016; Zeng et al., 2020).

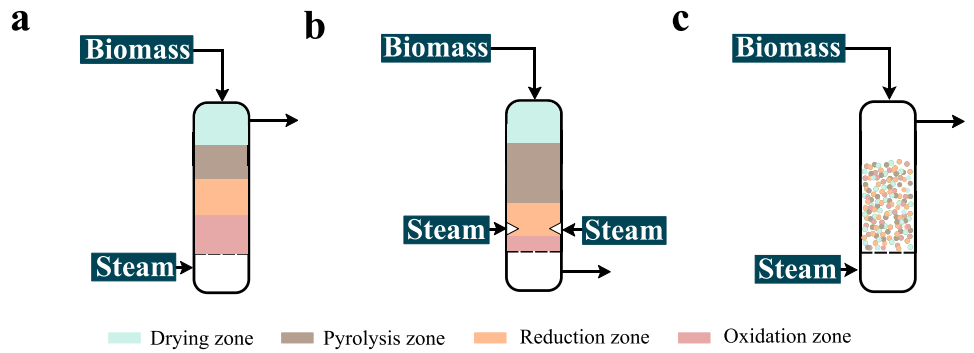

Figure 1.6. Fixed bed updraft (a) and downdraft (b), and fluidized bed (c), with their reaction zones.

1.2.3. Tar

Although the syngas accounts for the main product stream in the biomass gasification, other undesired compounds are also formed, as are tars (condensable aromatic and polyaromatic hydrocarbons) and other trace contaminants, such as nitrogen compounds (NH_3 and HCN), sulphur-containing inorganic compounds (H_2S, COS and CS_2), halogen compounds (HCl and Cl) and alkali (Na, K) and heavy metals (Sikarwar et al., 2016; Rakesh and Dasappa, 2018).

The composition yields and characteristics of the gasification products depend on the composition and structure of the biomass, process conditions (such as temperature, gasifying agent, pressure, residence time or use of catalyst) and reactor type. Even small changes in process conditions could affect the overall performance of the gasification process, and therefore the quality of the final product gas (Shayan et al., 2018; Suryawanshi et al., 2021). Thus, clean woody biomass leads to a product gas with very low concentrations of NH_3, H_2S and HCl, as it contains low amounts of sulphur, nitrogen and chlorine compounds, whereas the use of low-cost residual biomass, such as agricultural residues, manure, sewage sludge or waste, leads to relatively much higher concentrations (Pinto et al., 2008; Schweitzer et al., 2018; De

Almeida et al., 2020). In comparison with the latter contaminants, tar is present in higher amounts in the product gas, and special attention will therefore be paid in Section 1.3. Table 1.1 shows the major impurities present in the product gas and their effect on the gasification process.

Tar is a complex mixture of high molecular weight aromatic hydrocarbons (between 1 and 5 rings), which are especially problematic, as they may cause fouling, corrosion and blocking of downstream equipment and many environmental problems. Nevertheless, the tar contains a significant amount of energy that could be transformed into syngas (Li and Suzuki, 2009; Guan et al., 2016; Islam, 2020; Gao et al., 2022). Therefore, tar removal strategies have been extensively developed to reduce the tar content. Figure 1.7 shows a schematic representation of these methods. Overall, these strategies may be classified as follows: i) primary, to remove tar in the gasifier, or ii) secondary, the in-line cleaning of the syngas produced. Regarding the primary methods, the first measures adopted usually involve the design of the gasifier, the use of in situ catalysts, and the adequate control of operating conditions (temperature, equivalence ratio, and gasifying agent). The secondary methods do not interfere with the gasifier operation and they could be classified into physical (cyclones, cooling towers/wash columns, electrostatic precipitators and so on) and chemical treatments (thermal and catalytic process and partial oxidation). Primary tar elimination methods significantly reduce the process cost, but they may not be efficient enough to remove tar. In these cases, the combination of in situ and in-line methods may be a good option (Devi et al., 2003; Anis and Zainal, 2011; Valderrama Rios et al., 2018; Hanchate et al., 2021; Li et al., 2021b)

Table 1.1. Impurities formed in biomass gasification and the associated problems.

Type of impurities	More common compounds	Associated problems
Nitrogen	- Mainly NH_3 and HCN - Traces of pyridines, quinolines…	- NO_x Emissions - Gas conditioning needed - Poisoning of downstream catalyst
Sulphur	- Mainly H_2S and COS - Traces of thiophenes, mercaptans…	- Interaction with alkali metals leads to emissions, deposits and corrosion - Gas conditioning needed - Poisoning of downstream catalyst
Chlorine	- Mainly HCl - Traces of CH_3Cl	- Emissions, corrosion and ash sintering - Interaction with K leads to deposition and agglomeration. - Ash softening temperature decreased
Alkali and alkaline earth metals	- Forming salts	- Involved in ash deposition and deposit formation. - Ash melting temperatures lowered (Na, K) or increased (Mg, Ca). - Reaction with Si and S leads to deposition, agglomeration, fouling and corrosion - Ash disposal -Ash melting behaviour
Heavy metals	- Traces of Hg, Cd	- Emissions - Ash disposal costs increase
Tars	- Aromatic and polyaromatic hydrocarbons	- Ease for condensing - Corrosion, fouling and clogging on downstream equipment - Gas conditioning needed - Deactivation of downstream catalyst

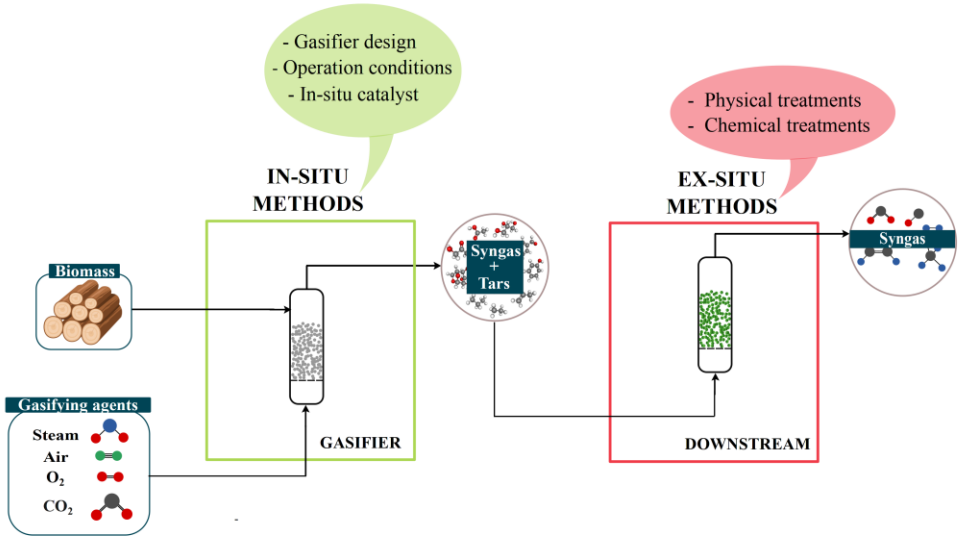

Figure 1.7. Schematic representation of tar removal strategies.

It is noteworthy that several primary tar removal strategies have been proposed in this thesis in order to enhance biomass steam gasification efficiency. Thus, a novel gas-solid contact regime based on the spouted bed reactor has been developed and the overall process has been optimized, i.e., reactor design, operating conditions and primary catalysts. Sections 1.3 and 1.4 focus on the mentioned points. More specifically, Section 1.3 gives a comprehensive overview of the tar issue, whereas Section 1.4 reviews the main primary measures for tar elimination in the biomass gasification. An extensive literature survey has been carried out in order to assess the effect operating conditions (temperature, ER and S/B), primary catalysts (natural and supported metal catalysts) and modifications and improvements in reactor design have on the tar content in the produced gas.

1.3. TAR ISSUE

1.3.1. Tar definition and classifications

Tar is an ambiguous term that describes a complex mixture of condensable hydrocarbons. Given the diversity of institutions and researchers working on biomass gasification, there is a great number of tar definitions and tar sampling techniques. Thus, the Gasification Task from the IEA Bionergy Agreement, US Department of energy (DOE) and the DGXVII from the European Commission agreed to define tar as hydrocarbons with molecular weight higher than benzene (Rabou et al., 2009). To sum up, tar is thick brown-black colored highly viscous liquid, which includes single-ring to multiple-ring aromatic compounds along with other oxygen containing hydrocarbons and complex polycyclic hydrocarbons (Font Palma, 2013; Hanchate et al., 2021).

Two different tar classifications can be found in literature. The first one was reported by Evans and Milne (1997) and grouped tar compounds into 4 lumps according to their reactivity (primary, secondary, alkyl-tertiary and condensed tertiary tar) as shown in Table 1.2. However, the distinction between secondary and tertiary compounds is not always straightforward, as they may overlap (Rabou et al., 2009). Thus, Energy Research Center of the Netherlands (ECN) proposed a more clear tar classification, which also ranks the large amount of unconverted tar compounds. According to this classification, tar compounds are divided into five classes based on their molecular weight, solubility and condensability (Table 1.2): GC undetectable tar, light aromatics, heterocycles, light and heavy PAHs. Both methods are commonly used to classify tar depending on the subsequent application, and they are in fact complementary.

Table 1.2. Tar classification methods, their properties and typical compounds (Anis and Zainal, 2011; Guan et al., 2016; Valderrama Rios et al., 2018; Zeng et al., 2020)

Classification method	Basis of classification	Nomenclature	Description	Properties	Typical compounds
Milne	Reactivity, appearance	Primary	Cellulose, hemicellulose and lignin derived oxygenated compounds	Low molecular weight oxygenated hydrocarbons	- Acids, sugars, alcohols, ketones, aldehydes, cathecol, guaiacol, anisol, vanillin
		Secondary	Product from the conversion of primary products (phenolic and olefin compounds)	Alkyl phenols Singles-ring aromatics	-Phenol, cresol, xylene
		Alkyl tertiary	Aromatic compounds with methyl branches	Methyl derivative aromatics with one or more rings	- Methyl acenaphthylene, methyl naphthalene, toluene, indene
		Condensed tertiary	Policyclic aromatic compounds without branches	Polynuclear aromatic hydrocarbon (PAH) series without substituents	- Benzene, naphthalene, acenaphtylene, anthracene, phenanthrene, pyrene

Table 1.2. Continued.

Classification method	Basis of classification	Nomenclature	Description	Properties	Typical compounds
ECN-TNO-UT	Molecular weight, solubility and condensability	Class I	GC undetectable compounds	- Very heavy compounds with 8 or more rings - Not detected by GC - Calculated by subtracting the GC detectable tar from the total gravimetric tar	
		Class II	Heterocyclic compounds	- Single ring aromatics containing heteroatoms - High solubility in water	- Pyridine, phenol, cresol, quinoline, isoquinoline
		Class III	Light aromatic compounds	- Single ring aromatic compounds - Without condensability and solubility problems	- Toluene, ethylbenzene, xylenes, styrene
		Class IV	Light PAHs	- 2-3 ring aromatic compounds - Condense at low temperatures	- Indene, naphthalene, methylnaphthalene, biphenyl,acenaphthalene, fluorene, phenanthrene, anthracene

1.3.2. Tar formation and growth mechanisms

In order to prevent or reduce tar production, a thorough understanding of its formation and growth is essential. However, tar formation and growth mechanisms remain challenging, as they are very fast and complicated process. This is probably associated with the complex nature of biomass, as it has a heterogeneous chemical composition, including different polymeric units and cross-linkages in its constituents (lignin, cellulose and hemicellulose), and the competing reactions involving highly reactive species (radicals with complex chemistry), producing a large number of PAH isomers (Shukla and Koshi, 2011; Zhou et al., 2014). Apart from being the tar main compounds, PAHs are very problematic, especially the heavier ones. Therefore, knowledge of their formation mechanism and evolution is of vital significance for the optimization of the gasification process (Qin et al., 2015).

Lignin is considered a potential precursor of PAH formation, since it is the only fraction in the biomass with aromatic nature. Tar formation during biomass gasification follows several sequential steps. When biomass is fed into the gasifier, it first dries and then starts to decompose (Eq. (1.1)). The operating temperature is responsible for the nature of the tar produced. Temperatures below 500 ºC lead to a tar mainly formed by oxygenate organic compounds, which is usually known as primary tar. Examples of primary tars are vanillin (4-hydroxy-3-methoxybenzaldehyde, $C_8H_8O_3$), catechol (1,2-dyhydroxybenzene, $C_6H_6O_2$), guiacol (2-methoxyphenol, $C_7H_8O_2$) and anisol (metoxibenzene, C_7H_8O). However, temperatures above 500 ºC are capable of converting primary tars into secondary tars, since dehydroxylation, demethoxylation and demetehylation reactions take place simultaneously (Shen et al., 2014; Zhou et al., 2018). Secondary tar is mainly made up of branched and heteroatom compounds. Higher temperatures make tars to grow, and therefore evolve to more stable compounds, PAHs, (tertiary tars), such as naphthalene, phenantrene, anthracene, pyrene… (Valderrama Rios et al., 2018). Figure 1.8 shows the tar evolution in the 500-100 ºC temperature range.

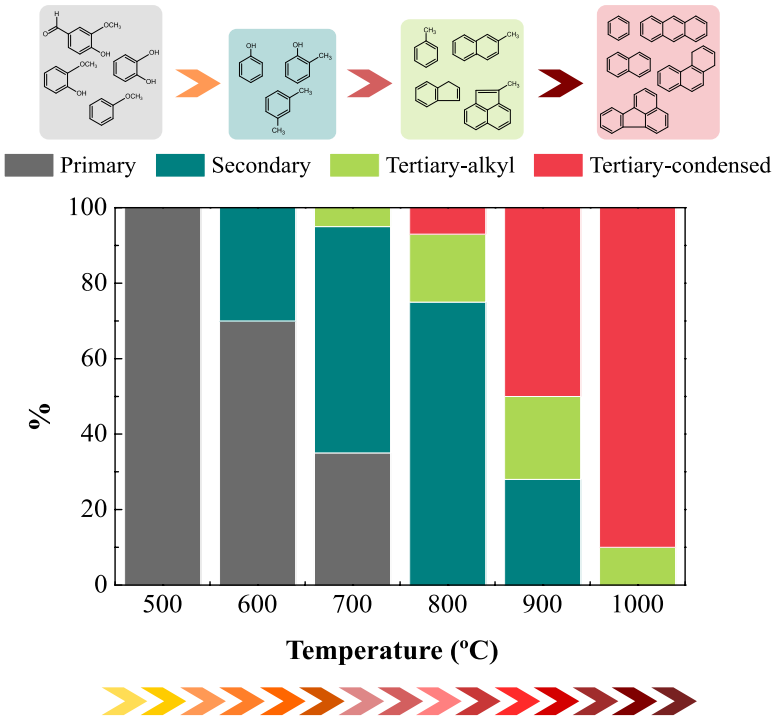

Figure 1.8. Tar compound distribution in the 500-1000 ºC temperature range.

The formation of PAHs and their growth is initiated when the PAH precursors are produced. There are two main pathways for PAH formation: one considers benzene as the precursor, whereas the other considers phenol (Yu et al., 2014; Qin et al., 2015). Benzene could be produced by the primary pyrolysis of the lignin or by the combination of light alkenes through dehydrogenation and Diels-Alder type reactions. In the case of phenol, it is generated when the ether bond in the lignin breaks under acid conditions. With benzene as precursor, PAHs could be formed by its ring condensation reaction or hydrogen abstraction and addition reactions of unsaturated light hydrocarbons, such as acetylene, vinyl, methyl... The PAH formation from benzene precursors is shown in Figure 1.9. However, when phenol is the precursor, phenolic compounds lose CO radical to form cyclopentadiene, which in turn loses one H atom to generate ciclopentadienyl radical. Then two cyclopentadienyl radicals combine into naphthalene. Naphthalene loses H radical to give indenyl, which reacts

with cyclopentadiene generating aromatic compounds with more than two rings. This reaction pathway could be seen in Figure 1.10.

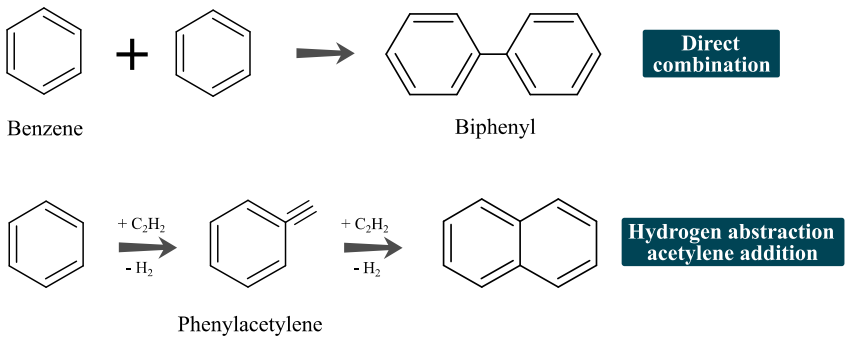

Figure 1.9. PAH formation from benzene precursors.

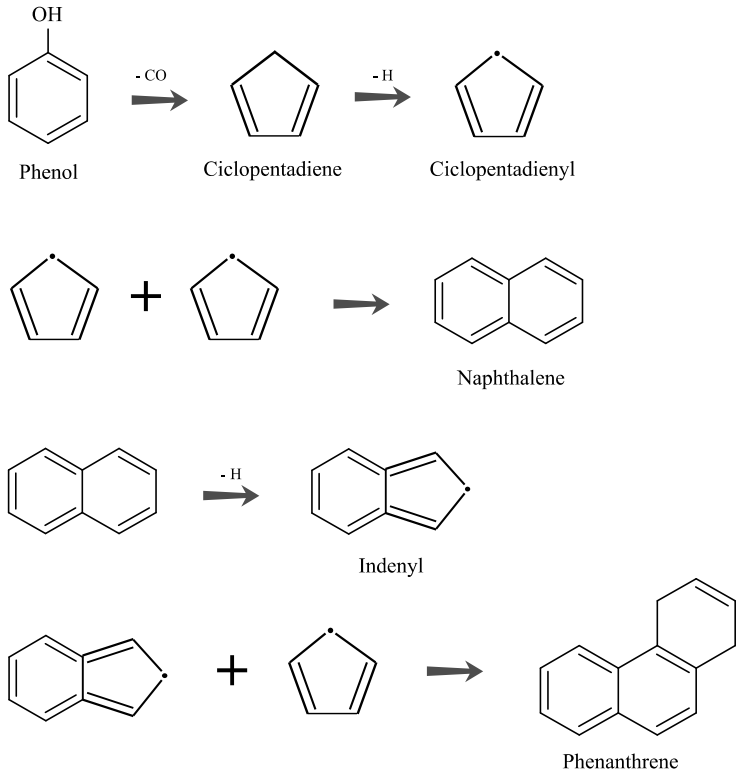

Figure 1.10. PAH formation from phenol precursors.

Thus, to reduce the yield of PAH tar, the formation of the precursors or the growth of PAH tar from the precursors needs to be reduced (Qin et al., 2015; Nguyen et al., 2018). According to Qin et al. (2015), H_2 suppresses the formation of large PAH, as hydrogen intermediates preferably react with carbon-containing intermediates, reducing the possibility of reactions involving carbon containing species to produce larger compounds.

The growth mechanism of the tar is not clear yet and a lot of research has been done in order to understand it. Thus, several authors have reported different alternatives for tar growth, such as aromatic ring-ring condensation and acetylene addition (Böhm et al., 1998), particle filler model (Dong and Hüttinger, 2002), aryl-aryl combination followed by H_2 elimination and ring cyclization (Unterreiner et al., 2004) and condensation of aromatic radicals with neutral species. The hydrogen-abstraction/acetylene-addition (HACA) mechanism has been widely used to describe the evolution of PAHs (Wang and Frenklach, 1997; Font Palma, 2013; Liu et al., 2019) although other researchers point out that it is a rather slow mechanism (Shukla and Koshi, 2011; Reizer et al., 2019). Additionally, Shukla and Koshi (2011) proposed several tar growing pathways based on reactions involving radical mechanisms: HAVA (hydrogen abstraction and vinyl radical addition) (Shukla and Koshi, 2012), PAC (phenyl addition and cyclization) (Shukla et al., 2008; Shukla and Koshi, 2010) and MAC (methyl addition and cyclization) (Shukla et al., 2010). The studies carried out by the same authors pointed out that PAC is the most efficient mechanism for PAH growth, MAC is more efficient than HACA, but less than PAC and HAVA is faster than HACA. It seems that the formation of PAHs and their role may be related to the complex combination of the mechanisms described above and their efficient pathways. Overall, these mechanisms are based on consecutive dealkylation/decarboxilation (tar aromaticity is enhanced by the cleavage of alkyl groups attached to the aromatic rings), dimerization (direct combination of aromatic rings) and cyclization reactions that may occur simultaneously, which lead to the growth of light aromatic compounds to give heavier ones (Fuentes-Cano et al., 2013).

1.3.3. Tar drawbacks

The major challenge of biomass gasification is related to tar formation, as it requires cleaning and upgrading of the product gas, which restricts its industrial viability (Li and Suzuki, 2009). Technical and economic problems concerning tars have given rise to cancel several investments in the past (Gredinger et al., 2018). Overcoming tar-associated problems is crucial for achieving economically and environmentally efficient energy recovery from biomass gasification (Arena et al., 2010). In fact, tar formation wastes 5-15 % of the effective energy from biomass gasification, reducing the process efficiency (Qin et al., 2015). All tar compounds are undesired in the product gas, as they may polymerize into more complex structures on downstream pipelines, heat exchangers or filters, which leads to corrosion, fouling and clogging. Consequently, process efficiency decreases and emissions and operational costs increase. Thus, tar issue is closely linked to operational problems, gas downstream applications and human and environmental risks, as summarized in Table 1.3.

Tar amount and its composition are influenced by the type of gasifier (which determines the contact mode and mass and heat transfer rates), composition of the biomass used as feedstock and, especially, operating conditions (such as temperature, gasifying agent, pressure, residence time or use of catalyst), as shown in Section 1.4. Tar concentration depends on the gasification technology, as shown in Figure 1.11. Tar content for entrained flow reactors and circulating fluidized beds is low, with their ranges being 0-5 g Nm^{-3} and 0-10 g Nm^{-3} range, respectively. However, much higher tar concentrations are produced in conventional spouted beds and updraft fixed bed, up to 140 g Nm^{-3}. Dual and bubbling fluidized beds and downdraft fixed beds lead to moderate tar levels, with a peak value of 50 g Nm^{-3} (Asadullah, 2014a; Claude et al., 2016; Arregi et al., 2018; Valderrama Rios et al., 2018). The total amount of tar in the product gas determines the downstream application. Thus, applications directed towards the production of motor fuels, such as H_2 production, Fischer-Tropsch synthesis, methanol and natural gas synthesis, only accept a very low tar level, below 1 mg Nm^{-3}, whereas power generation equipment, such as gas turbines, gas engines, fuel

cells or boilers, accept higher limits (Harb et al., 2020). As observed in Figure 1.11, the tar concentrations in the standard gasification technologies remains above the acceptable range for mentioned applications. Thus, tars need to be removed or converted in order to avoid unacceptable levels of maintenance in the upgrading processes.

Table 1.3. Side effects of the tar in the biomass gasification process (Anis and Zainal, 2011; Guan et al., 2016; Rakesh and Dasappa, 2018; Zeng et al., 2020).

Side effects	Explanation
Pipeline blockage at low temperatures	Below 300 ºC, tar in the gaseous stream may condense quickly and attach easily to the gas pipelines, resulting in their obstruction and operational disruption
Corrosion on downstream equipment	The acid nature of the tar may cause severe corrosion in downstream equipment
Catalyst deactivation in downstream reactor (if used)	Tars could deposit on the catalyst surface and block the active sites, shortening its lifetime.
Reduction of process efficiency	Tar accounts for 3-5 % of the total energy in the feedstock or 10-15 % of the energy in the product gas, reducing the total energy utilization and process efficiency.
Production of phenolic wastewater	As phenolic compounds are abundant in the tar, a great deal of wastewater is produced in the gas cleaning, which must be treated.
Human and environmental risks	Most of tar compounds are carcinogenic, so the human and environmental health is in danger when released.

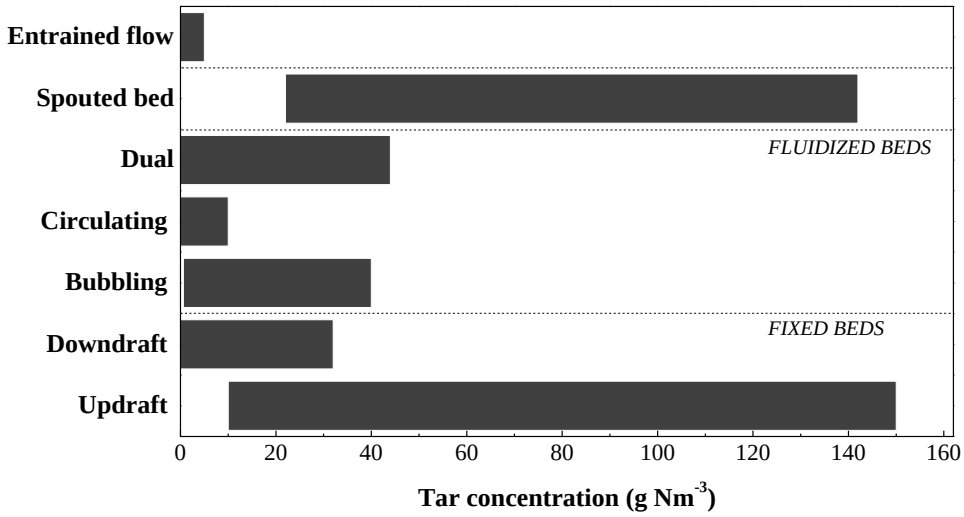

Figure 1.11. Tar concentration obtained in the gasification technologies (Asadullah, 2014a; Claude et al., 2016; Arregi et al., 2018; Valderrama Rios et al., 2018)

Likewise, not only does the total tar concentration indicate the suitability of the end-use application, but tar conforming compounds also play a key role, as all tar components present in the product gas contribute to the overall tar dew point. Tar dew point is the temperature at which the partial pressure of the tar equals the tar saturation pressure. Thus, as the tar dew point is kept at very low levels, fouling problems by tar condensation are minimized. Undoubtedly, heavy PAHs dominate tar dew point. Even for concentrations below 1 mg Nm^{-3}, a dew point below 100 ºC is impossible to obtain. However, light aromatics are not condensable even at concentrations of 10 g Nm^{-3}. In the case of heterocycles and light PAHs, they need to be partially removed to keep the dew point at approximately 25 ºC. As light aromatic compounds do not play an important role in this matter, tar removal strategies must focus on reducing heterocycles and light and heavy PAHs in order to ensure a successful application of the product gas (Anis and Zainal, 2011; Rakesh and Dasappa, 2018; Valderrama Rios et al., 2018).

1.3.3.1. Effect of tar on downstream applications

The product gas from biomass gasification could be used in the generation of power and heat and production of H_2 and second-generation fuels, such as methanol, dimethyl ether and natural gas and so on. The processes for the synthesis of these fuels are encouraging, but they are still under development due to their complexity (Engvall et al., 2011; Molino et al., 2018). Table 1.4 gives an overview of the tar limits, as well as the problems and challenges associated with both applications.

Currently, most of the gas obtained in the biomass gasification is used for power generation. There are different devices to produce electricity, such as gas turbines, gas engines, boilers and fuel cells. The tar containing gas obtained at the exit of the gasifier cannot be directly used in these equipments because it may cause corrosion in the cylinder, blockage of the gas flow line and valves, piston choking, blade corrosion and erosion, high consumption of lubricating oil and so on. Thus, the gas must meet stringent requirements regarding tar concentration after conditioning for smooth operation of these devices (Sansaniwal et al., 2017b).

The main advantage of steam turbine and boiler combination is that the expanding fluid is completely isolated from the gas combustion fumes. Consequently, there is no specific tar limitation and the product gas can directly be used without further treatment and without producing corrosion, fouling and plugging of the rotating parts. However, commercially available steam turbines have an extremely low efficiency of electricity generation, in the 10-20 % range, and they are expensive, which make them unviable option (Arena et al., 2010; Asadullah, 2014b).

In the case of gas turbines, the turbine components are exposed to combustion products and their electrical efficiency is higher than those of boiler and steam turbine combination. Gas turbines can accept hot gas for combustion and, as temperature is higher than the dew point of the tar, it could stay in vapor phase. Due to high exhaust gas temperatures, they are ideal for adding an additional energy recovery system, such

as a steam cycle, i.e., integrated gasification combined cycle (IGCC). To date, the IGCC electrical efficiency has reached over 42 %. Nevertheless, at 400 ºC tars may dehydrate and form carbon deposits, which cause fouling, plugging and abrasion of turbine blades. Thus, the tar level must be below 5 mg Nm^{-3} to meet the manufacture's specification (Arena et al., 2010; Asadullah, 2014a; Situmorang et al., 2020).

Regarding gas engine, it is not so sensitive to gas impurities compared to gas turbine, allowing a gas with 100 mg Nm^{-3} of tar concentration. On the one hand, special attention should be paid to heavy tars species, as they could deposit on the engine manifold and cylinder wall. On the other hand, polycyclic aromatic hydrocarbons do not tend to deposition, although they may influence gas emissions from engine exhausts and wastewater from the gas conditioning units (Prando et al., 2016). In this case, the decontamination of the gas could be achieved with quite inexpensive equipment, which makes the solution viable and competitive. Its advantages include low investment, maintenance and running costs, reliability, high operating efficiency, compact and robust structure and simple operation and maintenance (Arena et al., 2010; Situmorang et al., 2020). However, the engines are designed for gasoline and diesel, and consequently the injection systems require some modifications (Molino et al., 2016). Many co-generation units for the production of thermal energy with electricity using gas engines are installed and working successfully in the world (Sikarwar et al., 2016).

Solid oxide fuel cells (SOFC) produce electricity via electrochemical conversion of H_2 and CO in the product gas, whereas CH_4 is internally reformed to H_2 and CO. This electrochemical conversion is possible thanks to their operation at high temperature and a catalyst contained in their anode. They offer the possibility of highly efficient electricity production (over 40 % electric conversion efficiency could be obtained), which could reach 60 % or more when the exhaust heat from SOFC is used in combined cycle application or cogeneration. Moreover, compared to traditional power generation devices, fuel cells have lower impact to the environment, as the product gas is not burned (Molino et al., 2016; Ud Din and Zainal, 2017). Nevertheless, feeding tar

containing product gas could result in significant deactivation from carbon deposition, which hinder the fuel transport, block active sites of anodes and, as a result, reduce the electrical efficiency and durability of the fuel cell (Lorente et al., 2012; Liu and Aravind, 2014). Thus, the tar limits are even more stringent than for gas turbines, below 1 mg Nm^{-3}, which lead to the absence of large scale applications.

Concerning fuel synthesis processes, such as Fisher-Tropsch, methanation and natural gas synthesis, tar containing product gas causes the same type of problem, as all of them are catalytic process. Thus, the catalyst employed in each case is the most damaged element by tars, as it is rapidly deactivated by coke formation. Since coke is refractory in nature under the reaction conditions, it blocks the active site of the catalyst, and consequently the overall reactive sites of the catalyst decrease until the entire catalyst becomes inactive (Asadullah, 2014a; Molino et al., 2016). Therefore, the product gas should be thoroughly cleaned before using in these synthesis processes, with the acceptable tar concentration limit being below 1 mg Nm^{-3}. Up to date, there is not much experience on the large-scale use of biomass as feedstock for fuel production, although it may be of great interest due to the rise in the prices of fossil fuel, as well as climate change issues and the increase in the energy demand in the transportation sector (Engvall et al., 2011; Rauch et al., 2016).

Table 1.4. Tar limitations and problems and challenges associated with power generation devices and fuel synthesis processes.

	Tar limits (mg Nm^{-3})	Problems	Challenges
Power generation			
Boiler/steam turbine	No specific restrictions	- Although there is little chance for tar condensation, the gas produced after burning should meet local emission requirements.	- Obtaining higher energy efficiency with smaller boilers (< 150 MWth)
Gas turbine	5 mg Nm^{-3}	- As they used hot gas, carbon deposits could be form.	- Improving abrasion and erosion resistance of turbine blades.
Gas engine	100 mg Nm^{-3}	- Turbine blades are very sensitive to tar. - Heavy tars could deposit on the engine manifold and cylinder wall	- Modification of the gas injection system
Fuel cells	< 1mg Nm^{-3}	- Tar could condensate in fuel injection system - Tar could cause corrosion and carbon deposition, and consequently degrade the anodes	- Development of anodes resistant to carbon deposition -Improving durability of the fuel cells
Fuel synthesis			
Fisher Tropsh synthesis	< 1mg Nm^{-3}	- Catalyst deactivation by coke formation	-Development of high activity catalyst with excellent resistance to coke without high cost -Improving process energy integration
Methanol synthesis	< 1mg Nm^{-3}		
Methanation	< 1mg Nm^{-3}		

1.3.3.2. Effect of tar on human´s health and environment

There is a growing interest in developing biomass gasification for sustainable energy production. As biomass adsorbs CO_2 through photosynthesis during daylight, the use of biomass for energy conversion is net neutral in CO_2 emissions (Luo et al., 2018). However, power generation from biomass gasification poses several key hazards. Tar contains a great amount of highly toxic and carcinogenic aromatic hydrocarbons, which could be risky for humans and environment if disposed into water sources, such as rivers and underground water (Ashok et al., 2020; Gao et al., 2021).

There are stipulated concentrations from which tar compounds are deemed toxic and carcinogenic. The limit concentrations vary depending on the exposure time. Occupational Safety and Health Administration (OSHA) has established the exposure limits of the following tar compounds: toluene, 200 ppm (753.70 mg m^{-3}), whereas the values for naphthalene and phenol are much lower, 10 ppm (52.35 mg m^{-3}) and 5 ppm (19.23 mg m^{-3}), respectively. In the case of anthracene, pyrene and fluoranthrene, OSHA has identified them as typical components of the benzene-soluble fraction of coal tar pitch volatiles, with their limit being 0.2 mg m^{-3}.

1.3.4. Tar analysis

As tars caused multiple problems on downstream equipment, the determination of their content in the product gas and their online monitoring over time are crucial for process control. Qualitative and quantitative measurements of the tar in the gaseous stream help to assess the effectiveness of the cleanup and conditioning processes and verify the adequacy of the cleaned gas for its final use (Meng et al., 2012; Rakesh and Dasappa, 2018). Operating conditions and the peripheral equipment of the gasification plant, as well as the experience of the user, influence the tar formation, detection and sampling. Therefore, standardized tar analysis methods are needed for comparison purposes (Gredinger et al., 2018).

Various different technologies are available to measure the tar load of the product gas, which could be divided into two groups: off-line and online techniques. Conventional off-line analysis are characterized by capturing a known amount of the sample from the main gas stream and bringing into an analytical laboratory for further chemical analysis, whereas the online methods allow measuring the tar content directly in the product gas (Li and Suzuki, 2009; IEA Bioenergy, 2018).

Since there are numerous methods for tar measurement, their selection should be based on the information desired (qualitative or quantitative results, information about chemical composition), final use of this information (industrial monitoring or R&D), reliability of the technique, cost and so on. In the case of industrial monitoring and analysis systems, they should be reliable, fast, not expensive and preferably online, and they should need low staffing without specific expertise.

1.3.4.1. Off-line methods

The overall process of tar off-line analysis comprises the following common steps: sampling of tars, preparation of the resulting sample (depending on the analytical technique, conditioning may include drying or removal of particulate material from the gas) and analysis of the sample, generally carried out by gas chromatography (GC) or high pressure liquid chromatography (HPLC). The most relevant off-line tar techniques are tar guideline/protocol, the solid phase adsorption (SPA) and solid phase micro-extraction (SPME).

1.3.4.1.1. Tar protocol

The tar guideline/protocol was the first technical guideline for sampling and analyzing biomass gasification tar and was developed by the European Committee for standardization (ECN) with the help of different European Research Institutes (VTT, KTH, DTI, MTG, NRE). Nowadays, it is a reference procedure for tar measurement and is standardized by the tentative standard CEN/TS 15439 (Neeft et al., 2008). It

consists on a sampling unit to adjust the gas temperature and pressure, a subsequent high temperature filter to remove particles, the tar condenser itself consisting of six impinger bottles with solvents placed in a temperature controlled bath and a gas pumping and flow measurement equipment placed after the tar collection bottles. In the series of impinger bottles, the first one acts as moisture collector, in which water condenses from the product gas by adsorption in isopropanol. After the moisture collector, the gases pass through a series of four impinger bottles with solvent (usually isopropanol) and a final empty bottle. The first four bottles are kept at a temperature of 20 ºC approximately in a water bath, whereas the last two ones are cooled to -20 ºC in a salt and ice bath in order the capture aerosols. Several authors studied the configuration of the impinger train in order to optimize the temperature profile of the gas flowing through the bottles, the type of solvent and its amount in each bottle (Virginie et al., 2012; Mahapatra and Dasappa, 2014; Patuzzi et al., 2016; Prando et al., 2016; Neubert et al., 2017; Neubauer et al., 2018).

In order to determine the amount of gravimetric tar in the product gas, the evaporation of the solvent in the four impinge bottles is required. Although the tar protocol quantifies the total tar amount, it does not provide information about its composition, as this requires an additional analysis in GC or GC/MS.

It is a reliable method for the quantification of the total tar amount. However, the implementation is difficult as it is a very time consuming method (the sampling time may be as long as 1 h) and requires specific knowledge and instrumentation, which becomes the analysis expensive. Moreover, it is not a suitable method when tar concentrations are very low (below 1 mg Nm^{-3}) and the handling of large volumes of solvents may pose safety risks (Gredinger et al., 2016, 2018).

The tar guideline also includes the Petersen column as an alternative analytical method for the impinger train. It consists of two washing stages filled with acetone, which is surrounded by a cooling jacket. In the first stage, the gas is washed using an impinger and in the second stage, washing efficiency is improved by generating a large amount of small bubbles in order to retain the tar droplets. The outlet of the column is

connected to a pump to force gas flow and to a gas meter to measure the volumetric flow through the column during sampling. As Petersen column is a single unit, it makes easier the tar sampling than the impinger bottles (Neeft et al., 2008; Li and Suzuki, 2009; Rakesh and Dasappa, 2018).

1.3.4.1.2. Solid phase adsorption (SPA)

SPA sampling and analysis method was originally developed by KTH in the 1990's (Brage et al., 1997), with the main objective being to reduce the time for tar sampling and sample preparation. It is based on tar extraction from the gas sample by adsorption onto a solid-phase column and subsequent off-line desorption and analysis of the loaded solid cartridge. The tar containing gas sample crosses the sorbent (amino-based, activated carbon or a combination) which retains the tar compounds. Afterwards, the column is desorbed using a solvent and tar compounds are analyzed using GC (Israelsson et al., 2013). The tar sampling is carried out by inserting a syringe needle (attached to the solid phase extraction column) into the process line via a rubber septum, which allows reducing the tar sampling to 1 min. However, the total time invested for one measurement is high, as the column needs to be prepared before each sampling and the final laboratory analysis is very laborious (Brage et al., 1997).

The selection of the column sorbent is vital, as the reliability of the tar quantification depends on it. There are different types of SPA columns, which differ in composition and size. The 100 and 500 mg amino-based LC-NH_2 column is the most used one, as it is reliable for tar compounds ranging from naphthalene to pyrene (Brage et al., 1997; Siedlecki et al., 2009; Israelsson et al., 2013; Horvat et al., 2016a). However, this column is not able to capture volatile organic compounds, such as benzene, toluene and xylenes, nor tar compounds heavier than pyrene (González et al., 2012; Osipovs, 2013). Some studies showed that the volatile organic compounds produced during biomass gasification might be collected by modifying the column with some amount of activated carbon in series (Dufour et al., 2007; Osipovs, 2008, 2009). Moreover, some investigation groups have adapted the methodology of SPA sampling to meet their

analysis requirements by varying the sorbent of the column, the sampling conditions, the sampling storage and the elution procedure of tar compounds from the column (Dufour et al., 2007; González et al., 2012; Horvat et al., 2016b; Neubert et al., 2017).

According to several studies (Brage et al., 1997; Dufour et al., 2007; Osipovs, 2013; Neubert et al., 2017), the values of tar obtained with tar protocol and SPA sampling procedures are consistent. Thus, they concluded that SPA technique is simple in use, inexpensive, fast and allows high accuracy and reproducibility in the results, which makes it an adequate method for sampling gas with low tar concentration.

1.3.4.1.3. Solid phase micro-extraction (SPME)

SPME is being developed by KTH with the aim of improving SPA technique for the analysis of tar compounds in the product gas. However, it has been already applied in the analysis of organic compounds contained in water, air or solid matrices (Campíns-Falcó et al., 2009; Parkinson et al., 2010; Ghaffar et al., 2012; Pan et al., 2013; Zhang et al., 2014; Ibragimova et al., 2019; Tursumbayeva et al., 2019; Peñalver et al., 2020; Ruiz-Jimenez et al., 2020). This method is based on the extraction of analytes from a sample by adsoption onto a solid stationary phase and subsequent desorption of the analytes in an analytical equipment. The stationary phase used is silica fiber coated with 50 μm polydimethylsiloxane (PDMS). As the fiber is small and its shape is cylindrical, it is possible to integrate it into a device that works like a standard syringe, which fits into the injector of a gas chromatography. Once tar compounds have been absorbed onto the PMDS phase, the fiber is placed in the GC injector, where the analytes are directly desorbed without needing a solvent extraction step. This technique is suitable for the analysis of a gas with very low tar content (clean syngas), as it ensures attaining lower detection limits than SPA analysis (Ahmadi et al., 2013a).

Several aspects of this technique are crucial for measuring tar correctly, such as the choice of the stationary phase selection and sampling temperature. The adsorption capacity of tar compounds on the stationary phase depends on the affinity between the

fiber and the tar compounds, i.e., their polarity. Since PDMS is a non-polar phase, the affinity increases as the polarity of the compounds is lower (Duan et al., 2011; Fernández-Amado et al., 2016). Moreover, the sampling temperature greatly influences the adsorption on the fiber, as each compound has an optimum temperature that maximizes sensitivity while condensation is avoided. The optimum temperature for light and polar compounds is set at 21 ºC, which shifts to higher temperatures for heavier tar compounds to be condensed. Thus, this technique is limited to measure very low tar concentrations (Ahmadi et al., 2013a). The main differences between off-line techniques are gathered in Table 1.5.

Table 1.5. Comparison of off-line tar measuring techniques.

	Tar protocol	SPA	SPME
Principle	Cold trapping in liquid solvent (isopropanol)	Adsorption in a solid phase (amino-based, active carbon…)	Adsorption in a solid stationary phase (silica fiber with PDMS)
Sampling time	1 h	1-2 min	10 min
Desorption time	-	1 h	-
Analysis time	1 h	1 h	1 h
Advantages	- Robust method - Measures the total tar	- Easy and fast sampling - Smaller amounts of solvent - No loss of tar adsorbed tar by solvent evaporation and aerosol formation - High accuracy and reproducibility	- Easy and rather fast sampling - Solvent-free sampling - Suitable for measuring very low tar amounts
Shortcomings	- Long sampling times - Bulky and complicated sampling - Large solvent volumes - Loss of adsorbed tar by solvent evaporation and aerosol formation - Inadequate for low tar concentration - Low precision	- Only measures GC detectable compounds - Inadequate for heavy tars - BTX must be analyzed within few hours to avoid their desorption	- Under development -Application in raw product gas uncertain - Only measures GC detectable compounds - Non-aromatic C5+ hydrocarbons might compete with the tar compounds for the adsorption sites - Not standard procedure available
Tar detection limit	>5 mg Nm^{-3}	>2.5 mg Nm^{-3}	<0.1 mg Nm^{-3}
Application	Laboratory use	Laboratory use	Laboratory use

1.3.4.2. Online methods

As shown in section 1.3.4.1, off-line methods are time consuming (sampling times ranging from 1 min to 1 h) and require specific knowledge and instrumentation. Moreover, they need further laboratory analysis, which may require days or even weeks after sampling, making these methods inadequate for process monitoring. For further development of tar reduction strategies, a robust analytical device capable of monitoring continuously the tar concentration and fast enough to be used for process control is needed (Gredinger et al., 2018; Neubauer et al., 2018; Borgmeyer and Behrendt, 2020). Online tar analysis could be employed to monitor the general gasification process, the efficiency of tar scrubbers or catalytic reformers and their optimization, which would allow extending the life of gas engines and other downstream equipment (Gredinger et al., 2016). The development of online tar measurement techniques tries to address the drawbacks of off-line methods. Although several universities and research institutions have developed their own tools for measuring tar, which have been applied in many scientific works (Carpenter et al., 2007; Ahmadi et al., 2013b; Patuzzi et al., 2013; Gredinger et al., 2018), there is a need for simple and robust devices for industrial operation without requiring any highly skilled analytical expertise. The technologies used for this aim are based on molecule ionization and detection by flame (FID) or by photons (PID), optical methods, such as laser and UV-LED induced fluorescence and mass spectroscopy, i.e., molecular beam mass spectroscopy (MBMS) and ion molecular reaction spectroscopy (IMR-MS). Other techniques has also been tested in the online tar monitoring, such as tar dew point analyzer, high temperature reactor (HTR) (Israelsson et al., 2014), liquid UV-VIS spectroscopy (Kaufman Rechulski et al., 2012; Edinger et al., 2016) and volatility tandem differential mobility analyzer (VTDMA) (Gall et al., 2018). Table 1.6 compares online tar measuring techniques.

1.3.4.2.1. FID analyzer

FID online tar analyzer was initially developed by the Institute of Combustion and Power Plant Technology (IFK) and refined in the past years together with Ratfisch Analysensysteme GmbH for commercialization purposes. In fact, the previous company commercialized it with the name of TA120-3, although nowadays the purchase of this device is no longer possible. The measurement principle is based on a differential measurement of the organically bound carbon compounds present in the product gas, which is carried out using a flame ionization detector (FID). This device has two sample loops independently connected to FID. The only difference between the two loops is the cooled filter located before the FID in one of the loops, where tars are retained. Thus, the unaltered gas sample passing through the FID gives information about the total hydrocarbon content, whereas the gas sample crossing the filter indicates the total non-condensable hydrocarbon content. Detailed technical measurement principles and specifications of this device could be found elsewhere (Gredinger et al., 2016, 2018). It enables a fast and simple quantification of the total hydrocarbon concentration, non-condensable hydrocarbon concentration and tar concentration (by difference). Tar contents in the product gas in the 0-120 g Nm^{-3} range are detectable and each analysis takes around 60-90 s. Moreover, its use is quite easy, as it is not required any specific knowledge or training. Furthermore, it could be used in different sampling points as it is rather light (around 10 kg). One of the major challenges of this analyzer is the selection of an adequate tar filter, since the calculation of tars is performed through difference. If tars are not properly adsorbed or if other compounds are also absorbed (such as benzene) the accuracy of the tar concentration measurement can be negatively affected (Gredinger et al., 2016). Furthermore, filter changing and the overall maintenance of the equipment is quite easy. The online tar analyzer was tested and compared with off-line techniques, such solid phase adsorption (Meng et al., 2012) and tar protocol (Gredinger et al., 2018; Neubauer et al., 2018).

1.3.4.2.2. PID analyzer

Photo ionization detector (PID) based online tar analyzer was developed jointly by BTG and KTH. The fundamental element of the detector is an ultraviolet lamp filled with a gas, which generates photons and excites tar compounds. As a result, positively charged molecules produce a current directly proportional to the concentration of the compounds. The gas filling the UV lamp plays a key role in the detection of the compounds, as the emitted light has different wavelengths, and therefore different compounds could be detected. In this way, the lamp filled with xenon can detect aromatic compounds, such as toluene, phenol, naphthalene, acenaphthene, biphenyl, flourene, anthracene and pyrene. The recorded PID signal accounts for the total signal from all excited compounds, i.e., the total tar concentration, but is unable to quantify individual tar compounds. However, PID based tar analyzer could be suitable for online qualitative monitoring of tar, as PID signal stabilizes within a minute, the response time is of a few seconds and is very sensitive to low tar concentrations (<10 mg Nm^{-3}). In fact, the PID sensitivity is between 10 and 50 times higher than that of FID. The most challenging issue of this device is the fouling of the excitation chamber, which leads to a decrease in the PID response over time, and therefore the operation must be interrupted for periodic cleaning (Ahmadi et al., 2011, 2013b).

1.3.4.2.3. Optical analyzer

The optical online tar monitoring systems are based on fluorescence spectroscopy. The principle behind fluorescence spectroscopy for online tar measurement is a linear correlation between fluorescence signal and the tar concentration in a gas. In the first setup, Nd:YAG laser was used as the light source for analyte excitation. However, in the last few years light emitting diodes (LED) have been used to reduce the equipment cost (laser, spectrograph and CCD camera) and reinforce the robustness of the system for industrial application. UV-photons emitted from the LED are absorbed by tar compounds, raising their electronic state to excited ones. PAHs in the tar are excited by

wavelengths longer than 250 nm and release fluorescence upon relaxation. The optical setup is composed of a heated (up to 350 ºC) measurement cell, which allows optical access to tar containing gaseous streams through quartz glass windows constantly flushed by nitrogen to avoid tar condensation. The fluorescence light emitted by tar compounds in the cell is directed by an optical fiber to a UV/vis spectrometer, where the signals are detected. The whole measurement equipment is placed into a box to avoid ambient light influence. Several universities and research centers have developed laser and LED induced fluorescence based devices (Sun et al., 2010; Baumhakl and Karellas, 2011; Meng et al., 2012; Mitsakis et al., 2013; Patuzzi et al., 2013; Capper et al., 2017; Neubauer et al., 2018; Borgmeyer and Behrendt, 2020). However, none of them have been capable of running for a long time-frame in a plant environment. Thus, long-term stability of the laser is a challenge and fouling of the optical windows is troublesome even if the windows are heated up to 300 ºC (Borgmeyer, 2019). More recently, Borgmeyer and Behrendt (2020) have setup their LED-based system cooled by water, which exhibited no fluctuations regardless of the environmental conditions. Moreover, optical window purging with hot nitrogen during operation enabled continuous operation without operator interaction for several weeks, as no tar was condensed on the cell windows.

1.3.4.2.4. Online mass spectrometers

Online mass spectrometers have also been applied for continuously measuring a wide range of tar compounds with high sensitivity. Unlike most of the analytic mass spectrometers, which are coupled to a GC for the separation of the gaseous compounds, the online mass spectrometers setups are coupled to molecular beam (MB) and ion molecule reaction (IMR).

In the MBMS system, sampled gases are first extracted and the resulting supersonic expansion causes the fast cooling of the sample, inhibiting condensation or reaction. Thus, the analyte is preserved in its original state, allowing light gases to be sampled simultaneously with heavier condensable and reactive species. The subsequent mass

spectrometry analysis generates instantaneously the chemical fingerprint of the sample, enabling to observe its time-resolved behavior. The MBMS online analyzer was originally developed to study prompt thermochemical phenomena and has been extensively used by US National Renewable Energy Laboratory (NREL) in several other applications (Magrini et al., 2007; Sykes et al., 2009; French and Czernik, 2010; Haddix et al., 2016). Carpenter et al. (2007) investigated the use of a molecular beam mass spectrometer as an alternative method for quantifying real-time tar concentrations in biomass gasification and compared the results with those obtained with tar protocol, which showed they were consistent. This device could be used to sample directly from harsh environments, including high-temperature, wet and particulate gas streams. However, there is no pre-separation of the observed peaks, and isomers cannot be distinguished, making it difficult to interpret the mass spectra. Moreover, this system is quite complex, big in size and expensive, which makes its use unviable in industrial applications.

The French Alternative Energies and Atomic Energy Commission (CEA) have adapted IMR-MS setup for online tar measurement. A low ionization energy inert gas (Xe or Kr) is used as ion source because high ionization energies fragment molecules and lead to more complex mass spectra and multiple overlapping intensities. In this technique, an inert gas is ionized by electron impact, which reacts under vacuum conditions with the sample gas according to the ion molecule reaction in a reaction chamber. The ionized sample gas is then conducted to a classical quadrupole and mass spectrometer. Defoort et al. (2014) tested this equipment in biomass steam gasification, measuring the released wet and dry gases. In the case of wet gas, it was diluted with nitrogen, which led to less consistent results, as the values were close the detection limit of the equipment. However, the masses corresponding to benzene, toluene, thiophene, phenol, indene, acenaphthylene, biphenyl+acenaphthene, fluorene, phenanthrene+anthracene were well defined. As soft ionization is used, fragmentation of molecules is avoided, but the need for building a fragmentation database at such low ionization potential arises.

The status of the presented techniques for tar sampling and measuring is diverse. The development of some of them has been suspended, whereas others are commercially available or still under development. Tar protocol and SPA off-line techniques are actively used. Although SPA method is less time consuming and cumbersome than tar protocol and provides adequate results, tar protocol is still more frequently used in both industrial and scientific environments. Many research groups have reported the use of this technique to measure the amount of tar in the biomass gasification processes (De Andrés et al., 2011a; Virginie et al., 2012; Barisano et al., 2016; Rapagnà et al., 2018; Benedikt et al., 2019; Mauerhofer et al., 2019; Fuentes-Cano et al., 2020; Gupta et al., 2020). In the case of SPME technology, it seems that it has been abandoned after its first demonstration with clean syngas. Regarding the introduced online methods, only MBMS and IMR-MS setups are commercially available up to now. MBMS and IMR-MS equipment for online quantification of tar during biomass gasification are being commercialized by Extrel and V&F (Airsense model) companies respectively. However, both setups are so expensive (around 300,000 $) that they are not used to monitor and control tar concentration in gasification processes. Some years ago, a FID online analyzer was commercialized by Ratfisch Analysensysteme GmbH with the name of TA120-3, but nowadays the purchase of this device is no longer possible. Technical challenges and restrictions hindered the scientific and commercial success, and therefore further development of the technique is needed (Gredinger et al., 2018). At this time, the development of a PID based commercially available device is stopped because the fouling problems of the UV lamp have not been solved yet. However, it may have a great potential when they are solved. In the case of optical methods, UV-LED based ones seem to be more promising for process control than laser ones as they are much cheaper, but there is still a lot of work ahead to eliminate the associated problems.

Table 1.6. Comparison between online tar measuring techniques.

Technique	Detected tar compounds	Tar detection limit	Advantages	Limitations	Status
FID online tar analyzer	Total tar concentration	0-120 g Nm^{-3}	-Fast and easy quantification of tar concentration -Short measurement time: 60-90 s -Easy to use -Simple maintenance -Light and robust	- Maximum operating temperature: 300 ºC -Impossibility of determine individual tar composition -Filter change	Discontinuation
PID online tar analyzer	Total tar concentration	0-50 g Nm^{-3}	- Short response time: few seconds - Very sensitive to low concentrations - Linear response to tar compounds - Non-destructive analysis	- Maximun operating temperature: 300 ºC - Impossibility of determining individual tar composition - Fouling of the excitation chamber - Changes in tar composition negatively affect the accuracy of the quantification	On hold
Laser induced fluorescence	Some tar species	0-20 g Nm^{-3}	- High-precision - High fluorescence signals - Linear correlation between fluorescence signal and tar content - Non-invasive	- Very expensive (not suitable for industrial applications)	On hold

Table 1.6. Continued.

Technique	Detected tar compounds	Tar detection limit	Advantages	Limitations	Status
Led induced fluorescence	Some tar species	0.5- >10 g Nm^{-3}	- Low price: promising for industrial applications - Stability of optical power - Linear correlation between fluorescence signal and tar content - Non-invasive	- Low optical power - Limited tar compounds can be detected at a single wavelength - It is difficult to translate the absorbance into tar concentration (more than one tar species causes absorbance at the same wavelength) -Fouling on optical windows is problematic -Only can measure light and heavy polyaromatics	On hold
Molecular beam mass spectrometer	Some tar species	Near-universal detection	- Robust equipment for monitoring hot raw product gas - High reproducibility and sensibility -Near-universal detection - Commercially available	-Complex system -Expensive equipment -Quantification could be complicated -Possible interference with other gas compounds	Commercial
Ion molecule reaction mass spectrometry	Some tar species	Near-universal detection	- Capable of measuring BTX and PAHs at low and high concentrations -Commercially available	-Need for building a fragmentation database for low ionization potential -Expensive equipment	Commercial

1.4. PRIMARY STRATEGIES FOR TAR ELIMINATION

Tar removal is one of the main concerns in biomass gasification, since it condenses at low temperatures leading to the blockage and fouling of process equipment, such as pipes, heat exchangers and particle filters (Devi et al., 2003; Anis and Zainal, 2011; Arregi et al., 2018). In this regard, several strategies have been proposed and analyzed in order to reduce or even completely eliminate the tar compounds from the fuel gas. These measures can be classified into two different groups: i) primary methods, wherein the tar is removed inside the gasifier by selecting optimum operating conditions, using adequate bed materials or catalysts or even by a proper design of the gasifier, and; ii) secondary methods, where the tar is reduced downstream the gasifier. These latter ones can be divided into physical/mechanical (filters, cyclones and scrubbes) and chemical systems (thermal and catalytic tar cracking) (Anis and Zainal, 2011). Despite these strategies have been proved to be effective for tar elimination, their use is sometimes not economically feasible (Claude et al., 2016).

This section provides an overview of the main primary strategies for tar elimination in biomass gasification. Accordingly, the influence the main operating conditions (temperature, S/B and ER and gasifying agent), biomass characteristics and the different primary catalysts used in the literature is analyzed in Sections 1.4.1, 1.4.2 and 1.4.3, respectively. Moreover, the main advances in reactor design development and the new strategies implemented in the reactor itself for tar removal will be discussed in Section 1.4.4.

1.4.1. Operating conditions

The suitable selection and control of the operating conditions during biomass gasification is of uttermost importance for the reduction or almost complete removal of tar compounds in the flue gas. Amongst the operating parameters that affect the gasification performance, the most influential ones are as follows: temperature, gasifying agent, steam/biomass (S/B) ratio, equivalence ratio (ER), residence time and

pressure. Moreover, the type of biomass and its features (ash content, particle size and moisture) may greatly influence the distribution of the products obtained in the process (Parthasarathy and Narayanan, 2014). It should be noted that the type of gasifier used also conditions the optimum selection of these parameters (Devi et al., 2003).

1.4.1.1. Temperature

Gasification temperature is one of the most influential parameter in terms of tar formation and H_2 production (Parthasarathy and Narayanan, 2014). The temperature range at which gasification is usually conducted varies from 700 to 1200 ºC, although most of the research studies operate between 800 and 900 ºC to obtain high conversion rates (Hanchate et al., 2021). It should be noted that the temperature range selected also depends on the gasifying agent used (air, oxygen, steam or their mixtures) and the type of gasifier, with a correct fluidization regime being essential for a homogeneous temperature profile inside the gasifier in order to ensure suitable operation (Devi et al., 2003). Thus, the selection of an optimum temperature is of uttermost importance, since it influences the chemical reactions involved in the gasifier, and therefore modifies both the distribution and the composition of the products obtained. In fact, controlling the temperature inside the reactor is necessary for enhancing process characteristics, and consequently control the tar concentration in the product gas. Thus, at low gasification temperatures, high tar concentrations are obtained (Hanchate et al., 2021), whereas at higher temperatures, tar content is significantly reduced due to the promotion of tar cracking and reforming reactions (Gil-Lalaguna et al., 2014). The latter positively enhance a gas stream rich in H_2, with low values of CO and CH_4 concentration (Parthasarathy and Narayanan, 2014; Arregi et al., 2018; Hanchate et al., 2021).

The influence temperature has on the tar content in the gaseous stream has been analyzed by several researches (Göransson et al., 2011; Kirnbauer et al., 2013; Meng et al., 2018b; Yahaya et al., 2020). Accordingly, a wide range of reactor configurations have been employed, with the most common ones being fixed bed (updraft, downdraft

and crossdraft), fluidized bed, entrained flow, spouted beds and plasma reactors (Mahinpey and Gomez, 2016; Arregi et al., 2018; Ren et al., 2019a). Figure 1.12 compares various results reported in the literature wherein the influence gasification temperature has on tar content is analyzed. As will be shown later, (Section 1.4.1.2), the tar content is considerable affected by the type of gasifying agent. For the sake of clarity, the graphs in Figure 1.12 have been ordered according to the gasifying agent used, i.e., steam (Figure 1.12a), air or O_2 (Figure 1.12b), and their mixtures (Figure 1.12c).

As observed in Figure 1.12, regardless the gasifying agent used, the tar content is reduced as temperature is increased. Thus, Tian et al. (2020) investigated the influence reaction temperature (700–900 °C) has on the component distribution in the gas stream, lower heating value (LHV), tar content, gas yield and H_2/CO ratio using a fluidized bed system for air-steam gasification of rice husk. Two bed materials were tested and a considerable tar reduction was attained when gasification runs were conducted at 900 ºC (they reported tar values of 2.17 and 0.15 g Nm^{-3} with silica sand and coal bottom ash, respectively). Guo et al. (2020) reported a tar reduction to one third (from 6.2 g Nm^{-3} at 700 °C to 2.02 g Nm^{-3} at 900 °C) in the corn straw gasification runs conducted in a bench-scale internally circulating fluidized bed when the ER was 0.21. Rapagnà et al. (2000) conducted the steam gasification of almond shells in a fluidized bed using olivine as bed material. A decrease in tar content from 6.1 to 0.5 g Nm^{-3} was observed as temperature was increased from 770 to 820 °C. A conical spouted bed reactor (CSBR) was used by Erkiaga et al. (2014) who analyzed the influence of temperature in the pinewood sawdust steam gasification using sand as bed material. The tar content was significantly reduced from 364 to 142 g Nm^{-3} as temperature was increased from 800 to 900 ºC due to the enhancement of tar cracking and reforming reactions.

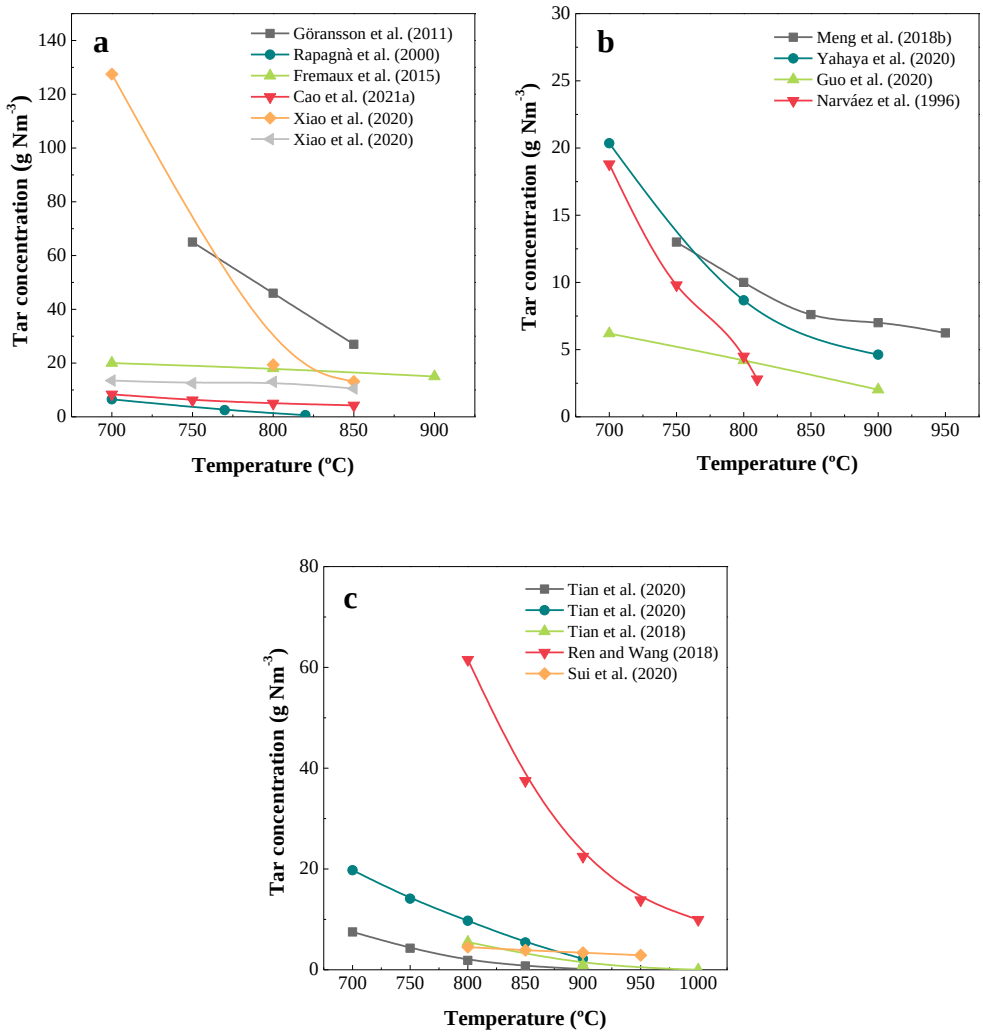

Figure 1.12. Influence of gasification temperature on tar content in the gaseous product stream. Gasifying agent: (a) steam, (b) air/O_2 and (c) mixtures of steam-air (Narváez et al., 1996; Rapagnà et al., 2000; Göransson et al., 2011; Fremaux et al., 2015; Meng et al., 2018b; Ren and Wang, 2018; Tian et al., 2018, 2020; Guo et al., 2020; Sui et al., 2020; Xiao et al., 2020; Yahaya et al., 2020; Cao et al., 2021a).

Moreover, gasification temperature not only affects the tar content, but also influences its composition (Meng et al., 2018b). It is to note that the diversity of tar classification

by the researches hampers the straight comparison of the literature results. In general, as gasification temperature is increased, the tar is mainly formed by highly stable species (light and heavy polycyclic aromatic compounds (PAHs)) because light aromatics (1 ring) and heterocyclic compounds are considerably removed (Milne et al., 1998; Devi et al., 2003; Meng et al., 2018b; Valderrama Rios et al., 2018). Mayerhofer et al. (2012) analyzed the influence temperature (750-840 ºC) has on tar composition using a fluidized bed reactor for the steam gasification of wood pellets. They observed that high temperatures were essential for the formation of secondary and tertiary aromatic and polyaromatic tar species. Similar results have been reported in the literature (Calvo et al., 2012; Kuba and Hofbauer, 2018; Guo et al., 2020).

1.4.1.2. Gasifying agent

The selection of the gasifying agent greatly influences the tar content and its composition in the gaseous stream, as well as the reaction rate and the heating value of the produced gas, as a result of the different gasification reactions involved when one gasifying agent or another is selected. The choice between them depends on the balance between the final product gas specifications and process costs (Devi et al., 2003; Molino et al., 2018; Hanchate et al., 2021). Several gasifying agents have been employed in the literature, the most common ones being steam, air, O_2, CO_2 and their mixtures. In terms of obtaining a gas with low amounts of tar, oxygen is the best candidate. However, the operating costs are extremely high due to the energy required for oxygen production. Thus, air is most widely used, although higher tar concentrations are produced. More recently, special attention has been paid to biomass steam gasification because a gas with higher hydrogen content is obtained, although higher tar concentrations are also produced. On the other hand, steam gasification reactions are highly endothermic and an external energy supply is demanded. In view of these facts, air and steam mixtures seem to be promising from both economy and chemistry points of view, since the partial combustion of the biomass particle inside the gasifier supplies the heat required for the process, with tar formation and hydrogen production being moderate (Campoy et al., 2009; Gil-Lalaguna et al., 2014; De Sales et

al., 2017). Figure 1.13 compares some literature results in which the effect air, steam and O_2-air/steam mixtures has on tar concentration under similar operating conditions is evaluated.

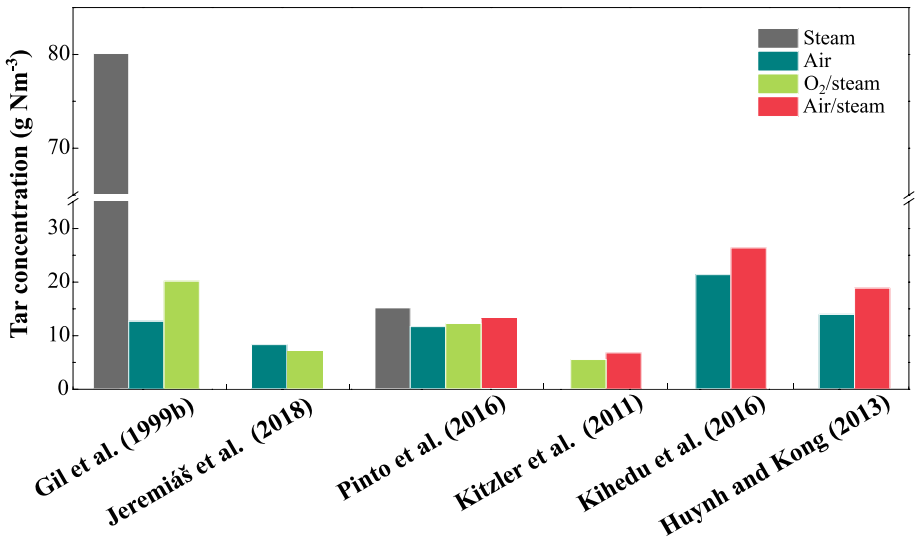

Figure 1.13. Influence of the gasifying agent on tar concentration (Gil et al., 1999b; Kitzler et al., 2011; Huynh and Kong, 2013; Kihedu et al., 2016; Pinto et al., 2016; Jeremiáš et al., 2018).

When comparing the results obtained with different gasification agents, it is very important to measure the gas yield on a dry inert free basis to avoid the dilution effect of N_2. As shown in Figure 1.13, Gil et al. (1999b) and Pinto et al. (2016) studied the effect of the type of gasifying agent on tar concentration and the highest tar concentrations were recorded for steam, 80 and 15 g Nm^{-3}, respectively. In addition, both authors obtained lower tar concentrations with air and O_2/steam mixtures. However, much lower differences could be observed for the tar concentrations obtained by Pinto et al. (2016). With regard to the research carried out by Gil et al. (1999b) involving air and O_2/steam gasification, the gas yield was not measured on a N_2 free basis, which certainly explains the higher influence noticed. Jeremiáš et al. (2017) also compared the influence of air and O_2/steam on the gasification of wood chips in a fluidized bed and showed that the mixture was slightly more effective in tar

reduction. As for Kitzler et al. (2011), the comparison was done between mixtures, concluding that the one with O_2 is the best to reduce the tar concentration. However, the high cost of O_2 does not balance that small decrease. Pinto et al. (2016) drew the same conclusion when adding O_2 to steam, as tar reduction was of only 5 %.

Furthermore, Huynh and Kong (2013) and Kihedu et al. (2016) noted the same declining trend as the previous authors when they used air and air/steam mixtures, with the tar concentration being higher for the mixture. Both authors reported that tar was reduced by around 26 % when air was used. The results from Figure 1.13 bring to light that O_2 containing mixtures led to the lowest tar concentration followed by air.

There is no much literature regarding how tar composition is affected by using one or another gasifying agent. Jeremiáš et al. (2017) reported that steam mixtures resulted in a tar with a lower amount of heavy PAHs compared to air-only gasification. In fact, the amount of this lump was reduced by almost half, from 11 wt% in air gasification to 6 wt% in O_2/steam gasification. In this line, Corella et al. (1999) reported that tars produced in the steam gasification were easier to remove that tars obtained in air gasification. In the study carried out by Jeremiáš et al. (2017), the amounts of heteterocycles and light aromatics obtained with O_2/steam mixture and air were almost the same, around 3 wt% for heterocycles and 41 wt% for light aromatics. Consequently, the amount of light PAHs was higher for O_2/steam mixture (51 wt%) than for the air gasification (45 wt%). According to Gil-Lalaguna et al. (2014), steam containing gasifying mixtures led to a decrease in the fraction of light PAHs, as it seems that polymerization reactions were prevented when using steam. The same authors (Gil-Lalaguna et al., 2014) analyzed the composition of the gasification medium feeding sewage sludge in a fluidized bed and stated that N-aromatics and light PAHs were the most sensitive tar lumps to the steam/O_2 ratio.

It should be noted that the fuel mass ratio and gasifying agent, i.e., steam to biomass ratio (S/B), equivalence ratio (ER) and gasifying ratio (GR) when steam, air or O_2-steam mixtures are used, respectively, are the most influential parameters in the removal of tar, and they are therefore discussed in detail in the following subsections.

1.4.1.1.1. Influence of S/B ratio

Steam is regarded as the most suitable gasifying agent for the production of H_2 rich syngas (Cao et al., 2020). Moreover, a gas with a high heating value in the range of 10-15 MJ m^{-3} is obtained, which makes its use attractive for energy production (Parthasarathy and Narayanan, 2014; Sansaniwal et al., 2017a). The endothermic nature of steam gasification reactions may involve an increase in the energy requirements of this process, thereby increasing the costs compared to the use of other gasifying agents such as air. Moreover, the use of steam provides the additional advantage of avoiding a costly separation process (Devi et al., 2003; Arregi et al., 2018). The main reactions involved in the biomass steam gasification are as follows: drying, pyrolysis, char gasification, reforming, cracking and water gas shift (WGS) reactions (Erkiaga et al., 2014; Mazumder and de Lasa, 2016; Cao et al., 2020).

S/B ratio is one of the key parameters involved in steam gasification. It is defined as the mass flow rate of the steam fed into reactor divided by the biomass mass flow rate. An increase in S/B ratio enhances WGS and steam reforming reactions, and therefore a higher gas yield is obtained at the same time as tar and char formations are hampered. However, an excess of steam could lead to a reduction in temperature, and consequently enhance tar formation. Figure 1.14 shows some studies wherein the influence of S/B ratio on tar concentration is analyzed.

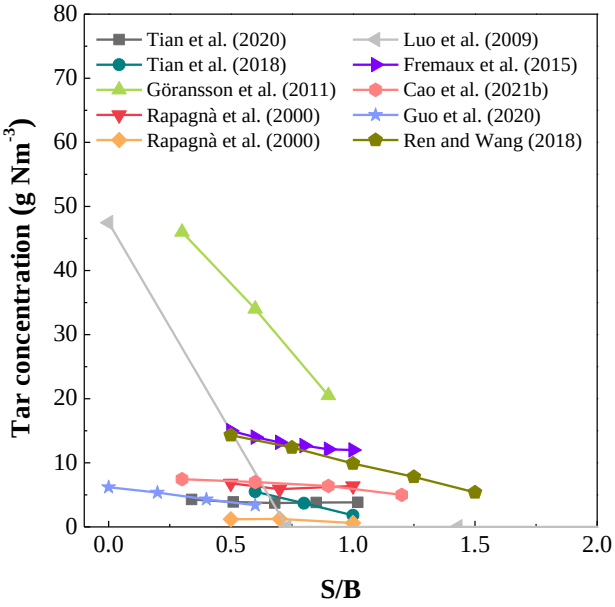

Figure 1.14. Influence of S/B ratio on tar concentration (Rapagnà et al., 2000; Luo et al., 2009; Göransson et al., 2011; Fremaux et al., 2015; Ren and Wang, 2018; Tian et al., 2018; Guo et al., 2020; Cao et al., 2021b).

As shown in Figure 1.14, high S/B ratios lead to an improvement in tar removal. Among all the studies, the one by Goranssön et al. (2011) shows that tar concentration is mostly influenced by the S/B ratio. These authors (Göransson et al., 2011) studied the effect of S/B ratio in the 0.3-0.9 range in a dual fluidized bed and reported that the tar concentration was reduced by more than half, from 46.0 to 20.5 g Nm^{-3}. Furthermore, Ren and Wang (2018) and Tian et al. (2018) observed a more moderate decrease in tar concentration when S/B ratio was varied from 0.6 to 1 and from 0.5 to 1.5, revealing that the amount of tar gradually declined from 5.5 to 1.8 g Nm^{-3} and from 14.3 to 5.4 g Nm^{-3}, respectively. However, other authors (Rapagnà et al., 2000; Fremaux et al., 2015; Guo et al., 2020; Cao et al., 2021b) presented in Figure 1.14 concluded that an increase in S/B ratio slightly affect tar concentration. In fact, Luo et al. (2009) did not note any tar for S/B ratios higher than 0.73 in a fixed bed reactor, whereas they recorded a tar concentration of 47.8 g Nm^{-3} when no steam was in the

feed. Taking the results of these studies into account, it could be concluded that there is an optimum S/B ratio that strikes a balance involving high H_2 productions, low tar concentrations and external energy requirements.

Studies dealing with the influence of S/B ratio on tar composition are scarce and mostly the comparison between them turns to be difficult, as tar definitions are usually diverse. In general, it is agreed that steam addition changes tar composition, leading to a decline in the amount of light tar compounds (Qin et al., 2010; Göransson et al., 2011). Erkiaga et al. (2014) and Guo et al. (2020) conducted a detailed study in which the influence of S/B ratio was analyzed for the different tar lumps. However, different conclusions were drawn, which might be related with the different operating conditions used in one and the other. On the one hand, Guo et al. (2020) varied the S/B ratio in the 0-0.6 range maintaining the reaction temperature at 700 ºC and ER=0.21 in air-steam gasification experiments. They concluded that an increase in the S/B ratio led to a decrease in the amount of heterocycles and light aromatics from 5 and to 2.5 and 47 wt%, respectively, whereas those of light and heavy PAHs increased from 11 and 1 to 28 and 5 wt%, respectively, and the content of GC undetectable compounds decreased slightly from 19 to 17.5 wt%. On the other hand, Erkiaga et al. (2014) analyzed the influence of S/B ratio between 0 and 2 at 900 ºC in the biomass steam gasification and the opposite trend was observed for the heterocyclic compounds and the light PAH fraction. They concluded that the main effect of increasing the amount of steam was an increase in heterocyclic compounds (from 10 to 15.5 wt%) and a reduction in light PAHs (from 70 to 66 wt%), although these effect was rather limited. In fact, increasing the S/B ratio from 1 to 2 did not change the tar composition.

1.4.1.1.2. Influence of ER

Air has been extensively used as gasifying agent, since it promotes combustion and partial oxidation reactions, providing the energy required for the gasification process. However, a syngas of low heating value is produced in the air gasification of biomass due to the dilution with N_2 (Asadullah, 2014b; Sansaniwal et al., 2017a).

ER is a crucial factor affecting the air gasification performance. It is defined as the actual air supply divided by the stoichiometric air required for complete combustion (Guo et al., 2014; Sansaniwal et al., 2017b). In biomass gasification, it usually varies from 0.20 to 0.40. ER values below 0.2 result in incomplete gasification, and therefore more tar and char are formed and a low heating value gas (Alauddin et al., 2010; Claude et al., 2016; Sikarwar et al., 2016). Figure 1.15 compares some results obtained in different studies in which the tar concentration was monitored by increasing ER. All selected studies have in common that all of them gasify lignocellulosic biomasses, although they have differences in the reactor type, operating conditions, mainly gasifier temperature, and the way heat is provided to reactor (allothermal or authotermal). When a gasifier is authotermical, a higher ER implies a higher reaction temperature, so it may be difficult to distinguish between the temperature or ER effect on the tar concentration (Kaewluan and Pipatmanomai, 2011a).

As observed in Figure 1.15, an increase in ER leads to a reduction in tar concentration. When increasing ER, oxidation and exothermic reactions are enhanced, which promote the combustion of volatiles and carbon. Thus, tar cracking reactions are favoured and so the reaction between tar and moisture in the raw material, producing more H_2, CO and other light gases (Guo et al., 2020). However, excessively high ER values result in higher gas yields (though more diluted) and shorter residence times, which avoids tar reduction. An optimum ER should strike a balance between high calorific value gas and low tar concentrations (Cao et al., 2021b). In this line, Sui et al. (2020) varied ER from 0.12 to 0.24 at 800 ºC in a fluidized bed gasifier and considered ER of 0.2 as an optimum value, as tar content did not significantly changed when ER was further increased to 0.24. Furthermore, Guo et al. (2014) reported a higher ER (0.32) as the optimum one. In fact, these authors studied the effect of ER between 0.18 and 0.37 in a downdraft fixed bed, which has poorer heat and mass transfer rates than fluidized beds, and noted that tar content dropped from 2.5 to 0.52 g Nm^{-3} when the ER was increased to 0.32, but it hardly changed for higher ERs. Due to the dilution effect of N_2, high ER ratios involve high amounts of N_2, which reduces the tar concentration. Therefore, in these cases it would be necessary to check the tar yields (defined as the amount of tar

produced in mass divided by the amount of biomass in the feed) to determine the real effect of ER in tar elimination.

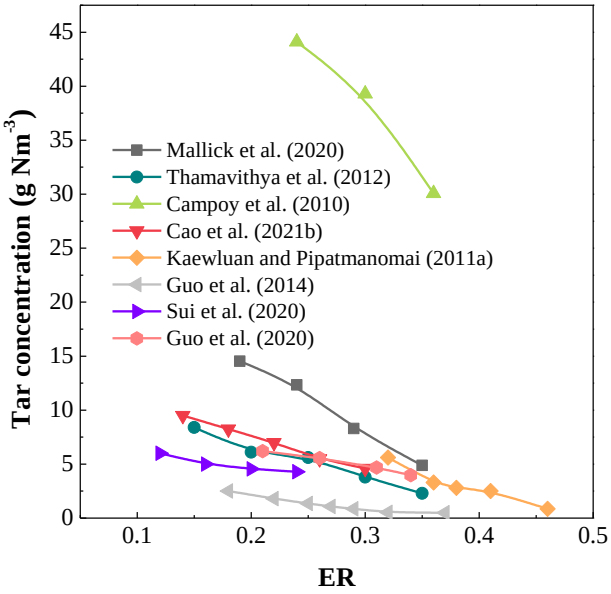

Figure 1.15. Influence of ER on tar concentration (Campoy et al., 2010; Kaewluan and Pipatmanomai, 2011a; Thamavithya et al., 2012; Guo et al., 2014, 2020; Mallick et al., 2020; Sui et al., 2020; Cao et al., 2021b).

Regarding the influence of ER on tar composition, Guo et al. (2020) varied it between 0.21 and 0.34 in an autothermal fluidized bed and monitored the amounts of different tar lumps. The contents of heterocyclic compounds and light aromatics decreased with an increase in the ER, whereas those of light and heavy PAHs increased. According to these authors, as the ER increased, the O_2 in the air promoted the oxidation of heterocycles and light aromatics, leading to the cleavage of C-H and C-O bonds and formation of free H and O radicals. These free radicals enhanced dimerization reactions and H_2-abstraction-C_2H_2 addition sequence reactions, forming aromatics with a higher number of rings. Mallick et al. (2020) gave also a very similar explanation.

1.4.1.3. Pressure

Gasification process may be carried out at atmospheric pressure or under higher pressures. In fact, special attention should be paid to the operating pressure as it might provide certain advantages from a chemical point of view, but also some challenges from an operational perspective (Couto et al., 2013; Sansaniwal et al., 2017b; Molino et al., 2018; Hanchate et al., 2021).

Following Le Chatelier's principle, some reactions are accelerated at high operating pressures due to chemical equilibrium shift towards the side with fewer moles, which hinders reforming and cracking reactions in the gas phase. Thus, an increase in the amount of tar is expected with increasing pressure (Mayerhofer et al., 2012; Motta et al., 2018). However, according to Mayerhofer et al. (2012), the total gas pressure also influences the release of primary/secondary tar, as evaporation decrease leads to longer residence times of primary/secondary tars, and therefore cracking is enhanced and tar composition changed. As for Wolfesberger et al. (2009), they pointed out that pressure has an influence on tar concentration depending on the gasifier design. Thus, pressurized operation is suitable for large-scale processes since heat transfer in the bed is much more efficient, and consequently gasification performance improves, reducing tar concentration (Motta et al., 2018). One of the advantages of the pressurized operation is that, depending on the final application of the produced syngas, it might not require an additional compression, as it is the case of syngas burning on turbines or engines. With regards to the challenges involving the pressurized gasification, feeding biomass is quite tricky, operation is more expensive and high amounts of purging gas are needed. Although the equipment size is smaller when higher pressures are employed because lower gas volumes are treated, they are 4 times more expensive than the equipment used in atmospheric gasification. Therefore, pressurized gasification is only advisable if the syngas needs to be compressed for its final application (Couto et al., 2013; Claude et al., 2016; Sansaniwal et al., 2017b; Molino et al., 2018).

In the literature, there is a discrepancy regarding the effect of pressure on tar concentration. As shown in Figure 1.16, some authors reported that elevated pressures reduce the tar concentration, whereas others concluded that tar content increases by increasing pressure. Thus, Wolfesberger et al. (2009) carried out biomass gasification at 825 ºC in the 70 kW air-blown pressurized unit and found that the tar content declined from 4.4 to 1.7 g Nm^{-3} when the pressure was increased from 1 to 5 bar. These authors suggested that increasing pressure, the gas linear velocity declines due to the influence of pressure on the density of the gaseous phase, and therefore the residence time increases and the tar concentration decreases.

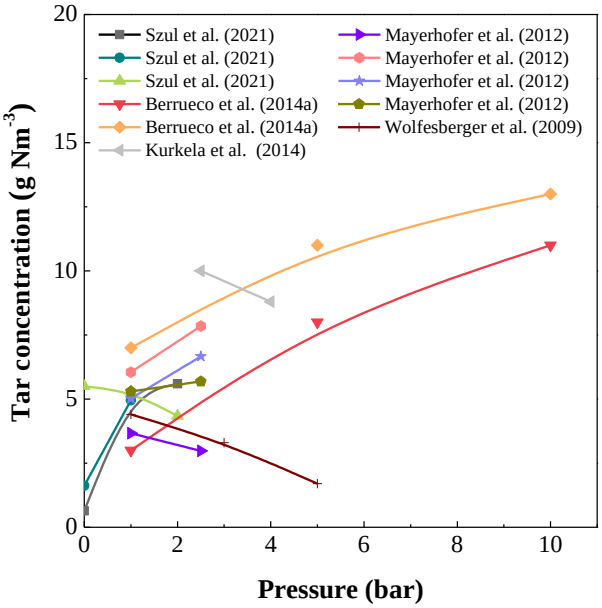

Figure 1.16. Influence of the operating pressure on tar concentration. (Wolfesberger et al., 2009; Mayerhofer et al., 2012; Berrueco et al., 2014a; Kurkela et al., 2014; Szul et al., 2021).

Mayerhofer et al. (2012) changed the pressure in the 1-2.5 bar range in an allothermal bubbling fluidized bed operating at 750 and 800 ºC with S/B ratios of 0.8 and 1.2. They reported a raising tendency for tar concentration under all the conditions studied with increasing pressure, except for the experiment at 800 ºC and using a S/B ratio of

2. Likewise, Berrueco et al. (2014b) also revealed that elevating the pressure from 1 to 10 bar in a fluidized bed reactor, tar concentration increased from 3 to 11 g Nm^{-3} for Norwegian spruce and from 7 to 13 g Nm^{-3} for Norwegian forest residue. However, Szul et al. (2021) used an autothermal fluidized bed reactor to analyse the influence of pressure in the 0-2 bar range on the gasification of softwood, bark and lignin at 850 ºC, and found that tar concentration increased with pressure for bark and lignin, from 0.64 to 5.6 g Nm^{-3} and from 1.62 to 4.95 g Nm^{-3}, respectively, whereas a slightly decreasing trend was observed for the softwood, from 5.50 to 4.34 g Nm^{-3}. Kurkela et al. (2014) also reported a slightly declining trend for tar concentration (from 10 to 8.8 g Nm^{-3}) when the pressure ranged between 2.5 and 4 bar, although they pointed out that the gasifier became unstable and operational changes were needed. The same authors suggested that a bubbling fluidized bed would be more adequate for operating at high pressures than a circulating fluidized bed.

Regarding the effect of pressure on tar composition, Mayerhofer et al. (2012) observed that heterocyclic compounds were hardly affected or slightly reduced with increasing pressure, whereas the concentration of light PAHs increased. The most significant change was reported for naphthalene, which rose from 0.61 g Nm^{-3} to 1.79 g Nm^{-3}. However, Wolfesberger et al. (2009) found the opposite tendency for tar concentration, reporting that the amount of naphthalene and heterocycles increased from 40 and 3 to 52 and 6 wt%, respectively and that of light PAHs decreased from 35 to 20 wt%, with the one of light aromatics remaining steady.

1.4.1.4. Residence time

Residence time determines how many, and to what extent, consecutive reactions can take place at certain temperature (Paasen and Kiel, 2004). Thus, residence time is a crucial parameter, which should be considered in order to design a gasifier. Short residence times hinder tar cracking and reforming reactions and low conversion efficiencies are obtained, whereas high residence times allow greater exposure of tar to the gasifying agent, which reduces tar formation and leads to higher process efficiency

(Valderrama Rios et al., 2018; Singh Siwal et al., 2020). However, the literature has barely studied its influence on the gasification performance. That is, the studies were not mainly focused on tar concentration, although a few ones dealt with experimental and simulations runs analyzing the effect of residence time on syngas compositions (Hernández et al., 2010; Agu et al., 2019; Rupesh et al., 2021). Paasen and Kiel (2004) studied the effect of gas residence time by sampling the gas at different freeboard heights, which corresponded to 1.2 and 5.4 s, and reported that tar concentration decreased from 22.63 to 17.54 g Nm^{-3}. Regarding individual tar lumps, the concentration of light and heavy PAHs increased, whereas the of concentration heterocyclic and light aromatic compounds decreased with increasing residence time, which is in agreement with the results of Kinoshita and Wang (1994). The latter adjusted the residence time between 3.2 and 4.8 s by varying the nitrogen flowrate at 800 ºC and concluded that tar concentration was hardly influenced by residence time.

1.4.2. Biomass characteristics

The main biomass characteristics influencing gasification performance are biomass type, moisture content and particle size. The following subsections deal with the effect of biomass type and its features (moisture and particle size) on the product distribution, mainly tar concentration.

1.4.2.1. Biomass type

Biomass could be classified into different groups according to their origin: agricultural biomass, forest biomass, municipal biomass and biological biomass (Hanchate et al., 2021). All biomasses are mainly composed of cellulose, hemicellulose and lignin, and their proportion depends on the original biomass type (Parthasarathy and Narayanan, 2014). These principal components play a crucial role in biomass gasification, which also applies to the ashes produced. In fact, the proportion between these biomass components determines process performance. Thus, the celloluse and hemicellulose amount is associated with the gas yield and the lignin amount with the tar yield.

Generally, biomasses with high amounts of lignin and volatile matter lead to high amounts of tar concentration, whereas those with high amounts of cellulose or fixed carbon lead to low tar contents (Sikarwar et al., 2016; Molino et al., 2018; Hanchate et al., 2021).

Figure 1.17 shows the variation in the tar concentration for different types of biomasses based on the investigations carried out in the literature. As observed, there is no clear tendency. It seems that other factors, such as reactor type and operating conditions, may have a major influence on tar composition than the biomass type.

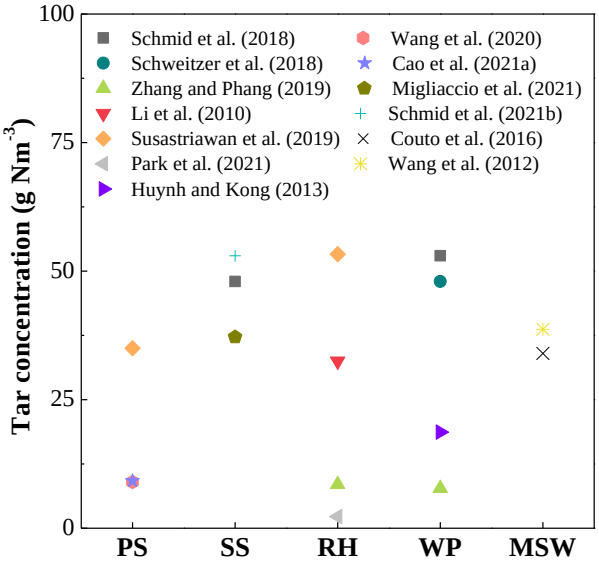

Figure 1.17. Tar concentration for various biomass feedstocks (PS: pine sawdust; SS: sewage sludge; RH: rice husk; WP: wood pellets; MSW: municipal solid wastes) (Li et al., 2010; Wang et al., 2012; Huynh and Kong, 2013; Couto et al., 2016; Schmid et al., 2018, 2021b; Schweitzer et al., 2018; Susastriawan et al., 2019; Zhang and Pang, 2019; Wang et al., 2020; Cao et al., 2021a; Migliaccio et al., 2021; Park et al., 2021)

1.4.2.2. Moisture

Generally, woody and some herbaceous biomasses contain a moisture content below 15 wt%. However, some freshly harvested biomasses could have moisture contents of up to 60 wt% (Sikarwar et al., 2016).

The moisture percentage of the biomass has a great effect on the energy balance of the reactor. When a biomass with high amount of moisture (above 40 wt%) is fed, gasification temperature decreases, and therefore the process efficiency is reduced, as water evaporation is a highly endothermic process. In fact, an extra of 2260 kJ are needed to vaporize a kilogram of moisture in the biomass. According to the literature (Sikarwar et al., 2016; Motta et al., 2018; Cao et al., 2020), biomass with less than 35 wt% of moisture should be treated to strike a balance between high quality syngas with low tar concentration and costs-benefits. Feeding biomass with a moisture content in the 10-15 wt% range is ideal for an adequate operation of the feeder and gasification performance, as some moisture could be advantageous (Bronson et al., 2012).

In the case of handling high moisture content biomass, low feeding rates are advisable in order to maintain bed conditions stable, and therefore operate with high efficiency in the process (Bronson et al., 2016). Moreover, additional heat must also be supplied, either externally or by introducing some air or O_2 (Sikarwar et al., 2016; Motta et al., 2018). Regarding the reactor configuration, updraft fixed bed could operated with 60 wt% of moisture, whereas the downdraft ones could only efficiently handle a moisture content of up to 25 wt% (Sansaniwal et al., 2017a; Molino et al., 2018). Thus, co-gasification is gaining attention in order to handle high moisture content biomasses (Kaewluan and Pipatmanomai, 2011b; Pinto et al., 2016). Furthermore, previous treatments, such as drying, torrefaction or hydrothermal upgrading are also recommended in these cases (Motta et al., 2018).

Figure 1.18 shows some of the studies in which the influence of the biomass moisture content on tar concentration was reported. The studies carried out by Paasen and Kiel

(2004) in a bubbling fluidized bed by varying the moisture content in the 10-43 wt% range showed that some moisture could be beneficial to the gasification process, as the enhancement of WGS and CH_4 and tar steam reforming reactions reduced tar concentration from 14.3 to 9.2 g Nm^{-3}. Likewise, Pfeifer et al. (2011) in a dual fluidized bed reactor reported for similar moisture contents (6-40 wt%) that the highest tar concentration (7.5 g Nm^{-3}) were measured when the biomass with the lowest moisture content (6 wt%) was fed and the lowest (4.9 g Nm^{-3}) when the biomass with 20 wt% moisture content was fed. For moisture contents of up to 40 wt%, tar concentration increased slightly, but these values were still below those for 6 wt% moisture content. Furthermore, Bronson et al. (2016) did not observed a significant reduction in the tar concentration (from 38.2 to 36.4 g Nm^{-3}) when wet fine biomass was gasified, whereas the reduction was more remarkable, from 26.7 and 16.0 to 16.6 and 11.5 g Nm^{-3}, respectively, for moderate and coarse wet particles. Unlike the previous authors, who supplied extra heat to keep constant the reactor temperature, Kaewluan and Pipatmanomai (2011b) experienced a reduction of 60 ºC in both bed and freeboard temperatures when increasing the moisture content from 9.5 to 18.1 wt%, which led to higher tar concentrations. As for the evolution of tar composition with increasing biomass moisture content, no clear trend may be deduced for the results shown by Bronson et al. (2016) and Paasen and Kiel (2004).

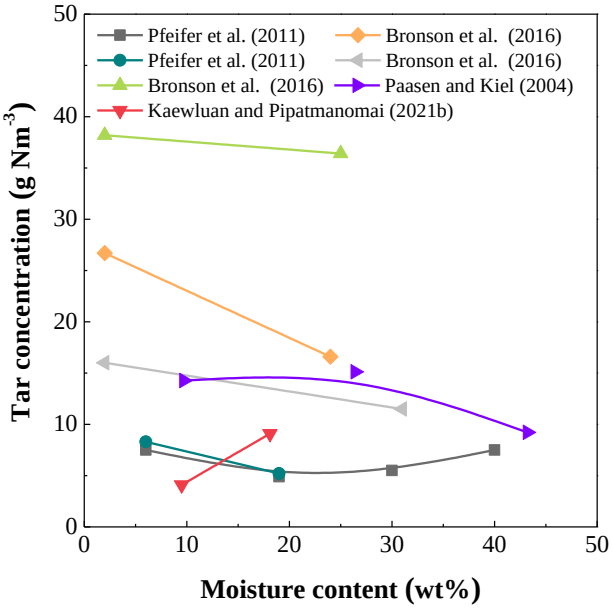

Figure 1.18. Influence of the biomass moisture content on tar concentration (Paasen and Kiel, 2004; Kaewluan and Pipatmanomai, 2011b; Pfeifer et al., 2011; Bronson et al., 2016).

1.4.2.3. Particle size

Biomass particle size is closey related to the limitations of the initial steps in the gasification process, such as the heating of the particle, pyrolysis and diffusion of gaseous products inside the biomass particle, and therefore to process efficiency. Since smaller biomass particle sizes have larger surface area per mass unit, which means higher heat and mass transfer rates between phases, it can be foreseen that biomass size will enhance the gasification performance (Parthasarathy and Narayanan, 2014). However, reducing biomass particle size below 1 mm increases exponentially energy consumption, which corresponds to around 10% of the output energy obtained in the gasification process (Kaushal and Tyagi, 2012; Moiceanu et al., 2019; Warguła et al., 2022). Therefore, it is essential to develop a versatile gasification technology that may

handle large biomass particles without compromising heat and mass transfer phenomena (Arregi et al., 2018).

Although the effect of biomass particle size has only been studied by few researchers using a variety of reactors, different trends and impact levels could be observed on tar concentration. On the one hand, Lv et al. (2004), Luo et al. (2009), Hernandez et al. (2010) and Tian et al. (2018) have reported that particle size reduction improved the gasification performance by increasing gas production, and at the same time tar amount was reduced. On the other hand, other authors (Li et al., 2004; Jand and Foscolo, 2005; Rapagnà and di Celso, 2008; Erkiaga et al., 2014) stated that influence of particle size in tar removal is negligible. Thus, Erkiaga et al. (2014) studied the effect of particle size on biomass steam gasification using 0.3-1 mm (fine), 1-2 mm (medium) and 2-4 mm (coarse) sawdust particles in a conical spouted bed reactor, and concluded that particle size played a minor role at 850 ºC because heat transfer rates in the bed were so high that the limitations of the physical steps were minimized. Thus, tar concentration increased only slightly as biomass particle size was increased, from around 243 g Nm^{-3} for fine and medium sawdust to 263 g Nm^{-3} for coarse sawdust. Regarding the influence of biomass particle size on tar composition, the same authors observed almost the same composition for all the biomass fractions (20-25 wt% for heterocycles, 5-8 wt% for light aromatics, 58-62 wt% for light PAHs and 10-12 wt% for heavy PAHs) concluding that particle size has no influence on the subsequent tar cracking process. Anyway, particle size could play a significant role when other technologies are used, probably due to their lower heat and mass transfer rates.

Moreover, some other researchers (Van Der Drift and Van Doorn, 2008; Wilk and Hofbauer, 2013; Bronson et al., 2016) concluded fine particles could have a negative impact on gasification performance as they yielded a gaseous product with the highest tar loading. According to these authors, the presence of a greater amount of tar when fine biomass particles were fed could be partially ascribed to their entrainment. A fraction of the biomass particles was entrained from the bed just after feeding because their terminal velocity was lower than the operating velocity. As the volatiles are

mostly released in the freeboard of the gasifier, they are less likely to be reformed, and tar formation is therefore enhanced. In relation to the tar composition, Bronson et al. (2016) gasified three different size forestry residues (<3.17 mm, 3.17-6.35 mm and 6.35-19.05 mm) in an air-blown fluidized bed and they only observed differences in tar composition for the gravimetric tars.

1.4.3. Primary catalysts

The use of catalysts also has a positive impact on reducing the amount of tar generated in the biomass gasification, since they decrease the heat and mass transfer resistances through the particles providing an alternative lower-energy pathway for reaction. The selection of a suitable catalyst with reforming and cracking activity could deplete the formation of tar compounds and precursors (Sikarwar et al., 2016). These catalysts may be used as primary catalysts directly in the gasifier, or as secondary catalysts in downstream catalytic processes. Thus, the use of in situ primary catalysts is a promising method to reduce the tar concentration in comparison with the use of a more expensive secondary catalytic cracking reactor downstream (Devi et al., 2003; Narnaware and Panwar, 2021; Ruoppolo et al., 2021). A large number of materials with significant activity for tar cracking and reforming have been used as primary catalysts. In the following subsections, the role different primary catalysts have in tar reduction will be reviewed. Accordingly, these catalysts have been divided into three main groups: natural catalysts, metal catalysts and others.

1.4.3.1. Natural catalysts

A wide variety of natural catalysts have been thoroughly researched as primary catalysts, with olivine, dolomite and limestone having received much attention, due mainly to their low cost, abundance and moderate activity. However, other minerals have also been used as primary catalysts, such as magnesite (Siedlecki et al., 2009; Tuomi et al., 2015; Serrano et al., 2016; Di Marcello et al., 2017), ilmenite (Larsson et al., 2014; Berdugo Vilches et al., 2016; Pushp et al., 2018; Pio et al., 2020), limonite

(Hurley et al., 2012; Niu et al., 2017) and feldspar (Fürsatz et al., 2021; Pissot et al., 2021).

Dolomite is a calcium and magnesium carbonate mineral, ideally $CaMg(CO_3)_2$, olivine is a magnesium and iron silicate represented by the general formula $(Mg, Fe)_2SiO_4$ and limestone is a carbonate sedimentary rock, mostly composed of calcite and aragonite minerals ($CaCO_3$). All of them may also contain several metal trace elements. The chemical composition of these natural catalysts varies from source to source, as well as their surface areas, pore sizes and their distribution. Moreover, their catalytic activity can be improved by calcining at temperatures above 900 ºC, as decarbonate (only for dolomite and limestone) and the oxides migrate to the surface (Sutton et al., 2001; Shen and Yoshikawa, 2013; Guan et al., 2016; Ramadhani et al., 2020; Narnaware and Panwar, 2021). Thus, the catalytic activity of these natural catalysts in the biomass gasification seems to be related to CaO-MgO solution in the dolomite, MgO and Fe_2O_3 phases in the olivine and CaO in the limestone. Regarding their performance, olivine has an outstanding mechanical resistance, comparable to that of sand, whereas both dolomite and limestone are so fragile that they undergone severe attrition when used in fluidized bed reactors. Consequently, they produced a large amount of fine particles, which leads to unstable operation. However, the activity of dolomite is reported to overcome that of olivine (Devi et al., 2005a; Koppatz et al., 2011; Kook et al., 2016).

Typically, industrial-size plants use olivine as bed material, as calcium-rich layers on the surface of the particles appear after days of operation (Kuba et al., 2017). These layers emerge from the interaction of the bed material particles with the woody biomass ash, which improve the catalytic activity of the olivine, and therefore enhance tar reduction (Mauerhofer et al., 2018). Figure 1.19 compares the tar concentration results obtained by several authors when using diverse natural catalysts as primary catalysts in the biomass air/steam gasification. As shown, the results acquired with inert sand have been taken as a reference (associated with the thermal catalytic effect). In order to shed light on the efficiency of these catalysts for removing tar, Figure 1.19a shows the role of olivine and activated olivine, Figure 1.19b the performance of olivine

and dolomite and Figure 1.19c the comparison between dolomite and magnesite/MgO and limestone/CaO.

As observed in Figure 1.19a, the use of olivine and activated olivine as in-bed catalysts improved the results obtained with the silica sand. Christodoulou et al. (2014) and Meng et al. (2018b) obtained very similar tar concentrations for both sand and olivine in the biomass air gasification carried out in a circulating fluidized bed, accounting 51.5 and 71.7 % of tar reduction with olivine. In the same line, Koppatz et al. (2011) reported a bit higher tar values and a lower tar removal capacity of olivine in a dual fluidized bed reactor at 850 ºC, from 10.8 to 7.7 g Nm^{-3} (tar reduction of 30.5 %). However, Berdugo-Vilches et al. (2016) report much higher tar contents in their experiments conducted at 800 ºC, although the introduction of olivine as primary catalysts significantly reduced tar concentration by approximately 18 %. The differences observed in the capacity of olivine for tar removal might be related to the iron species present in the olivine surface (Rauch et al., 2004; Kuhn et al., 2008a). Regarding the use of activated olivine, a noticeable tar reduction was reported by Kirnbauer et al. (2012) with an used olivine (rich in Ca) and Berdugo-vilches et al. (2016) with a K-loaded olivine, from 20.6 and 46 g Nm^{-3} to 4.6 and 25 g Nm^{-3}, respectively. Nevertheless, Fürsatz et al. (2021) did not observed much difference in their runs with used olivine (with a non-negligible content of heavy metals), as tar concentration only decreased by approximately 10 %, from 20.9 to 18.8 g Nm^{-3}.

Figure 1.19b confirms that the dolomite is more catalytically active for tar reduction than olivine. Rapagnà et al. (2000) compared the use of sand, olivine and dolomite at 770 ºC in a fluidized bed reactor and reported a drastic tar reduction from 43 g Nm^{-3} with sand to 2.4 g Nm^{-3} with olivine and 0.6 g Nm^{-3} with dolomite. Other authors also observed that dolomite performance overcomes that of olivine, with the tar content being reduced from 13.2 to 11.4 g Nm^{-3} (Miccio et al., 2009), 2.1 to 1.0 g Nm^{-3} (De Andrés et al., 2011a) and 9.1 to 7.2 g Nm^{-3} (Ma et al., 2019) in a fluidized bed reactor.

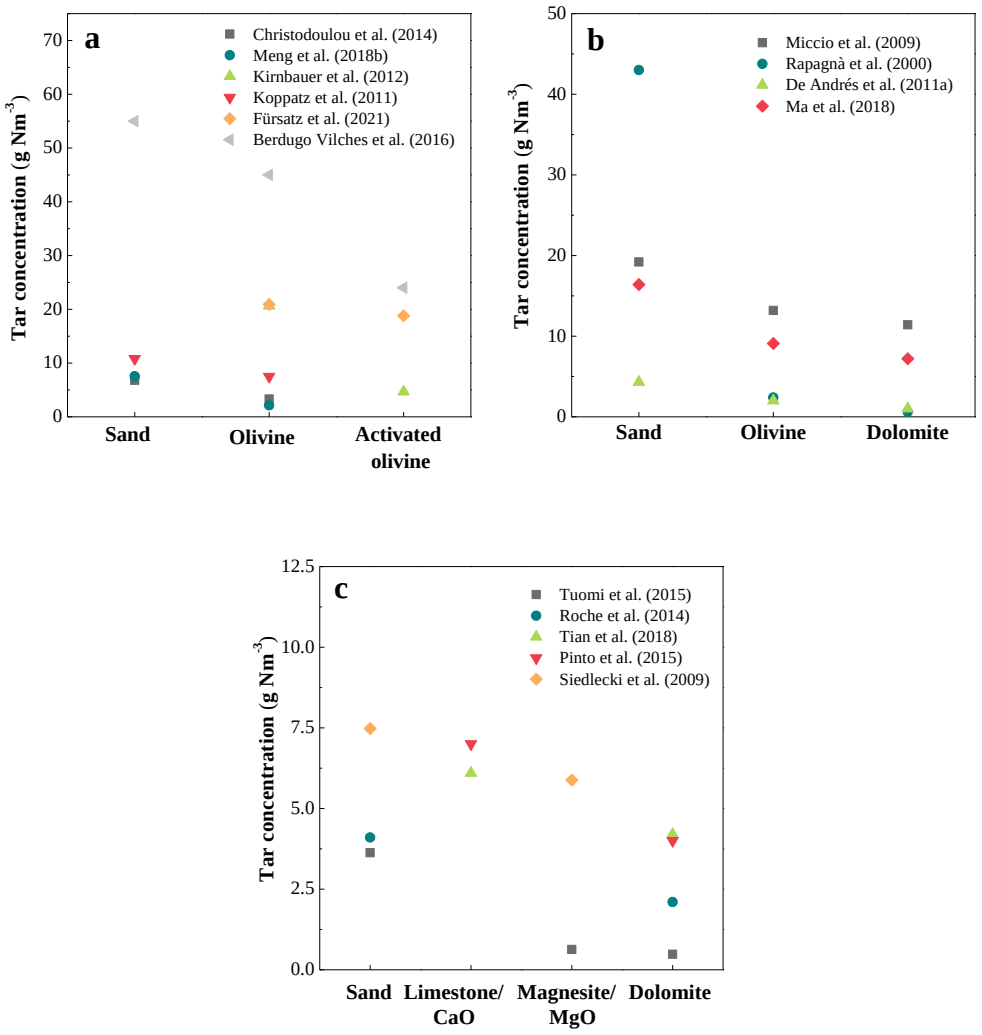

Figure 1.19. The influence of different natural catalysts on tar concentration. Natural catalysts: (a) sand, olivine and activated olivine, (b) sand, olivine and dolomite and (c) sand, dolomite, magnesite/MgO and limestone/CaO. (Rapagnà et al., 2000; Miccio et al., 2009; Siedlecki et al., 2009; De Andrés et al., 2011a; Koppatz et al., 2011; Kirnbauer et al., 2012; Christodoulou et al., 2014; Roche et al., 2014; Pinto et al., 2015; Tuomi et al., 2015; Berdugo Vilches et al., 2016; Meng et al., 2018b; Tian et al., 2018; Ma et al., 2019; Fürsatz et al., 2021).

Figure 1.19c aims to determine the effect of individual dolomite components, i.e., MgO and CaO, on tar concentration. As observed, better results were obtained with dolomite in comparison with magnesite/MgO or limestone/CaO. These three natural catalysts improved the results obtained with the inert sand. Tuomi et al. (2015) tested the performance of MgO and dolomite in a fixed bed reactor at 850 ºC and obtained a lower amount of tar when using dolomite, 0.48 g Nm^{-3}, than rather than MgO, 0.63 g Nm^{-3} (tar concentration was of 3.63 g Nm^{-3} with sand). Similarly, Siedlecki et al. (2009) reported that magnesite reduced tar concentration by 21 % compared to sand. Furthermore, Pinto et al. (2015) and Tian et al. (2018) analyzed the effectiveness of the in-bed use of limestone and dolomite in air/steam gasification carried out in a fluidized bed and reported that tar concentration decreased from 6.1 and 7 g Nm^{-3} to 4.2 and 4.0 g Nm^{-3} when a dolomite bed is used instead of limestone.

The use of in situ primary catalysts not only affects the tar content, but also influences its composition. Independent of the natural primary catalyst used, literature studies (Pfeifer et al., 2004; Miccio et al., 2009; Serrano et al., 2016) show that light PAHs were the main tar lump, among which naphthalene, acenaphthylene, fluorene, phenanthrene and indene are noteworthy. Moreover, heavy PAH still remained, with fluoranthene and pyrene being the most abundant compounds. To sum up, primary natural catalysts lead to a tar fraction made up of highly stable compounds.

The in situ use of natural catalysts is an attractive method to remove tar, although the tar content in the product gas may not meet the requirements to use it in downstream applications. However, they can act as a guard catalyst and avoid the rapid deactivation of an expensive secondary catalyst by carbon deposits.

1.4.3.2. Metal catalysts

Supported metal catalysts have been extensively used in the steam reforming of biomass tar model compounds, especially transition metal catalysts (Sutton et al., 2001; Shen and Yoshikawa, 2013; Shahbaz et al., 2017). Amongst them, nickel based

catalysts are the most used ones in both research and industrial processes. In fact, there are a lot of commercially available Ni catalysts and they are supported on a wide variety of materials, such as Al_2O_3, ZrO_2, TiO_2, CeO_2, MgO and even olivine and dolomite natural ores (Artetxe et al., 2017; Wang et al., 2017; Xiao et al., 2017b; Cao et al., 2018; Savuto et al., 2018; Tan et al., 2020). These catalysts not only have a high catalytic activity for tar removal, but they are also active for methane reforming and WGS reactions, which leads to an increase in the gas and hydrogen yields (Sutton et al., 2001; Ren et al., 2019a). However, catalysts containing nickel are very toxic and undergo a rapid deactivation caused by carbon deposits on the catalyst surface (Świerczyński et al., 2007; Kuhn et al., 2008b; Guan et al., 2016; Sun et al., 2019). Thus, Fe based catalysts have recently attracted an increasing attention for tar reduction, as iron is cheaper and less toxic than nickel. The activity of iron based catalysts is related to the tar cracking and reforming capacity of metallic iron and WGS reaction enhancement capacity of magnetite (Fe_3O_4) (Nordgreen et al., 2006; Virginie et al., 2010a, 2012; Rapagnà et al., 2011; Quan et al., 2017).

The literature dealing with in situ metal catalysts for the biomass air and/or steam gasification is scarce, with Al_2O_3 and olivine supports being the most researched. Miccio et al. (2009, 2016) impregnated Fe and Ni with Al_2O_3 and tested in the air/steam gasification of spruce wood pellets (ER=0.17 and S/B=0.66) in a bubbling fluidized bed. They reported similar tar concentrations for both catalysts, i.e., 8.4 g Nm^{-3} for Fe/Al_2O_3 and 8 g Nm^{-3} for Ni/Al_2O_3. Besides, Assadullah et al. (2004) tested the performance of $Rh/CeO_2/SiO_2$ catalyst and a commercial steam reforming catalyst G-91 (14 wt%Ni) in the air gasification of cedar wood, and obtained a negligible tar amount when $Rh/CeO_2/SiO_2$ catalyst was used, whereas tar concentration was of about 30 g Nm^{-3} when G-91 catalyst was used. Dolomite was also used as catalyst support by Chaiprasert and Vitidsant (2009) and tested in coconut shell steam gasification at 800 ºC in a fluidized bed reactor once it was impregnated with Ni and small amounts of Pt, Co and Fe promoters.

Figure 1.20 shows the influence of iron and nickel based in situ catalysts on tar concentration and compares with that of pure olivine. As observed, metal loading to olivine reduces the tar amount in the process. Thus, Virginie et al. (2012) studied the performance of 10 wt%Fe/olivine catalyst in the biomass steam gasification at 850 ºC in a dual fluidized bed and reported that tar reduction was more significant in the presence of Fe/olivine in the bed than with olivine (5.1 and 2.6 g Nm^{-3} of tar content for olivine and Fe/olivine respectively). Moreover, Barisano et al. (2016) used the same catalysts in the biomass steam/O_2 gasification at 890 ºC in an internally circulating bubbling fluidized bed and noted the total content was reduced by 38 % (from 10.1 to 6.2 g Nm^{-3}).

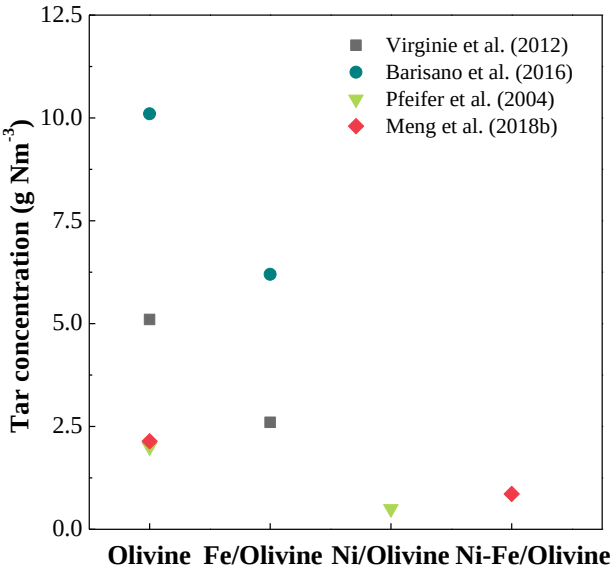

Figure 1.20. The influence of olivine based metal catalysts on tar concentration. (Pfeifer et al., 2004; Virginie et al., 2012; Barisano et al., 2016; Meng et al., 2018b).

Regarding Ni incorporation, Pfeifer et al. (2004) added 20 % of 5wt%Ni/olivine catalyst to a bed of olivine to study tar removal activity in a 100 kWth dual fluidized bed reactor, and obtained a tar concentration as low as of 0.5 g Nm^{-3}. Meng et al.

(2018b) reported a slightly higher value of tar concentration (0.86 g Nm^{-3}) when Ni-Fe/olivine catalysts was used for pine sawdust air gasification carried out in a circulating fluidized bed. The literature comparison in Figure 1.20 points out that the Ni/olivine catalyst is the most effective in terms of tar removal.

With respect to tar composition, Barisano et al. (2012) reported that naphthalene was the major tar compound when using Fe/olivine catalyst, with its amount being still very high. Furthermore, they observed a significant removal of phenol, methyl phenol, 1-methyl phenol, 1-methyl naphthalene, dibenzofuran, 1-H phenalene, 2-phenyl naphthalene and pyrene. Thus, they concluded the more stable tar compounds were difficult to remove even with the Fe/olivine catalyst.

1.4.3.3. Other types of catalysts

A big effort has been made in the biomass gasification field to search low cost in situ catalysts with high catalytic activity for tar abatement. Thus, apart from natural catalysts, other materials, such as γ-alumina, FCC spent catalyst or cement have also been tested. The γ-alumina and the FCC spent catalyst are of acid character, whereas cement is basic. Although γ-alumina has been widely used as catalysts support, it has also been employed in biomass gasification. Thus, Kuramoto et al. (2009) and Matsuoka et al. (2008) verified the effectiveness of γ-alumina for removing tar and yielding hydrogen. Concerning the use of the FCC spent catalyst, it is a highly interesting application, since it allows prolonging the lifetime of a refinery waste material (Abu El-Rub et al., 2004; Ferella et al., 2016).

Figure 1.21 compares the research work carried out by various authors wherein the above materials were employed as primary catalysts. However, the comparison of the results is not straightforward due to different operating conditions and technologies used, which led to unclear trends. In any case, it is noteworthy that the use of these in-bed catalysts improved tar removal over that corresponding to the inert sand. In addition, this figure also shows that alumina has been the most tested material,

probably due to its suitable mechanical properties and cracking activity (Nam et al., 2020).

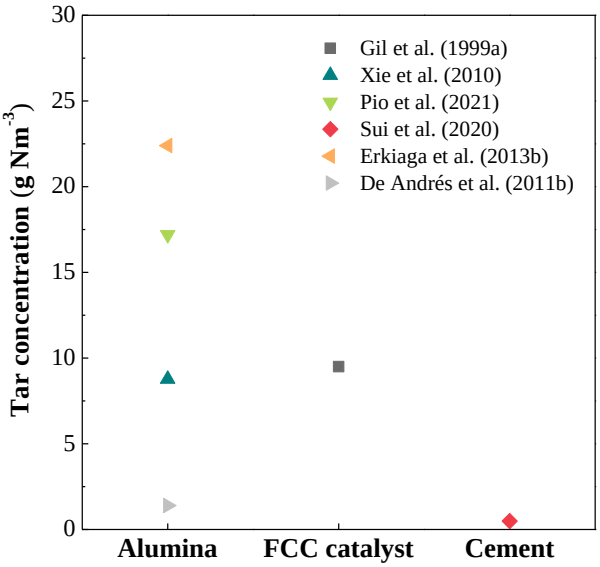

Figure 1.21. The influence of γ-alumina, FCC spent catalyst and cement primary catalysts on tar concentration (Gil et al., 1999a; Xie et al., 2010; De Andrés et al., 2011b; Erkiaga et al., 2013b; Sui et al., 2020; Pio et al., 2021).

1.4.4. Modifications in reactors and innovative designs

Although the use of in-bed catalysts and the optimization of the operating conditions (temperature, ER and S/B) allows improving the gasification process performance, they may not be sufficient to attain the gas purity required for cold gas applications (Table 1.4). In this context, further measures involving redesign of the gasifier or development of innovative designs are needed to obtain a clean product gas (Gómez-Barea et al., 2013b).

According to Bridgwater (1995), there are three key strategies, which may improve the reactor performance in terms of tar reduction and obtain high process efficiencies. The first one is the injection of some air or pure O_2 along the reactor to promote the partial oxidation of the tars by creating various thermal levels in the gasifier. The next one is the use of heated bed materials to favour the tar cracking. The last one is to increase the residence time of the tars inside the reactor, as most volatiles are directly carried out by the gas flow without contacting the bed material. Accordingly, several attempts have been proposed in the literature to decrease tar concentration, such as the injection of secondary air/O_2, changes in reactor design and feeding mode, use of filter candles in the freeboard and staged gasification (drastic zone division of pyrolysis and reduction stages). These strategies will be discussed in the following subsections.

1.4.4.1. Secondary air/O_2 injection

Air staging has been widely applied in the coal combustion field, but not much in biomass or coal gasification. Although the main target for both processes is different (reduce the emissions of sulphur and nitrogen compounds in combustion and mainly tar elimination in gasification), both aim to promote the partial oxidation of the undesirable compounds (Cao et al., 2006; Fan et al., 2010; Robinson et al., 2016; Kang et al., 2017; Chai et al., 2020). In the gasification process, the staging injection of air/O_2 can significantly raise the temperature in the upper section of the reactor, and consequently improve the gasification performance to a great extent due to the oxidative atmosphere. In that way, a more uniform temperature profile is achieved in the gasifier. However, raising the temperature through secondary air injection in the freeboard may have a negative impact on the gas heating value (Narváez et al., 1996; Pan et al., 1999; Campoy et al., 2010; Thamavithya et al., 2012; Wang et al., 2019).

Thamavithya et al. (2012) placed the secondary air supply port 1100 mm above the primary air distributor in a spout-fluid bed and used secondary air to primary air ratios of 10, 20 and 30 % by keeping primary air flow rate constant. The temperature of the partial oxidation zone increased from 578 ºC with no secondary air to 742 ºC with 30

% secondary air supply , which caused tar content to reduce from 5.63 to 1.53 g Nm^3. Likewise, Campoy et al.(2010) investigated the effect of some primary measures on the performance of an air-blown fluidized bed gasifier and reported that the injection of secondary air (keeping SR constant and fixing the secondary to total air ratio at 11 %) reduced the gravimetric tar and the water-soluble tar compounds to 20 and 30 %, respectively. However, the total tar concentration was still high (20-23 g Nm^3) and the fraction of stable aromatic tar compounds in the gas increased significantly. Recently, Tsekos et al. (2021) investigated the effect of secondary air injection in a novel indirectly heated bubbling fluidized bed and achieved a 91 % reduction in the total tar content (from 45 to 4 g Nm^3) when 8 kg h^{-1} of secondary air was injected. Regarding tar composition, naphthalene, acenaphthylene, anthracene and toluene were the most abundant tar species, with naphthalene being the prevailing one by far. Even so, the secondary air injection entailed more than 87 % reduction in naphthalene concentration. Wang et al. (2019) conducted a more extensive research on the effect of the injection point and direction for coal gasification in a circulating fluidized bed. They concluded that higher injecting points led to a more remarkable improvement in the gasification performance and the tangential injection was more effective than the radical injection because of the preferable contact between gasifying agents and char particles.

Although secondary air/O_2 injection reduces tar concentration, in most cases it is not enough for the gas to meet the requirements in downstream applications. Thus, many research groups have decided to take some other complementary measures to reduce further tar concentration.

1.4.4.2. Candle filters in the freeboard

Under UNIFHY (UNIQUE gasifier for hydrogen production) European Project framework, joint R&D efforts by several research organizations and private companies throughout Europe managed to integrate biomass gasification and hot syngas cleaning and conditioning into one reactor vessel (Heidenreich and Foscolo, 2015). With this in

mind, they placed a catalytic hot gas filter (a commercially available ceramic candle filter) in the freeboard of a fluidized bed (Figure 1.22). The first record of inserting a catalytic filter within the biomass gasifier and testing in real process conditions was published by Rapagnà et al. (2009), although several previous studies dealing with hot gas catalytic filtration under simulated biomass gasification can be found in the literature (Engelen et al., 2003; Ma et al., 2005; Heidenreich et al., 2008). The main objectives of placing a filter candle in the freeboard were to improve the thermal efficiency of the whole process, allow tar conversion, remove trace elements and avoid particle entrainment in the gas at the reactor outlet, so delivering high purity syngas (Rapagnà et al., 2009, 2010). Regarding the advantages of this innovative solution, the operating temperature of the catalytic filter candle was closed to the process temperature, which favoured tar reforming reactions towards permanent gases, at the same time as particles and other trace elements, such as ammonia, were eliminated.

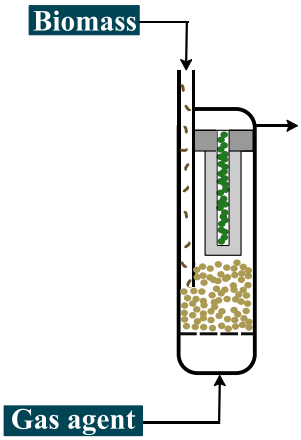

Figure 1.22. Scheme of a catalytic candle filter located in the freeboard of a fluidized bed reactor.

Experimental tests in fluidized bed gasifiers at laboratory and industrial scale using different types of filter candles (catalytic and non-catalytic) demonstrated their efficiency in tar reduction. Almost all their effort was devoted in the development of

adequate filtering material. At the beginning, Rapagnà et al. (2009) tested a commercially available DIA-SCHUMALITH type N filter supported on SiC with outer mullite membrane activated with Ni/MgO-Al_2O_3 catalyst (catalytic filter) or without being activated (non-catalytic filter) in the biomass steam gasification at 830 ºC with an S/B ratio of 1. They reported that the catalytic filter activation reduced tar concentration from 1.9 to 0.7 g Nm^{-3}. Subsequently, Rapagnà et al. (2010) used the previous non-catalytic filter with the hollow-cylindrical space filled with 6 wt%Ni/MgO catalysts and obtained similar tar concentration as with the catalytically active filter (of around 0.7 g Nm^{-3}). They reported that, although the reduction in methane and tar conversion was rather low, the catalytic performance of this filter element remained stable for a total gasification time of 22 h.

Al_2O_3 based grain-sintered candle filters involved a great improvement in the gasification performance. Thus, Rapagnà et al. (2012) compared the non-catalytic option of Al_2O_3 based filter with one in which Ni was integrated and observed a stable catalytic activity over 20 h of continuous steam biomass gasification, achieving an average tar conversion of 93.5 % (0.15 g Nm^{-3} of tar concentration was reported for the Ni impregnated catalytic filter). Moreover, Rapagnà et al. (2018) tested the performance of a new catalytically activated Al_2O_3 based hot gas filter candle, which was improved with an Al_2O_3 outer membrane and with an integrated catalytic ceramic foam. In this candle, a MgO-NiO catalytic layer system was applied on the filter support and a MgO-Al_2O_3-NiO based catalytic layer system was applied on the integrated catalytic ceramic foam. They obtained a product gas with a very low amount of tar (0.057 g Nm^{-3}) and free of dust when 20 % of dolomite was added to the olivine bed.

However, the main technical problem associated with the use of filter candles is related to the difficulty to impregnate the metal active phase directly on the ceramic filters due to their considerable size (the typical length of this filtering device is 1.5 m). Thus, with the aim of making the overall process more feasible in practice, Savuto el al. (2019) followed the strategy by Rapagnà et al. (2010) and proposed to fill the inner

empty space of commercial Al_2O_3 filtering candles with pellets of a steam reforming catalyst available in the market. They studied three different configurations: i) empty candle, ii) candle partially filled with catalyst pellets and iii) candle totally filled with catalyst pellets, and concluded that the runs with the partially filled candle led to the best results in terms of tar elimination (0.3 g Nm^{-3}). Moreover, the Ni catalyst was very stable for approximately 4 h, as no lower performance or degradation was observed for this time.

1.4.4.3. Location of the feeding point

In bench and lab scale plants, the feeding point is usually above the bed or on a middle location in the bed (Berrueco et al., 2014a; Rapagnà et al., 2018; Cao et al., 2021a), whereas in large pilot plants, the feeding point is at the lower part of the bed, more specifically near the gas distributor plate (Koppatz et al., 2011; Berdugo Vilches et al., 2016; Fürsatz et al., 2021; Wang et al., 2022).

According to Corella et al. (1988a), the location of the feeding point depends on the differences in biomass features, bed material and produced char/ash densities. In fact, biomass has a density 2-5 times lower than silica sand and this difference is 10 times or even higher for the char and/or ash formed in the biomass gasification. Therefore, there is a big tendency for biomass, char and ash to flow upward in the bed and segregate at the top. Thus, these authors investigated the effect of the feeding location on tar concentration and reported lower tar yields when biomass was fed at the lower section in the bed than from the top (4.5 vs. 13 wt%) in a bubbling fluidized bed. Thus, when biomass is feed from the top of the reactor, the contact between the fluidizing gas and bed material is very poor and the volatiles directly leave the reactor (low residence time). Consequently, a big amount of undesirable byproducts, such as tars and char, are formed. However, when the material is fed at the lower end of the bed, although a priori it could entail more operational problems than feeding from the top, there is sufficient time for the biomass to interact with the bed material and the gasifying fluid, enabling efficient carbon conversion and less tar formation. This is consistent with the

results by Gómez-Barea et al. (2013b), who stated that feeding the biomass at the bottom increases the residence time for tar conversion, thereby reducing the tar concentration, at the same time as leading to more stable and heavy (aromatic) tar compounds in the gas.

Other researches also selected in-bed feeding as the optimum one (Kern et al., 2013b; Wilk et al., 2013; Wang et al., 2019). Thus, Kern et al. (2013b) studied the influence of the position at which the biomass must be fed into a DFB gasifier. Steam gasification experiments of wood pellets carried out at 850 ºC and S/B=0.6 concluded that much lower tar contents were observed with in-bed feeding than with on-bed feeding, as tar concentration were reduced from 26.5 to 8.7 g Nm^{-3}. Likewise, Wilk et al. (2013) also showed that in-bed feeding was more favorable for wood pellet gasification in a DFB, although they hardly observed differences for the co-gasification of plastic waste and wood pellets. Wang et al. (2019) performed coal gasification runs in a CFB in order to compare on-bed feeding and by loop seal feeding (the feed was injected into the bed), and reported that coal feeding by loop seal was an effective way to improve the gasification performance because the residence time was prolonged by making the coal to circulate through the whole furnace. The same conclusion was drawn by Jaiswal et al. (2020) based on a computational particle fluid dynamics (CPFD) model for a fluidized bed reactor.

1.4.4.4. Multi-staged gasifiers

As explained in Section 1.2.1, the gasification process consists of several overlapped steps, such as heating and drying, pyrolysis, oxidation and gasification itself, making impossible to control and optimize the different steps separately in a conventional gasifier. Multi-stage gasification processes separate and combine the pyrolysis and the gasification steps in a single controlled one. Thus, a better understanding of the complex thermal conversion process, as well as the optimization of the conditions in the entire process, is attained (Han et al., 2018).

The most common strategy is to combine pyrolysis and gasification in a two- or three-stage gasification process, either in one unit or in separate reactor units combined in series. With both reactor configurations, high process efficiencies with high char conversion rates and high purity syngas with low tar concentration are possible. However, the complexity of the process is increased by combining different reactors (Heidenreich and Foscolo, 2015). According to Gómez-Barea et al. (2013b), staged gasification is the only method capable of maximizing process efficiency and minimizing secondary gas treatment (by avoiding complex tar cleaning) with reasonable simplicity and cost.

Several two-stage gasification concepts have been recently developed by separating pyrolysis and gasification zones. Pei et al. (2018) and Niu et al. (2019) developed a novel two-stage gasifier, consisting of a fluidized bed and an entrained flow bed connected in series. The fluidized bed was used in the first stage for converting biomass into raw gas, tar and char at approximately 650–700 °C, while swirl-melting furnace with liquid slagging was provided with temperatures above 1250 °C for tar cracking, char reforming and ash melting in the second stage. Continuous steady operation of the pilot plant demonstrated the feasibility of this two-stage gasification technology, as a significant improvement in fuel gas quality was obtained, i.e., the tar content was reduced from 14.25 to 0.95 g Nm^{-3} with the addition of the second stage in which an ER of 0.19 was used (Niu et al., 2019). As for Zeng et al. (2016) and Wang et al. (2022), they also used a two-stage gasification system, but in this case both opted for using a fluidized bed in the first stage and a riser in the second one. Zeng et al. (2016) reported tar values as low as 0.4 g Nm^{-3} in the air gasification of herb residues, with the temperatures in the pyrolyzer and gasifier being of around 700 and 850 ºC, whereas Wang et al. (2022) obtained higher values (of around 4.35 g Nm^{-3}) in the oxygen-rich air gasification of pine chips.

Gómez-Barea (2013a), Choi et al. (2016) and Pan et al. (2019), among others, implemented three-stage gasification. Usually three-stage gasifiers comprise pyrolysis, reforming and combustion steps separately. However, Choi et al. (2016) developed a

three-stage gasifier (UOS gasifier) consisting of an auger for biomass devolatilization, as well as fluidized and fixed bed reactors placed in series for reforming and cracking, but none of the reactors were used for char combustion. In an experiment they performed by feeding sewage sludge on activated carbon in the fixed bed, in which the temperature in the auger reactor was 710 °C and in the fluidized bed and fixed bed reactors 830 °C, the tar content in the gas stream was 22 mg Nm^{-3} (including N_2 flow). Pan et al. (2019) used a different reactor configuration based on three separated reactors called DTBG (decoupled triple bed gasifier), which consisted of a gas-solid countercurrent and solid-solid concurrent moving bed for pyrolysis, a gas-solid crosscurrent moving bed for the gasification/reforming of the volatiles on a catalyst, and a fast fluidized bed for char and catalyst coke combustion. This reactor configuration system was used in the steam co-gasification of sawdust and bituminous coal, which allowed reducing the tar content from 25.35 to 4.87 g Nm^{-3} when Fe/olivine catalyst was used instead of sand. Gómez-Barea et al. (2013a) also proposed a three-stage gasification (FLETGAS) process based on fluidized bed devolatilization, non-catalytic air/steam reforming of the gas coming from the devolatilizer, and chemical filtering of the gas and gasification of the char generated in the devolatilizer in a moving bed. Moreover, these authors compared their results with those obtained in the one-stage process and observed tar content was reduced from 31 to 0.01 g Nm^{-3} under similar conditions.

1.4.4.5. Modifications in reactor design

This section describes the most innovative modifications and redesigns carried out in DFB and fixed bed gasifiers with the aim of improving the gasification performance, specifically form the perspective of tar removal.

1.4.4.5.1. Changes in DFBs

Researchers from TU Wien (Benedikt et al., 2017; Benedikt et al., 2018; Mauerhofer et al., 2018; Fürsatz et al., 2021) proposed an advanced concept for gasification following the DFB technology. Figure 1.23 compares the classic and advanced designs of their DFB reactor. The classic design (Figure 1.23a), which is typically used at the existing industrial sized plants, consists of a bubbling fluidized bed as gasification reactor and a fast fluidized bed as combustion reactor. Both reactors are connected via two loop seals from their lower and upper parts. The bed material leaving the combustion reactor is separated from the flue gas via a cyclone and then introduced into the gasification reactor again, as it works as heat carrier for the overall endothermic gasification. The produced char is used as fuel and transported to the combustion reactor, where it is burned with air. Additional fuel can be introduced into the combustion reactor to control the gasification temperature and compensate the relatively high heat losses of the experimental pilot plant. In this process, the flue gas stream and the product gas stream are separated, leading to a N_2-free product gas.

In order to improve the gas-solid contact within the gasification reactor, an advanced design was developed (Figure 1.23b). This innovative design is equipped with two gravity separators on top of the reactors. Compared to the use of cyclones, the gas and particle velocities are lower, which leads to smooth separation of the bed material from the gas streams, allowing the use of relatively low abrasion resistance materials, such as calcite. Therefore, calcite can also be used without profuse continuous replacement of the bed material. Besides these developments regarding separators, the key innovation is related to the design of the gasification reactor. The gasification reactor consists of two main parts, as follows: the lower part with the biomass feeding point, which works as a bubbling fluidized bed, and the upper part operating as a countercurrent column with turbulent fluidized bed zones. The countercurrent column results from the hot bed material, which is separated from the flue gas stream and introduced into this column. Furthermore, the column is equipped with constrictions, which lead to a distribution of the bed material hold-up over the height of the column.

As a result, the interaction of bed material and the product gas in the upper part of the gasification reactor is increased significantly. To sum up, this innovative design allows using soft materials due to the gentle separation units and, furthermore, increasing the gas-solid contact and residence time of the product gas through geometrical modifications in the gasification reactor.

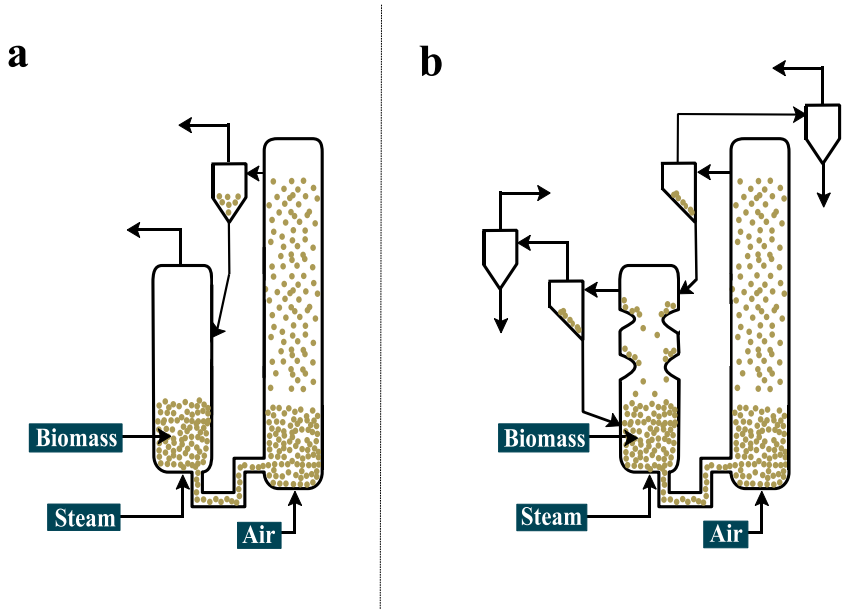

Figure 1.23. Traditional (a) and advanced (b) designs of the 100 kWth BFB pilot plant at TU Wien.

Benedikt et al. (2017) conducted gasification tests with wood and calcite as bed material in their novel plant and compared the results with those corresponding to a conventional plant using olivine under similar conditions. The results showed that the new configuration led to a product gas with remarkably lower tar content (1.87 g Nm^{-3} rather than 8.65 g Nm^{-3}), i.e., a decrease of 78 %. The higher tar conversion in the new configuration was explained by the coupling of two effects, as are: (i) The more active bed material (calcium oxide) enhanced steam reforming reactions and (ii) the higher temperatures in the countercurrent column for cracking reactions. Moreover, no heterocyclic tar components were detected in the runs with calcite and the percentage

of class 5 tar was significantly lower in the runs conducted in the improved pilot plant. Since the development of this innovative design, great effort and work have been devoted to test the performance of the plant using a great variety of lignocellulosic materials (softwood, hazelnut sheels, bark, sugarcane bagasse, rice husk, straw and so on), residual biogenic fuels (chicken manure), bed materials (limestone, feldspar, quartz and mixtures) and different operating conditions, as reviewed by Schmid et al., (2021a).

More recently, Di Carlo et al. (2019) proposed a cold model of a novel pilot scale dual bubbling fluidized bed gasifier-HBF2.0 (100 kWth of biomass input). It consists of two concentric cylindrical fluidized beds inside a single vessel; the external is for gasification and the internal for combustion. The two fluidized beds are interconnected with a baffle plate, which contains an opening at the base and another one at the bed surface, to allow bed material circulation and operation at different temperatures and superficial velocities. Heat is exchanged between the combustor and the gasifier by the circulation of the bed material: sand and residual char in the slow bed (gasifier) flow into the fast bed through the lower orifice and hot sand is recycled back into the slow bed through the upper orifice. The main novelties of this design are i) the system is compact, and thus suitable for small scale applications, with both reaction chambers (gasification and combustion) being integrated in one cylindrical body; ii) the heat exchange between the two chambers occurs by the circulation of the bed material and also by conduction/convection through the wall of the internal cylinder; iii) the higher temperature chamber (combustor), operating at 900-950 ºC, is thermally insulated; this reduces the drawback of thermal losses in small scale applications; iv) the longer residence time in the combustor (bubbling bed) allows complete burning of char particles.

Kuba et al. (2018) implemented two measures on-site to optimize the Senden DFB power plant. The first measure was based on bed particle activation through ash layer formation. According to Kuba et al. (2017) and Fürsatz et al. (2021), layered olivine particles (used) have higher catalytic activity compared to those of fresh olivine, as

they have Ca-rich surfaces active for tar reduction. Thus, a new line for recycling layered olivine and a hopper were installed. This recycling line connects the combustion reactor with the hopper, where the used olivine is discharged and stored, which is used to compensate the bed material losses. Regarding the second measure, separately regulated additional fluidization nozzles were introduced into the inclined wall of the gasifier to improve the mixing of the biomass and catalytically active bed material, and so avoid segregation, which led to further decrease in the tar content in the product gas. After implementing these two modifications, these authors reported that the layered olivine reduced tar concentration from 17.7 (before optimization) to 14.2 g Nm^{-3}, and even a more significant reduction when nozzles were installed (to 10.3 g Nm^{-3}). Two operation points for optimizing long-term running were suggested by Kuba and Hofbauer (2018).

1.4.4.5.2. Changes in fixed beds

The installation of additional nozzles is a strategy that has also been used in downdraft gasifiers to avoid the bypass of volatiles through relatively cold zones, and consequently improve gasification performance (Susanto and Beenackers, 1996; Machin et al., 2015; Rahman et al., 2021). According to Susanto and Beenackers (1996), multiple air nozzles or ring type oxidation zones are only valid up to a few hundred kg h^{-1} capacity at best. With the aim of scaling up a concurrent gasifier, these authors installed a separate combustion chamber within the reactor and developed a downdraft moving bed gasifier with internal recycle. By establishing a recycle gas flow countercurrently with the solids feed, the heat transfer to the bed above the oxidation zone is greatly improved, which resulted in a more complete pyrolysis of the solids when entering the reduction zone. Thus, the recycle system greatly reduced the tar content in the gas produced to values below 0.1 g Nm^{-3}. They also observed that tar content decreased by increasing the recycle ratio (recycle gas to gasifying air) to 0.6, but no further tar reduction was observed for higher ratios. Furthermore, Machin et al. (2015) changed the entry angle of the gasification agent to the combustion chamber from 90 to 72º, creating a swirl flow. Thus, this fluid dynamic behaviour allowed

increasing the mixing of the gasifying agent with the pyrolysis gases. Consequently, the temperature inside the combustion chamber was homogenized, thus diminishing the formation of cool areas between the nozzles. In addition, this modification increased the residence time of the gas inside the combustion chamber, thereby increasing the thermal cracking of the tar in this zone and decreasing the tar concentration in the producer gas. The tar in this new configuration did not overcome 10 mg Nm^{-3}. More recently, Rahman et al. (2020, 2021) gathered the modifications of the previous two authors and proposed a low-tar biomass (LTB) gasifier. This reactor is provided with a separate combustor inside the reactor in the partial oxidation zone and the gasifying agent is fed into the combustor from the top of the reactor by three nozzles inclined 120º and oriented towards the center of the combustor. The use of wood chips with a moisture content of 11-34 wt% resulted in a very low tar content of 10.6 mg Nm^{-3}.

Kurkela et al. (2021) introduced a catalytic modification in their reactor design. The gasifier is a combination of the updraft gasification and a second catalytic step integrated within the upper part of gasifier, which is VTT's third fixed-bed gasifier design called staged fixed-bed gasifier (SXB). The primary gasification stage takes place in a traditional counter-current fixed bed reactor, whereas tar reforming and cracking reactions are catalytically enhanced in the secondary stage. A steel plate separates both stages, which has four holes. These holes are equipped with Venturi-type inlet distributors, which allow feeding a small amount of air into their axes in order to avoid the formation of tar deposits that may gradually block the distributor holes. The secondary stage made up of horizontal baskets filled with catalyst and assembled at four vertical levels, each having four catalyst wings, resulting in a total amount of 16 catalyst wings. The raw gas from the lower updraft bed flows through the holes of the division plate into the secondary gasification zone and joins the secondary gasification gases (to induce partial combustion reactions and increase temperature), which are introduced through a catalytic distributor system. The scheme of this reactor is shown in Figure 1.24.

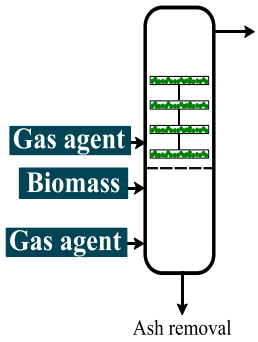

Figure 1.24. Scheme of VTT's staged fixed-bed gasifier.

2

EXPERIMENTAL

2.1. MATERIALS

2.1.1. Feed

The biomass used was forest pinewood waste from *pinus insignus*, which covers most of the Cantabrian watershed (150000 ha, accounting for 40 % of the total wooded forest area) and involves most of the biomass production in the Basque Country (almost 90 % of the annual pruning). This raw material was not treated with any product and its main features are summarized in Table 2.1.

Table 2.2. Characterization of the biomass used.

Ultimate analysis (wt%)	
Carbon	49.33
Hydrogen	6.06
Nitrogen	0.04
Oxygen	44.57
Proximate analysis (wt%)	
Volatile matter	73.4
Fixed carbon	16.7
Ash	0.5
Moisture	9.4
HHV (MJ kg^{-1})	**19.8**

In order to ease continuous feeding, it was crushed, ground and sieved to a particle size in the 1-2 mm range and then airdried to a moisture content below 10 wt%. The ultimate analysis was carried out in a *LECO CHNS-932* and *VTF-900* elemental

analyzers. The ultra-microbalance *SARTORIUS M2P* (precision ± 0.001 mg) was connected on line to a computer for processing the data provided by the analyzer. As shown in Table 2.1, the amount of N in the sawdust is almost negligible, and therefore the empirical formula is as follows: $CH_{1.47}O_{0.67}$.

Moreover, the proximate analysis was conducted in a *TA Instruments TGA Q5000IR* thermogravimetric analyzer. Firstly, the sample was subjected to an isothermal period at 105 ºC for 80 min under inert atmosphere to determine the moisture content by weight loss. Subsequently, the sample was heated to 800 ºC following a 15 ºC min^{-1} ramp, and kept at this temperature for 30 min. This weight loss corresponds to the volatile matter. Finally, the inert gas was substituted by air and both flow rate and temperature were maintained for 5 min, which caused the combustion of the fixed carbon. The remaining solid matter was related to the ash content, which was calculated by difference. Lastly, the higher heating value (HHV) was measured in a *Parr 1356* isoperibolic bomb calorimeter.

2.1.2. Primary catalysts

Several primary catalysts were tested, i.e., two of them of basic character (olivine and dolomite) and active for reforming biomass-derived oxygenates and the other two of acid character (FCC spent catalyst and γ-alumina) and active for cracking. Furthermore, silica sand and Fe/olivine catalyst were also checked as in-bed materials. Minerals Sibelco supplied the olivine, dolomite and silica sand, Petronor refinery (Somorrostro, Viscay, Spain) the FCC spent catalyst and Alfa Aesar the γ-alumina. All materials were sieved to obtain the desire particle size. Prior to use as bed material, the dolomite was calcined at 900 ºC for 4 h in a muffle oven, as these conditions ensure the decomposition of calcium and magnesium carbonates. The characterization of the catalysts used is shown in Table 2.2 except for the Fe/olivine catalyst. The detailed characterization of the 5 wt%Fe/olivine catalysts is explained in Section 7.1. The physical properties of the primary catalyst (specific surface area, pore volume and average pore size), chemical composition and acidity were determined by N_2

adsorption–desorption, X-ray fluorescence (XRF) spectrometry and NH_3 temperature programmed desorption (TPD) techniques respectively. These techniques are thoroughly explained in Section 2.3.

Table 2.2. Properties of the primary catalysts.

	Sand	**Olivine**	**FCC catalyst**	**γ-alumina**	**Calcined dolomite**
Physical properties					
S_{BET} ($m^2\ g^{-1}$)	-	0.18	143	100	17.42
V_{pore} ($cm^3\ g^{-1}$)	-	-	0.04	0.42	0.05
d_{pore} (Å)	-	-	101	167	113
d_p (µm)	90-150	90-150	90-150	250-400	150-250
$\rho_{apparent}$ ($kg\ m^{-3}$)	2600	3300	1246	1666	1275
Chemical properties					
MgO (wt%)	-	48.79	-	-	43.61
SiO_2 (wt%)	98.0	43.18	-	0.02	0.12
Fe_2O_3 (wt%)	-	7.68	0.19*	-	0.02
CaO (wt%)	-	0.12	-	-	56.07
Al_2O_3 (wt%)	-	0.04	53.79	99.98	0.15
Na_2O (wt%)	-	0.06	0.29*	-	0.01
TiO_2 (wt%)	-	0.02	-	-	0.02
MnO (wt%)	-	0.11	-	-	-
Re_2O_3 (wt%)	-	-	2.50	-	-
P_2O_5 (wt%)	-	-	0.62	-	-
Cu (ppm)	-	-	24	-	-
Ni (ppm)	-	-	741	-	-
V (ppm)	-	-	3335	-	-
Acidity					
A_T ($\mu mol_{NH3}\ g_{cat}^{-1}$)	-	-	124	80	-

2.2. CATALYST SYNTHESIS

The methodology for preparing the Fe/olivine catalyst is described below. Thus, the catalyst was synthesized by wet impregnation method after the proper conditioning of the support.

2.2.1. Wet impregnation method

Wet impregnation is by far the most used method for the synthesis of supported heterogeneous catalyst, as it is a simple, inexpensive and generates little waste. In general, the support is impregnated with a precursor-containing solution and dried, followed by further activation treatments, such as calcinations or reduction (Sietsma et al., 2006). Metal salts used as catalyst precursor are dissolved in the impregnating solution and added to the support by means of a rotatory evaporator or rotavapor, which allows evaporating the solution under reduced pressure and moderate temperatures. *Büchi rotavapor R-114* was employed, which operated under vacuum at 70 ºC. As shown in Figure 2.1, this rotavapor is consituted by the following components: a motor unit to rotate the evaporation flask where the support is, a vacuum pump to reduce the pressure within the evaporator system, a water bath to heat the sample, a spiral condenser cooled by tap water to condense the evaporated solution, a mechanical device to lift the evaporation flask from the heating bath and a flask at the bottom of the condenser to collect the distilled solvent.

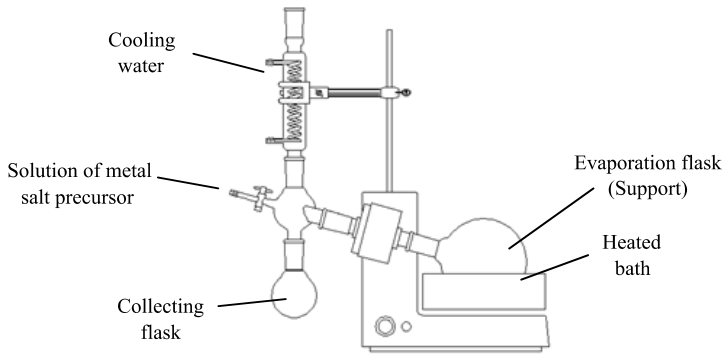

Figure 2.1. Scheme of Büchi rotavapor R-114.

2.2.1.1. Fe/olvine catalyst

Olivine was selected as catalyst support and Fe as metallic active phase. Thus, an aqueous solution of $Fe(NO_3)_3 \cdot 9H_2O$ (Panreac AppliChem, 98 %) was prepared with the amount of salt precursor required to attain the desired final metal content on the catalyst. A relatively low metallic load (5 wt%) was used, as the physical properties of olivine hinder a suitable dispersion for high metal loads due to its non-porous nature. After the impregnation, the catalyst was dried during a couple of days in an oven at 100 ºC and calcined at 1000 ºC for 4 h in a muffle oven. The heating rate in the calcination was 5 ºC min^{-1}.

2.3. CATALYSTS CHARACTERIZATION

A detailed characterization of the fresh and deactivated catalysts was carried out. Regarding to the fresh catalysts, different techniques were performed to understand their initial catalytic activity, whereas in the case of the spent catalysts, they were used to ascertain their main causes of deactivation. These characterization techniques are explained in the following subsections.

2.3.1. N_2 adsorption-desorption isotherms

The structure of the catalysts was analyzed in a *Micromeritics ASAP 2010* equipment and the specific surface area, pore volume and average pore size were determined. N_2 adsorption-desorption techniques for specific surface determination are based on multilayer adsorption and the application of the simplified Brunauer-Emmett-Teller (BET) equation in the 0.01-0.2 relative pressure range. The total pore volume was calculated taking into account the total amount of adsorbate at the inflexion point on the high-pressure plateau, whereas the pore size distribution was determined by Barrett, Joyner, and Halenda (BJH) method.

The experimental procedure consisted in a previous sample degasification at 150 ºC for 8 h to remove any impurities of the sample, followed by a N_2 adsorption-desorption in multiple equilibrium stages until the sample was saturated at cryogenic temperatures (liquid N_2).

2.3.2. X-ray fluorescence (XRF)

The chemical composition (wt%) of each catalyst was measured by means of XRF spectrometry in the Central Research Services (SGIker) at the University of the Basque Country (EHU/UPV). XRF analysis were carried out under vacuum atmosphere using a sequential wavelength dispersion X-ray fluorescence (WDXRF) spectrometer *(Axios 2005, PANalytical)* equipped with a Rh tube, and three detectors (gaseous flow,

scintillation and Xe sealing). From 200 mg of each powder sample, a bead was prepared by melting the powder with litium borate (Merck, Spectromelt A12) in a 1:20 ratio, using an induction microfurnace at 1200 ºC. The calibration lines were performed by means of well characterized international patterns of rocks and minerals.

2.3.3. Temperature programmed reduction (TPR)

TPR analysis allows determining the reduction temperature of the different metallic phases in the catalysts. In this technique, the catalyst is exposed to a reducing gas, usually H_2 diluted in argon, while the temperature is raised linearly. The H_2 consumed is measured continuously, and the reduction rate is therefore determined.

These assays were performed in an *AutoChem II 2920 Micromeritics*. Around 200 mg of the fresh catalyst was placed in a U-shape tube which was heated to 900 ºC with a heating rate at 10 ºC min^{-1} in a reduction atmosphere (10 vol% hydrogen in argon) Prior to the reduction experiments, the catalyst was heated under He stream to 200 °C in order to remove water or any impurities. A thermal conductivity detector (TCD) was used to analyze the hydrogen consumption of the samples and its signal was recorded continuously. A cold trap of 1-propanol/N_2 (liq.) was located between the sample and the detector to retain the water formed during the reduction, and therefore prevent interferences in the TCD signal.

2.3.4. X-ray diffraction (XRD)

XRD analysis was performed to analyze the inner crystalline structure of the calcined, reduced and deactivated catalyst, as every crystalline solid has itwn own characteristic difractogram. This non-destructive technique provides information about the crystallographic orientation, qualitative and quantitative phase identification, crystallite size and polymorphism, among others. In this thesis, the XRD analysis was used to identify the possible reducible metal species in the catalysts subject to TPR analysis.

The XRD analyses were conduted in the SGIker Central Service at the University of the Basque Country EHU/UPV, by using a *Bruker D8 Advance diffractrometer* with CuKα1 radiation, equipped with a Germanium primary monochromator, Bragg-Brentano geometry, with a CuKα1 wavelength of 1.5406 (Å), corresponding to an X-ray tube with Cu anticathode. Sol-X dispersive energy detector was used, with a window optimized for CuKα1 for limiting the fluorescence radiation. Thus, a monochromatic X-ray beam impinges on the crystalline material and the diffracted beam or the intensity of the elastically scattered electrons is measured as a function of the diffracted 2θ angle. Thus, diffraction spectra were obtained in 2θ angles in the 10-90º range and indexed by comparing with JCPDS files (Joint Committee on Powder Diffraction Standards)

2.3.5. Temperature programmed desorption of NH_3 (NH_3-TPD)

The total acidity was determined by NH_3-TPD in an *AutoChem II 2920 Micromeritics*. The experimental procedure consisted in outgasssing 200 mg of the catalyst under He stream at 550 ºC for 10 min with a heating rate of 15 ºC min^{-1}. Afterwards, the sample was cooled down, stabilized at 100 ºC and exposed to 0.05 cm^3 min^{-1} of NH_3 until sample saturation. The NH_3-saturated sample was then heated up 550 ºC following a heating rate of 5 ºC min^{-1} under He stream to remove the physisorbed NH_3. The ammonia desorption was followed with a TCD detector.

2.3.6. X-ray photoelectron spectroscopy (XPS)

XPS analysis was carried out to record in detail the elements making up the surface, and quantify and analyze their oxidation states. XPS measurements were conducted in the SGIker Central Service at the University of the Basque Country (EHU/UPV), using a SPECS system equipped with a *Phoibos 150 1D-DLD analyzer* and a monochromatic Al-Kα radiation source (1486.7 eV). Prior to the analysis, the spectrometer was calibrated with Ag (Ag $3d^5$ / 2368.26 eV) and the samples were outgassed. An initial scan was carried out using a step energy of 1 eV, dwell time of 0.1 s and a pass energy

of 80 eV followed by a detailed scanned using a step energy of 1 eV, dwell time of 0.1 s and a pass energy of 30 eV. CasaXPS 2.3.16 software was used to fit the spectra according to Gauss-Lorentzian model.

2.3.7. Temperature programmed oxidation (TPO)

Carbon deposition on the deactivated catalyst was ascertained by TPO in a thermobalance (*TGA Q5000 TA Instruments*) coupled in-line to a mass spectrometer (*Thermostar Balzers Instrument*). This device allows recording the signals at 14, 18, 28 and 44 atomic numbers, corresponding to N_2, H_2O, CO and CO_2, respectively. The coke content was determined based on CO_2 signal as it is impossible to distinguish between the water formed in the combustion of the coke and that corresponding to sample moisture. It should be noted that the CO content is negligible (the metallic species of the catalyst oxidize CO to CO_2 instantaneously). Coke content is defined as follows:

$$C_C = \frac{m_{CO_2}\ 12 g_C/44\ g_{CO_2}}{W} \cdot 100 \qquad (2.1)$$

where m_{CO2} is the CO_2 mass produced in the combustion and W the catalyst mass after completey burning the coke.

The experimental procedure consisted in the stabilization of the signal under N_2 stream (50 mL min^{-1}) at 100 ºC, followed by the oxidation of the sample with air by increasing temperature to 800 ºC using a ramp of 5 ºC min^{-1} and maintaining this final temperature for 30 min to ensure complete carbon combustion. Finally, the sample was cooled down to room temperature.

2.4. BENCH SCALE PLANT

The scheme of the bench scale plant used for biomass steam gasification is shown in Figure 2.2. This plant was fine-tuned and optimized based on the previous experience of the research group in cold fluid dynamic studies (Olazar et al., 1992, 1993a,c, 1994a,b) and the design and use of other plants fitted with the conical spouted bed reactor (CSBR) in the biomass pyrolysis and gasification (Aguado, 1999; Amutio, 2011; Erkiaga, 2014; Alvarez, 2015), pyrolysis of tyres (Velez, 2004; Arabiourrutia, 2007; Lopez, 2008), plastics pyrolysis and gasification (Gaisan, 2002; Elordi, 2010; Artetxe, 2012; Erkiaga, 2014), pyrolysis and in-line reforming of plastic wastes (Barbarias, 2015) and pyrolysis and in-line reforming of biomass (Arregi, 2017; Santamaria, 2019).

This bench scale plant is made up of the following components: 1) solid feeding system, 2) gas feeding system, 3) water feeding system, 4) reaction system, 5) product separation system, 6) control system, and 7) gas analysis system.

Moreover, the plant is equipped with a differential pressure gauge for detecting any increase in pressure drop caused by filter clogging. The description of each component of the unit plant is described below.

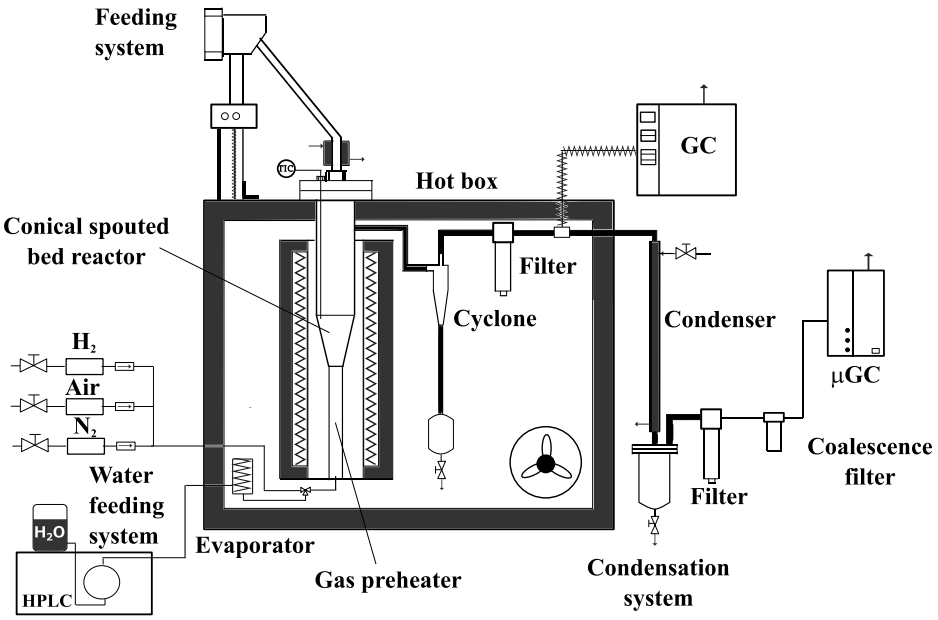

Figure 2.2. Scheme of the bench scale gasification plant.

2.4.1. Solid feeding system

Biomass was continuously fed into the gasifier by means of a piston feeder. This system (Figure 2.3) consists of a cylindrical vessel of 200 mL volume equipped with a vertical shaft connected to a 60 cm stroke piston placed below the material bed. When the piston rises, the biomass is pushed towards the top of the feeding system at the same time as the whole system is vibrating by means of an electric engine to prevent biomass agglomeration.

The biomass is loaded into the dispenser through an inlet located at the top of the feeding system. As the piston ascends, the biomass drops into the reactor through a 3/4" tube cooled with tap water to avoid biomass degradation, and so pipe clogging, before the reactor inlet. Moreover, a very small nitrogen flow of an inert gas (N_2) is introduced through a 1/8" tube from the top of the feeding vessel in order to ease the solid flow into the reactor and avoid the condensation of steam in the dispenser.

Dosing regulation rates are controlled from the control system, programmed for a speed between 0 and 100 %, where the maximum value of 100 % corresponds to the maximum flow rate of 1.7 g min^{-1} of biomass.

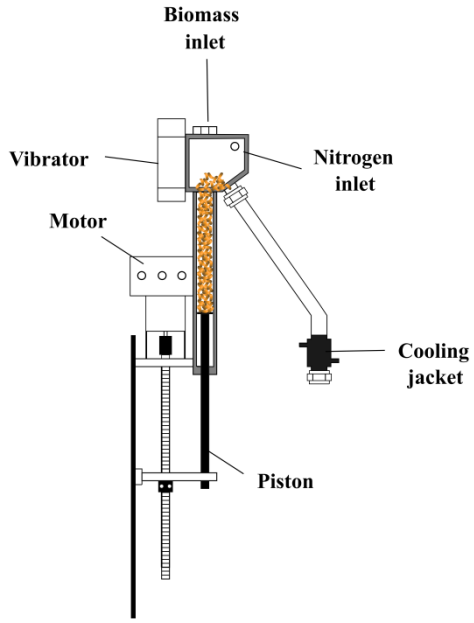

Figure 2.3. Solid feeding dispenser.

2.4.2. Gas feeding system

The pilot plant is provided with a gas feeding system, which allows feeding N_2, air and H_2 into the reactor through its lower part. The gas lines are joined together in a "T" junction in order to feed a single inlet gaseous stream into the reactor. The gas feeding system is made up of the following components:

- *Manual valves:* They allow the entrance of each gas to the system by manual opening. Each gas line has its own valve.

- *Mass flow controllers (MFCs).* The flow rate of the gases was measured by means of three mass flow controllers *(Brooks SLA5800),* one for each gas. These MFCs have a maximum design pressure of 8 bar, and inlet and outlet pressures of 4 and 2 bar, respectively. The N_2 flow controller supply a maximum flow rate of 40 L min^{-1}, that of air 20 L min^{-1} and that of H_2 5 L min^{-1}.

- *Non-return valves:* They allow flow circulation only in one direction and are fitted to ensure that the gas flows through the tubes in the right direction, when pressure conditions may otherwise cause reverse flow. They are located subsequent to the mass flow controllers.

2.4.3. Water feeding system

Water was fed by means of an *ASI 521* pump that allows a precise measuring of the flow rate. It is a positive displacement pump and its maximum design flow rate is 10 mL min^{-1}. The water circulates through a pressure-regulating valve *(back pressure),* which prevents its backward flow circulation and generates an overpressure of 34 bar in the pump head in relation to the reaction system, improving pump operation. The water stream was vaporized by an evaporator placed inside the hot box and prior to the entrance of the reactor.

2.4.4. Reaction system

The reaction system consists of a spouted bed reactor equipped with the fountain confiner and a non-porous draft tube. The reactor is placed into a forced convection oven, which is 1830x1950x1000 mm stainless steel box provided with 100 mm insulation of quartz wool with fiberglass reinforcement fabric. The hot box is kept at a temperature of 300 ºC to avoid the condensation of tars prior to chromatographic analysis.

As many of the applications of the conical spouted bed reactors (biomass, plastics, and tyres pyrolysis, drying of fine particles, coating powders and so on) involve operation using coarse and fine particle mixtures or very wide particle size distributions, high gas velocities are required, and therefore fine particle entrainment occurs. Thus, in order to overcome these limitatios, the fountain confiner was developed. The fountain confiner is a tube welded to the lid of the reactor, which has the lower end of the tube close to the surface of the bed and confines the gases produced during the gasification process, forcing them to describe a downwards trajectory.This reactor may also operate in the conventional spouting regime by using a lid without confiner. The main dimensions of the reactor are shown in Figure 2.4 and are as follows: cylindrical section diameter (D_C) 95 mm, height of the conical section (H_C) 150 mm, cone included angle (γ) 30°, length of the fountain confiner (H_G) 330 mm, and total height of the reactor (H_T) 430 mm. The cone base diameter is 20 mm, and the internal diameter of the fountain confiner (D_G) 54 mm, with its volume being of around 0.8 L. The height from the reactor base to the lower end of the confiner is 105 mm. These dimensions were established based on the prior knowledge by our research group on the spouted bed reactor fluid dynamics for different materials (Olazar et al., 1992, 1993b, 1994a, 1995; San José et al., 1993, 1995; Altzibar et al., 2017; Pablos et al., 2018; Estiati et al., 2019).

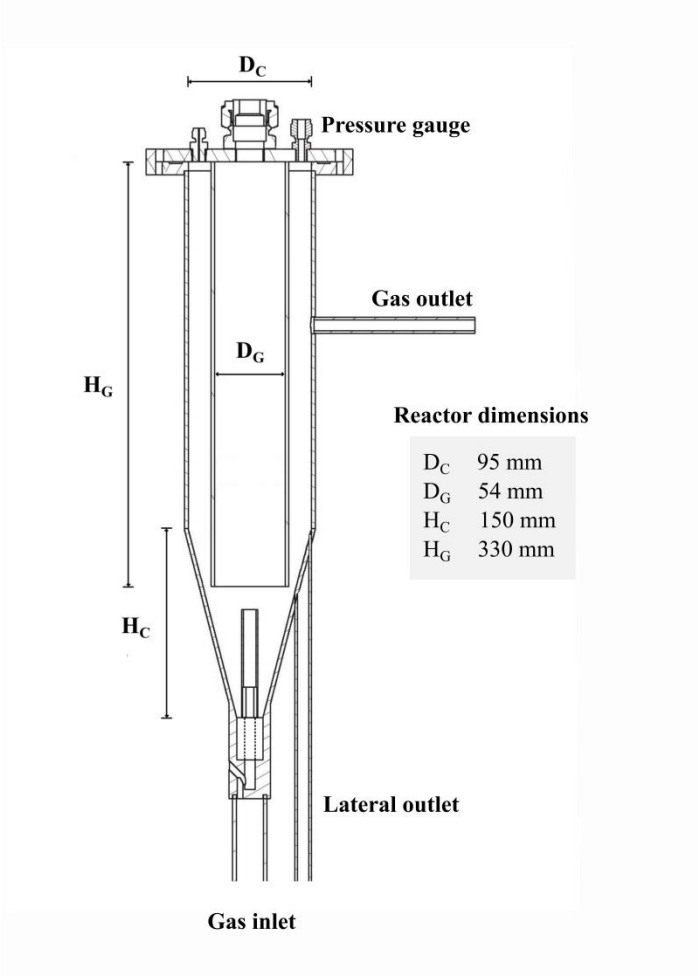

Figure 2.4. Scheme of the conical spouted bed reactor provided with fountain confiner and draft tube and its main dimensions (mm).

The gas inlet diameters (D_0) used are 5.5 and 8 mm for the draft tubes of 8 and 10 mm diameter (D_T), respectively. The base diameter (Di) is 20 mm independently of the draft tube used. The entrainment zone height (L_H) for the 8 mm draft tube is 15 mm, and two entrainment zone heights were assayed for the 10 mm draft tube, i.e., 15 and 25 mm. This parameter plays a crucial role in the spouting regime behavior; that is, higher solid circulation rates are attained for higher entrainment zones (Altzibar et al., 2013a; Nagashima et al., 2013; Estiati et al., 2020; De Brito et al., 2021). The total

height of all the draft tubes (L_T) is 85 mm. The design and dimensions of the draft tubes are shown in detail in Figure 2.5.

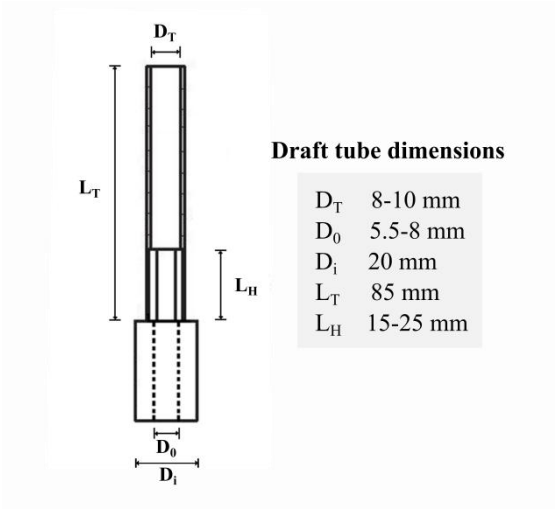

Figure 2.5. Scheme of the non-porous draft tube and its dimensions.

Besides the solid feeding tube, the reactor is provided with a 1/8" inlet on the lid, where a thermocouple is coupled to control the bed temperature, and 1/4" inlet for the pressure gauge. It is to note that the biomass inlet is located at the centre of the lid, and therefore biomass was fed into the fountain confiner.

The gas preheater is welded to the lower part of the reactor. The reactor is located within a radiant oven provided with two independent sections, with 2500 W power each, which provides the heat for operating up to 900 ºC. The temperature in each section is controlled by means of thermocouples placed at the gaseous stream inlet (lower section) and in the bed (upper section), with the latter being used for the monitoring of gasification temperature.

2.4.5. Product separation system

The bench scale plant is eqquiped with a particle retention system, consisting of a cyclone and a filter.

- *Cyclone.* The volatile stream leaving the reactor passes through a high efficiency cyclone to remove the fine char or bed material particles entrained from the reactor. The gaseous stream enters through a lateral inlet and leaves the cyclone from the top, whereas the particles drop down and leave the cyclone via a collection device fitted to its bottom.

- *Filter*. After the cyclone, the gases circulate through a sintered steel filter (40 μm) to retain the fines elutriated.

The volatile stream leaving the filter is then directed to a "T" junction, where part of the stream is taken to be injected in the gas chromatograph. The rest of the stream is driven to the condenstion system, fitted with a condenser, a separation tank and a coalescence filter.

- *Condenser*. The condenser consists of a double shell tube, whereby one tube is concentrically positioned within a larger one. The gaseous stream flows through the inner tube and tap water at room temperature flows through the surrounding shell.

- *Separation tank*. It is made of 1 L vessel in which a 40 μm stainless steel filter is located inside. Tars enter the filter and condense inside the vessel externally cooled by tap water. Thus, tar collection efficiency is greatly improved by inserting this filter, as it plays the role of an impingement device at the same time as increases the cooling surface area. A manual regulation valve located in the lower part of the tank allows discharging the liquid products, whereas the non-condensed gases leave the tank through the top.

- *Coalescence filter.* It is placed subsequent to the separation tank to ensure the retention of the microdroplets (fog) in the gaseous stream by coalescence. The maximum design pressure of this filter is 10 bar.

2.4.6. Control system

The unit control system is based on power line communications (PLC), with a 10" touch screen and a control panel provided with a power source, signal converters and electrical protections. The control system is located in a single box attached to the plant frame. Figure 2.6 displays the panel control of the pilot plant.

It incorporates an Ethernet port for the network control of the equipment, remote monitoring and downloading of Excel data files from a PC. It includes a fully implemented control firmware and fully developed user interface, as well as the necessary applications for data communication and downloading.

This control block is made up of a PLC system and its corresponding expansion modules. Both act as a central processing unit to which all the devices forming the system are connected to.

The control block is made up of the elements detailed below:

- PLC. Unitronics V1040 model, which includes:

  - 10.4" color touch screen

  - 9 programmable function keys

  - Dimensions 289x244.5x59.1 mm

- Expansion modules. Unitronics.

  - V200-18-E4XB snap-in I/O module. 18 digital inputs, 15 PNP outputs, 2 PNP/NPN outputs, 4 analog PT100/TC inputs and 4 analog outputs.

  - EX-AX2 expansion adapter

  - Analog input module IO-ATC8. 8 analog or thermocouple inputs.

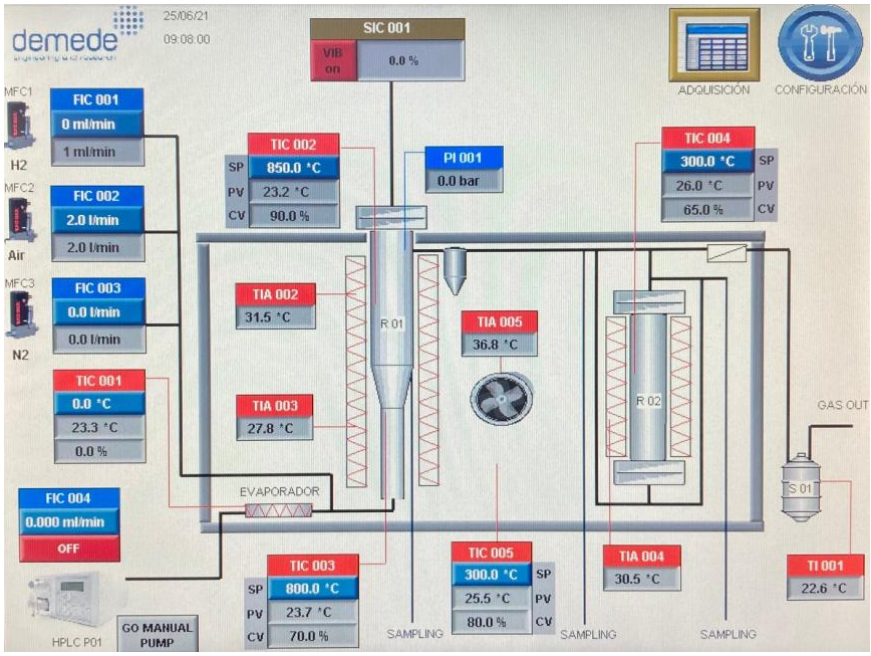

Figure 2.6. Control panel of the bench scale gasification plant.

2.5. OPERATING CONDITIONS

2.5.1. Hydrodynamic study

Runs were carried out in the spouted bed provided with fountain confiner by varying temperature, draft tube geometry and bed material (olivine) properties. Thus, the effect olivine particle size has on the performance of the bed was studied using four fractions obtained by sieving (90 to 150, 150 to 250, 250 to 355 and 355 to 500 μm) and that of olivine mass was analyzed by varying this parameter between 100 and 250 g. The influence of draft tube geometry was analyzed by changing the diameter of the tube and the height of the entrainment zone. Temperature was varied from room temperature to gasification conditions (800 ºC). The experimental conditions studied are summarized in Table 2.3.

The minimum spouting velocity (u_{ms}) and the fountain enhanced spouting velocity (u_{ef}) were determined by direct observation under the conditions studied. The fountain enhanced regime is reached for high gas velocities of around four times higher than the minimum spouting one and is characterized by a fountain height reaching the top of the confiner.

Table 2.3. Experimental conditions used in the hydrodynamic study of the fountain confined conical spouted bed.

Operating conditions	
Olivine mass (g)	100 and 250
Olivine particle size (μm)	90-150, 150-250, 250-355 and 355-500
Draft tube/gas inlet diameter (mm)	10/8 and 8/5.5
Entrainment zone height (mm)	15 and 25
Temperature (ºC)	25, 200, 400, 600 and 800

Given that the main aim of the fountain enhanced regime is to improve the conical spouted bed reactor´s performance for biomass gasification process, temperature profiles were determined in the bed because this parameter plays a crucial role in tar cracking reactions. The profiles were determined by introducing a thermocouple through the top of the fountain confiner and measuring bed temperature at different heights. Apart from the thermocouple used for reactor temperature control, which was located in the annular region at approximately 50 mm from the reactor base, the measurements were taken at the top of the draft tube (85 mm from the bottom), at an intermediate position between the top of the draft tube and the lower end of the confiner (93 mm from the bottom), at the lower end of the confiner (101 mm from the bottom), at three different heights inside the fountain confinement device (183, 266 and 348 mm from the bottom) and at the top of the fountain (431 mm from the bottom). Temperature profile measurements were conducted under three different operating conditions at 800 ºC (measured in the annulus), with their velocities above the minimum spouting (u/u_{ms} ratios) being 1.2, 2.5 and 4, corresponding to very different hydrodynamic conditions, with the latter corresponding the fountain enhanced spouting regime. 100 g of olivine (250-355 μm) and a draft tube with 10 mm diameter (an inlet diameter, D_0, of 8 mm) with a height of the draft tube entrainment zone of 15 mm were used.

In order to determine the voidage in the fountain region under given operating conditions, the decrease in the annulus bed height was measured from the static condition to the operating conditions under study. This reduction in bed height was produced due to the amount of olivine transferred into the fountain region under the fountain enhanced regime. To measure the bed height in the annulus under operating conditions, a fine steel bar provided with flat base was introduced from the top of the reactor. The bar was lowered until the flat base was supported on the surface of the bed. The difference between static bed height and that corresponding to operating conditions indicates the amount of solid transferred from the annulus into the fountain. Bed voidage was determined under gasification conditions, operating at 800 ºC with a

bed of 100 g of olivine (250-355 μm) and a draft tube with 10 mm diameter (an inlet diameter, D_0, of 8 mm) with a height of the draft tube entrainment zone of 15 mm.

This measurement is based on the assumption that voidage in the bed annulus is similar in both loose bed and spouting conditions (San José et al., 1998a). Furthermore, the use of a non-porous draft tube and fine particles minimizes air percolation into the annulus and the subsequent aeration of this region that may lead to a voidage increase. Moreover, under fixed bed conditions there are no solids in the draft tube except in the lower section corresponding to the entrainment zone. Accordingly, the solid volume conveyed to the fountain is determined from the solids transferred from the annulus (decrease in the annulus height) and the amount of solids transferred from the entrainment zone in the lower end of the spout.

2.5.2. Gasification experiments

Biomass steam gasification experiments were conducted using a draft tube with a diameter of 8 mm (internal diameter 5.5 mm) and an entrainment zone height of 15 mm. The optimum dimensions and geometry of this tube were determined based on the hydrodynamic results obtained in Chapter 3 under gasification conditions. Thus, these geometric factors allow operating under enhanced fountain regime wih low steam flow rates, and they also ensure great turbulence, development of the fountain region and fluidization stability (Lopez et al., 2017).

The runs were carried out in continuous mode by feeding 0.75 g min^{-1} of biomass. In all the experiments, the same steam flow rate of 1.5 mL min^{-1} was used, which corresponds to 1.86 NL min^{-1} (under normal conditions). Accordingly, the runs were performed with a steam/biomass (S/B) of 2.

All the experiments were performed in continuous mode for 20 min in order to ensure steady state process. Steam gasification kinetics is very fast above 800 ºC and steady state is attained in a short period of operation. In addition, the runs were repeated

several times (at least three) under the same conditions in order to guarantee reproducible results.

2.5.2.1. Effect of the regime

The bed contained 100 g of olivine, and two particles sizes were used, i.e., 90-150 μm and 250-355 μm. The selection of these olivine particle size ranges pursued the fine tuning of the hydrodynamic performance of the reactor, as the minimum spouting velocity strongly depends on particle size (Lopez et al., 2017; Tellabide et al., 2020a). Thus, operating with the coarse olivine fraction the gas velocity used corresponds approximately to 1.5 times the minimum spouting velocity (1.5 u_{ms}), and so the reactor operated under conventional spouting regime. Nevertheless, in the experiments performed with the fine olivine, the same gas velocity used accounted for approximately four times the minimum spouting one (4 u_{ms}), and the fountain enhanced regime was therefore attained.

In addition, experiments with and without the fountain confiner were carried out at 850 ºC and using coarse olivine (250-355 μm), with gas velocity corresponding in both cases to approximately 1.5 times u_{ms} (conventional spouting regime). Moreover, the results obtained with the confiner under conventional spouting regime were compared with those obtained with this device operating in the enhance fountain spouting regime under the same conditions, i.e., 850 ºC and S/B=2, by replacing the coarse olivine with the fine one in the bed. Therefore, the role of the vigorous gas-catalyst contact in the fountain enhanced regime was assessed.

2.5.2.2. Effect of temperature

The reactor was loaded with 100 g of olivine, with particles in the 90-150 μm range. This particle size was established to operate under fountain enhanced spouting regime; that is, with a gas velocity of around 4 times higher than the minimum spouting one (Lopez et al., 2017). The effect temperature has on the distribution of products and

their composition were studied by means of runs at 800 ºC, 850 ºC and 900 ºC of 20 min time on stream.

2.5.2.3. Effect of the primary catalysts

Gasification experiments were carried out at 850 ºC with steam as a gasyfing agent. As the density of the primary catalysts studied differs greatly, the bed mass and particle size were adjusted accordingly to operate under comparable hydrodynamic conditions. Thus, the same bed volume was used in all the experiments. Moreover, the particle size of each material was selected in order to ensure operation under enhanced fountain regime, i.e., the spouting velocity should be four times higher than the minimum one (u_{ms}) (Lopez et al., 2017; Cortazar et al., 2018). As the same steam flow rate was used in all the runs, a larger particle size was required for materials with lower densities in order to obtain the same spouting regime. Thus, the runs with olivine and silica sand were carried out using a bed of 100 g and a particle size in the 90-150 um range. The beds of dolomite contained 53 g of particles with a size in the 150-250 μm range, those of FCC 55 g in the 90-150 μm range and those of γ-alumina 45 g in the 250-400 μm range. Similar strategies were reported in the literature on catalytic biomass gasification in bubbling fluidized beds when the same steam flow rate was used in all the runs (Berdugo Vilches et al., 2016).

2.5.2.4. Effect of the iron addition

Continuous gasification experiments were performed at 850 ºC. The bed consisted of 100 g of either calcined olivine or Fe/olivine catalyst, with their particle size being in the 90-150 μm range. Prior to the reactions, the iron catalyst was subjected to an in situ reduction process at 850 ºC for 4 h with a stream containing 10 vol% of H_2 to ensure complete reduction to Fe^0 phase.

2.6. PRODUCT ANALYSIS

2.6.1. Tars and permanent gases

Samples of the volatile stream leaving the reactor were analyzed in-line by means of a gas chromatography (GC) and the permanent gases were analyzed in a gas micro-chromatograph (microGC). The samples were injected into the GC through a line thermostated at 280 ºC to avoid the condensation of the tars. The sampling point of the non-condensable gases was located after the condensation and filtering sections to prevent from column contamination. In order to check the reproducibility of the experiments, several samples were taken in each run under steady state conditions.

2.6.1.1. Gas chromatography

The gas chromatograph *GC Agilent 7890* is provided with a six-port rotary valve, an injector, a column and a flame ionization detector (FID).

Figure 2.7 illustrates the scheme of the sampling valve of the chromatograph. With the valve in "off "position, ports 1→6→3→2 and 4→5 are connected. The carrier gas (H_2) supply and the column are attached to ports 4 and 5, respectively, so the carrier gas flows directly into the column in this valve position and reaches the detector. A gas-sampling loop is attached to the valve at ports 6→3, which allows a gaseous sample to be introduced into the column. A suction pump connected to the vent makes the sample to flow through the loop.

Injection occurs when the six-port valve is moved to the "on" position. A pneumatic actuator allows the rotation of the sampling valve, reversing the flow direction. As the ports 4→3→6→5 are connected, the carrier gas flows first through the sample loop, flushing the sample loop into the injector. A *split/splitless* type injector was used and only a small fraction of the sample was injected into the column, whereas the

remaining was sent to vent. The valve must remain in "on" position for sufficient time to flush the loop completely.

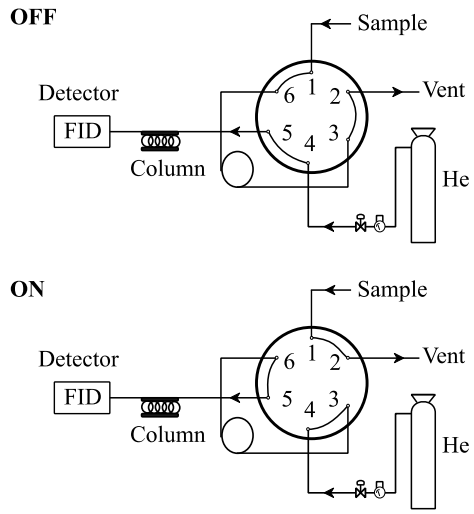

Figure 2.7. Sampling system of the *GC Agilent 7890*.

The column used is a HP Pona, which is 50 m long, 0.2 mm in internal diameter and has a coating thickness of 0.5 μm. The temperature program used in the chromatographic oven (Figure 2.8) was as follows: 2 min at 40 ºC in order to attain a good separation of gaseous products; and a sequence of 25 ºC min^{-1} up to 320 ºC and 7 min at this temperature to ensure that all products were outside the column.

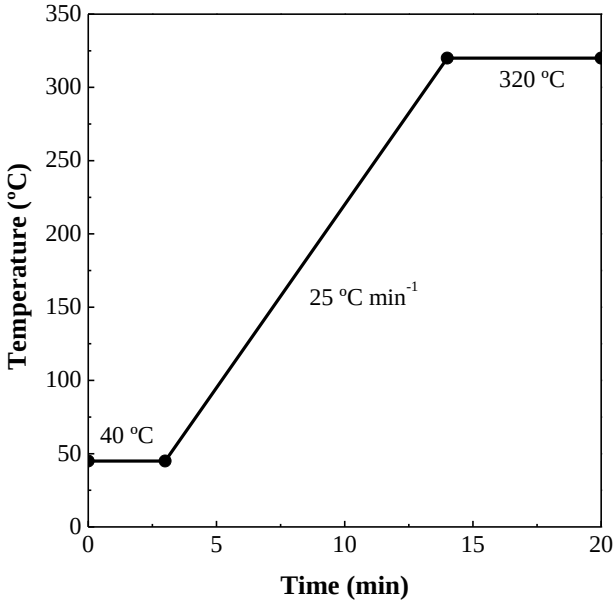

Figure 2.8. Temperature program of *GC Agilent 7890*.

The *GC Agilent 7890* chromatograph is equipped with a FID detector, which is the most widely used type of detector in gas chromatography. The FID signal is proportional to the number of carbon atoms in a pure hydrocarbon molecule (Kállai et al., 2001). However, the heteroatomic compounds are partially oxidized, and the signal is usually reduced. In the case of oxygenated compounds, they generate a lower response per molecule or mass because oxygen is already oxidated. In other words, the same amount of an oxygenated compound yields a lower peak of less area than its saturated counterpart does. Therefore, appropriate response factors must be calculated for the oxygenated compounds in the tar (McMinn, 2000).

Standard mixtures of known concentration were prepared for response factors determination. The most significant tar compounds were mixed with different hydrocarbons (the compounds must have different retention times to avoid peak overlapping), allowing to establish their response factor compared to that hydrocarbon. Considering that hydrocarbons response factor is equal to unity, the following

expression was used to calculate the response factors of the oxygenated compounds in the tar:

$$\frac{f_{OX}}{f_{HC}} = \frac{m_{OX}}{m_{HC}} \frac{A_{HC}}{A_{OX}} \quad (2.2)$$

where f_{ox} and f_{HC} are the response factors, m_{ox} and m_{HC} the masses and A_{ox} and A_{HC} the chromatographic areas of the oxygenated compound and the hydrocarbon, respectively.

Table 2.4 displays the response factors of the oxygenated compounds in the tar fraction. It is to note that the response factors depend on the type of bond between C and O, and on the relative proportion of C, H and O.

Table 2.4. Response factors of the most significant oxygenated compounds in the biomass steam gasification.

Compound	M_W (g mol^{-1})	Formula	Response factor
Phenol	94	C_6H_6O	1.2
Methyl phenol	108	C_7H_8O	1.15
Dibenzofurane	168	$C_{12}H_8O$	1.1

A typical chromatogram for biomass gasification at 850 ºC is shown in Figure 2.9.

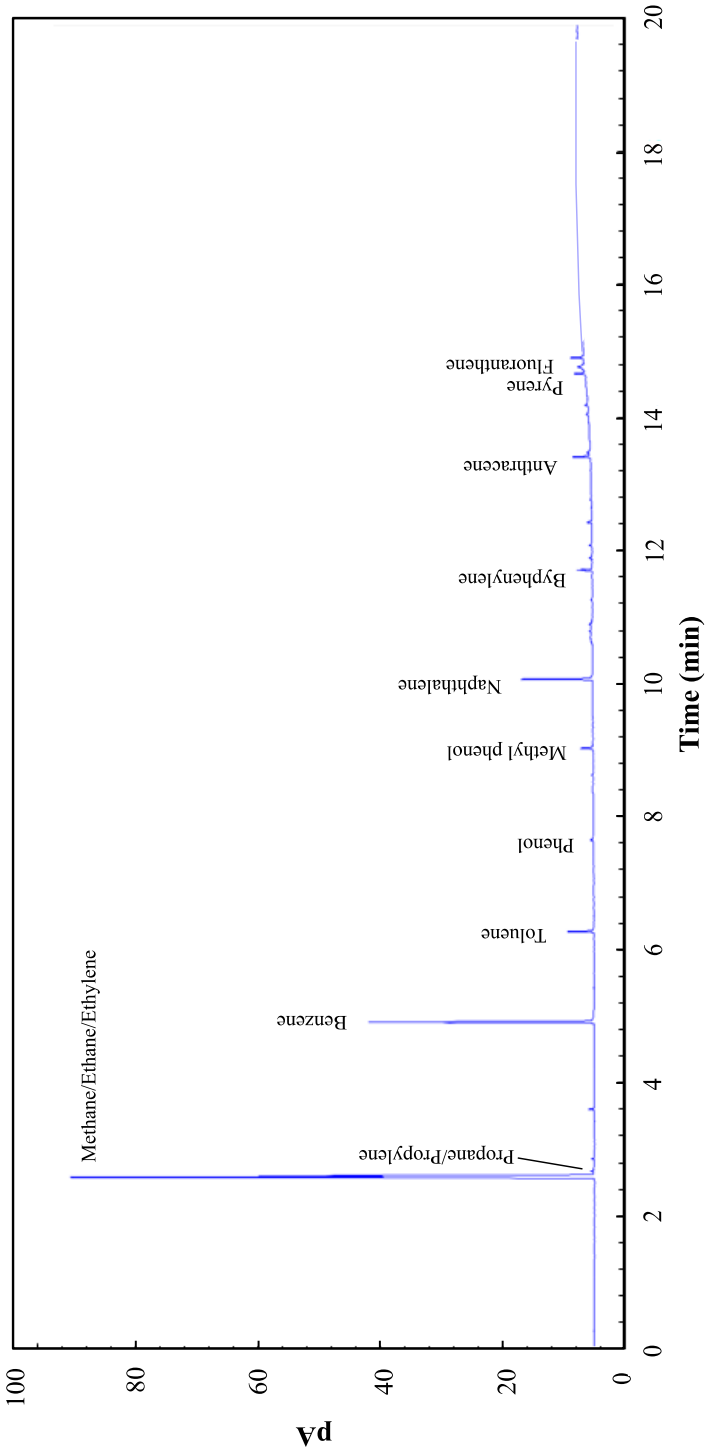

Figure 2.9 Cromatograph obtained in the biomass steam gasification with olivine at 850 ºC.

2.6.1.2. Gas micro-chromatography

The concentration of H_2, CH_4, CO and CO_2 was quantified by means of a gas micro-chromatograph *Varian 4900*. Moreover, it was also used for determining the proportion of ethane/ethylene and propane/propylene, as these compounds cannot be separated in the gas chromatograph (GC). The *Varian 4900* micro-chromatograph contains two different channels with three analytical modules, including injector, column and TCD.

- *Analytic channel A* is made up of a molecular sieve capillary column, Molecular Sieve 5 (MS5, 10 x 0.12 mm) and micro TCD detector, where small molecules, such as H_2, O_2, N_2, CH_4 and CO are separated.

- *Analytic channel B* is provided with a capillary column Porapak Q (PPQ, 10 m x 0.32 mm) and micro TCD detector. This column separates CH_4, CO_2, ethylene, ethane, propylene and propane.

Each channel of the micro-chromatograph has a microinjector module with a *backflush* system. The flow diagram of the system is shown in Figure 2.10. *Backflash* to vent is an advanced technique used to prevent later-eluting compounds from reaching the analytical column and detector, aiming at keeping the column clean and reducing analysis time. A *backflush* system consists of a pre-column and an analytical column coupled at a pressure point, which makes it possible to invert the flow direction of the gas carrier through the pre-column at a certain time called *backflush* time. When all compounds have passed through the analytical column, where compound separation is carried out, the *backflush* valve switches (at the backflash time), reversing the flow in the pre-column, and sending the remaining compounds to vent.

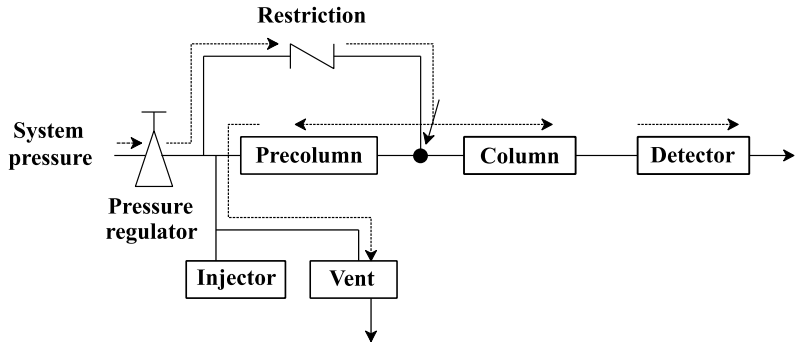

Figure 2.10. Flow chart of the backflush system in the micro-chromatograph *Varian 4900*.

The micro-chromatograph also controls the temperature of the injection system, with an independent temperature control up to 110 ºC at the sample inlet system and sample line of each channel. The instrument parameters of the chromatograph analytical method are shown in Table 2.5.

Table 2.5. Instrument parameters of the micro-chromatograph *Varian 4900* analytical method.

Parameter	MS5	PPQ
Column temperature (ºC)	90	90
Injector temperature (ºC)	110	110
Pressure (psi)	25	25
Backflush time (s)	7	7
Injection time (ms)	50	50
Analysis time (s)	200	200

Each channel is equipped with a TCD, which responds to the difference in thermal conductivity between the carrier gas alone and the carrier gas containing sample compounds. Table 2.6 shows the response factors of the compounds detected in the

micro-GC. These response factors are mandatory to determine the volume concentration of the compounds based on their chromatographic peak area.

Table 2.6. Response factors in the micro-GC *Varian 4900* for the identified compounds.

Compound	TCD 1	TCD 2
Hydrogen	55.4	-
Methane	4696.9	5589.5
Carbon monoxide	5101.1	-
Carbon dioxide	-	6699.9
Ethylene	-	7793.8
Ethane	-	7891.6
Propylene	-	9781.6
Propane	-	10282.5

2.6.2. Characterization of tars

2.6.2.1. Gas chromatography coupled with mass spectrometry (GC-MS)

Tar compounds were identified using a *Shimadzu 2010 chromatograph* coupled to a *Shimadzu QP2010S* mass spectrometer. The collected tar was dissolved in acetone to prevent fouling of the chromatographic components.

The gas chromatograph uses a *DB-1MS* column of 60 m length, 0.25 mm in diameter and 0.25 μm in thickness. The oven temperature programme was the same as that used in the gas chromatograph for the analysis of tars on-line, with the aim of easing the identification of tar compounds.

The analysis variables of the chromatograph are: pressure, 166.4 kPa; total flow, 6.5 mL min^{-1}; column flow, 1.57 mL min^{-1}; linear speed, 32 cm s^{-1}; purge flow, 3 mL min^{-1}

and *split* 100:1. The values of the variables of the mass spectrometer were: ion source temperature, 200 °C; interface temperature, 300 °C; solvent cut time, 4.5 min and the mass range detected, 40-400. The peaks were identified by comparing their spectra with those of the National Institute of Standards and Tecnology (NIST) library.

2.6.2.2. Fourier-transform infrared spectroscopy (FTIR)

Infrared spectroscopy (IR) consists in the absorption within the infrared region of the electromagnetic spectrum, being most commonly used for the identification of a compound or elucidation of the structure and composition of a sample. In this thesis, this technique was employed to study the tar composition, in terms of polar bonds of functional groups.

The analysis was carried out in a *FTIR Thermo-Nicolet 6700* spectroscope in transmission mode. The experimental procedure consisted in preparing a pellet of 150 mg of KBr (Aldrich, purity > 99 %) in which a drop of tar was placed in the middle, and then pressed it at 10 t cm^{-2} for 15 min. Prior to the analysis, and in order to substract the effect of the tar from the IR spectrum, a reference or background IR spectrum was recorded for a pellet of KBr. Infrared spectra of the tar was directly registered when the radiation hit the sample in the interval of 1000-3700 cm^{-1}.

2.6.2.3. Simulated distillation

Tars were fractionated by simulated distillation using a *GC Agilent 6890* provided with a FID detector and *Simdis 2887 fast* column, especially suitable for this purpose. The column is 10 m long, 0.53 mm in internal diameter and 0.88 µm of thickness. The tests were carried out according to the ASTM-D2887-84 standard (boiling range distribution of petroleum fractions by gas chromatography).

3

DEVELOPMENT AND HYDRODYNAMICS OF THE FOUNTAIN CONFINED SPOUTED BED (FCSB) FOR GASIFICATION

The spouted bed is an alternative fluid-particle contact method to fluidized beds, which has been successfully applied to systems in which conventional fluidization has yielded unsatisfactory results, especially when coarse materials are handled (Epstein and Grace, 2010). The main features of this technology are related to the well-defined cyclic movement of the particles, which allow for an excellent contact between the gas and solid particles, promoting high heat and mass transfer rates. This original fluid-particle contact makes spouted beds suitable for many industrial applications, such as drying (Benelli et al., 2013; Berghel and Renström, 2014; Sousa et al., 2019), coating (Da Rosa and Dos Santos Rocha, 2010; Mollick et al., 2015), pyrolysis (López et al., 2010; Alvarez et al., 2015; Fernandez et al., 2021b) and gasification (Erkiaga et al., 2013b; Lopez et al., 2015; Alvarez et al., 2019). Furthermore, several modifications of the original one reported by Mathur and Gishler (1955) have been proposed in order to increase the applicability range, as are two dimensional spouted beds (Swasdisevi et al., 2005; Saidi et al., 2015; Qiu et al., 2016) and spout fluid beds (Su et al., 2014; Knežević and Povrenović, 2015; Sutkar et al., 2015).

The aim of the Chapter 3 is to develop a novel gas-solid contact regime based on a conical spouted bed reactor for the optimization of its performance in biomass gasification. The conventional conical spouted bed is characterized by its short residence time, which is an excellent feature for minimizing undesired secondary reactions in pyrolysis processes (López et al., 2010; Alvarez et al., 2014). Nevertheless, it is a serious drawback for gasification, as short residence times hinder tar cracking reactions (Erkiaga et al., 2013a,b, 2014).

When designing gasifiers a critical point to consider is process efficiency in terms of gas composition and, especially, avoidance of tar formation (Devi et al., 2003; Larsson et al., 2021). According to Bridgwater (1995), there are three main design aspects of special significance for improving reactor performance: i) additional residence time after the gasification step, ii) direct contact with high temperature surfaces and iii) partial oxidation by injecting air or pure O_2. Several attempts were carried out to fulfill these objectives, and secondary air injection in the freeboard region of fluidized bed

gasifiers was reported as a suitable method to reduce tar content because it increases temperature in this region (Narváez et al., 1996; Pan et al., 1999; Thamavithya et al., 2012; Tsekos et al., 2021). Another strategy used for enhancing tar cracking is the separation of pyrolysis and reduction zones in the gasifier (Šulc et al., 2012; Gómez-Barea et al., 2013a; Wang et al., 2022).

The modifications proposed in this chapter for the conical spouted bed reactor pursue two of the guidelines proposed by Bridgwater (1995), i.e., residence time increase and additional direct contact with heat carrier particles in the bed fountain. The most significant modification lies in the fountain confinement, which was performed by welding a tube to the lid of the reactor, with the lower end of the tube being close to the surface of the bed (Figure 3.1). This device was originally designed with the aim of handling fine materials by retaining the particles in the fountain region, and therefore avoiding their entrainment from the bed (Altzibar et al., 2017). In addition, this system greatly contributes to the stability of the spouting regime and gas flow distribution in the reactor, with hardly any effect on pressure drop. The single previous reference of a device with certain similarity to the one developed here is the side-outlet spouted bed developed by Hattori et al. (1978, 1981). However, the aim of this configuration was not fine particle retention, but process scaling-up.

Fountain confined conical spouted beds allow operating with finer catalyst particles than conventional conical spouted beds, and therefore the gas flow rate for spouting is much lower. This point is of great significance, since it allows increasing residence time, and therefore promoting tar cracking (Gil et al., 1999b; Devi et al., 2003). Moreover, it also eases the adjustment of steam/biomass (S/B) ratio (or ER in the air gasification process) because the gasification agent also acts as fluidizing agent. This fact is of special significance, given that S/B ratio is a key parameter for process performance optimization (Ahmad et al., 2016; Singh Siwal et al., 2020). The longer residence time of the gas phase is attained by increasing the reactor volume, i.e., longer reactor's cylindrical section and fountain region height. A simple similar solution was successfully applied to improve the performance of a fluidized bed gasifier by

increasing the height of the freeboard region (Gil et al., 1999b).

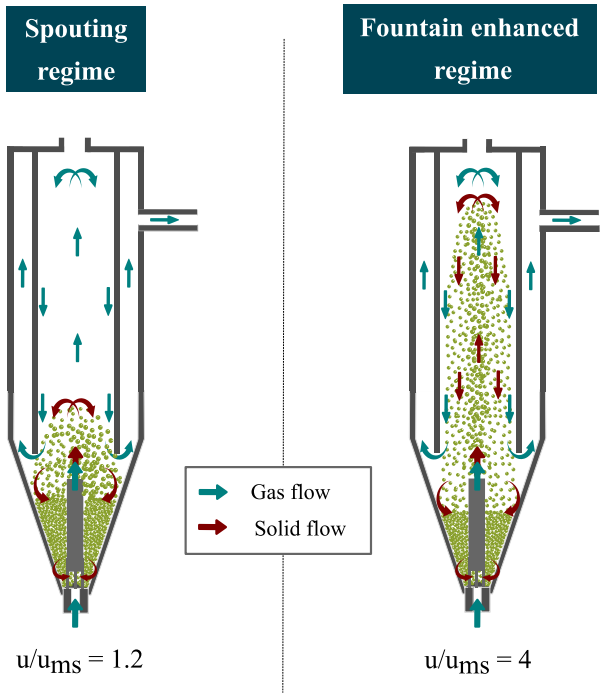

Figure 3.1. Schemes of the conventional spouting and the fountain enhanced regimes.

Furthermore, this device for confining the fountain also allows for modifying the residence time distribution. Thus, it avoids the direct release of the biomass derived gases from the reactor since it forces the gas to circulate through the confined fountain region. Therefore, the novel gas-solid contact regime developed in this study is based on the fountain confined conical spouted bed. The fountain enhanced spouting regime is attained by using a gas velocity four times the minimum spouting one. This regime is characterized by a severe expansion of the bed (in the fountain) and high turbulence. Figure 3.1 shows a scheme of the contactor operating with a gas velocity slightly above the minimum one (left) and with a gas velocity corresponding to the fountain enhanced regime (right), approximately four times the minimum one operating with fine materials; however, this ratio could be higher for coarse materials (Tellabide et al.,

2021b). The conditions in the latter regime promote contact between tar compounds in the gas phase and catalyst particles, which is essential to ensure tar elimination (Koppatz et al., 2012; Benedikt et al., 2017).

The use of a non-porous draft tube was also considered for the optimization of the fountain enhanced regime as it allows for operating with low gas flow rates for attaining high residence times (Luo et al., 2004; Thanit et al., 2005; Neto et al., 2008; Nagashima et al., 2009; Makibar et al., 2012; Altzibar et al., 2013b). In fact, the non-porous draft tube promotes high fountains (Makibar et al., 2012; Nagashima et al., 2013) by diverting most of the inlet gas stream through the draft tube, which enhances particle dragging, and therefore leads to additional gas-solid contact in the fountain.

As confining the fountain a clearly differentiated regime is attained, Section 3.1 analyzes the influence bed properties and draft tube design have on reactor´s hydrodynamics. In particular, Section 3.1.1 deals with the effect of bed particle size and bed mass on the minimum spouting velocities and fountain enhanced spouting velocities in the 20-800 ºC temperature range and Section 3.1.2 with the height of the draft tube entrainment zone and the combined effect of the gas inlet and draft tube diameters. On the other hand, Section 3.2 describes the temperature profile on fountain confiner since temperature determines the extent of gasification reactions. As well as temperature, the gas-solid contact between tars and the bed particles is essential for an efficient tar cracking reactions. Thus, Section 3.3 approaches the estimation of the fountain voidage. Finally, the discussion of the most relevant results is presented in Section 3.4.

3.1. INFLUENCE OF BED PROPERTIES AND DRAFT TUBE DESIGN ON THE REACTOR´S HYDRODYNAMICS

3.1.1. Influence of bed properties

In order to gain knowledge on the spouted beds provided with fountain confinement, the influence of different parameters was investigated operating at low and high gas velocities. Beds made up of olivine particles were analyzed using four fractions with their size ranges being 90-150, 150-250, 250-355 and 355-500 μm.

The first point to emphasize is the great stability in the fountain enhanced spouting regime, even with the finest olivine fraction. Thus, the combination of a non-porous draft tube with the fountain confinement system leads to a highly stable configuration.

Figure 3.2 shows the minimum spouting velocities and fountain enhanced spouting velocities obtained for beds made up of different particle sizes in the temperature range studied. Note that empty points correspond to minimum spouting velocity and solid points to enhanced fountain regime velocity. As observed, both with 10 (Figure 3.2a) and 8 mm (Figure 3.2b) draft tubes an increase in olivine particle size caused an increase in both the minimum and the fountain enhanced spouting velocities. In the case of the wider tube, this increase being more pronounced when comparing the velocity values obtained for the coarse and intermediate fractions (355-500 μm and 250-355). However, the opposite was observed with the fine tube, being the minimum and the fountain enhanced spouting velocities reduction more relevant for the 90-150 μm fraction (not studied with the 10 mm tube). Moreover, it should be noted that the stable hydrodynamic behavior attained with the finest particles is of special relevance, as it allows reducing the gas flow rate, and therefore increasing the residence time in the gasifier.

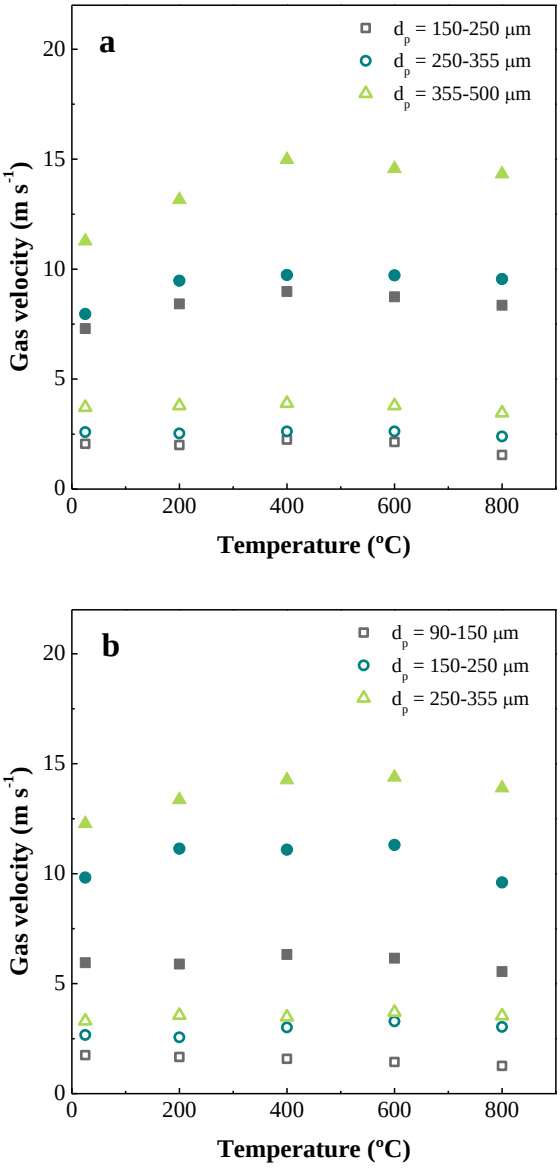

Figure 3.2. Effect of olivine particle size on the minimum spouting (empty points) and fountain enhanced spouting (solid points) velocities (per unit of inlet cross section): (a) $D_{0,}$ 8 mm; $D_{T,}$ 10 mm; olivine mass, 100 g and $L_{H,}$ 15 mm; (b), $D_{0,}$ 5.5 mm; $D_{T,}$ 10 mm; olivine mass, 100 g and L_H 15 mm.

Figure 3.2 also allows analyzing the influence of temperature on the minimum and fountain enhanced spouting velocities. As observed, the minimum spouting velocity hardly changed with temperature, with a slight decrease at the highest temperature under the different conditions studied. The literature information dealing with the evolution of the minimum spouting velocity with temperature is very scarce, especially for spouted beds provided with draft tube. Thus, Makibar et al. (2011) studied the effect temperature has on the minimum spouting velocity from 20 to 500 ºC in a conical spouted bed with non-porous draft tube. They observed a decreasing trend from 20 to 200 ºC, with this effect being less pronounced above this temperature. Wu et al. (2014, 2015) studied the influence of temperature on the minimum spouting velocity in a spout-fluid bed provided with a non-porous draft tube in a relatively narrow range from 20 to 227 ºC. These authors observed an increase in spouting velocity with temperature when low fluidizing gas velocity was used, but the trend was the opposite when higher velocities were introduced into the annulus (>0.02 m s^{-1}).

Regarding the evolution of the fountain enhanced spouting velocity with temperature a clearer trend was observed, with an initial increase to a peak value between 400 and 600 ºC and a subsequent slightly decrease at 800 ºC. These trends are explained by the complex effect of temperature on the gas phase momentum transfer to particles. Thus, on the one hand, gas viscosity increases with temperature, and therefore fluid-particle interaction is more significant, but, on the other, gas density decreases with temperature, which has an opposite effect on fluid-particle interaction (Ye et al., 1992).

The influence of olivine bed mass was analyzed by using two beds made up of 100 and 250 g (Figure 3.3). It should be noted that the results obtained for a bed of 150 g are not presented as they were very similar to those obtained for a bed of 100 g, for both minimum and fountain enhanced spouting velocities. This fact is explained by the limited effect of static bed height on the minimum spouting velocity when using nonporous draft tubes (Luo et al., 2004), especially when bed height is significantly above the entrainment zone (Altzibar et al., 2013b), as it was the case in this study. However, an increase in olive mass to 250 g led to an increase in both the minimum

and the fountain enhanced spouting velocities, with the increase being especially remarkable for the fountain enhanced velocity. This increase is explained by the fact that the bed height for 250 g of olivine was above the upper end of the draft tube (85 mm), which was not the case for the masses of 150 and 100 g. When the upper bed surface is significantly above the draft tube, particle circulation from the annulus into the spout occurs in the section above the draft tube, and the particles ascending in the spout collide with those incorporating in this upper section. All this phenomena are especially evident in the fountain enhanced spouting regime and lead to an increase in the velocity required for this regime.

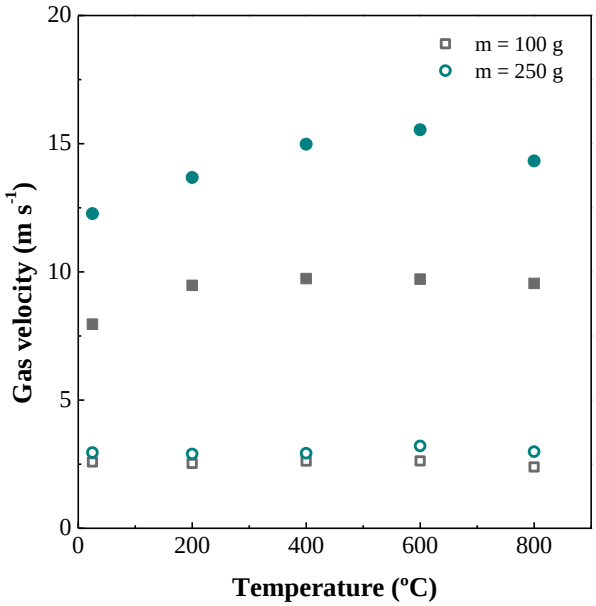

Figure 3.3. Effect of olivine bed mass on the minimum spouting (empty points) and fountain enhanced spouting (solid points) velocities. D_0, 8 mm; D_T, 10 mm; d_p, 250-355 μm and L_H 15 mm.

3.1.2. Influence of the draft tube design

Figure 3.4 shows the influence of the height of the draft tube entrainment zone on the minimum and fountain enhanced spouting velocities. As expected, an increase in this parameter caused an increase in the minimum spouting velocity, as reported by several authors (Ishikura et al., 2003; Luo et al., 2004; Neto et al., 2008; Makibar et al., 2012; Altzibar et al., 2013b). Thus, an increase in the entrainment zone height led to an increase in the solid incorporation from the annulus into the spout region, and therefore a higher solid circulation rate. Furthermore, this fact caused a higher pressure drop in the spout, which also modified the gas distribution between spout and the annulus, promoting the gas percolation into the annulus.

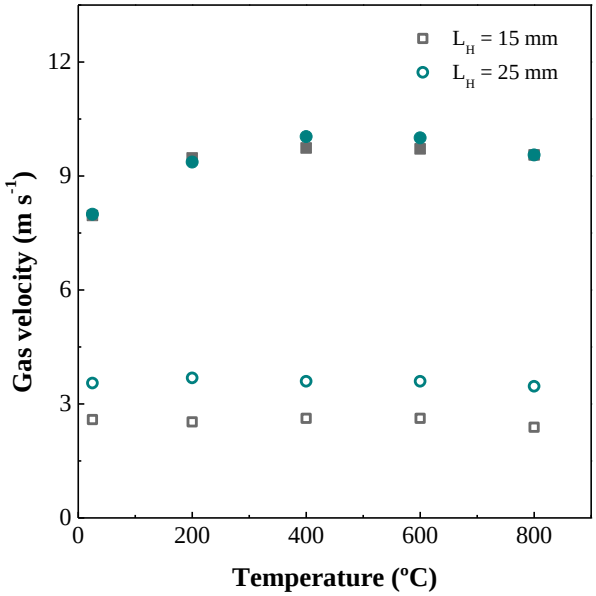

Figure 3.4. Effect of the height of the draft tube entrainment zone on the minimum spouting (empty points) and fountain enhanced spouting (solid points) velocities. D_0, 8 mm; D_T, 10 mm; olivine mass, 100 g and d_p 250-355 μm.

Nevertheless, a change in the height of the draft tube entrainment zone from 15 mm to 25 mm affected the velocity required for the fountain enhanced spouting regime. As mentioned above, an increase in this height promoted solid incorporation in the spouting regime, but the same result was also attained when spouting velocity was increased (Ishikura et al., 2003; Luo et al., 2004; Da Rosa and Freire, 2009; Shuyan et al., 2010; Nagashima et al., 2013). Given that the gas velocity required for the fountain enhanced spouting regime is much higher than for minimum spouting, it seems that the solid circulation rate and regime attained are mainly due to this high velocity in the range of entrainment zone heights used. There is surely a minimum value for the entrainment height, below which velocity is not the prevailing parameter. An explanation for this behavior may be the remarkable Venturi effect generated in the spout at the bottom of the contactor, due to the high gas velocity. Thus, the low pressure at the bottom zone in the spout promotes solids incorporation, which allows attaining high circulation rates whenever the surface (height of entrainment) available for incorporation is above a given minimum value. Furthermore, it seems there is a preferential solid cross-flow at the very lower end of the entrainment zone, which was observed for conventional conical spouted beds without draft tube (San José et al., 1998b).

The results shown in Figure 3.5 allow analyzing the combined effect of the gas inlet and draft tube diameters. As observed in Figure 3.5, the draft tube is welded to a perforated cylindrical piece that determines the gas inlet diameter. Accordingly, the draft tube of 10 mm internal diameter is combined with a gas inlet diameter of 8 mm and the draft tube of 8 mm internal diameter with an inlet diameter of 5.5 mm. Smaller gas inlet diameters than draft tube diameters were selected in order to ensure spouting stability and avoid gas flow diversion into the annulus zone (outside the draft tube) in the form of bubbles (Makibar et al., 2012; Altzibar et al., 2013a). As observed in Figure 3.5 the reduction in draft tube/gas inlet diameters caused an increase in both the minimum and fountain enhanced spouting velocities for the two olivine particle sizes studied. The same qualitative effect on spouting velocity was observed by other authors for both the draft tube diameter (Ishikura et al., 2003; Zhao et al., 2006) and the

gas inlet diameter (Altzibar et al., 2013a). Interestingly, Nagashima et al. (1999) reported that draft tube diameter reduction not only increased gas velocity but also improved gas diversion into the annular region.

It should be noted that although higher gas velocities were registered for the narrower draft tube/gas inlet diameters, a reduction in draft tube diameter entails using lower gas flow rates. Thus, there was a reduction of around 40 % in the gas flow rate needed to achieve both minimum spouting and fountain enhanced spouting velocities when draft tubes with narrow gas inlet diameters are employed.

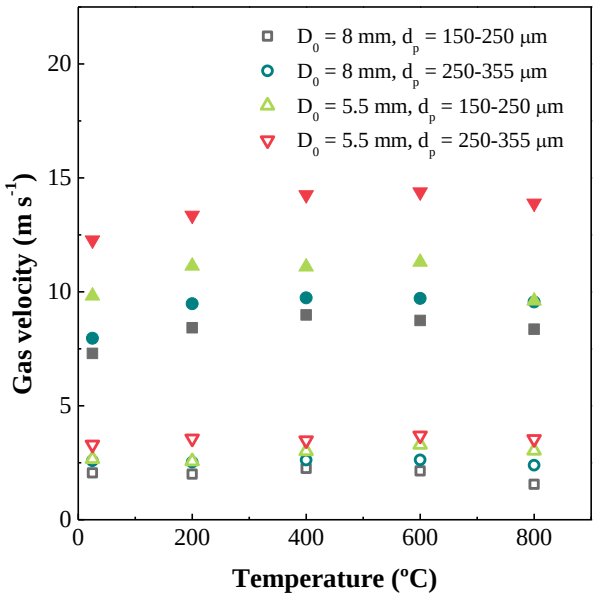

Figure 3.5. Effect of gas inlet diameter on the minimum spouting (empty points) and fountain enhanced spouting (solid points) velocities. L_H, 15 mm and olivine mass, 100 g.

3.2. TEMPERATURE PROFILES IN THE CONFINEMENT DEVICE

Temperature profiles in the gasifier greatly affect conversion, as they determine the extent of gasification and reforming reactions and, especially, tar cracking. The temperature in the spouted bed gasifier was measured at different heights, from the lower annulus region to the top of the confinement system. Furthermore, measurements were taken conducting the runs at different gas velocities, 1.2, 2.5 and 4 times the minimum spouting one. The lower velocity studied (1.2 times the minimum one) corresponded to the spouting regime and the top of the fountain reached the lower end of confinement device, in which temperature values were taken (T_3 in Figure 3.6). The highest velocity value studied (4 times the minimum one) corresponded the fountain enhanced spouting regime and the top of the fountain reached the upper end of the confiner, in which temperature values were taken (T_8 in Figure 3.6). Finally, operating with an u/u_{ms} ratio of 2.5 the fountain height reached approximately the position T_6. The aim of this study conducted at different velocities was to evaluate the effect fountain height has on the temperature profiles inside the fountain confiner.

As observed in Figure 3.6, temperature in the confinement region clearly increased with gas velocity, which is evidence that solid particles act as heat carrier and their circulation and the height reached are enhanced with gas velocity. The great temperature decrease at positions T_7 and T_8 was related to heat losses in the reactor upper section and the fact that the electric oven only provides heat up to the height of the gas outlet, between T_6 and T_7 (see Figure 3.6).

Numerous studies deal with the influence temperature has on biomass derived tar cracking and, although it is well-known that tar cracking strongly depends on the residence time and tar composition (Anis and Zainal, 2011; Mishra and Upadhyay, 2021), it is accepted that temperatures above 700 ºC are required to promote its effective cracking (Chen et al., 2009; Phuphuakrat et al., 2010; Tian et al., 2020) Accordingly, operation under fountain enhanced spouting regime increases the

effective volume in the fountain available for tar cracking reactions, as the high temperature zone is significantly increased.

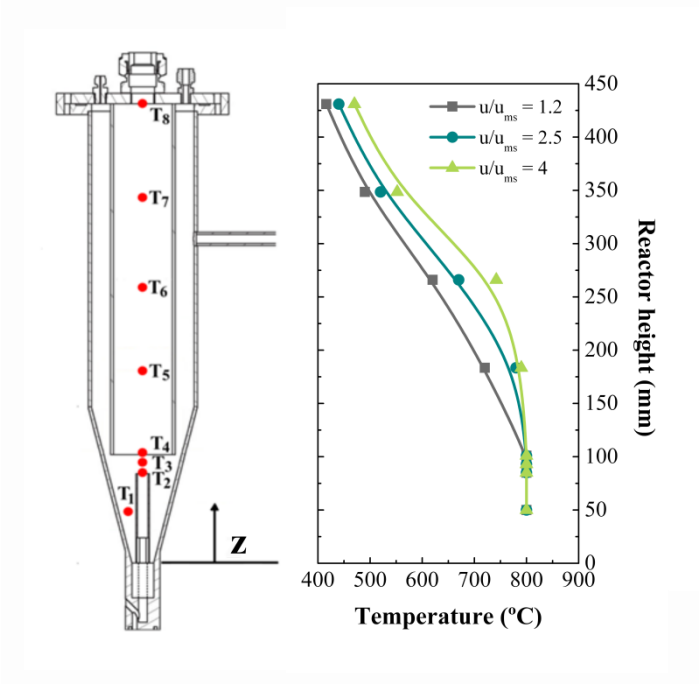

Figure 3.6. Vertical temperature profiles in the reactor operating at 800 ºC with different gas velocities, 1.2, 2.5 and 4 times u_{ms}.

3.3. STUDY ON FOUNTAIN VOIDAGE IN THE ENHANCED SPOUTING REGIME

In addition to temperature, the gas-solid contact between the tar compounds in the gaseous phase and the solid particles is also essential for an efficient tar cracking, as this contact promotes both the thermal and catalytic cracking. Accordingly, knowledge of fountain voidage in the fountain enhanced spouting regime is highly relevant.

The volume considered for voidage estimation was that from the bed surface to the top of the confinement device, i.e, the volume of the confiner plus the volume between the lower end of the device and the bed surface. Regarding the solid volume in the fountain region, it was determined based on the reduction of the annulus region height and the volume of particles located in the entrainment zone at the fixed bed condition, as described in Section 2.5.1.

The decrease in the annulus height observed from the fixed bed and to the enhanced fountain conditions was 1.8 cm (from 6 to 4.2 cm). This annulus volume reduction accounted for around 30 cm^3 of solid (approximately 48 % of the whole bed, i.e. 48 g of olivine). As the fountain region volume is 1000 cm^3 and considering olivine density, the average voidage in the fountain region is 0.98, which is of the same order as in the upper half in fast fluid beds (Kunii and Levenspiel, 1991). Furthermore, there are upward (in the fountain core) and downward (in the fountain periphery) circulation of both the gas and the solid, which means a countercurrent circulation of the ascending and descending fluid and the ascending and descending solid particles, with slip velocity being especially significant. Therefore, there is an efficient contact between the gas and the solid, which promotes high heat and mass transfer rates.

3.4. DISCUSSION

This thesis arises from the need to advance in the previous work conducted by Erkiaga (2014) on biomass steam gasification. She observed that although the use of primary catalysts and the optimization of the operating conditions (temperature, S/B ratio and particle diameter) improved the gasification process performance, tar content was still high. Thus, the reactor configuration was modified by inserting the fountain confiner with the aim of obtaining a syngas with lower tar amounts.

The incorporation of the fountain confiner in a conical spouted bed reactor pursued two key strategies, as are (i) increasing the residence time of the tars inside the reactor and (ii) increase their direct contact with heated bed materials. Previously, Gomez-Barea et al. (2013a) also put into practice the same strategies. Moreover, since this device was originally design to avoid particle entrainment when powders were used (Altzibar et al., 2017; Pablos et al., 2018), it allows operating with fine materials and increasing the u/u_{ms} ratio by modifying the hydrodynamic regime of the conventional spouted beds.

The development and characterization of the fountain enhanced regime carried out in this study are evidence of the potential of this new reactor configuration. The most influential parameter on the minimum spouting and fountain enhanced spouting velocities was particle size, with both regimes being stable even when operating with the finest particle size studied (90-150 μm). Furthermore, the effect of temperature was more remarkable on the fountain enhanced spouting velocity, i.e., it increased as temperature was raised to 400-600 ºC, but decreased for a further increase to 800 ºC. Regarding the height of the entrainment zone of the non-porous draft tube, it affected differently on the minimum spouting and on the fountain enhanced spouting velocities. Thus, an increase in this parameter caused an increase in the minimum spouting velocity, whereas it hardly affected the fountain enhanced spouting velocity. An increase in draft tube and gas inlet diameters caused the expected reduction in the velocity required for both regimes.

The results obtained in this chapter are encouraging for upcoming biomass steam gasification tests. The fountain enhanced regime allows greatly enlarging the fountain region, specially the height, as it improves the contact between reacting gases and the bed material due to the bed turbulence, increases the effective volume in the fountain available for tar cracking (temperature profile is more uniform) and narrows the residence time distribution. Use of fine particles, as well as narrow draft tube and gas inlet diameters allow reducing the gas flow rate at the same time as providing an excellent contact in the fountain region. In the words by Gil et al. (1999b) and Devi et al. (2003), both points are of great interest, since an increase in residence time promotes tar cracking. Moreover, the use of small particles also eases the adjustment of steam/biomass (S/B) ratio, which is consider a key parameter for process optimization, as steam is the fluidizing agent for the gasification process (Ahmad et al., 2016; Singh Siwal et al., 2020). It should be also highlighted that the enhanced fountain allows attaining a similar effect as the secondary air injection, i.e., it significantly raises the temperature in the upper section of the reactor. Secondary air injection in the freeboard was successfully employed bed by Narváez et al. (1996), Thamavithya et al. (2012) and Wang et al. (2019).

4

EFFECT OF THE FOUNTAIN CONFINER AND OPERATION REGIMES

Spouted beds are characterized by the short residence time of the gases which hinders tar conversion (Erkiaga et al., 2014), and therefore overall process efficiency (Gil et al., 1999b; Devi et al., 2003). In fact, tar in the syngas is the most challenging issue for the full scale development of biomass steam gasification (Anis and Zainal, 2011; Font Palma, 2013; Rakesh and Dasappa, 2018) because its causes severe operational problems, such as formation of aerosols, corrosion and clogging of pipes and process equipment. Primary or in situ tar elimination measures have been widely studied in the literature (Alauddin et al., 2010; Abdoulmoumine et al., 2015; Shahbaz et al., 2017; Narnaware and Panwar, 2021), with the most successful ones being the use of highly active catalysts and high temperatures combined with high residence times to promote catalytic or thermal tar cracking, respectively.

In order to improve the conical spouted bed performance for biomass gasification, different modifications were carried out following two of the guidelines proposed by Bridgwater et al. (1995), as are increasing the residence time and improving the contact between the gas and heat carrier particles. Therefore, it is clear that the hydrodynamic regime attained with the incorporation of a fountain confiner in the conical spouted bed reactor, as proved in Chapter 3, is suitable for achieving these objectives. The fountain confinement retains the gases generated during the gasification process, forcing them to describe a downwards trajectory. Thus, the advantages of the fountain enhanced regime compared to that of conventional spouting regime are checked in Chapter 4. They are worth mentioning the flexibility and stability of the spouting regime and the capability of increasing the fountain height in a controlled way in order to improve the contact between the reacting gases and the catalyst. Moreover, owing to the fountain confinement, the gas is forced to flow down to leave the confiner through its bottom, which increases the biomass derived volatile residence time in contact with the catalyst.

The main aim of this chapter is to assess the capability of the fountain confiner in a conical spouted bed reactor to lower tar formation in biomass steam gasification. The experiments were carried out in a bench scale plant described in Section 2.4 and the

experimental procedure followed is explained in Section 2.5 (Section 2.5.3.1). Although the main objective is to reduce the tar content, other process parameters are also analyzed. Thus, in Section 4.1 the reaction indices used are defined. Then, Section 4.2 explains the different spouting regimes and gas flow patternes developed in a spouted bed reactor. After that, Section 4.3 compares the performance of the hydrodynamic regimes described in Section 4.2 on biomass steam gasification, focusing on reaction indices in Section 4.3.1 and tar composition in Section 4.3.2. Moreover, a comparison with other biomass gasification technologies is made on Section 4.4. Finally, Section 4.5 discusses the most revelant results shown in Section 4.3.

4.1. REACTION INDICES

In order to quantify the process performance, the following reaction indices are defined:

- Gas yield (Y_{gas}, $Nm^3\ kg^{-1}$): It is defined by mass unit of biomass in the feed in the gasification process.

$$Y_{gas} = \frac{Q_{gas}}{m_0} \tag{4.1}$$

where Q_{gas} is the dry volumetric flow rate of the gas produced and m_0 is the mass flow rate of the biomass fed into the process.

- H_2 production (P_{H2}, wt%): It is defined by mass unit of the biomass in the feed and is calculated as follows:

$$P_{H_2} = \frac{m_{H_2}}{m_0} \cdot 100 \tag{4.2}$$

where m_{H2} and m_0 are the mass flow rates of H_2 produced and biomass in the feed, respectively.

- Tar concentration: It is defined as the amount of tar (in mass) per m^3 of dry syngas.

$$Tar\ content = \frac{m_{tar}}{Q_{gas}} \tag{4.3}$$

- Carbon conversion efficiency: It is defined as the ratio between the moles of C recovered in the gaseous product stream and those fed into the reactor.

$$X = \frac{C_{gas}}{C_{biomass}} \cdot 100 \tag{4.4}$$

4.2. STUDIED HYDRODYNAMIC REGIMES

Figure 4.1a shows schematically the solid and gas flow patterns in a conventional spouted bed. The role of the confinement is related not only to the modification of the solid behavior but also of the gas flow pattern (Figure 4.1b). Thus, the fountain confinement prevents the premature leaving of the gases at an initial stage in the biomass gasification and causes a downward gas flow inside the confiner. It is to note that biomass is fed in all cases from the top of the reactor, and therefore the volatiles in the conventional spouted bed gasifier leave immediately the reactor through the outlet located in the gasifier upper section (Figure 4.1a). This undesired situation leads to a short residence time of tars and other gaseous products and limits contact with the catalyst located in the conical section of the reactor. Thus, cracking and reforming reactions are hindered and lower conversion efficiencies are attained. On the other hand, when the reactor is equipped with the confiner and the biomass is fed within this device, the biomass derived volatiles cannot flow upwards, but the product stream must flow downwards to leave the confinement device, and then upwards through the shell between the confiner and the reactor wall (Figure 4.1b). Therefore, the gas circulation pattern attained with the fountain confiner not only increases the residence time of biomass derived gases but also improves the contact between the gaseous stream and the olivine.

Furthermore, the confined fountain leads to a highly stable hydrodynamic performance, which allows operating with finer materials and higher fountain heights. It also avoids the elutriation of bed material (Lopez et al., 2017; Pablos et al., 2020), and therefore a lower particle size olivine may be used with the same steam flow rate (and S/B ratio) as for bigger particles, which allows feeding a gaseous flow rate corresponding to a u/u_{ms} ratio of around 4, thereby attaining enhanced fountain regime (Altzibar et al., 2017; Tellabide et al., 2020b). This regime is characterized by a great bed expansion and turbulence, especially in the fountain region (see Figure 4.1c). These conditions favour a better contact between the gas phase and bed particles. In addition, biomass derived volatile residence time is increased and its distribution narrowed, which is a

key factor to promote tar elimination. Although the gas and solid flow patterns shown in Figure 4.1 are qualitative, the group is studying in depth the hydrodynamics in a larger cold unit with the aim of rigorously controlling the flow patterns of both the gaseous and the solid phases (Atxutegi et al., 2019; Tellabide et al., 2021a). Thus, it is observed that, under enhanced fountain regime conditions, the gas goes upwards preferably through the core of the fountain and goes downwards through the periphery (see the arrows in Figure 4.1c); that is, gas stream lines are associated with those of the particles.

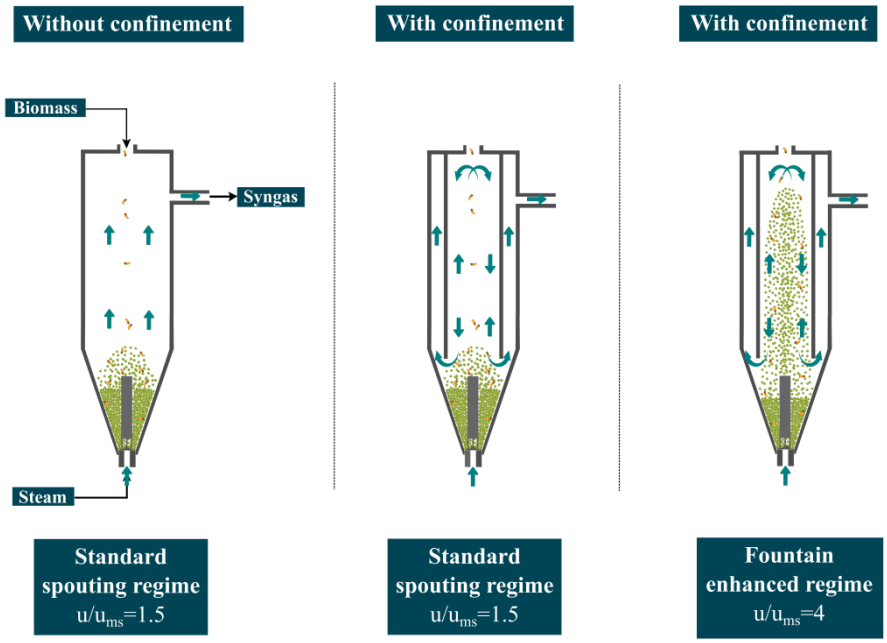

Figure 4.1. Different spouting regimes and gas/solid flow patterns developed in conical spouted beds: (a) standard spouting regime without fountain confiner, (b) standard spouting regime with fountain confinement and (c) enhanced fountain regime with fountain confinement.

A comparative study was carried out in order to evaluate the influence the fountain confinement device has on the efficiency of biomass steam gasification. Thus, experiments were conducted with and without the confinement system (Figures 4.1a

and 4.1b), at 850 ºC with the coarser olivine size (250-355 μm), using a u/u_{ms} ratio of 1.5, corresponding to standard spouting regime in both cases; that is, the same hydrodynamic conditions were used in both cases. Furthermore, in order to determine the influence the enhanced fountain regime has on the gasification process, the results under the mentioned conditions were compared with those obtained under enhanced fountain regime (Figure 4.1c). These results correspond to a relative velocity of 4 (u/u_{ms}= 4) and were obtained with the olivine whose particle size is in the 90-150 μm range. Thus, the experiments with the fountain confiner (Figures 4.1b and 4.1c) were performed under similar residence times (same reactor geometry and gas flow rate), so the differences in the gasification performance should be associated with the different gas-catalyst contact in the reactor, especially in the fountain region.

4.3. COMPARISON OF THE PERFORMANCE OF DIFFERENT HYDRODYNAMIC REGIMES ON BIOMASS GASIFICATION

4.3.1. Gasification performance

Figure 4.2 compares gas yield, H_2 production, tar content and carbon conversion efficiency results obtained for the three configurations described in Section 4.2. These indices are defined in Section 4.1.

As observed in Figure 4.2, all the process parameters were signicantly improved inserting the fountain confiner. The higher extent of steam reforming of tar and gaseous hydrocarbons entailed an increase in gas yield (Figure 4.2a) and hydrogen production (Figure 4.2b) and a decrease in tar concentration (Figure 4.2c). Thus, under convetional spouting regime gas and H_2 productions increased from 1.08 and 3.5 to 1.23 Nm^3 kg^{-1} and 4.5 wt% respectively due to the incorporation of the fountain confiner. Figure 4.3 illustrates the influence of the confinement system and spouting regime on product gas composition. Inserting the fountain confiner, H_2 concentration increased from 36.2 to 41.6 vol%, whereas that of CO decreased, and so the H_2/CO ratio increased from 1.09 to 1.4. The effect on CO_2 was less remarkable, although a slightly higher concentration was achieved operating with the fountain confiner. On the other hand, the concentration of methane and the other gaseous hydrocarbons decreased. These results clearly show a higher extent of steam reforming of methane (Eq. (1.8)) and tar (Eq. (1.3)) and water gas shift (Eq. (1.7)) reactions when the fountain confiner was used. These results are related to the increase in the gas residence time and the best contact of the gas with the catalyst attained when the fountain confiner was used.

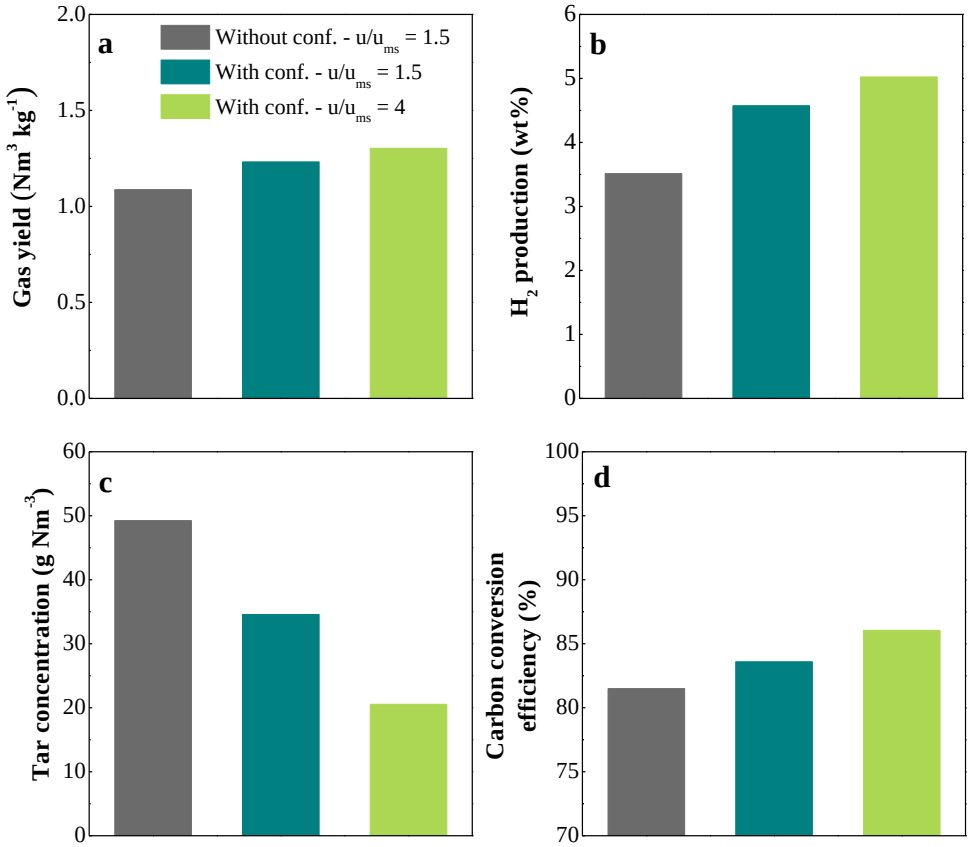

Figure 4.2. Influence of the confinement system and spouting regime on gas yield (a), H_2 production (b), tar concentration (on a dry basis) (c) and carbon conversion efficiency (d). Operating conditions: T, 850 ºC; S/B, 2; u/u_{ms}, 1.5 (4 for fountain enhanced regime); olivine particle diameter, 250-355 µm (90-150 µm for fountain enhanced regime).

It is to note that the incorporation of the fountain confiner caused a decrease in tar content in the syngas (Figure 4.3c). Thus, the tar content was of 49.2 g Nm^{-3} without fountain confiner, but decreased to 34.6 g Nm^{-3} when this device was inserted. These results were of the same order as those reported by Erkiaga et al. (2013b) for biomass steam gasification in a conical spouted bed reactor of slightly lower scale using olivine

and γ-alumina as primary catalysts at 900 ºC. The lower tar content values obtained in the latter, 30.1 and 22.4 g Nm^{-3}, respectively for olivine and γ-alumina, were explained by the higher temperature favouring tar elimination (Carpenter et al., 2010; Göransson et al., 2011; Koppatz et al., 2011; Erkiaga et al., 2014; Xiao et al., 2020; Cao et al., 2021a).

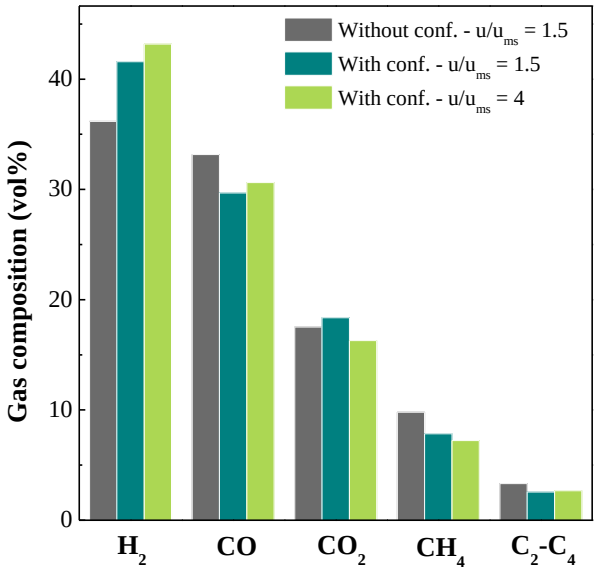

Figure 4.3. Influence of the confinement system and spouting regime on gas composition. Operating conditions: T, 850 ºC; S/B, 2; u/u_{ms}, 1.5 (4 for fountain enhanced regime); olivine particle diameter, 250-355 μm (90-150 μm for fountain enhanced regime).

The carbon conversion efficiency also increased when the confinement system was used (Figure 4.2d), i.e., a value of 83.6 % was attained instead of 81.5 % without this system. These values were slightly higher than those reported by other authors in fluidized bed reactors under similar conditions (Franco et al., 2003; Carpenter et al., 2010; Berdugo Vilches et al., 2016). However, Berdugo Vilches et al. (2016) used a fluidized bed reactor operating at 850 ºC with bauxite as the optimum primary catalyst, and they reached a value of 85 %. Niu et al. (2017) obtained a remarkably high carbon

conversion efficiency value (87.6 %) at 850 ºC in a downdraft gasifier, and Song et al. (2012) reached efficiency values of up to 90 % and , but in this case a dual bed was used, and consequently char fraction was burned.

It should be noted that the carbon conversion efficiency improvement using the fountain confiner is mainly related to tar elimination, given that similar char yields were obtained with and without confiner, 6.5 and 6.2 wt%, respectively. The char values reported in the literature on biomass steam gasification vary in a wide range given that it depends on gasification conditions, biomass composition and reactor design (Di Blasi, 2009). In fact, heterogeneous char gasification (Eqs. (1.9) and (1.10)) is a slow process even at 900 ºC, and therefore it is the limiting step in biomass gasification kinetics (Gómez-Barea and Leckner, 2010; Bryan Woodruff and Weimer, 2013; Lopez et al., 2016; Cortazar et al., 2020). Accordingly, char yield strongly depends on its residence time in the gasifier. Thus, different authors obtained char yields of around 10 wt% using different reactor designs (Gil et al., 1999b; Carpenter et al., 2010; Umeki et al., 2010; Rapagnà et al., 2018), but values well below than those obtained in this study, between 2 and 4 wt%, were also reported in fluidized beds (Michel et al., 2011b) and free fall reactors (Wei et al., 2007).

These results evidence the interest of the fountain confiner for the biomass gasification process, given that the use of this simple device improved biomass derived volatile residence time and the contact of the gas with the catalyst, and therefore enhanced biomass conversion efficiency and reduced the tar content in the syngas.

The aforementioned results were improved under fountain enhanced regime by decreasing olivine particle size and increasing the fountain height. The most significant effect of the operation under enhanced fountain regime was the increase in H_2 production to 5.0 wt% (Figure 4.2b), which corresponded to a H_2 concentration of 43.2 vol%. This result reveals the potential of this regime for the production of a H_2-rich syngas. Koppatz et al. (2011) reported a H_2 production of 4.2 wt% in a dual fluidized bed reactor operating at 850 ºC using olivine as primary catalyst. In the same line, Michel et al. (2011a) obtained a H_2 production of 4.9 wt% in a fluidized bed with

olivine bed at 860 ºC. In addition, higher values, in the range from 6.5 to 7.3 wt%, were obtained in fluidized beds using Fe and Ni modified olivine catalysts (Michel et al., 2011b; Rapagnà et al., 2011). Recently, pyrolysis and in-line reforming has been proposed as a direct route for H_2 production from biomass and other solid wastes (Barbarias et al., 2016; Lopez et al., 2018; Santamaria et al., 2021) with some H_2 productions reported being above 10 wt% (Xiao et al., 2013; Arregi et al., 2017; Santamaria et al., 2020a; Fernandez et al., 2022).

However, the effect the olivine particle size reduction and fountain height increase (fountain enhanced regime) had on the gas composition was rather limited (Figure 4.3). In the same line, Koppatz et al. (2012) studied the influence the particle size reduction had on the performance of a dual fluidized bed gasifier. Thus, in spite of the improvement in the turbulence and gas-solid contact by increasing u/u_{mf}, the influence on gas composition was limited.

It is also especially remarkable the reduction of tar content in the gas from 34.6 g Nm^{-3} under conventional spouting regime to 20.6 g Nm^{-3} under enhanced fountain regime (Figure 4.2c). This result is associated with the improvement in the gas-catalyst contact and heat transfer rates in the fountain region due to the higher fountain height. In addition, the reduction in olivine particle size also improved the catalyst surface area available for cracking and reforming reactions. In fact, the catalytic activity of olivine is related to Fe content on its external surface (Devi et al., 2005a; Tursun et al., 2019). It is to note that the same effect was observed by Koppatz et al. (2012) and Kern et al. (2013a) by reducing the bed material particle size in the steam gasification of biomass and lignite, respectively, in a dual fluidized bed gasifier. Thus, particle size reduction favoured bed turbulence, heat transfer rates, gas-solid contact, and therefore tar elimination and conversion efficiency.

4.3.2. Tar composition

According to the criteria used by several researchers, the tar fraction accounts for hydrocarbons heavier than benzene (Devi et al., 2005b; Neeft et al., 2008; Rabou et al., 2009; Anis and Zainal, 2011; Narnaware and Panwar, 2021; Ruivo et al., 2021). Although different classifications for tar are found in the literature, in this thesis the criteria proposed by Rabou et al. (2009) was followed, i.e, the following tar fractions were considered: i) light aromatics, which are single-ring light compounds, such as toluene; ii) heterocyclic compounds, which are those made up of aromatic rings containing heteroatoms, such as phenol; iii) light polyaromatics (PAHs), which are two- or three-ring aromatic compounds, such as naphthalene and iv) heavy PAHs, with more than three rings, such as pyrene. In fact, tar composition, rather than total tar content, is the key factor for the application of the gaseous product stream. Heavy components, especially PAHs, are responsible for fouling and soot formation in pipes and gas engines, given that their low dew points cause condensation at concentrations below 1 mg Nm^{-3} (Anis and Zainal, 2011).

The effect of using fountain confiner and fountain enhanced regime on the tar fractions is shown in Figure 4.4. Moreover, Table 4.1 provides a detailed composition of the tar for the different reactor configurations and spouting regimes. As observed in Figure 4.4, all the tar fractions in the gas were reduced using fountain confiner, with this reduction being especially significant for heavy PAHs and less significant for light aromatics. In fact, the mass fraction of heavy PAHs was reduced from 31.75 to 21.85 wt%, whereas those of light PAHs and light aromatics increased from 47.38 and 10.25 to 52.05 and 12.83 wt%, respectively (see Table 4.1). These results were improved under fountain enhanced regime, which favoured the reduction of the content of all tar fractions, especially that of most problematic ones. The concentration of heavy PAH compounds decreased even more under fountain enhanced regime (to 10.19 wt%), which was one third of that obtained under conventional spouting regime. Other facts to be noted were the reduction in fluoranthrene concentration (to 5.15 wt%), which was due to the cracking of heavy compounds, and the increase in the concentration of light

polyaromatics (main fraction) in the 47.38-62.08 wt% range, which was explained by the better gas-solid contact. Naphthalene was the most abundant compound in all the configurations. Concerning the content of light aromatic and heterocyclic fractions, it seems they slightly increased in the 10.25-14.22 wt% and 9.50-10.33 wt% ranges, respectively.

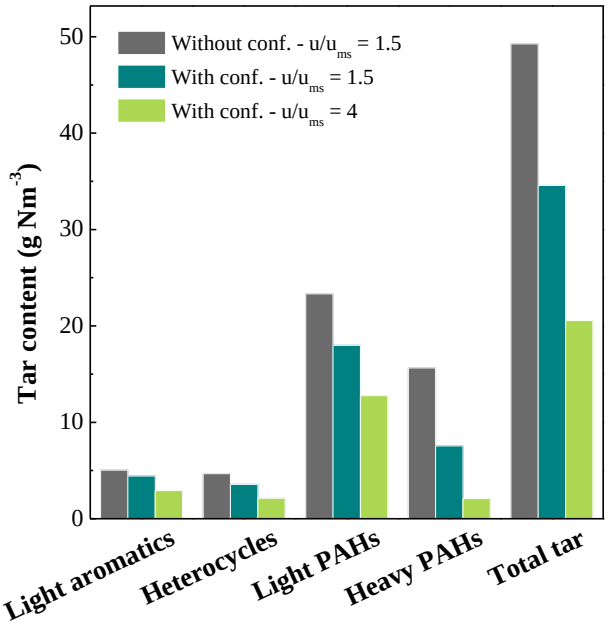

Figure 4.4. Influence of the confinement system and spouting regime on the tar composition. Operating conditions: T, 850 ºC; S/B, 2; u/u$_{ms}$, 1.5 (4 for fountain enhanced regime); olivine particle diameter, 250-355 µm (90-150 µm for fountain enhanced regime).

Table 4.1. Detailed tar composition (wt%) for the different reactor configurations and spouting regimes.

	Without conf. $u/u_{ms}=1.5$	**With conf.** $u/u_{ms}=1.5$	**With conf.** $u/u_{ms}=4$
Light aromatics	**10.25**	**12.83**	**14.22**
Toluene	10.25	12.83	14.22
Heterocycles	**9.50**	**10.31**	**10.33**
Phenol	2.41	3.63	3.16
Methyl phenol	7.09	6.68	7.17
Light PAHs	**47.38**	**52.05**	**62.08**
Indene	0.00	0.00	0.78
Naphthalene	21.45	24.10	32.40
1-Methyl naphthalene	0.00	1.49	1.57
2-Methyl naphthalene	1.01	1.31	1.47
Biphenyl	0.73	1.00	0.85
Acenapthene	0.00	0.00	0.00
Biphenylene	6.44	5.91	7.00
Dibenzofuran	0.46	1.79	3.58
Fluorene	1.46	1.87	1.96
1-H-Phenalene	2.74	2.65	2.69
Anthracene	8.78	7.78	6.28
Phenanthrene	2.97	2.28	1.16
9-Methyl anthracene	0.00	0.00	2.35

Table 4.1. Continued

	Without conf. $u/u_{ms}=1.5$	**With conf.** $u/u_{ms}=1.5$	**With conf.** $u/u_{ms}=4$
2-Phenyl naphthalene	1.02	1.88	0.00
Heavy PAHs	**31.75**	**21.85**	**10.19**
Pyrene	9.73	6.48	3.92
Fluoranthrene	19.57	13.48	5.15
4H-Cyclopenta[def]phenanthrene	2.45	1.88	1.12

4.4. COMPARISON WITH OTHER BIOMASS GASIFICATION TECHNOLOGIES

Table 4.2 compares the aforementioned results obtained in this chapter with those from the literature in other biomass gasification technologies under similar conditions. It should be highlighted that tar yield strongly depends on operating conditions, catalyst, gasifying agent and reactor configuration (Anis and Zainal, 2011; Ahmad et al., 2016; Rakesh and Dasappa, 2018; Narnaware and Panwar, 2021). Furthermore, the different tar sampling techniques and tar definitions make difficult a comparison of the results from the literature. Thus, the usual tar contents in the syngas obtained in fine tuned bubbling and dual fluidized beds are in the 10 to 40 g Nm^{-3} range (Xie et al., 2010; Göransson et al., 2011; Fremaux et al., 2015; Zhang and Pang, 2017; Ahlström et al., 2019), although higher (Gil et al., 1999b; Berdugo Vilches et al., 2016) and lower (Rapagnà et al., 2000; Tursun et al., 2019; Valin et al., 2020; Cao et al., 2021a) results were also reported. It should be noted that the tar yields reported in downdraft gasifiers are lower than those obtained in fluidized beds and spouted beds (Susastriawan et al., 2017), whereas the opposite is true in updraft gasifiers (Umeki et al., 2010; Aljbour and Kawamoto, 2013).

Table 4.2. Comparison of gas yields, H_2 productions, tar contents and carbon conversion efficiencies obtained in the biomass steam gasification in different technologies ([a] S/C ratio (molar), [b]expressed on a dry and ash free basis).

Reference	Reactor	Feed	Temperature (ºC)	S/B ratio	Catalyst/bed material	Gas yield (m^3 kg^{-1})	H_2 production (wt.%)	Tar content (g Nm^{-3})	Carbon conversion efficiency (%)
This study	Spouted bed	Pine wood	850	2	Olivine	1.09	3.51	49.2	81.5
This study	Fountain confined spouted bed	Pine wood	850	2	Olivine	1.23	4.57	34.6	83.6
This study	Enhanced fountain spouted bed	Pine wood	850	2	Olivine	1.30	5.03	20.6	86.1
Rapagnà et al. (2018)	Bubbling fluidized bed	Almond shells	820	0.72	Olivine (0.9)/dolomite (0.1)	1.58[b]	7.3[b]	2.13	-
Niu et al. (2017)	Downdraft	Pine wood	850	-	-	1.4	6.2	-	87.6
Zhang et al. (2017)	Dual fluidized bed	Pine wood pellets	820	2	Silica sand	0.82[b]	1.8[b]	10.3	-
Schweitzer et al. (2018)	Dual fluidized bed	Sewage sludge	820	1.5[a]	Silica sand	0.85[b]	3.6	122	-
Fremaux et al. (2015)	Fluidized bed	Waste wood	900	1	Silica sand	1.22	5.9	12.5	-
Koppatz et al. (2011)	Dual fluidized bed	Wood pellets	850	1.1	Olivine	1.13	4.2	10	-
Goransson et al. (2011)	Dual fluidized bed	Wood pellets	850	0.9	Silica sand	-	-	10	-
Michel et al. (2011a)	Fluidized bed	Miscathus giganteus	860	1	Olivine	1.2[b]	4.9	-	-

Table 4.2. Continued.

Reference	Reactor	Feed	Temperature (°C)	S/B ratio	Catalyst/bed material	Gas yield ($m^3\ kg^{-1}$)	H_2 production (wt.%)	Tar content ($g\ Nm^{-3}$)	Carbon conversion efficiency (%)
Tursun et al. (2019)	Decoupled triple bed	Pine sawdust	850	0.65	Olivine	1.07	3.62	7.3	-
Cao et al. (2021a)	Fluidized bed	Pine sawdust	850	1.2	Olivine	1.4	6.28	4.27	-
Valin et al. (2020)	Fluidized bed	Bark	850	0.88[a]	Olivine	1.22	4.91	2.3	75
Ahlström et al. (2019)	Dual fluidized bed	Pine wood pellets	870	0.61	Olivine	1.23	4.39	20.05	87
Berdugo-Vilches et al. (2016)	Dual fluidized bed	Wood pellets	815	0.84	Olivine	0.76[b]	2.2	44	-
Song et al. (2012)	Dual spout-fluidized bed	Pine wood	820	1.2	Silica sand	1.4	4.3	8	-
Aljbour et al. (2013)	Updraft	Cedar wood	850	1.5[a]	-	2.2	11	-	-
Wei et al. (2006)	Moving bed	Pine wood	800	0.35	-	0.83[b]	3	4	-
Xiao et al. (2020)	Dual loop gasifier	Pine sawdust and bituminous coal	850	0.63	Olivine	1.0	3.75	11.0	63

4.5. DISCUSSION

In this chapter, the advantages of inserting a fountain confiner in conical spouted bed reactor were evaluated. Other authors also modified their reactor design in order to improve the gasification process efficiency and tested the modified configurations under gasification conditions (Gómez-Barea et al., 2013a; Benedikt et al., 2017; Savuto et al., 2019; Kurkela et al., 2021).

The fountain confiner enhanced the efficiency of biomass gasification by favouring tar conversion. Thus, at 850 ºC, tar content was reduced from 49.2 g Nm^{-3} without confiner to 34.6 g Nm^{-3} when this device was used. The gas and H_2 productions and carbon conversion efficiencies were also remarkably improved. Moreover, small olivine particle sizes allowed operating under enhanced fountain regime, whose features are large fountain and high bed turbulence. These features allowed a better contact between olivine and the gases and, moreover, the olivine external surface available for catalytic reactions was enhanced. Thus, tar content in the gas product was reduced to 20.6 g Nm^{-3}. According to Koppatz et al. (2012) and Kern et al. (2013a), particle size reduction improved bed turbulence, heat transfer rates, gas-solid contact, and consequently tar elimination and conversion efficiency. Tar composition was also affected by operating under enhanced fountain regime. Interestingly, the presence of heavy PAHs was significantly reduced, whereas that of light PAHs and light aromatics increased. In the same line, other reaction indices, such as gas and H_2 productions were also improved when operating under enhanced fountain regime, with their values being 1.3 Nm^3 kg^{-1} and 5.0 wt%, respectively. Likewise, Benedikt et al. (2017) proposed an advanced design of their DFB reactor following similar strategies as taken for the development of the fountain enhanced spouted bed. They designed the upper part of the gasifier as a countercurrent column equipped with constrictions. Thus, turbulent fluidized bed zones were created in order to increase the interaction between the bed material and the product gas at the same time as attain higher temperatures. Their results showed that the new configuration led to a product gas with remarkably lower tar values of around 78 %.

These results clearly remark the effect of inserting a fountain confiner in conical spouted beds for gasification processes. Conical spouted bed reactors under fountain enhanced regime allow achieving results within the range of those corresponding to other technologies (Göransson et al., 2011; Ahlström et al., 2019; Valin et al., 2020; Cao et al., 2021a); that is, they significantly improve biomass conversion efficiency towards a hydrogen rich syngas. Moreover, the highly stable nature of enhanced fountain regime ensures a highly versatile process with a vigorous solid circulation pattern, which is essential for handling primary catalysts and feedstocks of different texture, granulometry and moisture content. Therefore, this technology is suitable for co-valorising other raw materials, such as wastes from the consumer society (plastics and tyres).

5

ROLE OF TEMPERATURE IN THE GASIFICATION PROCESS EFFICIENCY

Tar removal strategies have been extensively developed for obtaining a syngas with very low tar content. Overall, these stretegies may be classified into two groups, depending where tar is removed: in situ (or primary) methods, and post-gasification (or secondary) methods. Among the primary methods, the first measure adopted usually involves the design of the gasifier (addressed in Chapter 4), the optimization of the operating conditions and the use of in situ catalysts.

Among the operating conditions, temperature has a great impact on the overall kinetics of the gasification process since it can control the tar concentration in the product gas. In fact, controlling the temperature inside the reactor is necessary for enhancing process performance. This chapter addresses the effect of temperature on steam gasification of biomass in a bench scale unit fitted with a fountain confined spouted bed operating in continuous mode, whose scheme is shown in Figure 2.2. A detailed description of the plant and operating procedure are shown in Section 2.4 and 2.5 respectively. The temperature effect was studied in the 800-900 ºC range and its influence was determined on gasification performance (gas and H_2 productions, gas composition and tar content) as approaches the Section 5.1. Moreover, Section 5.2 analyzes the influence temperature has on tar composition which includes a detailed characterization. Thus, Section 5.2.1 deals with Fourier transform infrared spectroscopy (FTIR), Section 5.2.2 with gas chromatography coupled with mass spectrometry (GC/MS) and Section 5.2.3 with simulated distillation. Finally, the most significant results are discussed in Section 5.3.

5.1. EFFECT OF TEMPERATURE ON GASIFICATION PERFORMANCE

Temperature has a great impact on the overall kinetics of the gasification process, and must therefore be carefully controlled in order to improve gasification performance. Understanding the effect of temperature requires considering the main reaction steps involving biomass steam gasification as described in Chapter 1. The selection of temperature and the use of an in situ catalyst, such as olivine, enhance these reactions and condition the gas composition.

Figure 5.1 shows the influence temperature has on tar concentration, char yield, carbon efficiency and gas and hydrogen production, which are the parameters defining the efficiency of the gasification process. These indices are defined in Section 4.1. An increase in temperature led to larger productions of syngas and hydrogen (Figures 5a and 5b, respectively) due to the promotion of pyrolysis, gasification and reforming reactions (Eqs. (1.1-1.11)). Acordingly, the gas yield and H_2 production increased from 0.98 Nm^3 kg^{-1} and 2.9 wt% at 800 ºC to 1.65 Nm^3 kg^{-1} and 7.3 wt% at 900 ºC, respectively. Moreover, these results are supported by the amount of reacted water during the gasification, which increased from 7.72 wt% at 800 ºC to 34.68 wt% at 900 ºC. As the reaction temperature was higher, the amount of steam reacted was greater; that is, a larger amount of steam was involved in the WGS and reforming reactions, and gas and hydrogen productions were therefore enhanced.

Figure 5.2 illustrates the composition of the gases formed at different temperatures (800, 850, 900 ºC) for a steam/biomass (S/B) ratio of 2. As observed, an increase in temperature led to higher hydrogen content in the gaseous stream. Thus, hydrogen concentration increased from 33.6 vol% at 800 ºC to 49.6 vol% at 900 ºC. The concentration of CO decreased by increasing temperature due to WGS promotion, whereas the effect of temperature on CO_2 was almost negligible (only increased from 17.2 to 19.3 vol% in this range). Interestingly, the H_2/CO ratio of the syngas remarkably increased from 0.98 to 2.05 in the temperature range studied, which is

highly relevant for using this gas in the synthesis of hydrocarbons (Fischer–Tropsch) or oxygenates (methanol or dimethyl ether). Wei et al. (2007) reported that the inorganic species in the char have a positive catalytic effect on the WGS reaction (Eq. (1.7)) at high temperatures. The concentration of methane and heavier hydrocarbons (C_2-C_4) decreased as temperature was raised due to the enhancement of hydrocarbon reforming reactions (Eq. (1.8)). These trends agree quite well with the results reported by other authors for the steam gasification of biomass (Franco et al., 2003; Wei et al., 2007; Koppatz et al., 2011; Cao et al., 2021a).

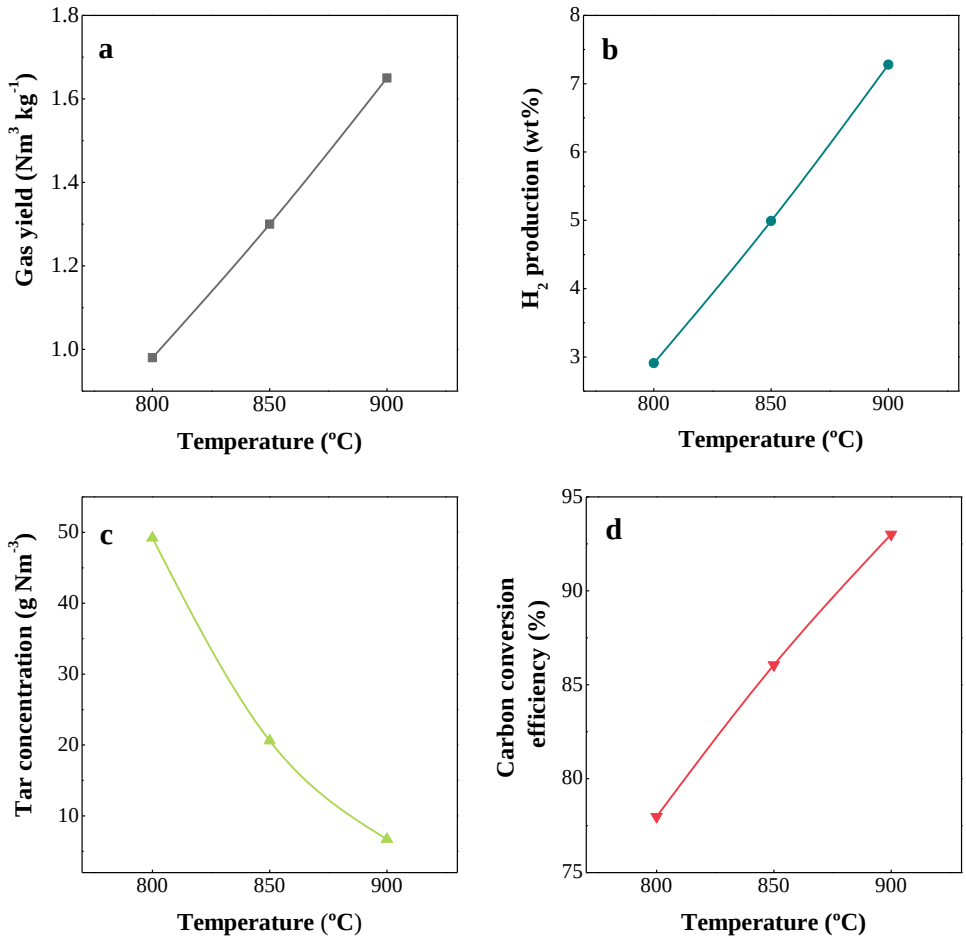

Figure 5.1. Effect of gasification temperature on gas (a) and hydrogen production (b), tar concentration (c) and carbon conversion efficiency (d).

Franco et al. (2003), Wei et al (2007) and Koppatz et al. (2011) also remarked higher H_2 and lower CO and CH_4 concentrations in the gaseous product when gasification temperature was increased. Berrueco et al. (2014a) and Sui et al. (2020) also obtained similar results in the air gasification. Conversely, Mayerhofer et al. (2012) obtained a higher CO content by increasing temperature due to the influence of char gasification reactions (Eqs. (1.10) and (1.11)).

Consequently, an increase in the gasification temperature reduced significantly the tar concentration, from 49.2 g Nm^{-3} at 800 ºC to 6.7 g Nm^{-3} at 900 ºC (Figure 5.1c). Likewise, char yield was also reduced by increasing temperature from 9.0 wt% at 800 ºC to 3.2 wt% at 900 ºC. Consequently, carbon conversion efficiency (Figure 5.1d) increased from 78 % at 800 ºC to 93 % at 900 ºC.

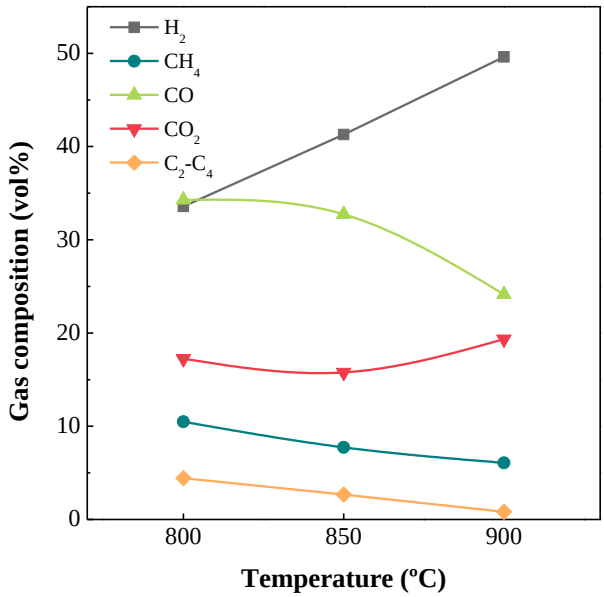

Figure 5.2. Effect of gasification temperature on the gas composition in the 800-900 ºC temperature range.

It is noteworthy that the overall gasification efficiency was greatly improved by using the fountain confiner with draft tube and operating under the fountain enhanced

spouting regime in the CSBR. In fact, Erkiaga et al. (2013b) performed the biomass gasification with olivine in a CSBR, but without these new modifications, and they attained a tar content of 30.1 g Nm^{-3} at 900 ºC. These authors studied the effect of temperature in the 800-900 ºC range with sand instead of olivine (Erkiaga et al., 2014). The tar content was reduced from 364 g Nm^{-3} at 800 ºC to 142 g Nm^{-3} at 900 ºC and the char yield from 8.9 to 4.5 wt%, respectively, which meant an increase in carbon conversion efficiency from 50 to 70 % (the value attained in this study was 93 %). In addition, the gas yield and H_2 production increased from 0.73 Nm^3 kg^{-1} and 1.8 wt% at 800 ºC to 0.96 Nm^3 kg^{-1} and 3.3 wt% at 900 ºC, respectively (the values obtained in this study at 900 ºC were 1.65 Nm^3 kg^{-1} and 7.3 wt%, respectively). The fountain confinement not only modifies the residence time distribution of the reactor, but also allows operating stably with high fountains (this circumstance is attained using fine materials), and there is therefore a great bed expansion and high turbulence. These hydrodynamic improvements described in detail in Chapter 3 promote the contact between olivine catalyst and tar compounds, thereby favouring tar elimination and H_2 production (Lopez et al., 2017; Cortazar et al., 2018).

The influence of temperature on product yields and gas composition was also studied with different gasification technologies and most of the authors agree that higher temperatures enhance these results (Michel et al., 2011a,b; Barisano et al., 2016; Niu et al., 2017; Cao et al., 2021a). Niu et al. (2017) used a downdraft gasifier and reported that the gas yield and hydrogen composition increased from 1.6 Nm^3 kg^{-1} and 5.0 wt%, at 850 ºC, to 2.7 Nm^3 kg^{-1} and 10.2 wt%, at 900 ºC, respectively. Michel et al. (2011b) operated in a fluidized bed reactor and obtained gas yields of 1 Nm^3 kg^{-1} at 800 ºC and 1.5 Nm^3 kg^{-1} at 900 ºC. In addition, they managed to produce 1.7 Nm^3 kg^{-1} of gas at 800 ºC by impregnating Ni to olivine and using it as a primary catalyst. The same authors reported (Michel et al., 2011a) lower char yields by increasing temperature in the 815-880 ºC range (from 3.6 to 2.7 wt%). In the same line, Barisano et al. (2016) managed to reduce the amount of char residue approximately by 70 % using an iron enriched olivine bed, which allowed them to reach 98 % carbon conversion in the

biomass steam/O_2 gasification process carried out in an internally circulating bubbling fluidized bed reactor.

Olivine is widely used as a primary catalyst in the biomass steam gasification due to its tar cracking activity and high attrition resistance. Several authors reported that olivine led to good results in tar abatement. Mayerhofer et al. (2012) studied the influence of temperature (750-850 ºC) on tar content in a fluidized bed made up of olivine and observed a reduction from 5.1 to 3.2 g Nm^{-3}. Kirnbauer et al. (2013), operating in a dual fluidized bed with olivine in the 750-870 ºC range, showed that tar content decreased from 7.8 to 4.5 g Nm^{-3}. Wei et al. (2006) used an externally circulating concurrent moving bed with olivine as bed material and reported a tar content of 0.6 g Nm^{-3} for the highest temperature (800 ºC). Carpenter et al. (2010) studied the influence of temperature (600-850 ºC) in the gasification of swichgrass in a fluidized bed reactor using olivine and observed that the amount of tar was reduced to one third, from 180 to 60 g Nm^{-3}. Rapagnà et al. (2000) also used a fluidized bed with olivine to study the effect of temperature in the 770-820 ºC range by gasifying almond and reported that tar was reduced from 6.1 to 0.5 g Nm^{-3}. Song et al. (2012) studied biomass steam gasification in a dual spout fluidized bed and obtained 8 g Nm^{-3} of tar at 820 ºC.

5.2. EFFECT OF TEMPERATURE ON TAR CHARACTERISTICS

5.2.1. FTIR analysis

The FTIR analysis allows detecting functional groups in the tars from biomass gasification, and therefore ascertaining their main chemical properties. Figure 5.3 shows the FTIR spectra of the tars obtained at different temperatures, whereas Table 5.1 summarizes the functional group assignment to the main absorption bands identified in these spectra (the numbers in Table 5.1 correspond to the different bands described in Figure 5.3). As observed in Figure 5.3, although there are differences in the absorbance corresponding to certain peaks, especially for the tar produced at 900 ºC, the spectra for the different temperatures were similar. The FTIR analysis revealed that the tars contained majorly a variety of aromatic compounds, together with aliphatic chains and oxygenated functional groups. A detailed description of the bands, and therefore the compounds contained in the tar, is as follows: The weak absorption band between 3700 and 3200 cm^{-1} (number 1 in Figure 5.3) corresponding to stretching vibrations of O-H bonds, is evidence of a limited presence of hydroxyl groups, such as phenols or alcohols. This band may also indicate the presence of water condensed and collected in the equipment itself. The band around 3050 cm^{-1} (2) is due to C-H stretching related to aromatic species, such as benzene or toluene (Montiano et al., 2015). Note that this band is less intense for the 900 ºC tar probably due to the severity of the gasification process at this temperature. The bands located in the 3000-2800 cm^{-1} range (3) correspond to aliphatic CH_2 and CH_3 groups (Michel et al., 2011a; Montiano et al., 2015). The small peaks in the 1780-1700 cm^{-1} region (4) are attributed to C=O stretching vibration from some oxygenated functionalities, such as carbonyl/carboxyl groups. The bands observed between 1650 and 1600 cm^{-1} (5) correspond to C=C stretching vibrations and reveal the presence of aromatics (Alvarez et al., 2017; Ordonez-Loza et al., 2021). According to Michel et al. (2011a), the stretching band close to 1600 cm^{-1} is very pronounced in the presence of phenol. Therefore, the absence of this band in the tar obtained at 900 ºC is evidence of a considerable

reduction in phenolic species. The peaks located between 1510 and 1450 cm^{-1} (6) suggest the presence of aromatic rings, whereas the peak at 1370 cm^{-1} (7) is assigned to CH_2 and CH_3 groups. The weak absorption bands between 1340 and at 1150 cm^{-1} (8) indicate the presence of syringyl units derived from lignin decomposition (Montiano et al., 2015; Lazzari et al., 2018). The absorption band at 1020 cm^{-1} (9) indicates again the presence of hydroxyl groups (Wang et al., 2014). Finally, the region between 900 and 675 cm^{-1} (10) corresponds to the C-H out-of-plane bending peaks derived from aromatic compounds (Alvarez et al., 2017). Besides, the bands at 690 and 820 cm^{-1} reveal the presence of aromatic mono-substitution, as is the case of phenol (at 900 ºC does not appear), whereas the presence of a band at 738 cm^{-1} is due to major aromatic bi-substitution (Michel et al., 2011a). Sun and Zhang (2017) ascribes the two absorption bands at about 815 and 750 cm^{-1} to systems containing 1,4-subsituted and 1,2-disubstituted aromatics, respectively.

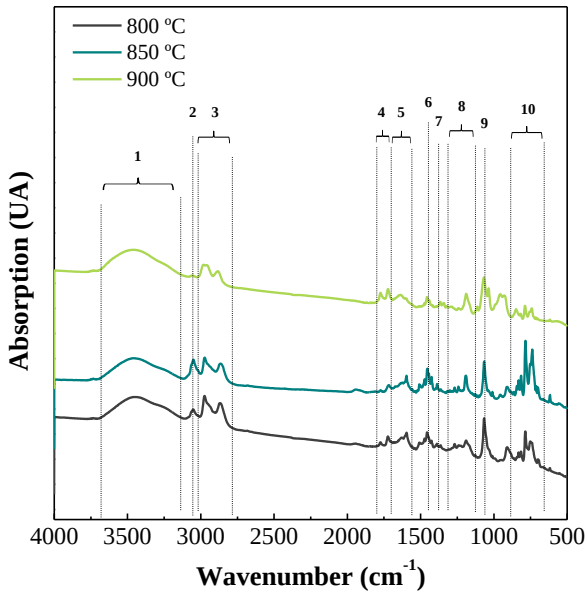

Figure 5.3. FTIR spectra of the tars obtained at 800, 850 and 900 ºC.

Table 5.1. Assignment of FTIR bands to functional groups and the corresponding tar compounds.

Band	Frequency range (cm^{-1})	Functional group	Type of compound
1	3700-3200	O-H stretching	Phenols, alcohols or water
2	3050	C-H stretching	Aromatic
3	3000-2700	C-H stretching	Alkanes
4	1750-1675	C=O	Carbonyl/Carboxyl
5	1650-1600	C=C stretching	Aromatic
6	1510-1450	C=C stretching (in ring)	Aromatic
7	1370	$-CH_2-$ or $-CH_3$	Alkanes
8	1340-1150	C–H and C-O stretching	Syringyl rings
9	1020	O-H stretching	Phenols
10	900-700	C-H out of plane blending	Aromatic

5.2.2. Chromatographic analysis

Figure 5.4 shows the influence temperature has on tar composition and Table 5.2 a detailed identification of tar compounds based on in-line GC and GC/MS analysis. Figure 5.4a reveals that the fraction of light PAHs increased sharply to 71.35 wt% at 900 ºC, but that of light aromatic compounds decreased from 15.35 wt% at 800 ºC to 2.49 wt% at 900 ºC, with no heterocyclic compounds at this temperature. Note that, although the concentration of the heavy PAH fraction passed through a minimum as temperature was raised, the yield of this fraction decreased at high temperatures due to

lower content of the total tar concentration (Figure 5.4b). Figure 5.4 allows concluding that light PAHs were the prevailing compounds in the tar.

Regarding the concentration of the individual compounds in the tar, Table 5.2 shows that tar composition shifted from phenolic compounds and alkyl-substituted PAHs to non-substituted PAHs (more stable species) as gasification temperature was increased. Thus, the concentration of phenol, 1-methyl phenol and other light PAH species (indene, 1-methyl naphthalene, biphenyl and acenapthene) decreased with temperature, whereas non-substituted and more stable compounds, such as naphthalene, anthracene or fluoranthene increased with temperature. The removal of light heterocyclic compounds in the presence of olivine above 850-900 ºC is well established in the literature (Devi et al., 2005a). Phenol decomposition occurs first with the dissociation of O-H bonds followed by: (i) ring opening caused by C-H scission and C=C rupture in positions 2 and 6, and (ii) C-O bond dissociation followed by C-H and C=C rupture. Both mechanisms lead to the formation of H_2, CO and light hydrocarbons in the presence of catalysts (Artetxe et al., 2016, 2017). Additionally, although to a lower extent, phenol may also be converted to naphthalene via decarbonylation followed by the Diels–Alder condensation reaction (Nitsch et al., 2013; Tursun et al., 2013; Pratali Maffei et al., 2020).

Table 5.2 also reveals that an increase in temperature led to either a gradual reduction or complete removal of branched or heterocyclic compounds, and so to a gradual formation of PAHs. Amongst the light PAHs, naphthalene was the major compound found in the whole range of temperatures studied followed by anthracene. Although their concentration increased by increasing temperature, the overall yield of light PAHs (including naphthalene and anthracene) underwent a slight decrease in this temperature range due to the lower content of tar (Figure 5.4b).

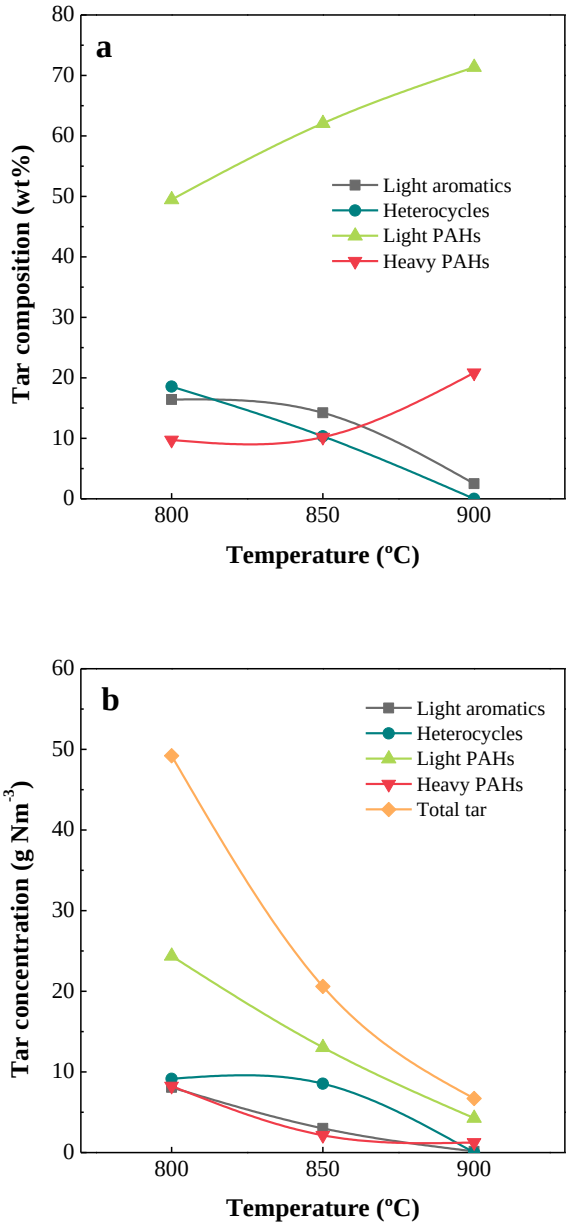

Figure 5.4. Evolution of tar composition (a) and tar concentration (b) in the gaseous stream with temperature.

Naphthalene is a very stable compound (with a similar reactivity as larger compounds, such as anthracene, phenanthrene and pyrene), and therefore high temperatures are

required for its elimination, which also enhance its formation from phenolic species. According to Valderrama Rios et al. (2018) the hydrogen abstraction reaction between hydrogen radicals and phenolic hydroxyls leads to phenoxy intermediates that may decompose into CO and cyclopentadiene radicals. Thereby, these cyclopentadiene radicals combine to form larger aromatic compounds like naphthalene. Morf et al. (2002) also determined that tertiary tars (more stable PAHs) were formed through H_2 abstraction-C_2H_2 addition followed by cyclization sequence or through the direct combination of single-ring species (phenol or benzene). In the former pathway, aromatic rings grow by H-abstraction, which activates aromatic molecules, and acetylene addition propagates molecular growth by cyclization. In the direct combination pathway, two benzene rings for example may lead to biphenyl, which reacts further towards PAH compounds. Kinoshita et al. (1994) concluded that the destruction of aromatic hydrocarbons like naphthalene or phenanthrene requires temperatures above 850 ºC. Under these conditions, naphthalene loses an H radical to form indenyl, which reacts with cyclopentadiene to form phenanthrene or undergoes a successive condensation to larger PAHs (Valderrama Rios et al., 2018). Other authors also observed that naphthalene is the most predominant tar compound in the 700-900 ºC range and its concentration is strongly dependent on temperature (Koppatz et al., 2011; Schmid et al., 2012; Kirnbauer et al., 2013; Tursun et al., 2013; Prasertcharoensuk et al., 2021).

In regards to heavy PAHs, fluoranthrene is the main compound in this fraction (Table 5.2) and its concentration peaks at 900 ºC (18.54 wt%), even though its yield decreases from 2.3 g Nm^{-3} at 800 ºC to 1.2 g Nm^{-3} at 900 ºC. The heaviest PAHs (ranging from benzo[kl]xanthene to benzo[a]pyrene) were only detected at 800 ºC. There is a huge controversy about the behavior of this fraction with temperature, given that the growth of PAHs can be either enhanced or suppressed by increasing process severity. Nguyen et al. (2018) stated that steam promotes the formation of reactive hydrogen intermediates and prevents the combination of carbon-containing species, and therefore hinders the growth of heavy PAHs. Similarly, Qin et al. (2015) concluded that high temperatures favor the production of more hydrogen radicals, which may easily

combine with small free radicals to produce more gas products. Thus, high temperatures (above 800 ºC), use of steam and olivine, as well as the fountain confined spouting regime (longer gas residence time than conventional spouting) avoid the growth of heavy species, and they are not therefore produced at 850 ºC. However, given that lighter species are faster removed at higher temperatures, their relative amount decreases. In the literature, different trends have been reported regarding this family. According to Devi et al. (2003), the concentration of these compounds increases with temperature. They stated that the mechanisms for the formation of heavy PAHs are not fully understood and that they may also be produced from the cracking of GC undetectable tar or from lighter tar compounds (heterocyclic compounds, light aromatics and light PAHs). Conversely, Tursun et al. (2013) observed that the highest concentration of heavy PAHs was attained at 800 ºC and then decreased at 850 ºC.

Table 5.2. Detailed composition (wt%) of the tar fraction obtained at different temperatures by GC/MS analysis.

Compound (wt%)	800 ºC	850 ºC	900 ºC
Light aromatics	**15.35**	**14.22**	**2.49**
Toluene	15.35	14.22	2.49
Heterocycles	**17.34**	**10.33**	**0.00**
Phenol	7.34	3.16	-
Methyl phenol	10.00	7.17	-
Light PAHs	**46.23**	**62.09**	**71.35**
Indene	7.47	0.78	-
Naphthalene	14.67	32.40	33.94
1-Methyl naphthalene	2.33	1.57	0.00
2-Methyl naphthalene	1.90	1.47	8.36
Biphenyl	0.94	0.85	-
Acenaphthene	0.80	0.00	-
Biphenylene	5.59	7.00	2.32
Dibenzofuran	2.24	3.58	8.73
Fluorene	0.69	1.96	1.52
1-H-Phenalene	1.35	2.69	3.06
Anthracene	4.12	6.28	7.25
Phenanthrene	1.56	1.16	1.51
9-Methyl anthracene	0.79	2.35	-
1-Methyl phenanthrene	0.52	-	-

Table 5.2. Continued.

Compound (wt%)	**800 ºC**	**850 ºC**	**900 ºC**
2-Phenyl naphthalene	1.27	-	4.65
Heavy PAHs	**15.64**	**10.20**	**20.84**
Pyrene	3.12	3.92	2.30
Fluoranthene	4.41	5.15	18.54
4H-Cyclopenta[def]phenanthrene	1.54	1.12	-
Benzo[kl]xanthene	0.51	-	-
11H-Benzo[b]fluorene	1.27	-	-
2-Methyl fluoranthene	0.82	-	-
1-Methyl pyrene	1.07	-	-
Benz[a]anthracene	0.80	-	-
Benzo[k]fluoranthene	0.51	-	-
Benzo[e]pyrene	0.79	-	-
Benzo[a]pyrene	0.81	-	-
Unidentified	**5.44**	**3.17**	**5.33**

5.2.3. Simulated distillation

In order to have a better assessment of the tar fractional composition, simulated distillation was applied to the tar samples obtained at 800, 850 and 900 ºC (Figure 5.5). The results confirm the trends observed in Table 5.2, i.e., an increase in the concentration of heavy and light PAHs by increasing temperature and a reduction in the light aromatic species, such as toluene and phenol. In fact, an increase in gasification temperature led to an increase in more stable compounds with lower boiling points. Thus, the tar fraction in the Vacuum Gas Oil (VGO) boiling range

increased from 11 % at 800 ºC to 30 and 40 % at 850 and 900 ºC, respectively. Conversely, the tar obtained at the lowest temperature (800 ºC) had the highest gasoline (22 %) and diesel (73 %) fractions. It is noteworthy that the distillation curves obtained for the tars of 850 and 900 ºC are quite similar, although the former is slightly lighter (lower average molecular weight). Figure 5.5 shows that 57 % of the tar derived from gasification at 850 ºC had the boiling range of diesel (between 160 and 355 ºC), whereas the one obtained at 900 ºC had only 49 % in this range.

Few studies were reported in the literature about the characterization of tars from biomass gasification by means of simulated distillation. Roets et al. (2014) obtained similar distillation curves as those shown in Figure 5.5 for coal-derived tars, with average boiling points being around 330 ºC. Shi et al. (2013) and Fidalgo et al. (2014) observed that most coal tar compounds were in the ranges of gasoil and heavier residues, whereas less than 5 wt% eluted below 260 ºC. Huang et al. (2011) performed simulated distillation for biomass tars and the boiling point ranged from 40 to 440 °C, with compounds ranging from C_7 to C_{29}. Moreover, other characterization techniques were also used for studying the boiling range distribution of gasification tars. Thus, thermogravimetric analysis (TGA) allowed determining that in most cases 60-70 % of the tar boiled above 250-300 ºC (Faúndez et al., 2001; Adegoroye et al., 2004). Likewise, the information obtained on tar characteristics and boiling points ranges by simple distillation is similar the one obtained by TGA and simulated distillation (Shi et al., 2013; Liu et al., 2021).

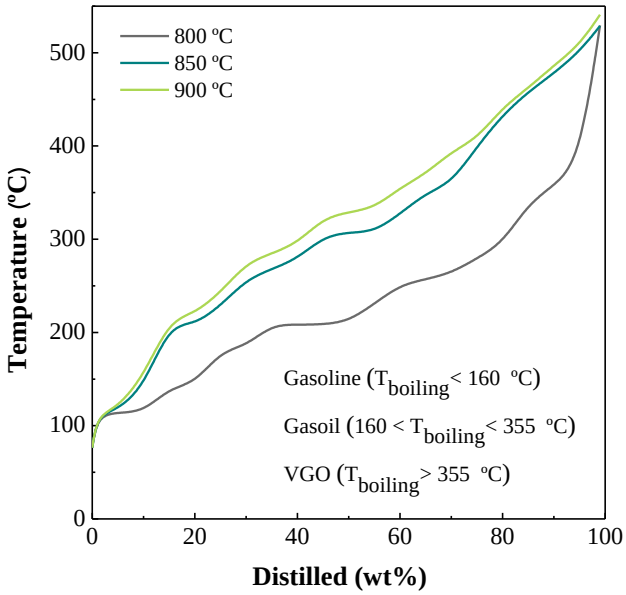

Figure 5.5. Comparison of simulated distillation curves for the tars obtained at 800, 850 and 900 ºC.

5.3. DISCUSSION

The aforementioned results of simulated distillation, FTIR and chromatographic analysis allow concluding that tar content reduces as temperature is increased due to the promotion of decomposition reactions, such as cracking and reforming. Thus, an increase in gasification temperature from 800 to 900 ºC improved process efficiency in terms of tar and char conversion, with the maximum carbon conversion efficiency being 93 % at 900 ºC. Regarding the tar content, it decreased by around 88 %, recording the lowest value (6.7 g Nm^{-3}) at 900 ºC. Moreover, tar composition also evolves from oxygenated organic compounds to more stable species in the range of secondary (non-aromatic and single-ring aromatic compounds) and tertiary tars (PAHs), at the same time as permanent gases are also formed when temperature is increased (Li and Suzuki, 2009; Font Palma, 2013; Hernández et al., 2013). Therefore, temperature increase also had a positive effect on hydrogen production, which increased from 2.9 wt% at 800 ºC to 7.3 wt% at 900 ºC. Analyzing tar composition, the major fraction in the 800-900 ºC range was that of light PAHs, although tar composition shifted from phenolic compounds and alkyl-substituted PAHs to more stable and heavier PAHs, such as naphthalene, anthracene or fluoranthene by increasing temperature, with naphthalene being the major compound at 850 and 900 ºC.

The mechanisms for the evolution and formation of tar species by increasing gasification severity is shown in Figure 5.6. Above 500 ºC, a series of tar formation and evolution stages take place, at the same time as the reactions described by Eqs. (1.2-1.11) are promoted. It is believed that non-aromatic compounds, such as cyclopentadiene, and monocyclic aromatic compounds, are PAH precursors and they derive from the breakage, decarboxylation and dehydrogenation of primary tars (Qin et al., 2015). Moreover, single ring aromatics may also be produced via Diels-Alder reactions of light alkenes in the permanent gases, followed by dehydrogenation of the cyclic compounds formed. Likewise, PAH precursors may follow two main pathways: (i) the formation of gases ranging from permanent ones to benzene, and (ii) the

formation of heavier compounds, such as light PAHs. Furthermore, PAHs may grow though two main mechanisms (Font Palma, 2013; Zhang and Pang, 2017): (i) the direct combination of two different aromatic species to form another aromatic compound with a higher number of rings, and (ii) consecutive additions of unsaturated light hydrocarbons, such as C_2H_2, to form aromatic intermediates, which are followed by cyclization and dehydrogenation reactions, resulting in an increase in the number of rings. Finally, non-aromatic cyclic compounds may also create aromatics (two molecules of cyclopentadiene could form naphthalene), which at the same time might be converted into heavier PAHs following the above-mentioned mechanism.

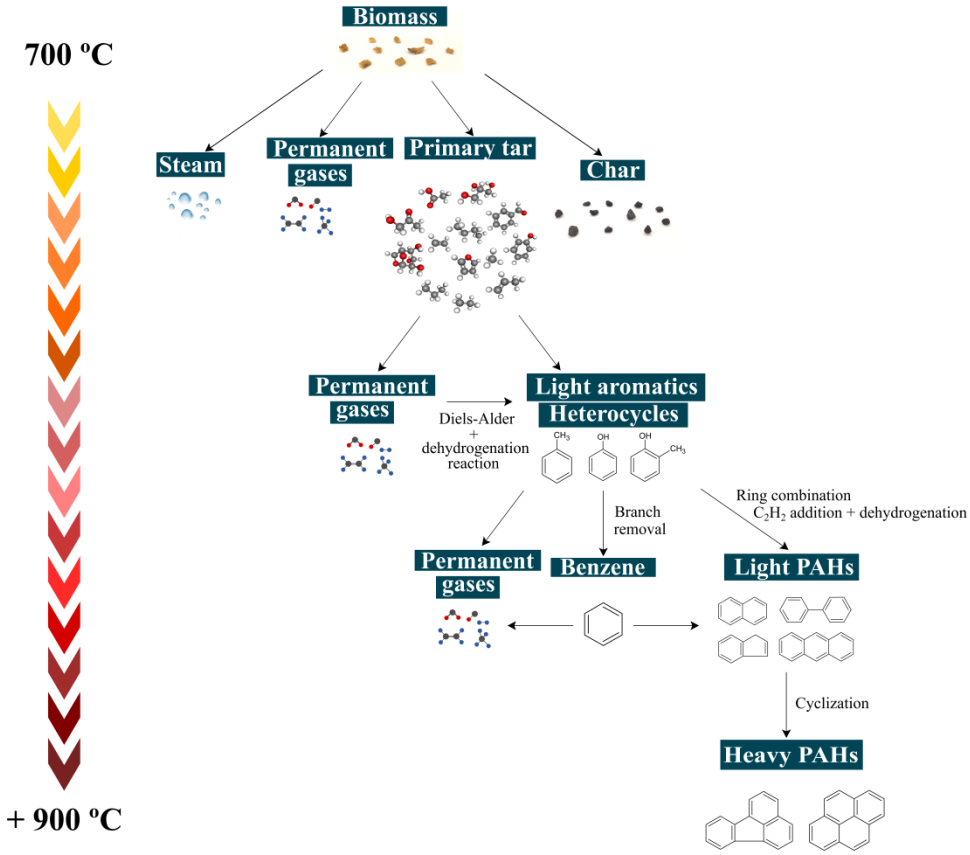

Figure 5.6. Tar formation and evolution pathways in the biomass gasification.

6

ROLE OF PRIMARY CATALYSTS IN THE GASIFICATION PROCESS EFFICIENCY

Primary tar elimination methods significantly reduce the process cost. Thus, apart from the reactor configuration (Chapter 4), the use of in situ catalysts is one of the most promising techniques for tar abatement (Shen and Yoshikawa, 2013; Claude et al., 2016; Guan et al., 2016; Schweitzer et al., 2018; Narnaware and Panwar, 2021). Given their low cost, natural minerals (mainly dolomite and olivine) have been extensively investigated as primary catalysts in biomass gasification. Dolomite is active for reforming, as well as for upgrading the quality of the gaseous stream and reducing tar content. However, its major drawback is its poor mechanical performance, producing a large amount of fine particles, and therefore unstable operation (Orío et al., 1997; Gil et al., 1999a; Gusta et al., 2009; Berrueco et al., 2014a; Islam, 2020). Olivine has outstanding mechanical resistance, comparable to that of sand, even at high temperatures, and it is slightly active for tar reforming. Nevertheless, its activity for reforming and cracking reactions is reported to be lower than that of dolomite (Rapagnà et al., 2000, 2018; Corella et al., 2004; Devi et al., 2005a; Koppatz et al., 2011; Pinto et al., 2014; Kook et al., 2016; Soria-Verdugo et al., 2019).

According to the literature, γ-alumina is effective in tar decomposition and enhances hydrogen production (Matsuoka et al., 2008; Kuramoto et al., 2009; Nam et al., 2020; Pio et al., 2021). Although it is an acid catalyst and has a lower reforming activity than dolomite, the literature reports a similar capacity for removing tar by cracking its components or intermediate components associated with its formation (Xie et al., 2010; De Andrés et al., 2011a). The use of a FCC spent catalyst is of particular interest, as it involves increasing the lifetime of a refinery waste material (Gil et al., 1999a; Abu El-Rub et al., 2004, 2008; Ferella et al., 2016; Fernandez et al., 2021a).

This chapter sets out to explore the potential of the fountain confined spouted bed reactor for the catalytic steam gasification of biomass. Thus, operating under an enhanced fountain regime greatly improves gas-solid contact, and therefore the potential benefits of using a primary catalyst in situ. The performances of the primary catalysts olivine, dolomite, γ-alumina and FCC spent catalyst were evaluated in the continuous steam gasification of sawdust at 850 ºC. Moreover, inert sand was also used

for a better evaluation of the catalytic performance of the proposed catalysts. All the experimental runs were carried out in the bench scale pilot plant described in Section 2.4. The characterization of the primary catalysts and experimental procedure are shown in Section 2.1 and Section 2.5 respectively and in the case of the latter, more specifically in Section 2.5.2.3. This chapter analyses the fountain confined conical spouted bed reactor's capacity for improving the efficiency of the gasification process using primary catalysts. Thus, Section 6.1 deals with the gasification performance (gas yield, H_2 production and carbon conversion efficiency) whereas Section 6.2 is focused on tar concentration and composition. Finally, the most relevant results are discussed in Section 6.3.

6.1. EFFECT OF PRIMARY CATALYSTS ON THE GASIFICATION PERFORMANCE

The influence of the in situ catalyst on the reaction indices (gas yield, H_2 production, tar content in the syngas and carbon conversion efficiency) are shown in Figure 6.1. The results obtained account for the effect of the catalysts on the main steps involved in biomass steam gasification (Eqs. (1.1-1.11)). In comparison with the results obtained with inert sand (associated with the thermal cracking effect), higher yields of gas and hydrogen and a lower tar concentration were attained due to the promotion of reforming, cracking and WGS reactions, and therefore the overall gasification efficiency was greatly improved by the use of the primary catalysts.

Among the tested materials, dolomite provided the best results followed by γ-alumina. Dolomite led to 7.3 wt% of H_2 and 1.60 $Nm^3\ kg^{-1}$ of gas yield, with tar concentration being 5.0 g Nm^{-3}, which accounted for a carbon conversion efficiency of 88.6 %. The lower activity of γ-alumina for the WGS reaction led to a slightly lower H_2 production, 6.7 wt%, even though the gas yield was similar to that of dolomite, 1.54 $Nm^3\ kg^{-1}$. The tar content was slightly higher for γ-alumina, 6.7 g Nm^{-3}, and therefore carbon conversion efficiency was slightly lower, 88.2 %.

Olivine had a smaller influence than dolomite and γ-alumina on the gasification process. Thus, H_2 and gas yields increased from 4.5 wt% and 1.25 $Nm^3\ kg^{-1}$, respectively, when a bed of sand was used, to 5.0 wt% and 1.30 $Nm^3\ kg^{-1}$, respectively, when olivine was used. The results of H_2 and gas productions with the FCC spent catalyst were similar to those with sand (4.5 wt% and 1.3 $Nm^3\ kg^{-1}$, respectively). Nevertheless, the tar concentration with the FCC spent catalyst was 16.2 g Nm^{-3}, which was significantly lower than with olivine (20.6 g Nm^{-3}) due to its cracking activity. Consequently, the carbon conversion efficiency was higher with the FCC spent catalyst than with olivine (86.9 % vs. 86.1 %). However, it should be noted that the Brønsted acid sites on the zeolite not only break the side chains of the tar, but they also stabilize the intermediate compounds (carbonium ions), which promotes condensation reactions

and PAH formation in the tar (Forzatti and Lietti, 1999). Furthermore, the influence of the primary catalysts studied on the char yield was almost negligible. Thus, the char yield with sand was 7 wt%, and the values obtained with the four catalysts were of around 6 wt%. Furthermore, this by-product may contribute to the overall economy of the gasification process. In fact, previous studies revealed that the char produced in the biomass steam gasification has high surface areas (even above 800 m^2 g^{-1}) and carbon contents, which are highly positive features for their application as adsorbents (Alvarez et al., 2019).

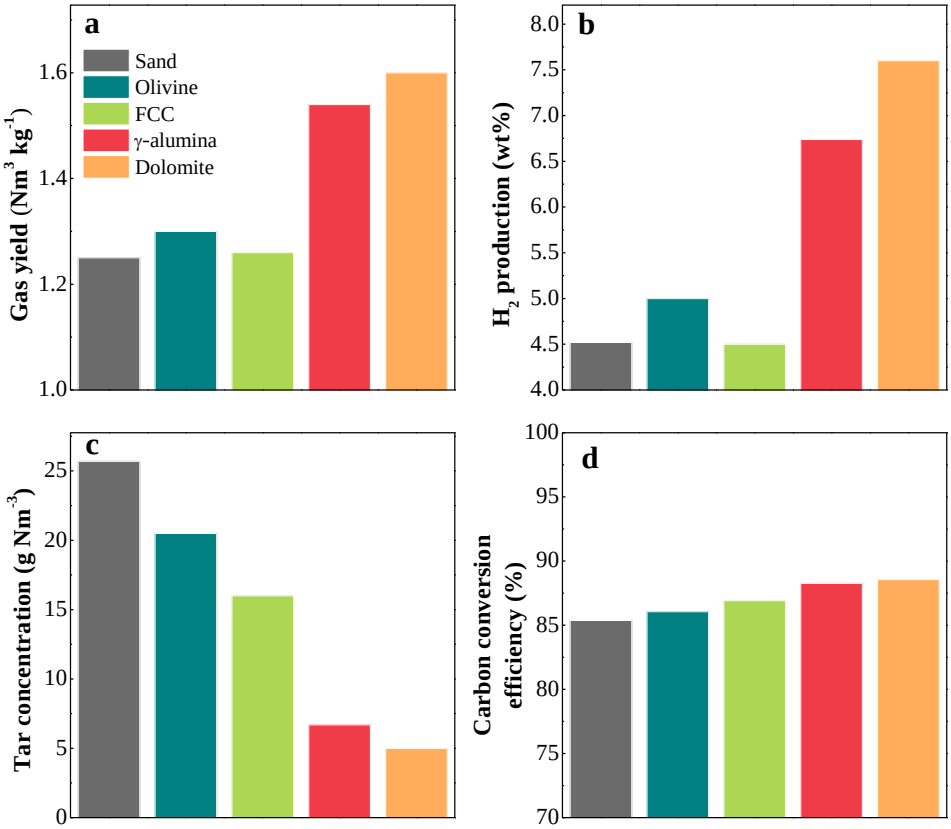

Figure 6.1. Effect of the primary catalysts on gas yield (a), H_2 production (b), tar concentration (on a dry basis) (c) and carbon conversion efficiency (d). Reaction conditions: 850 ºC; S/B ratio, 2.

A fact to note is that the improvement in the overall process efficiency observed in this study over the conventional conical spouted bed is due to the use of both the enhanced fountain and the primary catalysts. Thus, Erkiaga et al. (2013b) compared the influence of olivine and γ-alumina in a conventional spouted bed reactor at 900 ºC. They did not use draft tube nor fountain confinement device and observed that tar content was reduced from 142 g Nm^{-3} with sand to 30.1 and 22.4 g Nm^{-3} with olivine and γ-alumina, respectively. Nevertheless, although the operating temperature in this case was lower, tar concentration was remarkably lower (25.7 g Nm^{-3} with sand and 20.6 g Nm^{-3} with olivine), which was clearly due to the excellent performance of the fountain enhanced spouted bed reactor.

The performance of olivine and dolomite with that of silica sand has been compared in the literature for several gasification technologies. Koppatz et al. (2012) checked the behaviour of silica sand and olivine in a dual fluidized bed gasifier at 850 ºC. They observed a tar reduction of 30.5 %, from 10.8 to 7.5 g Nm^{-3}. Xiao et al. (2017a) also compared the performance of sand and olivine in a decoupled dual loop gasification system at 800 ºC and reported that tar concentration was reduced by approximately 76 %, from 59.8 to 14.1 g Nm^{-3}, and therefore carbon conversion efficiency increased to 73.3 %. Morin et al. (2017) stated that higher gas and H_2 productions and lower tar content obtained with olivine are associated with its catalytic activity for tar removal and WGS reaction.

Likewise, the effectiveness of dolomite in steam or air biomass gasification in terms of tar depletion has been also extensively reviewed. Thus, Rapagnà et al. (2000) compared the use of sand, olivine and dolomite at 770 ºC in a fluidized bed reactor and reported a drastic tar reduction from 43 g Nm^{-3} with sand to 0.6 g Nm^{-3} with dolomite, and to 2.4 g Nm^{-3} with olivine. In addition, Corella et al. (2004) and Devi et al. (2005a,b) studied the effectiveness of olivine and dolomite in air-blown fluidized bed biomass gasification and reported 47 % and 40 %, respectively, of reduction in tar content when a dolomite bed was used instead of olivine. However, Wei et al. (2007)

operating in a free fall reactor observed a negligible effect of olivine (similar to that of inert sand), whereas dolomite showed a slightly better performance.

Xie et al. (2010) tested the performance of dolomite and γ-alumina in a circulating spout-fluid bed reactor at 860 ºC and obtained H_2 and gas yields in the range of those in this study. However, they obtained a lower amount of tar when using dolomite, 3.7 g Nm^{-3} than γ-alumina, 8.8 g Nm^{-3}. Similarly, De Andrés (2011a) reported a good performance of dolomite and γ-alumina in the gasification of sewage sludge in a fluidized bed reactor, with tar content being reduced by 75 and 65 %, respectively, compared to sand, whereas tar content reduced by 50 % at most when olivine was used. In the same line, Manyà et al. (2005) proved the effectiveness of the in situ use of alumina by adding 5 wt% to a bed made up of sand, and reported a reduction in tar content of approximately 40 %.

Few studies have dealt with the use of the spent FCC catalyst in biomass gasification. Corella et al. (1988b) studied the behaviour of dolomite and FCC commercial catalyst (by adding them to the feed) in the steam gasification of biomass in a fluidized bed reactor at 750 ºC. Thus, they reported H_2 and gas yields of 4.4 wt% and 1.21 $Nm^3\ kg^{-1}$, respectively, for the FCC catalyst and 5.2 wt% and 1.33 $Nm^3\ kg^{-1}$, respectively, for the dolomite. Gil et al. (1999a) reported that tar content in the raw gas was decreased from 20.0 to 8.5 g Nm^{-3} by adding FCC catalysts (5 wt% in the feed) during biomass air gasification. They also observed a drastic tar reduction to below 1 g Nm^{-3} when 15-30 wt% of calcined dolomite is in the bed.

Although the natural dolomite catalyst led to the lowest tar yield, it undergoes severe attrition, which boosted the use of other catalysts with higher mechanical resistance (Islam, 2020). Thus, Xie et al. (2010) developed a synthetic CaO/Al_2O_3 catalyst that led to very similar H_2 productions and tar contents in the gas at 860 ºC (3.67 g Nm^{-3} for the synthetics catalyst and 3.73 g Nm^{-3} for the dolomite).

Other authors have developed olivine based catalysts in order to improve the tar cracking and reforming activity. Thus, the effect of adding Fe, Ni, K and Ca to the

olivine has been studied (Rapagnà et al., 2011; Kirnbauer et al., 2012; Virginie et al., 2012; Barisano et al., 2016; Berdugo Vilches et al., 2016; Kuba et al., 2017; Cortazar et al., 2021; Fürsatz et al., 2021). In all cases, higher values of gas and hydrogen productions were obtained and tar content was considerably reduced.

Unlike the above-mentioned authors, who reported dolomite underwent severe attrition and elutriation in fluidized beds, and therefore high amounts of dust to be retained at the reactor outlet, the loss of dolomite (or other catalysts) was negligible in this study. Even though dolomite attrition was considerable in the spouted bed reactor, the incorporation of the fountain confiner avoided the elutriation of the fines formed. In fact, this device was originally designed for handling fine powders without entrainment problems (Altzibar et al., 2017; Pablos et al., 2018, 2020). Moreover, the reactor configuration used in this thesis was a combination of the fountain confiner with a nonporous draft tube, which was demonstrated to be the optimum setup to avoid fine particle elutriation (Estiati et al., 2019).

The effect of the primary catalysts used on the composition of the gaseous fraction is shown in Figure 6.2. As observed, dolomite and γ-alumina behaved similarly, and they were those with the highest influence on gas composition. In fact, both catalysts favoured WGS and reforming reactions, which led to an increase in the concentration of H_2 and CO_2 and a reduction in that of CO (Gusta et al., 2009; De Andrés et al., 2011a; Yu et al., 2018). These catalysts also promoted steam reforming of CH_4 and light hydrocarbons, as deduced from their lower content. However, the influence of dolomite on the composition of the syngas was more remarkable, as deduced from the higher H_2 and CO_2 concentrations, 51.3 and 28.4 vol%, respectively. Moreover, the CO concentration with this catalyst was 13.0 vol%, leading to a H_2/CO ratio of 3.84. Thus, the activity of dolomite was related to CaO and MgO basic sites, with the increase in the Mg/Ca ratio and iron oxide content also promoting its activity (Shen and Yoshikawa, 2013; Shahbaz et al., 2017; Islam, 2020). Use of γ-alumina led to 49.3 vol% of H_2, but CO concentration was almost double that obtained with dolomite (22.1 vol%). Nevertheless, H_2/CO ratio was still quite high, of around 2.23. These results

suggest that dolomite may favour WGS reaction to a greater extent than γ-alumina. Anyway, the use of either dolomite or γ-alumina as in-bed catalyst involved 20-25 % improvement in the H_2 content.

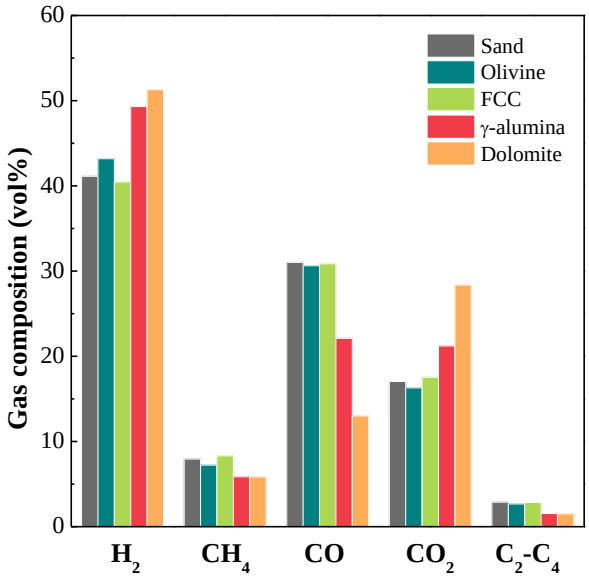

Figure 6.2. Influence of catalysts on gas composition. Reaction conditions: 850 ºC; S/B ratio, 2.

Olivine led to a gaseous stream with approximately 43.2 vol% of H_2, which was slightly higher than that obtained with inert sand, and similar CO and CO_2 contents. It is well kwon that iron-containing catalysts are active for WGS reaction, and the extent of this reaction depends on the presence and structure of the iron on the olivine surface (Swierczynski et al., 2006; Fredriksson et al., 2013; Cortazar et al., 2021). However, the FCC spent catalyst had a limited influence on the composition of the gas. In fact, the composition was very similar to that corresponding to the sand bed, i.e., approximately 40 vol% of H_2. Moreover, these results showed that the FCC spent catalyst led to slightly higher CH_4 and C_2-C_4 concentrations than those obtained with sand, which is attributed to the cracking of tar compounds on the Brønsted acid sites rather than their reforming (Abu El-Rub et al., 2008).

These results are consistent with those obtained by several authors. Wei et al. (2007) also reported that olivine did not improve significantly H_2 concentration in a free-fall reactor, whereas a noticeable difference was observed in the results between inert sand and dolomite. However, other authors reported a considerable increase in H_2 concentration when they used olivine as a primary catalyst instead of dolomite (Koppatz et al., 2011; Virginie et al., 2012; Berdugo Vilches et al., 2016; Ma et al., 2019). Rapagnà et al. (2000) and Koppatz et al. (2011) used fluidized beds reactors, and the former observed an increase of 18 % when using olivine instead of sand (from 35 vol% with sand to 41 vol% with olivine), and the latter of 20 % (from 43.5 vol% with sand to 52.2 vol% with olivine). Therefore, there is still great controversy about the catalytic activity of olivine. Constantinou et al. (2010) concluded that the activity of natural catalysts, such as dolomite, calcite or olivine, is correlated with their intrinsic surface site reactivity exhibited by the individual solid phases, which is influenced by the surface morphology and chemical composition of the primary catalysts. Thus, according to Rauch et al. (2004) and Kuhn et al. (2008a), Fe phase and its location play a crucial role in understanding the differences in the catalytic activity of olivine. In the case of dolomite, they agree on the fact that as it is fully decarbonated during the calcination process, CaO-MgO solution is formed, which enhances its catalytic performance in the biomass steam gasification over that of olivine (Hu et al., 2006; Gusta et al., 2009; Li et al., 2022).

Although many papers in the literature compare the performance of olivine with dolomite, those involving γ-alumina and the FCC spent catalyst as primary catalyst are much less. With regard to the use of the FCC spent catalyst, Gil et al. (1999a) and Corella et al. (1988b) reported a lower activity of the FCC catalyst compared to calcined dolomite. Xie et al. (2010) compared the activity of dolomite and γ-alumina at 860 ºC in a circulating spout-fluid bed and determined that both primary catalysts led to quite similar quality of syngas, with the one obtained with dolomite being richer in H_2 (51.5 vol% with dolomite vs. 48.9 vol% with γ-alumina).

Table 6.1 summarizes the aforementioned results obtained in this study and those reported in the literature for biomass gasification in other technologies under similar conditions and on different catalysts.

Table 6.1. Comparison of gas yields, H_2 productions and tar contents in different technologies using primary catalysts.

Reactor configuration	Temperature (ºC)	Catalysts	Gas yield ($Nm^3\ kg^{-1}$)	Tar production ($g\ Nm^{-3}$)	H_2 production (wt%)/(vol%)	References
Fountain confined spouted bed	850	Olivine	1.30	20.6	5.0/43.18	This study
		FCC catalyst	1.26	16.2	4.5/40.46	
		γ–alumina	1.54	6.7	6.7/49.31	
		Dolomite	1.60	5.0	7.3/51.3	
		Sand	1.25	25.7	4.5/41.12	
Conical spouted bed	900	Olivine	1.03	30.1	3.7/ 40.5	Erkiaga et al. (2013b)
		γ-alumina	1.12	22.4	4.3/43.6	
		Sand	0.92	142	3.1/37.8	
Dual fluidized bed	850	Olivine	1.13	7.5	4.79/35	Koppatz et al. (2011)
		Sand	0.99	10.8	3.09/41	
Decoupled dual loop	800	Olivine	1.02	14.1	3.71/40.8	Xiao et al. (2017)
		Sand	0.87	59.8	2.71/35.0	
Fluidized bed	770	Olivine	1.7	2.4	7.92/52.2	Rapargnà et al. (2000)
		Dolomite	1.9	0.6	9.41/55.5	
		Sand	1.1	43	4.28/43.6	
Circulating spout-fluid bed	860	Dolomite	1.29	3.73	5.84/51.51	Xie et al. (2010)
		γ-alumina	1.24	8.77	4.56/48.86	
		CaO/Al_2O_3	1.25	3.67	5.49/49.46	
Fluidized bed	750	FCC catalyst	1.21	-	4.37/40.3	Corella et al. (2004)
		Dolomite	1.33	-	5.23/44.1	
Free fall reactor	800	Dolomite	1.38	9.4	5.43/44	Wei et al. (2007)
Decoupled triple bed	850	Sand	0.5	25.35	1.66/37.21	Pan et al. (2019)
		Olivine	0.6	5.87	2.27/42.44	

Table 6.1. Continued.

Reactor configuration	Temperature (°C)	Catalysts	Gas yield ($Nm^3\ kg^{-1}$)	Tar production ($g\ Nm^{-3}$)	H_2 production (wt%)/(vol%)	References
Dual fluidized bed	780	Feldspar	1.17	25.4	3.72/35.6	Fürsatz et al. (2021)
		Olivine	1.36	20.9	4.37/36.0	
		Activted olivine	1.46	18.8	5.08/39.0	
		50 % Feldespar + 50 % Limestone	1.44	2.9	5.86/45.6	
		Limestone	1.36	1.9	5.74/47.3	
Dual fluidized bed	800	Sand	0.8	100	3.43/48	Schweitzer et al. (2018)
		Sand + 20 % limestone	-	15	-	
Bubbling fluidized bed	750	Kaolin	-	75	-	Soria-Verdugo et al. (2019)
		Olivine	-	17.27	-/39.2	
		Sepiolite	-	12.6	-/41.0	
Decoupled triple bed	850	Sand	0.76	32.8	2.07/30.5	Tursun et al. (2019)
		Olivine	0.95	11.6	3.43/40.4	
Dual fluidized bed	770	Olivine	1.36	20.9	4.75/39.1	Kuba et al. (2021)
		Sand + 10 % Limestone	1.41	11.1	5.34/42.4	
		Limestone	1.4	1.8	5.94/47.5	
Fluidized bed	950	Sand	-	6.92	-/38.1	Sui et al. (2020)
		Sand+ 9 % cement	-	0.49	-/50.3	

6.2. EFFECT OF PRIMARY CATALYSTS ON TAR COMPOSITION

PAHs are the tar components involving more problems for their removal, specially the heavier ones, and therefore knowledge of their formation or attenuation is of vital importance to optimize the gasification process.

The complexity of the reaction systems involved in gasification (Eqs. (1.1-1.11)) and Figure 5.6) and the heterogeneity of the primary catalysts hinder the interpretation of the results. Thus, the activity of the calcined dolomite is related to the formation of MgO-CaO component in the calcination process, which is the major active compound in the biomass steam gasification. Moreover, dolomite activity is found to increase as the content of Fe traces is increased. In the case of olivine, its catalytic activity for tar elimination depends on its magnesite (MgO) and iron oxide (Fe_2O_3) contents. In regards to the FCC spent catalyst and γ-alumina, their activity is related to their acid site content and surface area.

Figure 6.3 shows the influence of the primary catalysts on the tar composition. As observed, the nature of the tar was affected by the type of catalyst used. For any bed material, the most abundant species were light PAHs, which accounted for approximately 60 wt% of the whole tar mass. Dolomite led to a tar with a high concentration of heterocyclic compounds (10.22 wt%), the highest concentration of light aromatics (21.38 wt%) and the lowest of heavy PAHs (6.23 wt%). Therefore, based on tar formation and PAH growth mechanisms, dolomite seems to hinder the growth of PAHs in the scheme shown in Figure 5.6. In fact, Zhao et al. (2011) reported that CaO integrated in the dolomite is very effective in eliminating heavy PAHs. However, it was less efficient for cracking and reforming smaller aromatics, such as benzene or naphthalene. This result is related to the increase in H_2 production (Figure 6.1), since according to Nguyen et al. (2018) high H_2 concentrations in the reaction environment prevent the combination of carbon-containing species, which are the precursors of heavy tar molecules. The other catalysts (olivine, FCC spent catalyst and γ-alumina) led to a tar with a lower concentration of light aromatic compounds, of

around 15 wt%, which was slightly higher than that obtained with sand (11.05 wt%). It is noteworthy that the FCC spent catalyst and γ-alumina led to a very similar distribution of the various tar fractions, which is attributed to the acid character of both catalysts. Thus, the reaction pathway of both materials was very similar, i.e., both led to high fractions of heavy PAHs (16 wt%), which were similar to that obtained with sand (18.12 wt%). According to Forzatti and Lietti (1999), acid sites tend to stabilize carbon intermediates that condensate and form stable PAHs. The higher acidity of the FCC spent catalyst favoured their formation (Table 2.2). Dolomite led to the lowest amount of heavy PAHs, reaching a value of 6.23 wt%. In relation to heterocyclic compounds, higher fractions were obtained with dolomite and olivine (10 wt%), compared to sand and the FCC catalyst (5.70 wt%), whereas γ-alumina led to lowest fraction (2.77 wt%).

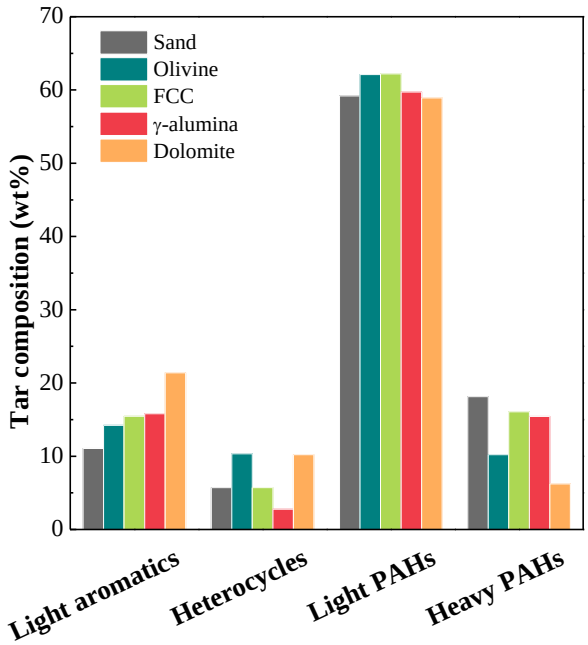

Figure 6.3. Effect of the bed material on tar composition. Reaction conditions: 850 ºC; S/B ratio, 2.

Table 6.2 shows the detected tar components and their concentration. As mentioned, the tar dew point, which depends on its concentration and composition, is a key factor for the valorization of the syngas product. Thus, monoaromatics are not condensable even at concentrations as high as 10 g Nm^{-3}, whereas polyaromatics of more than 4 rings cause severe problems at concentrations of around 1 mg Nm^{-3} (Anis and Zainal, 2011). As observed in Table 6.1, these catalysts managed to reduce all tar families to a higher or lesser extent and, especially, the more problematic PAHs.

For all the tested catalysts, naphthalene was the major tar compound. Dolomite led to the lowest naphthalene content, which was 26.31 wt% of the whole tar, whereas γ-alumina and the FCC spent catalyst led to the highest content (38 wt% approximately), which is higher than that obtained with the sand (33.52 wt%). In addition, based on the very small concentration of phenol obtained when both acid catalysts were used, 0.55 and 0.30 wt% for the FCC spent catalyst and γ-alumina, respectively, it is evident that they promoted phenol conversion towards naphthalene via decarbonylation followed by the Diels-Alder reaction (Corma et al., 2007). Moreover, the low amounts of 1-methyl naphthalene and 2-methyl naphthalene produced with these catalysts compared to sand suggests that they were also converted to naphthalene through dealkylation. In the case of olivine, the relative content of naphthalene was similar to that for sand, i.e., a slightly lower content of 32.40 wt%. Furthermore, it is noteworthy that fluoranthene and pyrene were the most refractory heavy PAHs.

As observed in Table 6.2, dolomite was the most effective primary catalyst to remove both light and heavy PAHs in the tar, with their concentrations being 3.0 and 0.3 g Nm^{-3}, respectively. Nevertheless, γ-alumina was the most effective in the abatement of heterocyclic compounds by cracking, with the concentration of light aromatics (toluene) being similar to that for dolomite. The previous results were a consequence of the catalysts features, since the activity of the catalysts' acid sites for condensation reactions seems to prevail over their activity for cracking (especially in the case of the FCC spent catalyst, which is more acid than γ-alumina). Therefore, the latter are less suitable primary catalysts than dolomite for biomass gasification.

Table 6.2. Detailed tar concentration (g Nm^{-3}) for the tested catalysts.

	Sand	Olivine	FCC	γ-alumina	Dolomite
Light aromatics	**2.8**	**2.9**	**2.5**	**1.1**	**1.1**
Toluene	2.8	2.9	2.5	1.1	1.1
Heterocycles	**1.5**	**2.1**	**0.9**	**0.2**	**0.5**
Phenol	0.3	0.6	0.1	0.0	0.1
Methyl phenol	1.2	1.5	0.8	0.2	0.4
Light PAHs	**15.2**	**12.8**	**10.1**	**4.0**	**3.0**
Indene	0.0	0.2	0.0	0.0	0.0
Naphthalene	8.6	6.7	6.1	2.5	1.3
1-Methyl naphthalene	0.1	0.3	0.1	0.1	0.1
2-Methyl naphthalene	0.3	0.3	0.2	0.2	0.2
Biphenyl	0.0	0.2	0.0	0.0	0.0
Acenaphthene	0.0	0.0	0.0	0.0	0.0
Biphenylene	1.9	1.4	1.0	0.2	0.2
Dibenzofuran	0.6	0.7	0.3	0.3	0.5
Fluorene	0.2	0.4	0.2	0.0	0.0
1-H-Phenalene	0.6	0.6	0.3	0.1	0.0
Anthracene	2.2	1.3	1.5	0.5	0.2
Phenanthrene	0.2	0.2	0.1	0.0	0.0
2-Phenyl naphthalene	0.4	0.5	0.2	0.2	0.4

Table 6.2. Continued.

	Sand	**Olivine**	**FCC**	**γ-alumina**	**Dolomite**
Heavy PAHs	**4.7**	**2.1**	**2.6**	**1.0**	**0.3**
Pyrene	1.8	0.8	0.9	0.3	0.1
Fluoranthene	2.5	1.1	1.5	0.6	0.2
4H-Cyclopenta[def]phenanthrene	0.3	0.2	0.1	0.0	0.0
Unidentified	**1.2**	**0.0**	**0.0**	**0.4**	**0.0**
Total tar	**25.7**	**20.6**	**16.2**	**6.7**	**5.0**

6.3. DISCUSSION

The results obtained in this study show that in situ use of dolomite, olivine, γ-alumina and FCC spent catalyst is a promising method to upgrade biomass-derived syngas. Not only did they reduce tar formation, but also improved syngas yield and its composition. Without any doubt, dolomite and γ-alumina significantly outperformed the other in bed materials (Figure 6.1). They significantly improved the composition of the gas, increasing hydrogen content in the gaseous stream to 51.3 vol% and 49.3 vol%, respectively, which corresponded to H_2 productions of 7.3 wt% and 6.7 wt%. Other primary catalysts also improved the results obtained with sand, but to a lesser extent. As some authors suggested (Rapagnà et al., 2000; Koppatz et al., 2011; Berdugo Vilches et al., 2016), this is explained by the higher extent of steam reforming, cracking and WGS reactions when comparing these primary catalysts to sand.

Besides their influence on the quality of the gas, the tested materials managed to remove tar, which was also observed by Gil et al., (1999a), De Andrés et al. (2011b), Erkiaga et al., (2013b), Cao et al., (2021a) and Fürsatz et al., (2021). The chemical composition and the nature of the primary catalysts play a key role in tar removal. According to Orío et al. (1997), Rauch et al. (2004), Devi et al. (2005b), Swierczynski et al.(2006), Kuramoto et al. (2009) and Islam (2020), the catalytic activity of dolomite and olivine natural catalysts in biomass gasification is related to CaO-MgO solution in the dolomite and MgO and Fe_2O_3 phases in the olivine, whereas the amount of acid sites and the surface area are the influential factors in FCC spent catalysts and γ-alumina. Thus, dolomite and alumina recorded the lowest tar values, 5.0 and 6.7 g Nm^{-3}, respectively, whereas the olivine and the FCC spent catalyst yielded higher contents, 20.6 and 16.2 g Nm^{-3}, respectively. It should be noted that a bed of inert sand led to a tar concentration of 25.7 g Nm^{-3}.

Although the most abundant tar species with any bed material were light PAHs, which accounted for approximately 60 wt% of the total tar concentration, the nature of tar was affected by the type of catalysts used (Figure 6.3). However, the complexity of the

gasification reaction system, as well as the heterogeneity of the primary catalysts, hinder the interpretation of the tar composition results. Dolomite turned out to be the most effective to deplete heavy PAH compounds, leading to the lowest amount (6.23 wt%). In the words of Nguyen et al. (2018), high H_2 productions avoid the combination of carbonaceous species, which are the main precursors of heavy PAHs. Nevertheless, both γ-alumina and FCC spent catalyst yielded much higher amounts (16 wt%), similar to that obtained with sand (18.12 wt%). Forzatti and Lietti (1999) stated that acid sites tend to stabilize carbon intermediates, which later on form stable PAHs. Furthermore, low amounts of phenol were obtained (Table 6.2) when both acid catalysts were used, 0.55 and 0.30 wt% for the FCC spent catalyst and γ-alumina, respectively, which evidenced the promotion of phenol conversion towards naphthalene via decarbonylation followed by the Diels-Alder reaction (Corma et al., 2007).

Moreover, the experimental research also showed the suitability of the fountain confined conical spouted bed when dolomite was used as in-bed material. Even though dolomite attrition was as significant as in fluidized beds, the incorporation of the fountain confiner avoided the elutriation of the fines formed, which is not the case in the other techologies. Several authors (Xie et al., 2010; Benedikt et al., 2017) reported high amounts of dust retained at the reactor outlet when fragile in bed materials were used.

7

EFFECT OF METAL ADDITION TO PRIMARY CATALYSTS

A large number of materials with significant activity for tar cracking and reforming have been used as primary catalysts. Natural minerals, such as dolomite and olivine, have attracted most of the attention because, apart from being active for tar cracking and reforming, they are inexpensive and abundant. Although the activity of dolomite is reported to overcome that of olivine, it is very fragile and undergoes severe attrition when used in fluidized beds. Furthermore, olivine has higher mechanical strength, comparable to that of sand (Rapagnà et al., 2000; Abu El-Rub et al., 2004; Corella et al., 2004; Gusta et al., 2009; De Andrés et al., 2011a; Koppatz et al., 2011; Li et al., 2021a; Nguyen et al., 2021). However, as it was shown in Chapter 6, the catalytic activity of these primary materials for tar conversion leaves room for improvement by metal phase addition.

Ni based catalysts are more effective for converting tar into hydrogen-rich gas, but they undergo a rapid deactivation by coke deposition and are toxic (Wang et al., 2005; Świerczyński et al., 2007; Kuhn et al., 2008b; Zhao et al., 2009; Zhang et al., 2013; Waheed et al., 2016; Sun et al., 2019; Farooq et al., 2021). Recently, iron based catalysts have gained considerable attention among the catalysts for tar removal. Compared to nickel, the use of iron reduces the catalyst cost and lowers its toxicity (Matsuoka et al., 2006; Virginie et al., 2010a,b, 2012; Rapagnà et al., 2011; Quan et al., 2017; Zamboni et al., 2017; Claude et al., 2019; Pan et al., 2019; Xu et al., 2019; Pudukudy et al., 2020). Apart from the well-known activity of metallic iron for tar reforming and cracking, magnetite (Fe_3O_4) has also been proven to be active for the WGS reaction (Martos et al., 2009; Dufour et al., 2011; Chou et al., 2019). Therefore, impregnation of natural minerals with iron seems to be an interesting alternative to synthesize primary catalysts.

This chapter assesses the potential benefits of the use of Fe/olivine catalyst in the fountain confined conical spouted bed for reducing the tar produced during biomass gasification. All the experimental runs were carried out at 850 ºC in the bench scale pilot plant described in Section 2.4 and the catalyst was prepared by wet impregnation method as explained in Section 2.2. Furthermore, this chapter approaches the role of

the active iron species and their behaviour in biomass steam gasification. Thus, an extensive characterization of the fresh catalyst is described in Section 7.1 according to the procedures explained in Section 2.3. Then, Section 7.2 shows the Fe/olivine catalyst performance on biomass steam gasification, where the catalyst activity (Section 7.2.1), stability over time (Section 7.2.2) and the main cause of the catalyst deactivation (Section 7.2.3) are discussed in deep. Finally, the most significant results are recapitulated in Section 7.3.

7.1. FRESH CATALYST CHARACTERIZATION

7.1.1. Physical properties and composition

Table 7.1 shows the physical properties of olivine and Fe/olivine catalysts, i.e., specific surface area, pore volume and average pore size. As observed, the specific surface area of the calcined olivine was as low as 1.92 m^2 g^{-1} and the pore volume 0.0023 cm^3 g^{-1}, which are evidences of its limited porous structure. Regarding the synthesized Fe/olivine catalyst, olivine physical properties were improved by iron impregnation. Thus, pore volume and average pore size became larger, which is due to the collapse of the inter-pore structure of olivine. Likewise, the specific area also increased, which may be attributed to the deposition of Fe on the external surface. This trend has also been reported for Ni impregnation on low porosity supports (García-García et al., 2015; Santamaria et al., 2018).

Table 7.1. Physical properties of the calcined olivine and Fe/olivine catalyst.

Catalyst	S_{BET} (m^2 g^{-1})	V_{pore} (cm^3 g^{-1})	d_{pore} (Å)
Olivine	1.92	0.0023	48.85
Fe/olivine	3.75	0.0076	80.85

The chemical compositions of the calcined olivine and the prepared catalyst are summarized in Table 7.2. The content of Fe in the olivine was of around 5.2 wt%. After impregnation, Fe content in the catalyst increased significantly, 10.2 wt%, which confirms that the metal content is that corresponding to the impregnation (5 wt%) plus that in the original olivine.

Table 7.2. Chemical composition (wt%) of the calcined olivine and the Fe/olivine catalyst.

Component (wt%)	MgO	SiO_2	Fe_2O_3	CaO	Al_2O_3	Na_2O	TiO_2	MnO
Olivine	45.98	42.10	7.52	0.11	0.10	0.07	0.03	0.11
Fe/olivine	42.08	38.68	14.71	0.12	0.24	0.06	0.02	0.10

7.1.2. Metallic properties

Figure 7.1 shows the diffractograms of the calcined olivine, fresh and reduced Fe/olivine. In the case of the calcined olivine, the XRD data reveal the main diffraction lines were characteristic to the olivine structure (($Mg_{1.81}$ $Fe_{0.19}$) (SiO_4)). Additional peaks corresponding to secondary crystalline phases may also be observed, such as enstatite ($MgSiO_3$) and quartz (SiO_2). According to and Świerczyński et al. (2006) and Michel et al. (2013, 2014) numerous phases of iron oxide may appear subsequent to olivine calcination, as are γ-Fe_2O_3, α-Fe_2O_3, Fe_3O_4 and $MgFe_2O_4$. The presence of these iron oxides is explained by the migration of the iron Fe^{2+} located within the internal structure of the olivine to its surface due to oxidation (Eq. 7.1) (Swierczynski et al., 2006; Morin et al., 2017). However, none of these phases was detected in this study. It should be noted that the calcination temperature used for the natural olivine was rather low (850 ºC) compared to other studies in the literature, in which they were over 1100 ºC. Kuhn et al. (2008a) performed XRD analysis to olivine calcined at 900 ºC during 2 h and they neither observed free Fe oxide phases. These oxide phases diffract in the same main lines as the olivine structure, but they were not strong enough to be detected and so inferred their presence.

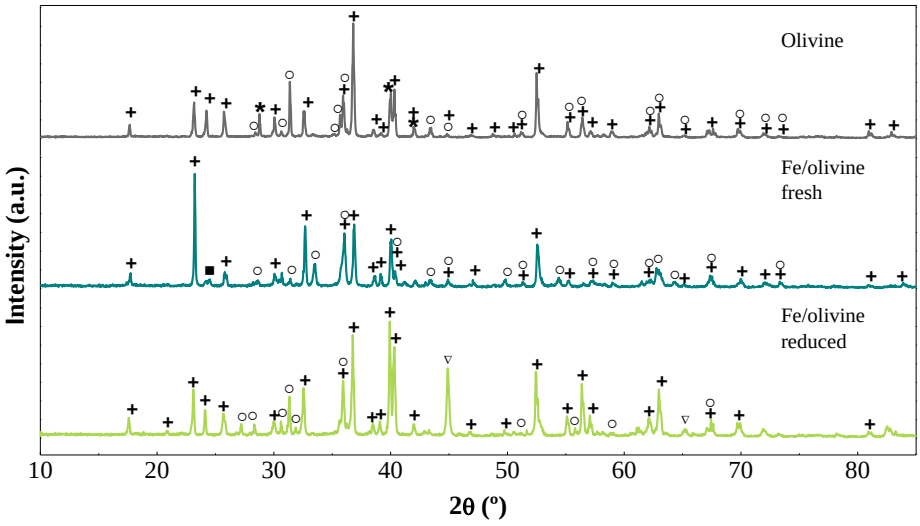

Figure 7.1. XRD patterns of the calcined olivine and fresh and reduced catalysts. Crystalline phases: (+)($(Mg_{1.81}\ Fe_{0.19})\ (SiO_4)$), (o) $MgSiO_3$, (*) SiO_2, (■) Fe_2O_3, (∇) Fe^0.

For the fresh and reduced Fe/olivine catalysts, the main crystalline forms were still those corresponding to olivine structure and $MgSiO_3$ enstatite phase, even though the olivine was subjected to iron impregnation, calcination and reduction. However, significant changes in the relative intensity of olivine structure and $MgSiO_3$ enstatite phases were noticed at 2Θ=21º, 31º and 36º, which indicated certain modifications in the crystallinity of the samples due to iron impregnation. In fact, the higher intensity of the diffraction lines in the reduced catalyst is evidence of its greater crystallinity compared to the calcined olivine or fresh catalyst, which was due to iron reincorporation into the olivine structure. In addition, hematite (α-Fe_2O_3) peak appeared at 2Θ=24º in the fresh catalyst, whereas for the reduced catalyst the presence of an intense peak of the metallic iron phase was observed at 2Θ=44º and a smaller one at 2Θ=65º. Iron oxide phases were not detected in the reduced sample, which is evidence of their full reduction. Other authors reported the same main lines for this catalyst (Virginie et al., 2010a,b; Meng et al., 2019). The SiO_2 lines detected in the

support disappeared in the catalyst. Michel et al. (2013) stated that olivine phase reacts with quartz at 1000 ºC to form enstatite phase.

$$(Mg,Fe)_2SiO_4+O_2 \rightarrow xMg_2SiO_4+(1-x)SiO_2+(2x-1)Fe_2O_3(\alpha)+2(1-x)MgFe_2O_4 \qquad (7.1)$$

7.1.3. Surface analysis

Figure 7.2 shows the XPS spectra for the samples in different binding energy ranges. This analysis revealed the main components on the surface of the samples, which were Si, Mg, Fe and O. No significant changes were observed in Si after iron impregnation and catalyst reduction, whereas more pronounced changes were detected in the peaks corresponding to Mg and Fe. In the case of Fe, its oxidation states are analyzed in detail later on. These variations are also visible in Table 7.3 and 7.4. Furthermore, peaks of other trace elements, previously detected by XRF, were not observed, which evidence that they were not located on the surface.

Table 7.3 shows the surface composition of the samples. The quantification of each element was carried out by integrating the intensities of Si 2p, Mg 2p, O 1s and Fe 2p using Scofield sensitivity factors. As observed, after iron impregnation, the amount of iron on the catalyst surface increased (from 6.2 to 8 %), which suggests that part of the impregnated iron was deposited on the surface of the catalyst, as evidenced by the increase in the BET surface of the catalyst (Table 7.1). However, the amount of Mg on the surface decreased (from 17.5 to 14.2 %) after iron loading. According to Frekdissön et al. (2013), after the oxidizing treatments, the surface is enriched in Fe at the expense of Mg. Furthermore, catalyst reduction with H_2 led to a decrease in the amount of Fe to 4.4 % and an increase in that of Mg to 22.1 % on the surface. Under reducing conditions, Fe clustered into large particles and incorporated into the olivine structure (Kuhn et al., 2008a). Regarding oxygen concentration, its oscillations on the surface of the catalyst are related to the oxidation state of iron.

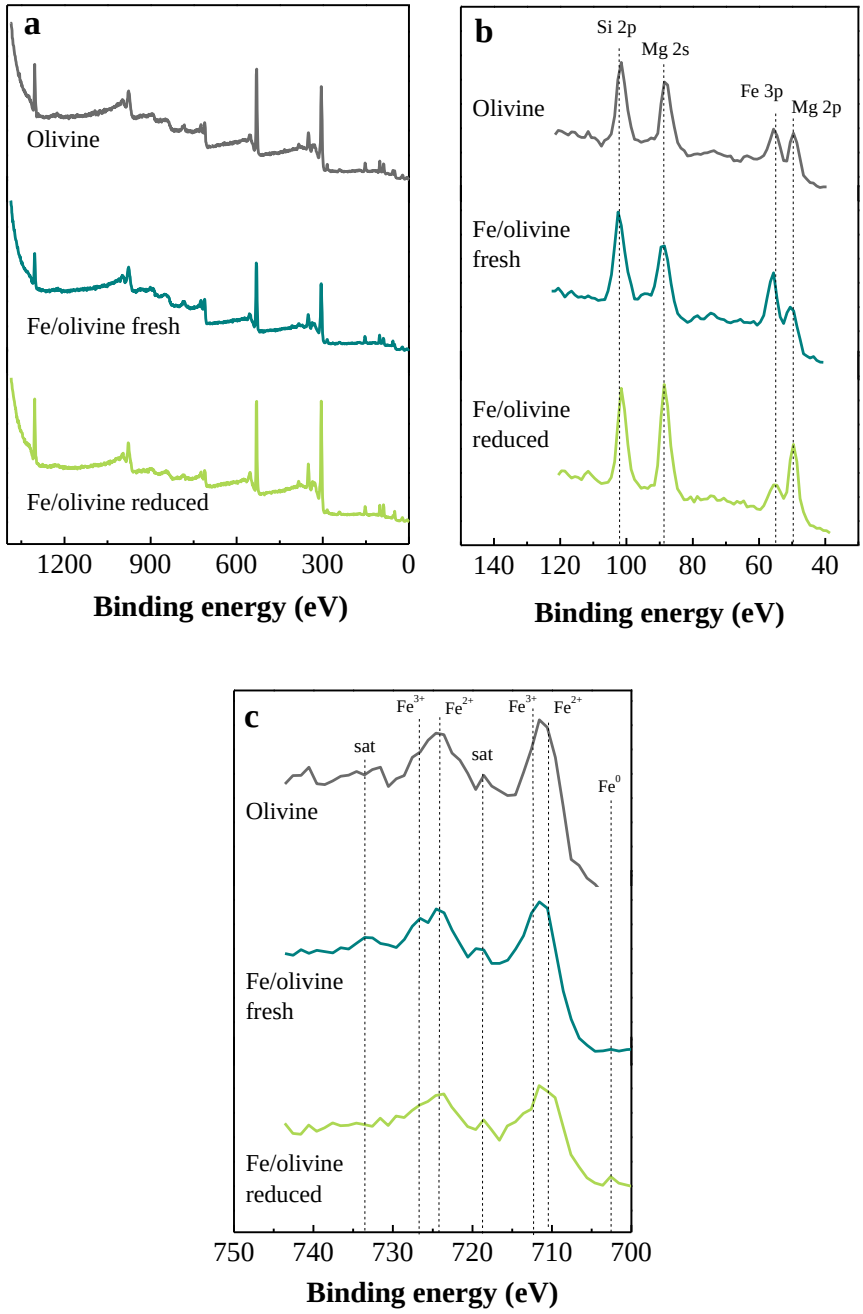

Figure 7.2. Wide XPS spectra (a), XPS spectra for low binding energy regions (b) and XPS spectra for Fe 2p (c) of the calcined olivine, and fresh and reduced Fe/olivine catalysts.

Table 7.3. Surface composition (%) of the calcined olivine and Fe/olivine catalysts.

Component (%)	Si	Mg	O	Fe
Olivine	15.8	17.5	60.6	6.2
Fresh Fe/olivine	15.1	14.2	62.7	8.0
Reduced Fe/olivine	14.6	22.1	58.9	4.4

XPS spectra in 700-750 eV binding energy range of the samples were analyzed to further understand the valence state of the iron in the calcined olivine and fresh and reduced Fe/olivine catalysts (Figures 7.2b and 7.2c). Accordingly, Fe 2p lines were used instead of Fe 3p because they were stronger. Moreover, Table 7.4 shows the iron distribution on the surface of the samples. Yamashita et al. (2008) reported that Fe $2p_{3/2}$ peak at 711 eV with satellite peak at 719 eV and Fe $2p_{1/2}$ peak at 725 eV with satellite peak at 732 eV were characteristic of Fe^{3+}, whereas Fe $2p_{3/2}$ peak at 709 eV with satellite peak at 714 eV and Fe $2p_{1/2}$ peak at 723 eV with satellite peak at 728 eV correspond to Fe^{2+}. In Figure 7.2c, the positions of these peaks are marked with dashed lines. Iron in Fe^{3+} state corresponds to Fe_2O_3 and $MgFe_2O_4$ compounds, whereas Fe^{2+} state is characteristic of iron in the olivine structure and FeO. In the calcined olivine, most of the Fe was as Fe^{3+} and doubled the amount of Fe as Fe^{2+}, which is evidence that a higher amount of iron led to free oxides on the surface than those remained within the olivine structure. The presence of free iron oxide phases (Fe^{3+}) stemmed from Fe migration from the olivine structure (Fe^{2+}) during the calcination process (Swierczynski et al., 2006; Fredriksson et al., 2013), although none of these compounds were detected by XRD analysis. Regarding iron distribution, the fresh Fe/olivine catalyst followed the same trend as the calcined olivine. However, when comparing the former with the calcined olivine, the amount of Fe^{2+} in the fresh catalyst increased (from 32.89 to 35.42 %), whereas that of Fe^{3+} decreased (from 67.11 to 64.54 %), although Fe^{2+}/Fe^{3+} ratio remained approximately constant. These results suggest

that, after impregnation, the iron within the olivine structure was preferably in the metallic state rather than forming free oxides. After reduction, a weak peak of metallic Fe appeared at 707 eV, which cannot be quantified due to its very small size. It seems that the metallic iron on the catalyst surface was oxidized due to its contact with air, but the iron inside the olivine remained in the metallic form, as was revealed by the XRD analysis (Figure 7.1). Moreover, the Fe^{2+}/Fe^{3+} ratio in the reduced catalyst was higher than that in the fresh one, with the amount of Fe^{2+} and Fe^{3+} being almost the same. Thus, the oxidation state of the iron located on the surface changed from a Fe^{3+} dominating state after oxidation to Fe^{2+} state after reduction (Fredriksson et al., 2013). Meng et al. (2019) observed the same trend for the iron distribution on the surface of the catalyst.

Table 7.4. Iron distribution (%) on the surface of the calcined olivine and fresh and reduced Fe/olivine catalysts determined by XPS.

	Fe^{2+} (%)	**Fe^{3+}(%)**
Olivine	32.89	67.11
Fe/olivine fresh	35.42	64.58
Fe/olivine reduced	48.95	51.05

7.1.4. Reducibility of metallic species

H_2-TPR experiments for the bed materials were carried out prior to their use in the reaction environment. The TPR profile of the catalysts enables determining the temperature needed for their reduction (Da Ros et al., 2021). As well-known, the profile depends not only on the nature of the metallic species, but also on the metal-support interactions. Moreover, as the metallic iron is supposed to be the active phase for hydrocarbon cracking, the reducibility of the catalysts is of great relevance (Nordgreen et al., 2006).

The TPR profiles of the calcined olivine and synthesized catalyst are shown in Figure 7.3. In the case of the calcined olivine, two small peaks were observed between 350 and 550 ºC. A third peak was also observed at a reduction temperature above 600 ºC. In the case of the first two peaks, their low reduction temperature is evidence that these species were easy to reduce. Thus, these peaks are attributed to the reduction of iron oxides on the olivine surface (Devi et al., 2005a). According to the XPS analysis (Table 5), the surface of the calcined olivine was presumably made up of Fe_2O_3 and/or $MgFe_2O_4$, which migrated from the internal olivine structure during the calcination (Swierczynski et al., 2006; Kuhn et al., 2008a; Virginie et al., 2010a; Meng et al., 2019). Thus, the peak at 350 ºC is assigned to the reduction of Fe_2O_3 and the peak at 550 ºC to the reduction of Fe_3O_4, as the reduction of Fe_2O_3 to metallic Fe occurs in two steps ($Fe_2O_3 \rightarrow Fe_3O_4 \rightarrow Fe^0$) (Virginie et al., 2010a; Quan et al., 2017). The peak that might appear at higher temperatures is associated with the reduction of iron phases inside the olivine grain, in which reduction is more difficult. The TPR profile of the Fe/olivine catalyst shows a broad reduction zone covering the range from 300 ºC to 700 ºC. Three main peaks may be observed, with the first two being associated with the two-step oxidation of Fe_2O_3 on the olivine surface and the peak above 600 ºC to the Fe atoms that migrated into the olivine support to form a very stable $MgFe_2O_4$ spinel phase (Meng et al., 2018a). In the case of the Fe/olivine catalyst, the reduction of iron phases inside the olivine grain was not observed due to the high stability of the olivine structure, i.e., higher temperatures are required for its reduction.

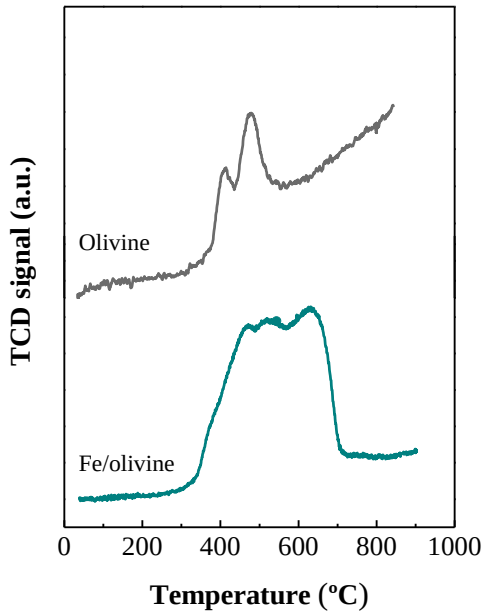

Figure 7.3. TPR profiles of the catalysts.

7.2. Fe/OLIVINE CATALYST PERFORMANCE

7.2.1. Initial activity of the Fe/olivine catalyst

The effect of Fe/olivine catalyst on the steam gasification process parameters (H_2 and gas productions, gas composition, carbon conversion and tar concentration and composition) was assessed and compared with that of calcined olivine.

As observed in Figure 7.4, all representative gasification parameters were significantly improved on the Fe/olivine catalyst. An increase in gas and hydrogen productions and a decrease in tar concentration was noticeable when 5 wt%Fe/olivine was used instead of convetional olivine (Figures 7.4a and 7.4b). Thus, gas production increased from 1.30 to 1.46 $Nm^3 kg^{-1}$ and so did the hydrogen production, from around 5.0 wt% on the olivine to 6.3 wt% on the iron impregnated catalyst. Figure 7.5 illustrates the product gas composition for the runs using 5 wt%Fe/olivine catalyst and calcined olivine. Iron impregnation led to an increase in H_2 concentration from 43.2 to 48.2 vol% and a reduction in that of CO, which implies that H_2/CO ratio increases from 1.41 for olivine to 3.26 for the iron catalyst. Consequently, CO_2 concentration increased to 28.2 vol%. From these results, it could be deduced that the addition of iron to olivine enhances the WGS reaction (Eq. (1.7)), as well as light hydrocarbon steam reforming and cracking reactions (Eqs. (1.2), (1.3) and (1.8)). Consequently, tar concentration was reduced approximately to half, from 20.6 to 10.4 g Nm^3, and carbon conversion efficiency accounted for 87.6 % (Figures 7.4c and 7.4d). According to several authors (Nordgreen et al., 2006; Fredriksson et al., 2013; Nam et al., 2016), the metallic Fe on the reduced catalyst enhances tar decomposition reactions. Moreover, the BET surface area (Table 7.1) and XPS analyses (Table 7.3) revealed that Fe was mainly located on the external surface of the catalyst, and was therefore easily accessible to the volatiles and promotes tar cracking and reforming reactions (Eqs.(1.2) and (1.3)).

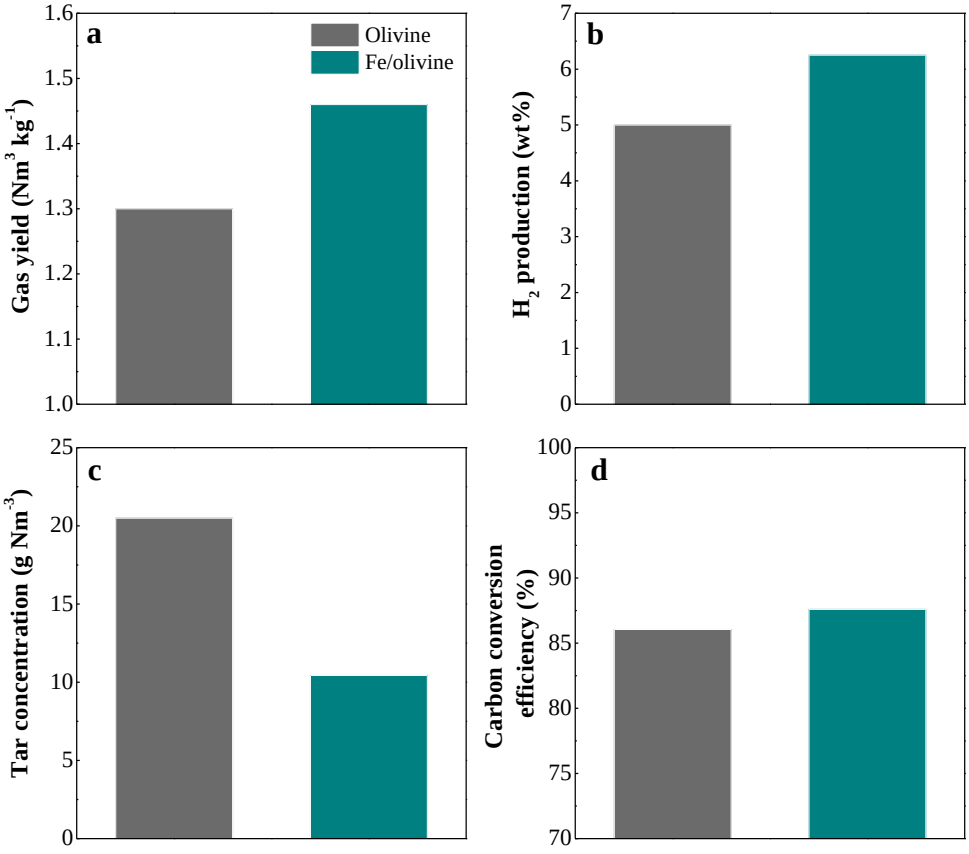

Figure 7.4. Influence of iron impregnation on the gas production (a), H_2 production (b), tar concentration (c) and carbon conversion efficiency (d). Reaction conditions: 850 ºC; S/B ratio, 2

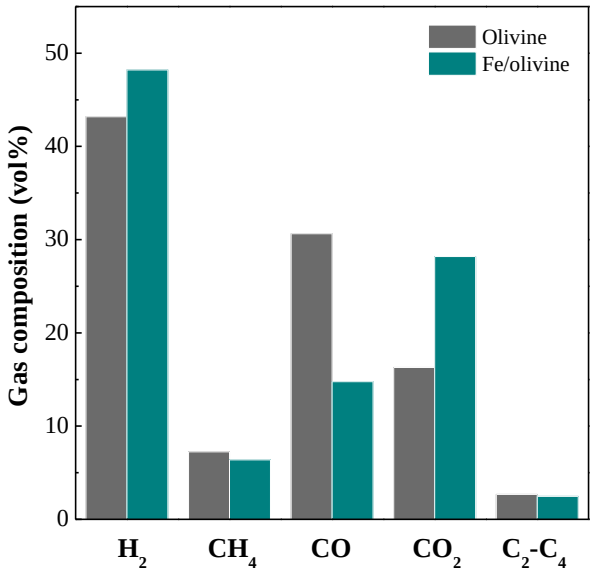

Figure 7.5. Influence of iron impregnation into olivine on gas composition. Reaction conditions: 850 ºC; S/B ratio, 2

Although there are many studies dealing with steam reforming of biomass tar model compounds using a wide variety of supported metal catalyst (Artetxe et al., 2016, 2017; Adnan et al., 2017; Ahmed et al., 2018; Cao et al., 2018; Savuto et al., 2018; Zou et al., 2018; Tan et al., 2020; Cavalli et al., 2021; Kim et al., 2021), those dealing with the effect of metal impregnated in situ catalysts on the biomass steam gasification are scarce, especially those carried out in laboratory pilot plants. Several authors reported the same trend as that obtained in this study for iron impregnated olivine and compared its activity with that of raw olivine using different gasification technologies (Rapagnà et al., 2011; Barisano et al., 2012, 2016; Virginie et al., 2012; Pan et al., 2019). Thus, Rapagnà et al. (2011) studied the performance of 10 wt%Fe/olivine catalysts in the biomass steam gasification at 820 ºC in a fluidized bed gasifier and obtained slightly higher reaction indices than in this study. They observed that H_2 and gas productions increased from 3.5 to 6.6 wt% (the gaseous stream contained 53 vol% of H_2) and from 1.0 to 1.4 Nm^3 kg^{-1}, respectively when an Fe/olivine catalyst was used instead of raw

olivine, whereas tar concentration was reduced by approximately 62 %, with the value being 2.25 g Nm^3 with the catalyst. Carbon conversion efficiency reached a value of 80 %, which was similar to that obtained with raw olivine. Virginie et al. (2012) used the same catalyst as the previous authors, but they used a dual fluidized bed. They reported that tar reduction was more notable in the presence of Fe/olivine in the bed than in the run with raw olivine (5.1 and 2.6 g Nm^{-3} of tar content for olivine and Fe/olivine at 850 ºC). In addition, Barisano et al. (2012, 2016) evaluated the performance of 10 wt%Fe/olivine catalyst in the biomass steam/O_2 gasification at 890 ºC in an internal circulating bubbling fluidized bed (ICBFB) and they reported 1.2 Nm^3 kg^{-1} and 3 wt% for the gas and H_2 productions. They also reported a reduction in the total tar content by 38 % (from 10.1 to 6.2 g Nm^{-3}), and 98 % of carbon conversion efficiency was therefore attained. However, Pan et al. (2019) used a lower Fe load in the catalyst (5 wt%Fe/olivine) for the steam co-gasification of pine sawdust and bituminous coal in a pyrolysis-reforming-combustion decoupled triple bed system (DTBG) at 850 ºC. All the studied reaction indices were improved, but the differences were not as remarkable as those observed for the biomass steam gasification. Thus, they obtained gas and H_2 productions of 0.66 Nm^3 kg^{-1} and 2.49 wt% (10 % higher in both cases) and a tar content as low as 4.87 g Nm^{-3} (17 % reduction).

Ni loading to olivine also enhances tar reforming activity in the biomass steam gasification, with the performance being even better than that of Fe/olivine catalyst. Thus, Pfeifer et al. (2004) studied tar removal activity of Ni/olivine catalyst in a 100 kWth dual fluidized bed reactor. After adding 20 % of 5 wt%Ni/olivine catalyst to a bed of olivine, the tar concentration was reduced by half and gas and H_2 productions increased to 1.0 Nm^3 kg^{-1} and 3.93 wt%, respectively at 850 ºC. Michel et al. (2011b) used in situ 3.9 wt%Ni/olivine catalyst in the biomass steam gasification carried out in fluidized bed at 800 ºC and reported a higher efficiency of the catalyst compared to raw olivine. Thus, they obtained H_2 and gas productions of 7.6 wt% and 1.7 Nm^3 kg^{-1}, instead of 3.4 wt% and 1 Nm^3 kg^{-1} with olivine, and less than 1 wt% of tar. More recently, Tursun et al. (2019) used 5 wt%Ni/olivine catalyst in a DTBG system consisting of a pyrolyzer, reformer and combustor, and reported that the catalyst not

only improved tar removal, but also enhanced H_2 and gas productions. Their results were slightly better than those obtained by Michel et al. (2011b), but the Ni loading was also slightly higher. They reported a gas production of 1.59 Nm^3 kg^{-1}, with H_2 concentration being 56.1 vol% (H_2 production of 8.0 wt%) and tar content as low as 0.6 g Nm^{-3}.

Regarding to tar composition, Figure 7.6 shows a significant reduction in the amount of heterocycles and heavy PAHs using Fe/olivine catalyst. In fact, the mass fraction of those lumps was reduced from 10.33 and 10.20 to 7.43 and 5.05 wt%, respectively. However, the percentage of light aromatics and PAHs in the total tar amount increased from 14.22 and 62.09 to 19.91 and 65.20 wt%. It is noteworthy that the Fe/olivine catalyst managed to reduce significantly the concentration of all tar families, as shown in Table 7.5. Based on the tar formation and PAH growth mechanisms (Cortazar et al., 2019), the Fe/olivine catalyst seems to hinder the growth of light PAHs into heavier ones, and the amount of the light PAHs was therefore higher. Furthermore, Diels-Alder reactions involving light alkenes in the permanent gases and phenols may produce light aromatics, and therefore its amount was increased (Nitsch et al., 2013; Qin et al., 2015; Meng et al., 2018c).

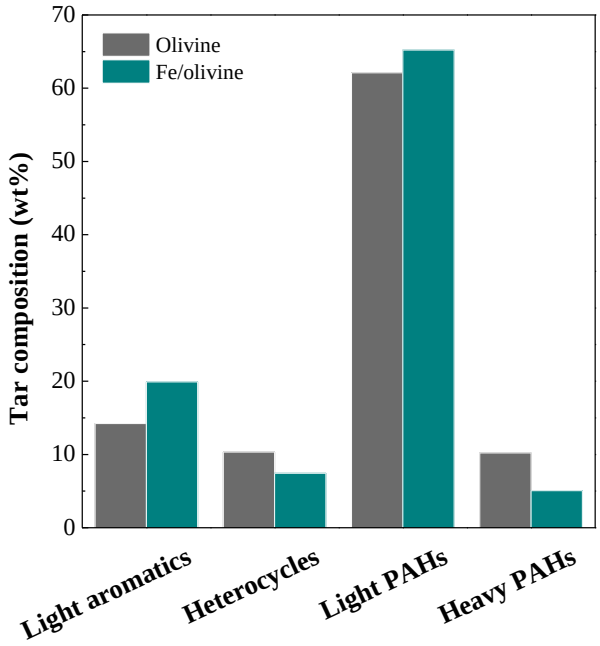

Figure 7.6. Influence of iron loading on tar composition.

Table 7.5 provides a detailed composition of the tar obtained with raw olivine and Fe/olivine catalyst. Naphthalene was the most abundant tar molecule for calcined olivine and Fe/olivine catalysts, although its concentration was reduced by 42 % approximately with the iron enrich catalyst. Barisano et al. (2016) reported a higher naphthalene reduction (of around 58 %) in the biomass steam/O_2 gasification. Moreover, compounds such as phenol, methyl phenol, 1-methyl naphthalene, dibenzofuran, 1-H phenalene, 2-phenyl naphthalene and pirene were significantly removed, as the catalyst managed to reduce their content beyond 60 %. Thus, it is clear that metallic iron is active for C-C and C-H bond breakdown (Nordgreen et al., 2006, 2012). The results in Table 7.5 also show the more stable tar compounds, which are those that are more difficult to remove. Using the Fe/olivine catalyst the concentration of toluene, naphthalene and anthracene was reduced, but their amounts were still rather high, as they are refractory to reforming/cracking reactions (Rapagnà et al., 2011). Therefore, all the efforts in the development of supported metal catalysts should be directed towards their capacity for removing the most refractory tar compounds.

Table 7.5. Detailed composition (g Nm^{-3}) of the tar obtained with calcined olivine and Fe/olivine catalyst.

	Olivine	**Fe/olivine**
Tar compound	**g Nm^{-3}**	**g Nm^{-3}**
Light aromatics	**2.99**	**2.08**
Toluene	2.99	2.08
Heterocycles	**2.17**	**0.78**
Phenol	0.66	0.30
Methyl phenol	1.51	0.48
Light PAHs	**13.04**	**6.81**
Indene	0.16	0.00
Naphthalene	6.80	3.97
1-Methyl naphthalene	0.33	0.16
2-Methyl naphthalene	0.31	0.27
Biphenyl	0.18	0.13
Biphenylene	1.47	0.58
Dibenzofuran	0.75	0.22
Fluorene	0.41	0.18
1-H-Phenalene	0.56	0.20
Anthracene	1.32	0.90
Phenanthrene	0.24	0.12
2-Phenyl naphthalene	0.49	0.08

Table 7.5. Continued.

	Olivine	**Fe/olivine**
Tar compound	**g Nm^{-3}**	**g Nm^{-3}**
Heavy PAHs	**2.14**	**0.53**
Pyrene	0.82	0.24
Fluoranthene	1.08	0.29
4H-Cyclopenta[def]phenanthrene	0.23	0.00

7.2.2. Stability of the Fe/olivine catalyst

The evolution of the gasification performance (Figure 7.7) and gas and tar compositions (Figures 7.8 and 7.9) were monitored for Fe/olivine with time on stream. The main properties of the Fe/olivine catalyst and their role on the biomass steam gasification explain these results.

Figure 7.7 illustrates the evolution of the reaction indices as a function of time on stream for Fe/olivine catalyst. Even though the performance of the calcined olivine remained stable after 140 min on stream, that of Fe/olivine catalyst underwent deactivation and the efficiency of the gasification process decreased with time on stream. Catalyst deactivation was especially evident by tar concentration, which increased by around 90 %, from 10.4 to 19.8 g Nm^{-3}, as shown in Figure 7.7c. After 140 min on stream, the amount of tar produced with the Fe/olivine catalyst reached almost that obtained with the calcined olivine (20.6 g Nm^{-3}). Other reaction indices also showed the deterioration of the catalyst. Thus, gas and H_2 productions declined from 1.46 and 6.2 to 1.35 Nm^3 kg^{-1} and 5.4 wt%, respectively (Figure 7.7a and 7.7b). However, the gas and H_2 productions were still above those obtained with calcined olivine, which suggests that although the catalyst was not able to maintain its original tar elimination capacity, it was still active in the WGS reaction. Likewise, a similar trend is observed in the evolution of the gas composition (Figure 7.8). H_2 concentration slightly decreased from 48.2 to 45.5 vol%, whereas that of CO increased from 14.3 to 20.2 vol%. CO_2 concentration remained almost stable at 24.9 vol%. A comparison of this performance with the stable calcined olivine shows that higher H_2 and CO_2 concentrations were obtained, whereas the value of CO was lower due to the enhancement of the WGS reaction. Concerning CH_4 and C_2-C_4 light hydrocarbons, they showed a slightly upward trend. In the case of the deactivated catalyst, CH_4 concentration was even lower (6.4 vol%) than that obtained with the calcined olivine and C_2-C_4 concentration reached a similar value as that with the calcined olivine (2.7 vol%). The latter results are evidence that the Fe/olivine catalyst was still active for steam reforming of CH_4 subsequent to 140 min on stream.

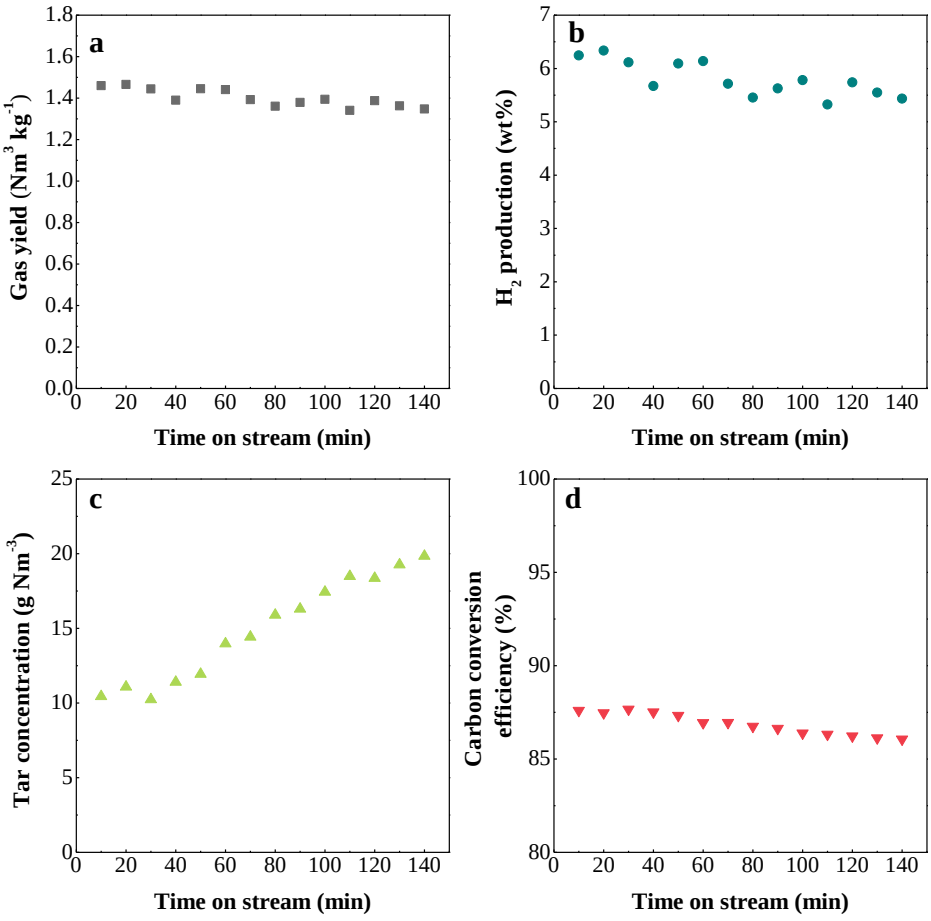

Figure 7.7. The evolution of gas production (a), H_2 production (b), tar concentration (on a dry basis), (c) and carbon conversion efficiency (d) with time on stream for Fe/olivine catalyst. Reaction conditions: 850 ºC; S/B ratio, 2.

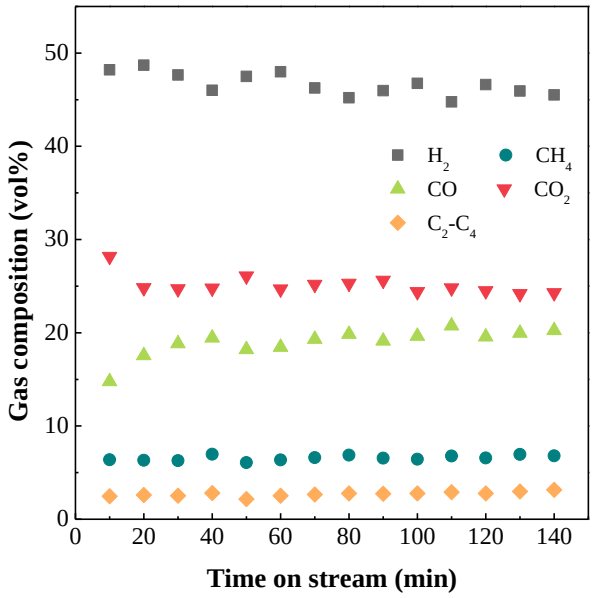

Figure 7.8. Gas composition as a function of time on the Fe/olivine catalyst. Reaction conditions: 850 ºC; S/B ratio, 2.

The evolution of tar lumps with time on stream is shown in Figure 7.9. As the Fe/olivine catalyst was deactivated, the amount of each tar family was similar to that obtained with the calcined olivine. Thus, the amount of light aromatics and PAHs declined from 19.91 and 64. to 15.24 and 57.47 wt%, whereas that of heterocycles and heavy PAHs increased from 7.43 and 5.05 to 10.82 and 11.63 wt% after 140 min on stream. Small differences were observed in the amount of light PAHs between the value with the calcined olivine and that with the deactivated Fe/olivine catalyst, which are related to the amount of unidentified compounds (there were more unidentified compounds with the deactivated catalyst). When the deactivation of the catalyst was not considerable, the Fe/olivine catalyst seemed to hinder the growth of light PAHs into heavier ones, and the amount of the light PAHs was therefore higher than for the calcined olivine. Moreover, Diels-Alder reactions involving light alkenes in the permanent gases and heterocyclic compounds may also have produced light aromatics,

which led to an increase in their amount (Nitsch et al., 2013; Qin et al., 2015; Meng et al., 2018c).

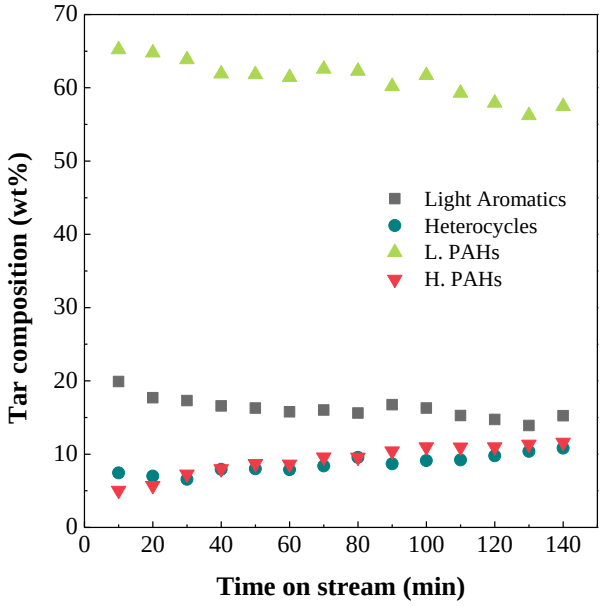

Figure 7.9. Tar composition with time on stream on the Fe/olivine catalyst. Reaction conditions: 850 ºC; S/B ratio, 2.

7.2.3. Causes of catalyst deactivation

The prevention and attenuation of catalyst deactivation is a challenging task. Thus, most catalytic processes undergo catalyst deactivation, and therefore understanding the deactivation mechanisms is vital. In the biomass gasification processes, deactivation is mainly caused by sulphur and chlorine poisoning or carbon deposition. However, catalyst physical changes, such as sintering, phase change and attrition may also lead to catalyst deactivation. The deactivated catalyst was characterized in detail in order to understand the main causes of catalyst activity decay.

7.2.3.1. Textural properties

Table 7.6 shows the values of the physical properties for the fresh and deactivated Fe/olivine catalysts. After 140 min on stream, the specific surface area of the Fe/olivine catalyst was significantly lower, with the reduction being even more noticeable in the pore volume and size, which underwent a more severe decrease. Therefore, the pores of the catalyst were partially blocked, which led to a decrease in the total surface area, as well as pore volume and size. The deactivated Fe/olivine catalyst had still a higher surface area and pore volume than the calcined olivine. However, the pore size was higher in the calcined olivine.

Table 7.6. Properties of the fresh and deactivated catalysts.

Catalyst	S_{BET} (m^2 g^{-1})	V_{pore} (cm^3 g^{-1})	d_{pore} (A)
	fresh/deactivated	*fresh/deactivated*	*fresh/deactivated*
Olivine	1.92	0.0003	78.33
Fe/olivine	3.75/2.47	0.0076/0.0021	80.85/34.76

7.2.3.2. Metallic properties

In order to assess the changes in the metallic structure of the Fe/olivine catalyst after the reaction, Figure 7.10 shows the XRD patterns of the reduced and deactivated catalysts. After the reaction, the main crystalline structures were still the olivine structure and the $MgSiO_3$ enstatite phase, although more diffraction lines corresponding to $MgSiO_3$ phase appeared in the deactivated catalyst. The most significant differences between both spectra are related to the iron phases. In the spectrum of the deactivated catalyst, there was no evidence of the presence of metallic iron, neither in 2Θ=44º nor 2Θ=65º diffraction lines. However, multiple lines of Fe_3O_4 or $MgFe_2O_4$ spinel phase were noticeable, which are evidence of a loss of active phase by oxidation of the metallic iron under reaction conditions. Virginie et al. (2012) also

reported the presence of intense diffraction lines corresponding to Fe_3O_4 or $MgFe_2O_4$ spinel phase after reaction.

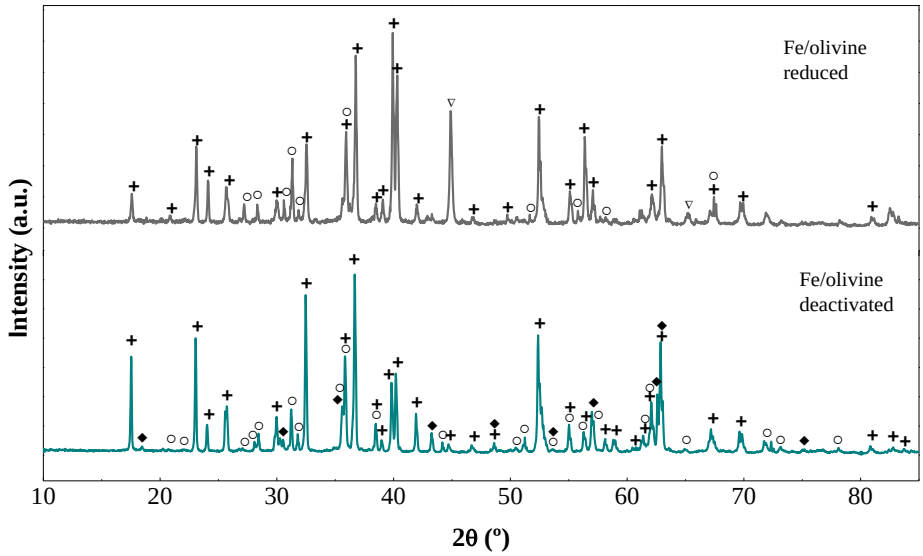

Figure 7.10. XRD patterns of reduced and deactivated catalysts. Crystalline phases: (+)(($Mg_{1.81}$ $Fe_{0.19}$) (SiO_4)), (o) $MgSiO_3$, (∇) metallic iron, (⬥) Fe_3O_4 or $MgFe_2O_4$ spinel phase.

7.2.3.3. Surface analysis

XPS analysis of the deactivated catalyst was carried out to determine the components located on the surface of the catalyst after reaction. The XPS spectra of the reduced and deactivated samples in different binding energy ranges are shown in Figure 7.11. This analysis revealed that, after the reaction, the main components on the surface of the samples are still Si, Mg, Fe and O (Figure 7.11b). However, the presence of K and Ca was also observed, although the amount of the latter on the surface could not be quantified because it was very small. Their existence was probably due to the biomass ashes. As shown in Figure 11c, metallic iron was not detected on the catalyst surface in the deactivated catalyst, which is consistent with the previous XRD results (Figure 7.10).

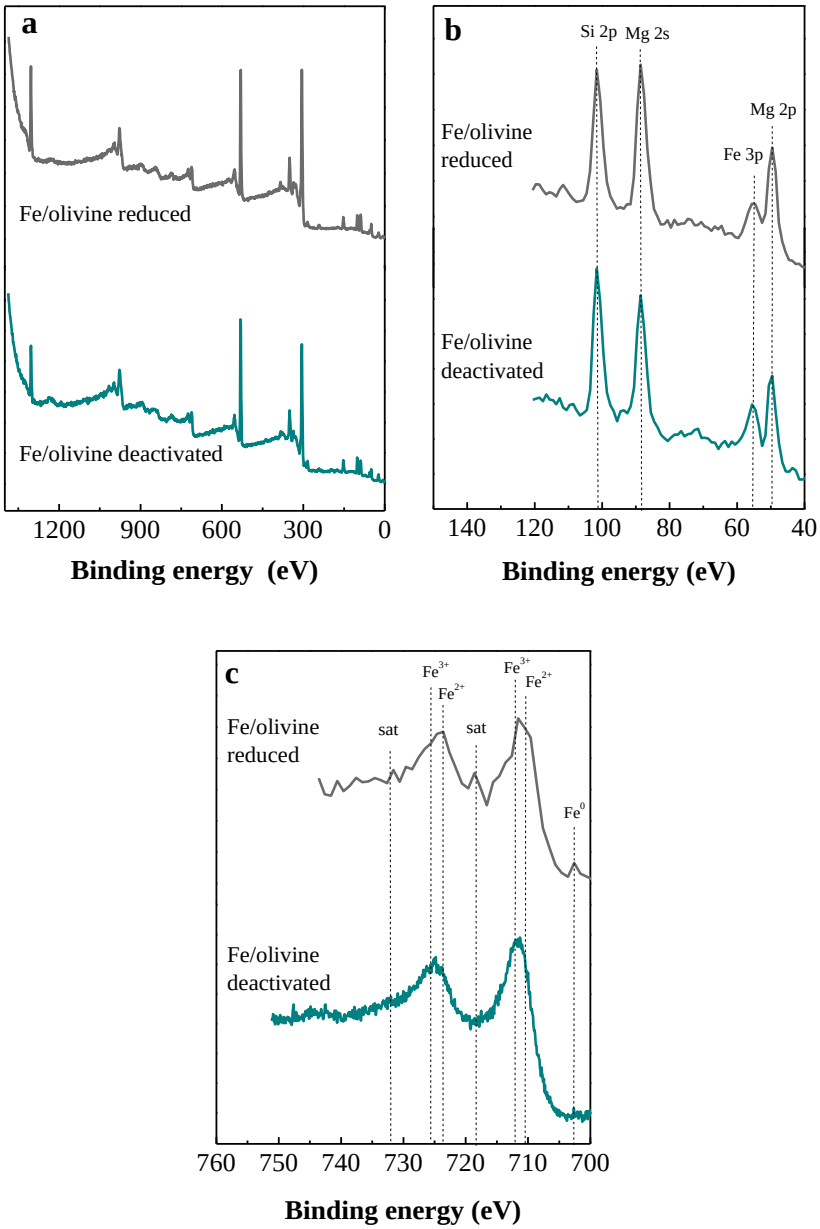

Figure 7.11. Wide XPS spectra (a), XPS spectra for low binding energy regions (b) and Fe 2p (d) of the reduced Fe/olivine and deactivated catalysts.

The surface composition and iron distribution in the reduced and deactivated catalysts are shown in Table 7.8. As observed, after the reaction there were small differences in

the amount of Mg and Fe on the catalyst surface. The amount of iron slightly increased from 4.4 to 5.1 % at the expense of Mg, which decreased from 22.1 to 18.4 wt%. However, the iron distribution remained constant (the amount of Fe^{2+} and Fe^{3+} compounds is the same), which is an indication that iron migration from the olivine structure into the surface happened. A comparison of this catalyst with the calcined olivine shows that the deactivated catalyst had more iron in the olivine structure and a higher amount of Fe^{2+} compounds on its surface. Iron migration from the inside to the surface or vice versa occurs in order to reach iron equilibrium in the structure (Virginie et al., 2012; Fredriksson et al., 2013). Regarding the amount of K on the deactivated catalyst surface (1.4 %), its origin is attributed to biomass ashes. Alvarez et al. (2019) reported the chemical analysis of the ashes of the same biomass used in this work and the amount of K_2O was 11.3 wt%. Moreover, at 850 ºC, potassium salts melt and they might have formed deposits on the deactivated catalyst surface.

Table 7.8. Surface composition (%) and iron distribution (%) in the reduced and deactivated Fe/olivine catalysts.

Component (%)	Si	Mg	O	Fe	K	Fe^{2+}/Fe^{3+}
Fe/olivine reduced	14.6	22.1	58.9	4.4	-	1
Fe/olivine deactivated	15.4	18.4	59.8	5.1	1.4	1

7.2.3.4. Reducibility of metallic species

Figure 7.12 shows the TPR curve of the fresh and spent catalysts. A single peak at 500 ºC with a small shoulder at a slightly higher temperature (590º C) was observed for the deactivated catalyst, which is evidence that the iron in the Fe/olivine catalyst was oxidized during the gasification process. As the XRD revealed, this peak should be attributed to the Fe_3O_4 or $MgFe_2O_4$ spinel phases detected. According to Meng et al. (2019), the difficulty for reducing the possible iron oxides is as follows: $MgFe_2O_4$>FeO>Fe_3O_4>Fe_2O_3. However, the low reduction temperature suggests that

this species was easy to reduce, i.e., it was probably Fe_3O_4. Furthermore, the shoulder at 590 ºC is attributed to the reduction of a small amount of $MgFe_2O_4$ spinel phase. In fact, it seems that most of the $MgFe_2O_4$ spinel phase did not undergo oxidization during the reaction, as it is a very stable compound.

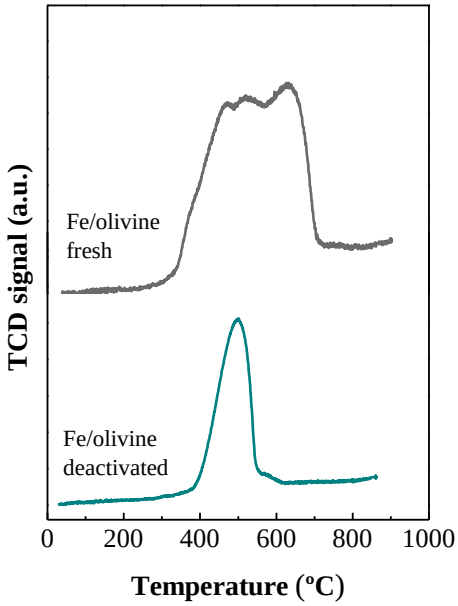

Figure 7.12. TPR profiles of the fresh and deactivated catalysts.

7.2.3.5. Coke deposition

As carbon deposition may cause catalyst deactivation, temperature programmed oxidation (TPO) was conducted on the spent Fe/olivine catalyst to quantify the amount of carbon settled. The total amount of coke and its composition depends on the operating conditions, mainly temperature and S/B ratio, as carbon deposition is a consequence of a balance between its formation and removal by gasification (Remiro et al., 2013). The TPO analysis revealed that a negligible amount of coke (0.11 wt%) was deposited on the catalyst after the reaction, which is evidence that high temperatures and steam promoted the in situ gasification of almost all the carbon that

may have formed. Figure 7.13 shows the TPO profile of the deactivated catalyst. Two different peaks are observed, which is an indication of the heterogeneous nature of the coke. According to the literature (Nahil et al., 2013; Waheed and Williams, 2013; Ochoa et al., 2018; Santamaria et al., 2020b; Fernandez et al., 2021b), the coke combustion temperature on supported metal catalysts is related to its location on the catalyst and composition. Low combustion temperatures are attributed to the coke deposited on the metallic sites (encapsulating coke), which may catalyse coke combustion, whereas higher combustion temperatures indicate that the coke is deposited on the support, which prevents coke combustion by metallic sites. Furthermore, even if the coke is deposited on similar locations, its combustion temperature is higher as the condensation degree is higher, i.e., more organized structures with lower H/C ratios.

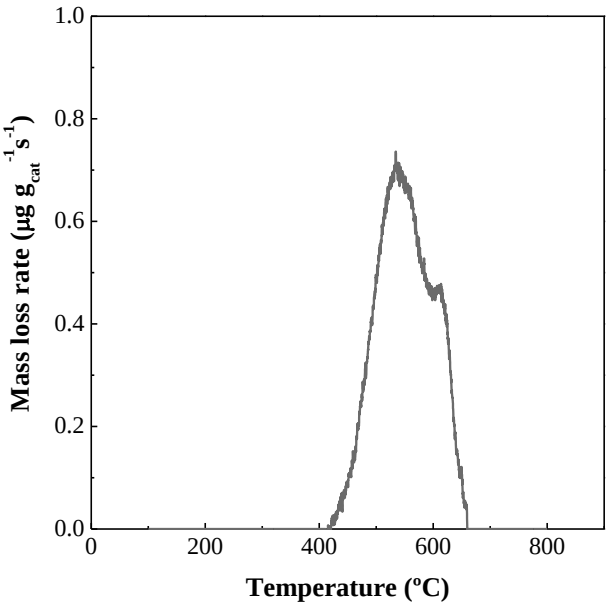

Figure 7.13. TPO profile of the deactivated Fe/olivine catalyst.

Figure 7.13 reveals the heterogeneity of the coke. Thus, two different carbon species were detected, with their combustion temperatures being 530 and 606 ºC. The peak at 530 ºC is attributed to the amorphous coke and the shoulder at 606 ºC to a coke with a

slightly more condensed structure. It seems that the severe reaction conditions prevented coke formation from the evolving compounds to more condensed ones due to the in situ gasification of the amorphous coke. Virginie et al. (2012) observed a similar TPO profile after biomass steam gasification experiments, although their carbon oxidation temperatures were slightly higher than those obtained in this work (585 and 630 ºC). As the coke content was very low (0.11 wt%), it cannot be stated that coke deposition caused catalyst deactivation.

7.2.3.6. Chemical composition

Table 7.9 shows the chemical composition of the fresh and deactivated Fe/olivine catalysts. XRF analysis revealed that there was no any iron loss due to attrition phenomena, which was also checked by sieving the deactivated catalyst (it had the same size range (90-150 μm) as prior to the runs). Meng et al. (2018b) and Claude et al. (2019) reported that the olivine catalysts synthesized by wet impregnation may undergo attrition, since the metallic species are mainly placed on the surface, and therefore their interaction with the support is rather weak. Some other authors studied this aspect. Thus, Virginie et al. (2012) reported an iron loss of 32 % after 12 h gasification in a dual fluidized bed and Rapagnà et al (2011) about 5 wt% during 320 min operation in a fluidized bed reactor.

Table 7.9. Chemical composition (wt%) of the fresh and deactivated Fe/olivine catalysts.

Component (wt%)	**MgO**	**SiO_2**	**Fe_2O_3**	**CaO**	**Al_2O_3**	**Na_2O**	**TiO_2**	**MnO**
Fe/olivine fresh	42.08	38.68	14.71	0.12	0.24	0.06	0.02	0.10
Fe/olivine deactivated	42.58	39.60	14.30	0.14	0.21	0.07	0.04	0.11

7.3. DISCUSSION

The gas composition in the gasifier environment plays a crucial role in the oxidation state of the iron located on the catalyst. During biomass steam gasification, metal Fe^0 was oxidized, as detected by XRD, XPS and TPR analyses. The operating methodology used in this study may have a significant impact, as it may have contributed to the catalyst oxidation, as explained in the experimental section. Thus, the fluidizing agent had to be changed from N_2 to steam and ensure suitable fluidization regime prior to starting biomass feed, which may have caused changes in the reaction environment. The presence of steam may have induced partial oxidation of the metallic phase at the beginning of the reactions. However, as biomass was fed into the reactor, the reaction environment shifted from oxidizing to reducing due to the high hydrogen concentration, and therefore the iron oxidized under steam atmosphere was reduced again. It should be noted that this problem can be avoided in full scale operation with continuous biomass feed.

A similar catalyst deactivation cause was observed in the in-line steam reforming of biomass fast pyrolysis volatiles on 10 wt%Co/Al_2O_3 catalyst by Santamaria et al. (2020a). Nordgreen et al. (2012) reported that, when the oxygen concentration in the reaction environment is too high, it would oxidise the metallic iron to wustite (FeO), and subsequently to magnetite (Fe_3O_4), since some locations favour these transformations. Based on the results obtained, when Fe was in the metallic state in the Fe/olivine catalyst, it showed a higher activity for reducing tar than when it was in the oxidized state (Figure 7.7c). Changes in tar removal capacity of the Fe/olivine catalyst with time on stream may also be related to the distribution of iron oxides. Nordgreen et al. (2012) also stated that the catalyst with metallic iron was capable of reducing the tar concentration above 60 %, whereas the catalyst with the oxidized iron only had a capacity of 18 %. The catalytic activity of iron oxides species increases with their reduction state (Fe_2O_3<Fe_3O_4<FeO<Fe^o) (Claude et al., 2019). After 140 min on stream, the tar concentration obtained with the deactivated Fe/olivine catalyst and that obtained with the calcined olivine were almost the same, which suggests the presence

of iron oxides led to the same tar removal performance as calcined olivine. The same trend was observed in the evolution of tar lumps. As the Fe/olivine catalyst was deactivated, the amount of each tar family was similar to that obtained with the calcined olivine. Undoubtedly, the oxidation of metal Fe^0 sites led to their decrease, and therefore caused catalyst deactivation, as was revealed by the characterization techniques.

Several studies pointed out that different Fe-phases may catalyze different reactions. Thus, Fe_2O_3 is reported to catalyze shoot and NO_x conversion, Fe_3O_4 to be active in the WGS reaction and metal Fe to catalyze Boudard reaction and tar removal reactions. Therefore, changes in the oxidation state of iron will drastically influence catalytic properties (Fredriksson et al., 2013). However, it seems that, after 140 min on stream, the Fe/olivine catalyst was still active for WGS and CH_4 steam reforming reactions, as shown in Figures 8a and 8b, which may be attributed to the Fe_3O_4 or $MgFe_2O_4$ spinel phase detected on the deactivated catalyst (Figure 7.10). However, the TPR analysis of the deactivated catalyst was more conclusive than XRD and XPS analyses, which allows inferring that Fe_3O_4 is the responsible, as the reduction temperature was rather low. Some authors proved Fe_3O_4 was active in the WGS reaction (Martos et al., 2009; Ratnasamy and Wagner, 2009; Fu et al., 2015; Chou et al., 2019; Chen et al., 2020).

.

8

SUMMARY

This thesis explores the potential of a novel reactor based on spouted bed technology, namely, the fountain confined spouted bed for the biomass steam gasification. With the fountain confiner and draft tube, and operatring under high u/u_{ms} ratios, a clearly differentiated regime called fountain enhanced regime is attained, which makes fountain confined spouted bed reactor highly efficient for this process.

In order to develop and characterize this novel regime, the influence of different operating parameters (temperature, gas flow rate, particle size and bed mass) and draft tube geometry (tube diameter and entrainment zone height) have on the reactor's hydrodynamics was analyzed. Fountain confinement allows enlarging greatly the fountain region, specially the height, which improves the contact between reacting gases and the catalyst, increases the effective volume in the fountain available for tar cracking (temperature profile is more uniform) and narrows the residence time distribution.

Biomass (1-2 mm pine sawdust) steam gasification experiments were conducted using a draft tube with a diameter of 8 mm (internal diameter 5.5 mm) and an entrainment zone height of 15 mm. The runs were carried out in continuous mode by feeding 0.75 g min^{-1} of biomass. In all the experiments, the same steam flow rate of 1.5 mL min^{-1} was used, which corresponds to 1.86 NL min^{-1} (under normal conditions). Accordingly, the runs were performed with a S/B ratio of 2. The main reaction indices considered were gas yield and composition, H_2 production, tar concentration and composition and carbon conversion efficiency.

The experiments for assessing the different hydrodynamic regimes attained in the biomass gasification were carried out at 850 ºC and using olivine as primary catalyst. The bed contained 100 g of olivine, and two particles sizes were used, i.e., 90-150 µm and 250-355 µm. Thus, operating with the coarse olivine fraction, the reactor operated under conventional spouting regime and, in those with the fine olivine, the fountain enhanced regime was attained. Experiments with and without the fountain confiner were carried out with the coarse olivine under conventional spouting regime. Moreover, the results obtained with the confiner under conventional spouting regime

were compared with those obtained with this device, but operating in the enhance fountain spouting regime. The use of the fountain confiner allows enhancing process versatility, increasing gas velocity over the minimum spouting one, increasing the fountain height and reducing olivine particle size (enhanced fountain regime). Thus, as a result of enhancing process efficiency, tar content was reduced from 49.2 g Nm^{-3} without fountain confiner to 34.6 g Nm^{-3} when this device was used, increasing gas and H_2 productions from 1.08 Nm^3 kg^{-1} and 3.5 wt% to 1.23 Nm^3 kg^{-1} and 4.5 wt%, respectively. Moreover, a greater improvement was attained under the enhanced fountain regime, as tar content was reduced to 20.6 g Nm^{-3}, with the reduction of heavy PAHs being especially remarkable. Likewise, gas and H_2 productions also improved, reaching a value of 1.3 Nm^3 kg^{-1} and 5.0 wt% respectively.

Consequently, the fountain confiner enhanced the efficiency of biomass gasification by favouring tar cracking Thus, at 850 ºC, tar content was reduced from 49.2 g Nm^{-3} without confiner to 34.6 g Nm^{-3} when this device was used. The gas and H_2 productions and carbon conversion efficiencies were also remarkably improved. Therefore, gas and H_2 productions increased from 1.08 Nm^3 kg^{-1} and 3.5 wt% to 1.23 Nm^3 kg^{-1} and 4.5 wt%.

The effect temperature has on the distribution of products and their character was studied by means of runs at 800 ºC, 850 ºC and 900 ºC. The reactor was loaded with 100 g of olivine, with particles in the 90-150 μm range. Not only did temperature have a positive effect on the gas yield and carbon conversion, but also played a crucial role in tar removal, as its concentration decreased from 49.2 g Nm^{-3} at 800 ºC to 6.7 g Nm^{-3} operating at 900 ºC. Moreover, temperature also enhanced hydrogen production recording a value of 7.3 wt% at 900 ºC. Regarding tar formation and its evolution pathway, as gasification temperature was increased the tar composition (analyzed by GC/MS, FTIR and simulated distillation techniques) evolved to more stable aromatic compounds (of higher molecular weight), such as naphthalene or fluoranthene, with heterocyclic or light aromatic compounds being almost absent at 900 ºC.

The performance of the primary catalysts olivine, dolomite, γ-alumina and FCC spent catalysts were evaluated at 850 ºC. Runs with silica sand were also carried out for comparison purposes. As the density of the primary catalysts studied differs greatly, the bed mass and particle size were adjusted accordingly to operate under comparable hydrodynamic conditions. Thus, the runs with olivine and silica sand were carried out using a bed of 100 g and a particle size in the 90-150 um range. The beds of dolomite contained 53 g of particles with a size in the 150-250 μm range, those of FCC 55 g in the 90-150 μm range and those of γ-alumina 45 g in the 250-400 μm range. These primary catalysts were characterized by means of N_2 adsorption-desorption, X-ray fluorescence (XRF) and temparture programmed desorption of NH_3.The benefits of the fountain confiner improved the gas-solid contact, and therefore favoured the primary catalysts reforming and cracking activity, enhancing H_2 production and reducing tar formation. Thus, dolomite and γ-alumina recorded the lowest values of tar, 5.0 and 6.7 g Nm^{-3}, respectively, which corresponded to 79 and 72 % tar reduction compared to the inert sand, whereas the olivine and the FCC spent catalyst recorded higher contents, 20.6 and 16.2 g Nm^{-3}, respectively. Regarding H_2 production, dolomite and γ-alumina led to a H_2 content in the gaseous stream of 51.3 vol% and 49.3 vol%, respectively, which correspond to H_2 productions of 7.3 wt% and 6.7 wt%, respectively.

Fe incorporation by wet impregnation on primary catalysts was proposed for enhancing their activity towards cracking, reforming and WGS reactions. The performance of Fe/olivine catalyst was tested at 850 ºC and compared with that of calcined olivine. Olivine was used as catalyst support and loaded with 5 wt%Fe. The bed consisted of 100 g of either calcined olivine or Fe/olivine catalyst, with their particle size being in the 90-150 μm range. Prior to the reactions, the iron catalyst was subjected to an in situ reduction process at 850 ºC for 4 h with a stream containing 10 vol% of H_2 to ensure complete reduction to Fe^0 phase. The catalyst was monitored by N_2 adsorption-desorption, X-ray fluorescence (XRF), temperature programmed reduction (TPR), X-ray powder diffraction (XRD) and X-ray photoelectron spectrometry (XPS), with the aim of determining the physical properties, chemical composition, reducibility, the metallic species and surface composition of the catalysts before and after the runs.

Moreover, temperature programmed oxidation (TPO) was also used to characterize the deactivated catalyst. The efficiency of the gasification process using olivine was considerably improved on the Fe/olivine catalyst, with the tar reduction being especially remarkable (to 10.4 g Nm^{-3}). After 140 min on stream, catalyst deactivation was particularly evident, as tar concentration increased to 19.9 g Nm^{-3} (90 % of that without Fe addition). However, Fe/olivine catalyst was still active for WGS and CH_4 steam reforming reactions, with gas and H_2 productions being 1.35 Nm^3 kg^{-1} and 5.4 wt%, respectively. Metal iron oxidation to Fe_3O_4 caused catalyst deactivation, as the reaction environment shifted from oxidizing to reducing conditions due to the experimental procedure.

The results obtained in this thesis shed light on the excellent performance of the fountain confined spouted bed reactor under enhanced fountain regime, as it overcomes the performance of the conventional spouted bed in biomass steam gasification. The fountain confinement not only modifies the residence time distribution of the reactor, but also allows operating stably with high fountains (this circumstance is attained using fine materials), and there is therefore a great bed expansion and high turbulence. These hydrodynamic improvements promote the contact between in-bed catalyst and biomass derived volatiles, thereby favouring tar elimination and H_2 production. Moreover, this novel reactor configuration showed high versatility and stability handling primary catalysts of different densities and granulometries, which is of uttermost relevance for the full scale development of the process. Indeed, fountain confined spouted bed reactors operating under fountain enhanced regime allow achieving results within the range of those corresponding to fine tunned fluidized beds.

9

CONCLUSIONS

The estudy conducted in this thesis allows drawing the conclusions detailed below, which are especially relevant for future research on biomass gasification and the industrial implementation of biomass valorization processes for H_2 production with low tar content.

Hydrodynamic study

A fountain enhanced spouting regime was attained for high gas velocities of around four times that corresponding to the minimum spouting one. Moreover, a large fountain region was developed in which the gas-solid contact was greatly improved, temperature profiles were more uniform than in conventional spouted beds and gas and solid residence times had a narrow distribution.

The most influential parameter on the minimum spouting and fountain enhanced spouting velocities was particle size, with both regimes being stable even when operating with the finest particle size studied (90-150 μm). For different draft tube designs, an increase in olivine particle size caused an increase in minimum and fountain enhanced spouting velocities, which was especially pronounced for the particles in 250-355 and 355-500 μm range. The effect of temperature was more remarkable on the fountain enhanced spouting velocity, i.e., it increased as temperature was increased to 400-600 ºC but decreased for a further increase to 800 ºC. However, the minimum spouting velocity hardly changed with temperature. Regarding the olivine bed mass, an increase from 100 to 250 g led to an increase in both minimum and fountain enhanced spouting velocities, with the increase being especially remarkable in the fountain enhanced velocity. The height of the entrainment zone of the non-porous draft tube affected differently on the minimum spouting and on the fountain enhanced spouting velocities. Thus, an increase in this parameter caused an increase in the minimum spouting velocity, whereas it hardly affected the fountain enhanced spouting velocity. An increase in draft tube and gas inlet diameters caused the expected reduction in the velocity required for reaching both regimes.

Given the high stability of the fountain enhanced spouting regime under a wide range of experimental conditions, several parameters may be fine-tuned in order to meet the most suitable conditions for biomass gasification process. Thus, the interest lies in reducing the gas flow rate in order to increase residence time, but maintaining at the same time an excellent contact in the fountain region. This objective can be achieved operating with the smallest particle size (90-150 μm), as well as the largest draft tube and gas inlet diameters.

Effect of the regime

The insertion of a fountain confiner in conical spouted bed reactors allowed modifying bed hydrodynamics, i.e., the residence time of the volatiles was increased and their contact with the catalyst improved. It also allowed operating with fine materials, and so increasing the u/u_{ms} ratio and improving bed turbulence and gas-solid contact. Furthermore, the confiner provided great stability to the bed and avoided fine particle elutriation.

Consequently, the fountain confiner enhanced the efficiency of biomass gasification by favouring tar cracking. Thus, at 850 ºC, tar content was reduced from 49.2 g Nm^{-3} without confiner to 34.6 g Nm^{-3} when this device was used. The gas and H_2 productions and carbon conversion efficiencies were also remarkably improved. Therefore, gas and H_2 productions increased from 1.08 Nm^3 kg^{-1} and 3.5 wt% to 1.23 Nm^3 kg^{-1} and 4.5 wt%, which also entailed the enhancement of the carbon conversion efficiency from 81.5 % to 83.6 %. Moreover, by reducing olivine particle size, it was possible to operate under enhanced fountain regime, whose features are great fountain height and high bed turbulence. These features allowed a better contact between olivine and the biomass derived volatiles, and tar content was therefore reduced to 20.6 g Nm^{-3}. Likewise, other reaction indices, such as gas and H_2 productions were also improved when operating under enhanced fountain regime, with their values being 1.3 Nm^3 kg^{-1} and 5.0 wt%, respectively, and carbon conversion efficiency 86.1 %. Tar composition was also affected by operating under enhanced fountain regime, with the

lump of light PAHs was the most abundant one in the different reactor configurations. In this regime, the presence of heavy PAHs was significantly reduced, whereas that of light PAHs and light aromatics increased.

Effect of the temperature

Operating under an enhanced fountain regime (attained by confining the fountain) makes the conical spouted bed reactor a suitable technology for biomass steam gasification, as it increases the gas residence time and gas-solid contact, which facilitates tar removal. An increase in gasification temperature improved process efficiency in terms of tar and char conversion, with the maximum carbon conversion efficiency being 93 % at 900 ºC. Moreover, temperature increase also showed a positive effect on hydrogen production, which increased from 2.9 wt% at 800 ºC to 7.3 wt% at 900 ºC. Tar content decreased by around 88 % in the 800-900 ºC range, recording the lowest value (6.7 g Nm^{-3}) at 900 ºC. Tar analysis (FTIR and GC) revealed that its composition was significantly influenced by temperature, opening a pathway for the evolution of its components to more stable species (enhanced when temperature was increased) in the range of secondary and tertiary tars (of higher molecular weight) due to rearrangement reactions. The major fraction in the 800-900 ºC range was that of light PAHs, although tar composition shifted from phenolic compounds and alkyl-substituted PAHs to more stable and heavier PAHs (non-substituted species) by increasing temperature, with naphthalene being the major compound at 850 and 900 ºC. Simulated distillation confirmed that the average boiling point of the tars increased (especially of those obtained from 800 to 850 ºC) when the gasification was performed at high temperatures.

Role of primary catalysts

The fountain confined conical spouted bed performs well in the biomass steam gasification with primary catalysts in situ. In fact, this reactor allows enhancing the

gas-solid contact, and therefore the catalytic activity by avoiding the elutriation of the fine catalyst particles formed, especially when dolomite is used.

The bed materials tested, olivine, dolomite, γ-alumina and FCC catalyst, proved to be beneficial in the biomass steam gasification, as they allowed not only reducing tar formation, but also improving syngas yield and its composition. Dolomite and γ-alumina significantly affected the composition of the gas. Thus, they increased hydrogen content in the gaseous stream to 51.3 vol% and 49.3 vol%, respectively, which corresponded to H_2 productions of 7.3 wt% and 6.7 wt%, respectively. This is explained by their activity for steam reforming, cracking and WGS reactions.

Concerning tar removal, dolomite and γ-alumina showed an excellent performance due to their respective reforming and cracking activities for depleting tar compounds and precursors in their formation. A bed of inert sand led to a tar concentration of 25.7 g Nm^{-3}, but this value was reduced to 5.0 and 6.7 g Nm^{-3} with dolomite and γ-alumina, respectively. Although the FCC spent catalyst did not show a significant reforming activity, it had still some cracking activity, which managed to reduce the tar concentration to 16.2 g Nm^{-3}. For all the catalyst studied, the more abundant species were light PAHs, which accounted for approximately 60 wt% of the total tar concentration. Dolomite's reforming activity turned out to be more effective to deplete the PAH compounds in the tar than the cracking activity of the acid catalysts, since the latter were not only active for removing heterocyclic compounds, but also for promoting the formation of PAH components.

Even though both dolomite and γ-alumina performed better in tar removal and reforming of hydrocarbons, olivine is also an interesting option, as it led to more stable fluidization behaviour, has suitable mechanical properties and is cheaper than γ-alumina.

Influence of iron loading

Iron incorporation to olivine proved to be beneficial in biomass steam gasification at zero time on stream, as it allowed not only reducing tar formation, but also improving syngas production and composition. Thus, gas production increased from 1.30 $Nm^3 kg^{-1}$ with calcined olivine to 1.46 $Nm^3 kg^{-1}$ with Fe/olivine catalyst, and similarly did hydrogen production, with the value being 6.25 wt%. Likewise, tar concentration was reduced approximately to half, from 20.6 to 11.4 g Nm^3. This was explained by the positive effect of metallic iron, which greatly favours WGS and light hydrocarbon steam reforming and cracking reactions. At zero time on stream, naphthalene was the most abundant tar compound for both the calcined olivine and Fe/olivine catalyst, although its concentration decreased to 42 wt% with the latter.

The evolution of the gasification performance and gas and tar compositions with time on stream was also monitored. The stability of the Fe/olivine catalyst was lower than that of calcined olivine, which was still stable after 140 min on stream. Catalyst deactivation was especially evident based on the tar concentration, which increased from 10.4 to 19.9 g Nm^{-3}, i.e., it almost reached the value obtained on the calcined olivine (20.6 g Nm^{-3}). Other reaction indices also showed the deterioration of the catalyst. Thus, gas and H_2 productions declined from 1.46 $Nm^3 kg^{-1}$ and 6.25 wt% to 1.35 $Nm^3 kg^{-1}$ and 5.44 wt%, respectively, but still remained above those obtained with the calcined olivine, suggesting the activity of the deactivated Fe/olivine catalyst for WGS and steam reforming of CH_4.

The characterization techniques revealed that the catalyst deactivation was due to the oxidation of the metallic iron into Fe_3O_4. The presence of steam in the reactor for a few minutes before starting biomass feed may have induced the partial oxidation of the metallic phase at the beginning of the reactions. However, as biomass feed started, the reaction environment shifted from oxidizing to reducing conditions, and the iron that may have oxidized became reduced again. These changes in the iron oxidation state have a great influence on the catalytic properties of the Fe/catalyst, and therefore on

the evolution of tar removal, as well on WGS and light hydrocarbon reforming reactions.

Although the experimental unit used in this study involves certain limitations for the operation with metallic catalysts during the start-up period, the results obtained shed light on the biomass steam gasification using Fe/olivine as primary catalyst in large-scale plants. .

10

NOMENCLATURE

Nomenclature

A_{ox}, A_{HC}	Chromatographic areas of oxygenated compounds and hydrocarbons
A_T	Total acidity, $\mu mol_{NH3}\ g_{cat}^{-1}$
$C_{biomass}$, C_{gas}	Moles of C fed into the reactor and those recovered in the gaseous product stream
C_C	Coke content, wt%
d_p	Particle diameter, μm
d_{pore}	Pore diameter, L
D_T, D_0, L_T, L_H	Design parameters of the draft tube: diameter of the draft tube, gas inlet diameter,total height of the draft tube and entrainment zone height, L
f_{ox}, f_{HC}	Response factor of oxygenates and hydrocarbons
H_G, D_G,	Design parameters of the fountain confiner: length of the fountain confiner, diameter of the fountain confiner, L
HHV, LHV	High and low heating values, $L^2\ T^{-2}$
H_T, H_C, D_G, D_i	Design parameters of the spouted bed reactor: total height, height of the conical section, diameter of the conical section, diameter of the bed bottom, L
m_0, m_{H2}	Mass flow rate of the feed and of the H_2 produced, $M\ T^{-1}$
m_{CO2}	Mass of CO_2 generated in the combustion, M
m_{ox}, m_{HC}	Mass of oxygenates and hydrocarbons, M
M_W	Molecular weight, $M\ mol^{-1}$
P_{H2}	H_2 production, wt%
Q_{gas}	Volumetric flow rate of the gas produced, $L^3\ T^{-1}$
S/B	Steam/biomass ratio
S_{BET}	BET specific surface, $L^2\ M^{-1}$

T	Temperature, K
u_{ms}, u_{ef}	Minimun spouting velocity, fountain enhanced spouting velocity, L T^{-1}
V_{pore}	Pore volume, L^3 M^{-1}
W	Catalyst mass, M
Y_{gas}	Specific gas yield, L^3 M^{-1}
Y_{H2}	H_2 yield, %

Symbols

γ	Angle of the conical section
θ	Position of the diffraction peak corresponding to the metal
λ	Length of the radiation wave
ρ	Density, M L^{-3}

Abbreviations

BET	Brunauer-Emmett-Teller
BJH	Barrett, Joyner, and Halenda
CFB	Circulating fluidized bed
CPFD	Computational particle fluid dynamics
DFB	Dual fluidized bed
DTBG	Decoupled triple bed gasifier
ER	Equivalent ratio
CSBR	Conical spouted bed reactor
FCC	Fluid catalytic cracking
FCSB	Fountain confined spouted bed

FID	Flame ionization detector
FTIR	Fourier-transform infrared spectroscopy
GC	Gas chromatograph
GR	Gasifying ratio
HACA; HAVA	H_2 abstraction and acetylene addition, H_2 abstraction and vinyl addition
HC	Hydrocarbon
HPLC	High pressure liquid pump
HTR	High temperature reactor
ICBFB	Internal circulating bubbling fluidized bed
IGCC	Integrated gasification combined cycle
IR	Infrared spectroscopy
JCPDS	Joint Committee on Powder Diffraction Standards
LED	Light emitting diode
LTB	Low-tar biomass
MAC	Methyl addition and cyclization
MBMS	Molecular beam mass spectroscopy
MFC	Mass flow controller
MS	Mass spectrometer
MS5	Molecular Sieve 5
NIST	National Institute of Standards and Tecnology
PAC	Phenyl addition and cyclization
PAH	Polyaromatic hydrocarbon
PC	Personal computer

PDMS	Polydimethylsiloxane
PID	Photo ionization detector
PLC	Power line communications)
PPQ	Porapak Q
S/B	Steam to biomass
SCWG	Super critical water gasification
SEM, TEM	Scanning electron microscopy, transmission electron microscopy
SOFC	Solid oxide fuel cells
SPA	Solid phase adsorption
SPME	Solid phase micro-extraction
SXB	Staged fixed-bed gasifier
TCD	Thermal conductivity detector
TGA	Thermogravimetric analysis
TPO, TPD, TPR	Temperature programmed oxidation, temperature programme desorption, temperature programmed reduction
UNIFHY	UNIQUE gasifier for hydrogen production
VGO	Vacuum Gas Oil
VTDMA	Volatility tandem differential mobility analyzer
WDXRF	Wavelength dispersion X-ray fluorescence
WGS	Water Gas Shift
XPS	X ray photoelectron spectroscopy
XRD	X-ray diffraction
XRF	X-ray fluorescence

11

BIBLIOGRAPHY

Abdoulmoumine, N., Adhikari, S., Kulkarni, A., Chattanathan, S., A review on biomass gasification syngas cleanup. *Appl. Energy*, **155**, 294-307 (2015).

Abu El-Rub, Z., Bramer, E.A., Brem, G., Review of catalysts for tar elimination in biomass gasification processes. *Ind. Eng. Chem. Res.,* **43**, 6911-6919 (2004).

Abu El-Rub, Z., Bramer, E.A., Brem, G., Experimental comparison of biomass chars with other catalysts for tar reduction. *Fuel*, **87**, 2243-2252 (2008).

Adegoroye, A., Paterson, N., Li, X., Morgan, T., Herod, A.A., Dugwell, D.R., Kandiyoti, R., The characterisation of tars produced during the gasification of sewage sludge in a spouted bed reactor. *Fuel*, **83**, 1949-1960 (2004).

Adnan, M.A., Muraza, O., Razzak, S.A., Hossain, M.M., De Lasa, H.I., Iron Oxide over Silica-Doped Alumina Catalyst for Catalytic Steam Reforming of Toluene as a Surrogate Tar Biomass Species. *Energy Fuels*, **31**, 7471-7481 (2017).

Agu, C.E., Pfeifer, C., Eikeland, M., Tokheim, L.A., Moldestad, B.M.E., Measurement and characterization of biomass mean residence time in an air-blown bubbling fluidized bed gasification reactor. *Fuel*, **253**, 1414-1423 (2019).

Aguado, R., Combustión y Pirólisis de Residuos de Madera en Spouted Bed Cónico, PhD Thesis, University of the Basque Country, Bilbao. (1999).

Aguado, R., Alvarez, S., San José, M.J., Olazar, M., Bilbao, J., Gas flow distribution modelling in conical spouted beds. *Comput. Aided Chem. Eng.,* **20**, 613-618 (2005).

Ahlström, J.M., Alamia, A., Larsson, A., Breitholtz, C., Harvey, S., Thunman, H., Bark as feedstock for dual fluidized bed gasifiers—Operability, efficiency, and economics. *Int. J. Energy Res.,* **43**, 1171-1190 (2019).

Ahmad, A.A., Zawawi, N.A., Kasim, F.H., Inayat, A., Khasri, A., Assessing the gasification performance of biomass: A review on biomass gasification process conditions, optimization and economic evaluation. *Renewable Sustainable Energy Rev.,* **53**, 1333-1347 (2016).

Ahmadi, M., Brage, C., Sjöström, K., Engvall, K., Knoef, H., Van de Beld, B., Development of an on-line tar measurement method based on photo ionization technique. *Catal. Today*, **176**, 250-252 (2011).

Ahmadi, M., Elm Svensson, E., Engvall, K., Application of Solid-Phase Microextraction (SPME) as a Tar Sampling Method. *Energy Fuels,* **27**, 3853-3860 (2013a).

Ahmadi, M., Knoef, H., Van de Beld, B., Liliedahl, T., Engvall, K., Development of a PID based on-line tar measurement method – Proof of concept. *Fuel,* **113**, 113-121 (2013b).

Ahmed, T., Xiu, S., Wang, L., Shahbazi, A., Investigation of Ni/Fe/Mg zeolite-supported catalysts in steam reforming of tar using simulated-toluene as model compound. *Fuel,* **211**, 566-571 (2018).

Ahmed, S.F., Rafa, N., Mofijur, M., Badruddin, I.A., Inayat, A., Ali, M.S., Farrok, O., Yunus Khan, T.M., Biohydrogen Production From Biomass Sources: Metabolic Pathways and Economic Analysis. *Front. Energy Res.,* **9,** 753878 (2021).

Alauddin, Z.A.B.Z., Lahijani, P., Mohammadi, M., Mohamed, A.R., Gasification of lignocellulosic biomass in fluidized beds for renewable energy development: A review. *Renewable Sustainable Energy Rev.,* **14**, 2852-2862 (2010).

Aljbour, S.H., Kawamoto, K., Bench-scale gasification of cedar wood – Part I: Effect of operational conditions on product gas characteristics. *Chemosphere,* **90**, 1495-1500 (2013).

Altzibar, H., Lopez, G., Estiati, I., Bilbao, J., Olazar, M., Particle cycle times and solid circulation rates in conical spouted beds with draft tubes of different configuration. *Ind. Eng. Chem. Res.,* **52**, 15959-15967 (2013a).

Altzibar, H., Lopez, G., Bilbao, J., Olazar, M., Minimum Spouting Velocity of Conical Spouted Beds Equipped with Draft Tubes of Different Configuration. *Ind. Eng. Chem. Res.,* **52**, 2995-3006 (2013b).

Altzibar, H., Estiati, I., Lopez, G., Saldarriaga, J.F., Aguado, R., Bilbao, J., Olazar, M., Fountain confined conical spouted beds. *Powder Technol.,* **312**, 334-346 (2017).

Alvarez, J., Lopez, G., Amutio, M., Bilbao, J., Olazar, M., Bio-oil production from rice husk fast pyrolysis in a conical spouted bed reactor. *Fuel,* **128**, 162-169 (2014).

Alvarez, J., Valorization of agro-forestry wastes and sewage sludge by fast pyrolysis in a conical spouted bed reactor, PhD Thesis, University of the Basque Country, Bilbao. (2015).

Alvarez, J., Amutio, M., Lopez, G., Bilbao, J., Olazar, M., Fast co-pyrolysis of sewage sludge and lignocellulosic biomass in a conical spouted bed reactor. *Fuel,* **159**, 810-818 (2015).

Alvarez, J., Lopez, G., Amutio, M., Mkhize, N.M., Danon, B., van der Gryp, P., Görgens, J.F., Bilbao, J., Olazar, M., Evaluation of the properties of tyre pyrolysis oils obtained in a conical spouted bed reactor. *Energy*, **128**, 463-474 (2017).

Alvarez, J., Lopez, G., Amutio, M., Bilbao, J., Olazar, M., Evolution of biomass char features and their role in the reactivity during steam gasification in a conical spouted bed reactor. *Energy Convers. Manage.*, **181**, 214-222 (2019).

Amutio, M., Estrategias para la Pirólisis Rápida de Biomasa en Reactor Spouted Bed Cónico, PhD Thesis, University of the Basque Country, Bilbao. (2011).

Amutio, M., Lopez, G., Alvarez, J., Olazar, M., Bilbao, J., Fast pyrolysis of eucalyptus waste in a conical spouted bed reactor. *Bioresour. Technol.*, **194**, 225-232 (2015).

Anis, S., Zainal, Z.A., Tar reduction in biomass producer gas via mechanical, catalytic and thermal methods: A review. *Renewable Sustainable Energy Rev.*, **15**, 2355-2377 (2011).

Arabiourrutia, M., Productos y Cinética de la Pirólisis Térmica y Catalítica de Neumáticos en Spouted Bed Cónico, PhD Thesis, University of the Basque Country, Bilbao. (2007).

Arena, U., Di Gregorio, F., Santonastasi, M., A techno-economic comparison between two design configurations for a small scale, biomass-to-energy gasification based system. *Chem. Eng. J.*, **162**, 580-590 (2010).

Arregi, A., Pyrolysis and in-line catalytic steam reforming of biomass and biomass/plastic mixtures for H_2 production. PhD Thesis, University of the Basque Country, Bilbao. (2017).

Arregi, A., Amutio, M., Lopez, G., Artetxe, M., Alvarez, J., Bilbao, J., Olazar, M., Hydrogen-rich gas production by continuous pyrolysis and in-line catalytic reforming of pine wood waste and HDPE mixtures. *Energy Convers. Manage.*, **136**, 192-201 (2017).

Arregi, A., Amutio, M., Lopez, G., Bilbao, J., Olazar, M., Evaluation of thermochemical routes for hydrogen production from biomass: A review. *Energy Convers. Manage.*, **165**, 696-719 (2018).

Artetxe, M., Producción de Olefinas a partir de Polietileno por Pirólisis y Craqueo en línea, PhD Thesis, University of the Basque Country, Bilbao. (2012).

Artetxe, M., Nahil, M.A., Olazar, M., Williams, P.T., Steam reforming of phenol as biomass tar model compound over Ni/Al_2O_3 catalyst. *Fuel*, **184**, 629-636 (2016).

Artetxe, M., Alvarez, J., Nahil, M.A., Olazar, M., Williams, P.T., Steam reforming of different biomass tar model compounds over Ni/Al_2O_3 catalysts. *Energy Convers. Manage.*, **136**, 119-126 (2017).

Asadullah, M., Miyazawa, T., Ito, S., Kunimori, K., Koyama, S., Tomishige, K., A comparison of $Rh/CeO_2/SiO_2$ catalysts with steam reforming catalysts, dolomite and inert materials as bed materials in low throughput fluidized bed gasification systems. *Biomass Bioenergy*, **26**, 269-279 (2004).

Asadullah, M., Biomass gasification gas cleaning for downstream applications: A comparative critical review. *Renewable Sustainable Energy Rev.*, **40**, 118-132 (2014a).

Asadullah, M., Barriers of commercial power generation using biomass gasification gas: A review. *Renewable Sustainable Energy Rev.*, **29**, 201-215 (2014b).

Ashok, J., Dewangan, N., Das, S., Hongmanorom, P., Wai, M.H., Tomishige, K., Kawi, S., Recent progress in the development of catalysts for steam reforming of biomass tar model reaction. *Fuel Process. Technol.*, **199**, 106252 (2020).

Atxutegi, A., Tellabide, M., Lopez, G., Aguado, R., Bilbao, J., Olazar, M., Implementation of a borescopic technique in a conical spouted bed for tracking spherical and irregular particles. *Chem. Eng. J.*, **374**, 39-48 (2019).

Barbarias, I., Proceso de Pirólisis y Reformado en Línea para la Producción de H_2 a partir de Residuos Plásticos, PhD Thesis, University of the Basque Country, Bilbao. (2015).

Barbarias, I., Lopez, G., Alvarez, J., Artetxe, M., Arregi, A., Bilbao, J., Olazar, M., A sequential process for hydrogen production based on continuous HDPE fast pyrolysis and in-line steam reforming. *Chem. Eng. J.*, **296**, 191-198 (2016).

Barisano, D., Freda, C., Nanna, F., Fanelli, E., Villone, A., Biomass gasification and in-bed contaminants removal: Performance of iron enriched olivine and bauxite in a process of steam/O_2 gasification. *Bioresour. Technol.*, **118**, 187-194 (2012).

Barisano, D., Canneto, G., Nanna, F., Alvino, E., Pinto, G., Villone, A., Carnevale, M., Valerio, V., Battafarano, A., Braccio, G., Steam/oxygen biomass gasification at pilot scale in an internally circulating bubbling fluidized bed reactor. *Fuel Process. Technol.*, **141**, 74-81 (2016).

Baruah, D., Baruah, D.C., Modeling of biomass gasification: A review. *Renewable Sustainable Energy Rev.*, **39**, 806-815 (2014).

Baumhakl, C., Karellas, S., Tar analysis from biomass gasification by means of online fluorescence spectroscopy. *Opt. Lasers Eng.*, **49**, 885-891 (2011).

Benedikt, F., Fuchs, J., Schmid, J.C., Müller, S., Hofbauer, H., Advanced dual fluidized bed steam gasification of wood and lignite with calcite as bed material. *Korean J. Chem. Eng.*, **34**, 2548-2558 (2017).

Benedikt, F., Schmid, J.C., Fuchs, J., Mauerhofer, A.M., Müller, S., Hofbauer, H., Fuel flexible gasification with an advanced 100 kW dual fluidized bed steam gasification pilot plant. *Energy*, **164**, 329-343 (2018).

Benedikt, F., Kuba, M., Schmid, J.C., Müller, S., Hofbauer, H., Assessment of correlations between tar and product gas composition in dual fluidized bed steam gasification for online tar prediction. *Appl. Energy*, **238**, 1138-1149 (2019).

Benelli, L., Souza, C.R.F., Oliveira, W.P., Spouted bed performance on drying of an aromatic plant extract. *Powder Technol.*, **239**, 59-71 (2013).

Berdugo Vilches, T., Marinkovic, J., Seemann, M., Thunman, H., Comparing Active Bed Materials in a Dual Fluidized Bed Biomass Gasifier: Olivine, Bauxite, Quartz-Sand, and Ilmenite. *Energy Fuels*, **30**, 4848-4857 (2016).

Berghel, J., Renström, R., An Experimental Study on the Influence of Using a Draft Tube in a Continuous Spouted Bed Dryer. *Drying Technol.*, **32**, 519-527 (2014).

Berrueco, C., Montané, D., Matas Güell, B., del Alamo, G., Effect of temperature and dolomite on tar formation during gasification of torrefied biomass in a pressurized fluidized bed. *Energy*, **66**, 849-859 (2014a).

Berrueco, C., Recari, J., Güell, B.M., Alamo, G.d., Pressurized gasification of torrefied woody biomass in a lab scale fluidized bed. *Energy*, **70**, 68-78 (2014b).

Böhm, H., Jander, H., Tanke, D., PAH growth and soot formation in the pyrolysis of acetylene and benzene at high temperatures and pressures: Modeling and experiment. *Symp. Int. Combust.*, **27**, 1605-1612 (1998).

Borgmeyer, J., Continuous On-Line Tar Monitoring in Hot Process Gases from Biomass Gasification by Means of Fluorescence Spectroscopy. PhD Thesis, Technische Universität, Berlin. (2019).

Borgmeyer, J., Behrendt, F., On-line tar monitoring using light-induced fluorescence: A setup for continuous operation in a biomass gasification plant environment. *Opt. Laser Technol.*, **123**, 105906 (2020).

Brage, C., Yu, Q., Chen, G., Sjöström, K., Use of amino phase adsorbent for biomass tar sampling and separation. *Fuel*, **76**, 137-142 (1997).

Bridgwater, A.V., The technical and economic feasibility of biomass gasification for power generation. *Fuel*, **74**, 631-653 (1995).

Bronson, B., Preto, F., Mehrani, P., Effect of pretreatment on the physical properties of biomass and its relation to fluidized bed gasification. *Environ. Prog. Sustainable Energy*, **31**, 335-339 (2012).

Bronson, B., Gogolek, P., Mehrani, P., Preto, F., Experimental investigation of the effect of physical pre-treatment on air-blown fluidized bed biomass gasification. *Biomass Bioenergy*, **88**, 77-88 (2016).

Bryan Woodruff, R., Weimer, A.W., A novel technique for measuring the kinetics of high-temperature gasification of biomass char with steam. *Fuel*, **103**, 749-757 (2013).

Calvo, L.F., Gil, M.V., Otero, M., Morán, A., García, A.I., Gasification of rice straw in a fluidized-bed gasifier for syngas application in close-coupled boiler-gasifier systems. *Bioresour. technol.*, **109**, 206-214 (2012).

Campíns-Falcó, P., Herráez-Hernández, R., Verdú-Andrés, J., Cháfer-Pericás, C., On-line determination of aliphatic amines in water using in-tube solid-phase microextraction-assisted derivatisation in in-valve mode for processing large sample volumes in LC. *Anal. Bioanal. Chem.*, **394**, 557-565 (2009).

Campoy, M., Gómez-Barea, A., Vidal, F.B., Ollero, P., Air–steam gasification of biomass in a fluidised bed: Process optimisation by enriched air. *Fuel Process. Technol.*, **90**, 677-685 (2009).

Campoy, M., Gómez-Barea, A., Fuentes-Cano, D., Ollero, P., Tar Reduction by Primary Measures in an Autothermal Air-Blown Fluidized Bed Biomass Gasifier. *Ind. Eng. Chem. Res.*, **49**, 11294-11301 (2010).

Cao, J.P., Ren, J., Zhao, X.Y., Wei, X.Y., Takarada, T., Effect of atmosphere on carbon deposition of Ni/Al_2O_3 and Ni-loaded on lignite char during reforming of toluene as a biomass tar model compound. *Fuel*, **217**, 515-521 (2018).

Cao, L., Yu, I.K.M., Xiong, X., Tsang, D.C.W., Zhang, S., Clark, J.H., Hu, C., Ng, Y.H., Shang, J., Ok, Y.S., Biorenewable hydrogen production through biomass gasification: A review and future prospects. *Environ. Res.*, **186**, 109547 (2020).

Cao, Y., Wang, Y., Riley, J.T., Pan, W., A novel biomass air gasification process for producing tar-free higher heating value fuel gas. *Fuel Process. Technol.*, **87**, 343-353 (2006).

Cao, Y., Bai, Y., Du, J., Study on gasification characteristics of pine sawdust using olivine as in-bed material for combustible gas production. *J. Energy Inst.*, **96**, 168-172 (2021a).

Cao, Y., Bai, Y., Du, J., Air-gasification of pine sawdust using dolomite as in-bed material: Effects of gasification conditions on product characteristics. *J. Energy Inst.*, **95**, 187-192 (2021b).

Capper, S., Khan, Z., Kamble, P., Sharp, J., Watson, I., Progression towards Online Tar Detection Systems. *Energy Procedia*, **142**, 892-897 (2017).

Carpenter, D.L., Deutch, S.P., French, R.J., Quantitative measurement of biomass gasifier tars using a molecular-beam mass spectrometer: Comparison with traditional impinger sampling. *Energy Fuels*, **21**, 3036-3043 (2007).

Carpenter, D.L., Bain, R.L., Davis, R.E., Dutta, A., Feik, C.J., Gaston, K.R., Jablonski, W., Phillips, S.D., Nimlos, M.R., Pilot-scale gasification of corn stover, switchgrass, wheat straw, and wood: 1. Parametric study and comparison with literature. *Ind. Eng. Chem. Res.*, **49**, 1859-1871 (2010).

Cavalli, A., Tetteroo, R., Graziadio, M., Aravind, P.V., Catalytic reforming of acetic acid as main primary tar compound from biomass updraft gasifiers: screening of suitable catalysts and operating conditions. *Biomass Bioenergy*, **146**, 105982 (2021).

Chai, Z., Zhu, Z., Wang, X., Wang, K., Sulfur conversions during coal char gasification with a two-stage air supply in a pilot-scale circulating fluidized bed gasifier. *Energy Sources Part A*, **42**, 421-431 (2020).

Chaiprasert, P., Vitidsant, T., Effects of promoters on biomass gasification using nickel/dolomite catalyst. *Korean J. Chem. Eng.*, **26**, 1545-1549 (2009).

Chen, C., Ren, H., Zhou, J., Luo, Y., Zhan, Y., Au, C., Lin, X., Jiang, L., Cu/Fe_3O_4 catalyst for water gas shift reaction: Insight into the effect of Fe^{2+} and Fe^{3+} distribution in Fe_3O_4. *Int. J. Hydrogen Energy*, **45**, 8456-8465 (2020).

Chen, Y., Luo, Y.H., Wu, W.G., Su, Y., Experimental investigation on tar formation and destruction in a lab-scale two-stage reactor. *Energy Fuels*, **23**, 4659-4667 (2009).

Choi, Y., Mun, T., Cho, M., Kim, J., Gasification of dried sewage sludge in a newly developed three-stage gasifier: Effect of each reactor temperature on the producer gas composition and impurity removal. *Energy*, **114**, 121-128 (2016).

Chou, C.Y., Loiland, J.A., Lobo, R.F., Reverse water-gas shift iron catalyst derived from magnetite. *Catalysts*, **9**, 773 (2019).

Christodoulou, C., Grimekis, D., Panopoulos, K.D., Pachatouridou, E.P., Iliopoulou, E.F., Kakaras, E., Comparing calcined and un-treated olivine as bed materials for tar reduction in fluidized bed gasification. *Fuel Process. Technol.*, **124**, 275-285 (2014).

Claude, V., Courson, C., Köhler, M., Lambert, S.D., Overview and Essentials of Biomass Gasification Technologies and Their Catalytic Cleaning Methods. *Energy Fuels*, **30**, 8791-8814 (2016).

Claude, V., Mahy, J.G., Douven, S., Pirard, S.L., Courson, C., Lambert, S.D., Ni- and Fe-doped γ-Al_2O_3 or olivine as primary catalyst for toluene reforming. *Mater. Today Chem.*, **14,** 100197 (2019).

Constantinou, D.A., Fierro, J.L.G., Efstathiou, A.M., A comparative study of the steam reforming of phenol towards H_2 production over natural calcite, dolomite and olivine materials. *Appl. Catal., B*, **95**, 255-269 (2010).

Corella, J., Herguido, J., Alday, F.J., Pyrolysis and Steam Gasification of Biomass in Fluidized Beds. Influence of the Type and Location of the Biomass Feeding Point on the Product Distribution. In A. V. Bridgwater, J. L. Kuester , (Eds.), *Research in Thermochemical Biomass Conversion*, 384-398, Springer Netherlands, Dordrecht, (1988a).

Corella, J., Herguido, J., Gonzalez-Saiz, J., Alday, F. J., Rodriguez-Trujillo, J., Fluidized Bed Steam Gasification of Biomass with Dolomite and with a Commercial FCC Catalyst. *Research in Thermochemical Biomass Conversion*, 754-765, Springer Netherlands, Dordrecht, (1988b).

Corella, J., Orío, A., Toledo, J.M., Biomass gasification with air in a fluidized bed: Exhaustive tar elimination with commercial steam reforming catalysts. *Energy Fuels*, **13**, 702-709 (1999).

Corella, J., Toledo, J.M., Padilla, R., Olivine or dolomite as in-bed additive in biomass gasification with air in a fluidized bed: Which is better? *Energy Fuels*, **18**, 713-720 (2004).

Corma, A., Huber, G.W., Sauvanaud, L., O'Connor, P., Processing biomass-derived oxygenates in the oil refinery: Catalytic cracking (FCC) reaction pathways and role of catalyst. *J. Catal.*, **247**, 307-327 (2007).

Cortazar, M., Lopez, G., Alvarez, J., Amutio, M., Bilbao, J., Olazar, M., Advantages of confining the fountain in a conical spouted bed reactor for biomass steam gasification. *Energy*, **153**, 455-463 (2018).

Cortazar, M., Lopez, G., Alvarez, J., Amutio, M., Bilbao, J., Olazar, M., Behaviour of primary catalysts in the biomass steam gasification in a fountain confined spouted bed. *Fuel*, **253**, 1446-1456 (2019).

Cortazar, M., Lopez, G., Alvarez, J., Arregi, A., Amutio, M., Bilbao, J., Olazar, M., Experimental study and modeling of biomass char gasification kinetics in a novel thermogravimetric flow reactor. *Chem. Eng. J.*, **396**, 125200 (2020).

Cortazar, M., Santamaria, L., Lopez, G., Alvarez, J., Amutio, M., Bilbao, J., Olazar, M., Fe/olivine as primary catalyst in the biomass steam gasification in a fountain confined spouted bed reactor. *J. Ind. Eng. Chem.*, **99**, 364-379 (2021).

Couto, N., Rouboa, A., Silva, V., Monteiro, E., Bouziane, K., Influence of the Biomass Gasification Processes on the Final Composition of Syngas. *Energy Procedia*, **36**, 596-606 (2013).

Couto, N., Monteiro, E., Silva, V., Rouboa, A., Hydrogen-rich gas from gasification of Portuguese municipal solid wastes. *Int. J. Hydrogen Energy*, **41**, 10619-10630 (2016).

Da Ros, S., Valter Flores, K.A., Schwaab, M., Barbosa-Coutinho, E., Fernandes, N.R.C., Pinto, J.C., Phenomenological approaches for quantitative temperature-programmed reduction (TPR) and desorption (TPD) analysis. *J. Ind. Eng. Chem.*, **94**, 425-434 (2021).

Da Rosa, C.A., Freire, J.T., Fluid Dynamics Analysis of a Draft-Tube Continuous Spouted Bed with Particles Bottom Feed using CFD. *Ind. Eng. Chem. Res.*, **48**, 7813-7820 (2009).

Da Rosa, G.S., Dos Santos Rocha, S.C., Effect of process conditions on particle growth for spouted bed coating of urea. *Chem. Eng. Process. Process Intensif.*, **49**, 836-842 (2010).

De Almeida, V.F., Gómez-Barea, A., Arroyo-Caire, J., Pardo, I., On the Measurement of the Main Inorganic Contaminants Derived from Cl, S and N in Simulated Waste-Derived Syngas. *Waste Biomass Valorization*, **11**, 6869-6884 (2020).

De Andrés, J.M., Narros, A., Rodríguez, M.E., Behaviour of dolomite, olivine and alumina as primary catalysts in air–steam gasification of sewage sludge. *Fuel*, **90**, 521-527 (2011a).

De Andrés, J.M., Narros, A., Rodríguez, M.E., Air-steam gasification of sewage sludge in a bubbling bed reactor: Effect of alumina as a primary catalyst. *Fuel Process. Technol.*, **92**, 433-440 (2011b).

De Brito, R.C., Tellabide, M., Atxutegi, A., Estiati, I., Freire, J.T., Olazar, M., Draft tube design based on a borescopic technique in conical spouted beds. *Adv. Powder Technol.*, **32**, 4420-4431 (2021).

De Sales, C.A.V.B., Maya, D.M.Y., Lora, E.E.S., Jaén, R.L., Reyes, A.M.M., González, A.M., Andrade, R.V., Martínez, J.D., Experimental study on biomass (eucalyptus spp.) gasification in a two-stage downdraft reactor by using mixtures of air, saturated steam and oxygen as gasifying agents. *Energy Convers. Manage.*, **145**, 314-323 (2017).

Defoort, F., Thiery, S., Ravel, S., A promising new on-line method of tar quantification by mass spectrometry during steam gasification of biomass. *Biomass Bioenergy*, **65**, 64-71 (2014).

Devi, L., Ptasinski, K.J., Janssen, F.J.J.G., A review of the primary measures for tar elimination in biomass gasification processes. *Biomass Bioenergy*, **24**, 125-140 (2003).

Devi, L., Craje, M., Thüne, P., Ptasinski, K.J., Janssen, F.J.J.G., Olivine as tar removal catalyst for biomass gasifiers: Catalyst characterization. *Appl. Catal., A*, **294**, 68-79 (2005a).

Devi, L., Ptasinski, K.J., Janssen, F.J.J.G., Van Paasen, S.V.B., Bergman, P.C.A., Kiel, J.H.A., Catalytic decomposition of biomass tars: Use of dolomite and untreated olivine. *Renewable Energy*, **30**, 565-587 (2005b).

Di Blasi, C., Combustion and gasification rates of lignocellulosic chars. *Prog. Energy Combust. Sci.*, **35**, 121-140 (2009).

Di Carlo, A., Moroni, M., Savuto, E., Pallozzi, V., Bocci, E., Di Lillo, P., Cold model testing of an innovative dual bubbling fluidized bed steam gasifier. *Chem. Eng. J.*, **377**, 119689 (2019).

Di Marcello, M., Tsalidis, G.A., Spinelli, G., de Jong, W., Kiel, J.H.A., Pilot scale steam-oxygen CFB gasification of commercial torrefied wood pellets. The effect of torrefaction on the gasification performance. *Biomass Bioenergy*, **105**, 411-420 (2017).

Dong, G.L., Hüttinger, K.J., Consideration of reaction mechanisms leading to pyrolytic carbon of different textures. *Carbon*, **40**, 2515-2528 (2002).

Duan, C., Shen, Z., Wu, D., Guan, Y., Recent developments in solid-phase microextraction for on-site sampling and sample preparation. *TrAC*, **30**, 1568-1574 (2011).

Dufour, A., Girods, P., Masson, E., Normand, S., Rogaume, Y., Zoulalian, A., Comparison of two methods of measuring wood pyrolysis tar. *J. Chromatogr. A*, **1164**, 240-247 (2007).

Dufour, J., Martos, C., Ruiz, A., Catalytic applications of magnetite: Hydrogen production through WGS reaction. *Magn. Struct. Prop. Appl.*, 209-236 (2011).

Edinger, P., Schneebeli, J., Struis, R.P.W.J., Biollaz, S.M.A., Ludwig, C., On-line liquid quench sampling and UV–Vis spectroscopy for tar measurements in wood gasification process gases. *Fuel*, **184**, 59-68 (2016).

Elordi, G., Térmica y Catalítica de Poliolefinas en un Reactor de Spouted Bed Cónico, PhD Thesis, University of the Basque Country, Bilbao. (2010).

Engelen, K., Zhang, Y., Draelants, D.J., Baron, G.V., A novel catalytic filter for tar removal from biomass gasification gas: Improvement of the catalytic activity in presence of H_2S. *Chem. Eng. Sci.*, **58**, 665-670 (2003).

Engvall, K., Kusar, H., Sjöström, K., Pettersson, L.J., Upgrading of Raw Gas from Biomass and Waste Gasification: Challenges and Opportunities. *Top. Catal.*, **54**, 949 (2011).

Epstein, N., Grace, J., Spouted and spout-fluid beds: Fundamentals and applications. Cambridge University Press, Cambridge (2010).

Erkiaga, A., Gasificación con vapor de Biomasa y Plásticos en Spouted Bed Cónico, PhD Thesis, University of the Basque Country, Bilbao. (2014).

Erkiaga, A., Lopez, G., Amutio, M., Bilbao, J., Olazar, M., Syngas from steam gasification of polyethylene in a conical spouted bed reactor. *Fuel*, **109**, 461-469 (2013a).

Erkiaga, A., Lopez, G., Amutio, M., Bilbao, J., Olazar, M., Steam gasification of biomass in a conical spouted bed reactor with olivine and γ-alumina as primary catalysts. *Fuel Process. Technol.*, **116**, 292-299 (2013b).

Erkiaga, A., Lopez, G., Amutio, M., Bilbao, J., Olazar, M., Influence of operating conditions on the steam gasification of biomass in a conical spouted bed reactor. *Chem. Eng. J.*, **237**, 259-267 (2014).

Estiati, I., Tellabide, M., Saldarriaga, J.F., Altzibar, H., Olazar, M., Fine particle entrainment in fountain confined conical spouted beds. *Powder Technol.,* **344**, 278-285 (2019).

Estiati, I., Tellabide, M., Pablos, A., Altzibar, H., Aguado, R., Olazar, M., Design Factors in Fountain Confined Conical Spouted Beds. *Chem. Eng. Process. Process Intensif.,* **155,** 108062 (2020).

European Parliament, Directive 2009/28/EC of the European Parliament and of the Council of 23 April 2009 on the promotion of the use of energy from renewable sources and amending and subsequently repealing Directives 2001/77/EC and 2003/30/EC. (2009).

Evans, R. J., Milne, T. A., Chemistry of Tar Formation and Maturation in the Thermochemical Conversion of Biomass. In A. V. Bridgwater, D. G. B. Boocock , (Eds.), *Developments in Thermochemical Biomass Conversion: Volume 1 / Volume 2*, 803-816, Springer Netherlands, Dordrecht, (1997).

Fan, W., Lin, Z., Kuang, J., Li, Y., Impact of air staging along furnace height on NOx emissions from pulverized coal combustion. *Fuel Process. Technol.,* **91**, 625-634 (2010).

Farooq, A., Moogi, S., Jang, S., Kannapu, H.P.R., Valizadeh, S., Ahmed, A., Lam, S.S., Park, Y., Linear low-density polyethylene gasification over highly active Ni/CeO_2-ZrO_2 catalyst for enhanced hydrogen generation. *J. Ind. Eng. Chem.,* **94**, 336-342 (2021).

Faúndez, J.M., García, X.A., Gordon, A.L., A kinetic approach to catalytic pyrolysis of tars. *Fuel Process. Technol.,* **69**, 239-256 (2001).

Ferella, F., Innocenzi, V., Maggiore, F., Oil refining spent catalysts: A review of possible recycling technologies. *Resourc. Conserv. Recycl.,* **108**, 10-20 (2016).

Fernandez, E., Santamaria, L., Artetxe, M., Amutio, M., Arregi, A., Lopez, G., Bilbao, J., Olazar, M., In line upgrading of biomass fast pyrolysis products using low-cost catalysts. *Fuel,* **296,** 120682 (2021a).

Fernandez, E., Amutio, M., Artetxe, M., Arregi, A., Santamaria, L., Lopez, G., Bilbao, J., Olazar, M., Assessment of product yields and catalyst deactivation in fixed and fluidized bed reactors in the steam reforming of biomass pyrolysis volatiles. *Process Saf. Environ. Prot.,* **145**, 52-62 (2021b).

Fernandez, E., Santamaria, L., Artetxe, M., Amutio, M., Arregi, A., Lopez, G., Bilbao, J., Olazar, M., Conditioning the volatile stream from biomass fast pyrolysis for the attenuation of steam reforming catalyst deactivation. *Fuel,* **312**, 122910 (2022).

Fernández-Amado, M., Prieto-Blanco, M.C., López-Mahía, P., Muniategui-Lorenzo, S., Prada-Rodríguez, D., Strengths and weaknesses of in-tube solid-phase microextraction: A scoping review. *Anal. Chim. Acta,* **906**, 41-57 (2016).

Fidalgo, B., Van Niekerk, D., Millan, M., The effect of syngas on tar quality and quantity in pyrolysis of a typical South African inertinite-rich coal. *Fuel,* **134**, 90-96 (2014).

Font Palma, C., Modelling of tar formation and evolution for biomass gasification: A review. *Appl. Energy,* **111**, 129-141 (2013).

Forzatti, P., Lietti, L., Catalyst deactivation. *Catal. Today,* **52**, 165-181 (1999).

Franco, C., Pinto, F., Gulyurtlu, I., Cabrita, I., The study of reactions influencing the biomass steam gasification process. *Fuel,* **82**, 835-842 (2003).

Fredriksson, H.O.A., Lancee, R.J., Thüne, P.C., Veringa, H.J., Niemantsverdriet, J.W.H., Olivine as tar removal catalyst in biomass gasification: Catalyst dynamics under model conditions. *Appl. Catal., B.,* **130-131**, 168-177 (2013).

Fremaux, S., Beheshti, S.M., Ghassemi, H., Shahsavan-Markadeh, R., An experimental study on hydrogen-rich gas production via steam gasification of biomass in a research-scale fluidized bed. *Energy Convers. Manage.,* **91**, 427-432 (2015).

French, R., Czernik, S., Catalytic pyrolysis of biomass for biofuels production. *Fuel Process. Technol.,* **91**, 25-32 (2010).

Fu, Z., Wang, J., Zhang, N., An, Y., Yang, Z., Effect of Cu doping on the catalytic activity of Fe_3O_4 in water-gas shift reactions. *Int. J. Hydrogen Energy,* **40**, 2193-2198 (2015).

Fuentes-Cano, D., Goḿez-Barea, A., Nilsson, S., Ollero, P., The influence of temperature and steam on the yields of tar and light hydrocarbon compounds during devolatilization of dried sewage sludge in a fluidized bed. *Fuel,* **108**, 341-350 (2013).

Fuentes-Cano, D., Von Berg, L., Diéguez-Alonso, A., Scharler, R., Gómez-Barea, A., Anca-Couce, A., Tar conversion of biomass syngas in a downstream char bed. *Fuel Process. Technol.,* **199**, 106271 (2020).

Fürsatz, K., Fuchs, J., Benedikt, F., Kuba, M., Hofbauer, H., Effect of biomass fuel ash and bed material on the product gas composition in DFB steam gasification. *Energy,* **219**, 119650 (2021).

Gaisan, B., Aspectos Básicos de la Tecnología de Pirólisis de Plásticos en un Reactor de Spouted Bed Cónico, PhD Thesis, University of the Basque Country, Bilbao. (2002).

Gall, D., Pushp, M., Larsson, A., Davidsson, K., Pettersson, J.B.C., Online Measurements of Alkali Metals during Start-up and Operation of an Industrial-Scale Biomass Gasification Plant. *Energy Fuels*, **32**, 532-541 (2018).

Gao, N., Salisu, J., Quan, C., Williams, P., Modified nickel-based catalysts for improved steam reforming of biomass tar: A critical review. *Renewable Sustainable Energy Rev.*, **145**, 111023 (2021).

Gao, N., Milandile, M.H., Quan, C., Rundong, L., Critical assessment of plasma tar reforming during biomass gasification: A review on advancement in plasma technology. *J. Hazard. Mater.*, **421**, 126764 (2022).

García-García, I., Acha, E., Bizkarra, K., Martínez de Ilarduya, J., Requies, J., Cambra, J.F., Hydrogen production by steam reforming of m-cresol, a bio-oil model compound, using catalysts supported on conventional and unconventional supports. *Int. J. Hydrogen Energy*, **40**, 14445-14455 (2015).

Gemechu, E. D., Kumar, A., Chapter 12 - The environmental performance of hydrogen production pathways based on renewable sources. In J. Ren, (Ed.), *Renewable-Energy-Driven Future*, 375-406, Academic Press, (2021).

Ghaffar, S., Hashmi, I., Awan, M.A., Nasir, H., Amjad, H., Determination of Volatile Organic Compounds (VOCs) in Potable Water Using Solid Phase Micro Extraction-Gas Chromatography (SPME-GC). *Arabian J. Sci. Eng.*, **37**, 1255-1262 (2012).

Gil, J., Caballero, M.A., Martín, J.A., Aznar, M.-., Corella, J., Biomass gasification with air in a fluidized bed: Effect of the in-bed use of dolomite under different operation conditions. *Ind. Eng. Chem. Res.*, **38**, 4226-4235 (1999a).

Gil, J., Corella, J., Aznar, M.P., Caballero, M.A., Biomass gasification in atmospheric and bubbling fluidized bed: Effect of the type of gasifying agent on the product distribution. *Biomass Bioenergy*, **17**, 389-403 (1999b).

Gil-Lalaguna, N., Sánchez, J.L., Murillo, M.B., Rodríguez, E., Gea, G., Air–steam gasification of sewage sludge in a fluidized bed. Influence of some operating conditions. *Chem. Eng. J.*, **248**, 373-382 (2014).

Gómez-Barea, A., Leckner, B., Modeling of biomass gasification in fluidized bed. *Prog. Energy Combust. Sci.*, **36**, 444-509 (2010).

Gómez-Barea, A., Leckner, B., Villanueva Perales, A., Nilsson, S., Fuentes Cano, D., Improving the performance of fluidized bed biomass/waste gasifiers for distributed electricity: A new three-stage gasification system. *Appl. Therm. Eng.*, **50**, 1453-1462 (2013a).

Gómez-Barea, A., Ollero, P., Leckner, B., Optimization of char and tar conversion in fluidized bed biomass gasifiers. *Fuel*, **103**, 42-52 (2013b).

González, I.O., Pastor, R.M.P., Hervás, J.M.S., Sampling of tar from sewage sludge gasification using solid phase adsorption. *Anal. Bioanal. Chem.*, **403**, 2039-2046 (2012).

Göransson, K., Söderlind, U., Zhang, W., Experimental test on a novel dual fluidised bed biomass gasifier for synthetic fuel production. *Fuel*, **90**, 1340-1349 (2011).

Gredinger, A., Schweitzer, D., Dieter, H., Scheffknecht, G., A Measurement Device for Online Monitoring of Total Tar in Gasification Systems. *J. Energy Res. Technol.*, **138**, 042205 (2016).

Gredinger, A., Spörl, R., Scheffknecht, G., Comparison measurements of tar content in gasification systems between an online method and the tar protocol. *Biomass Bioenergy*, **111**, 301-307 (2018).

Guan, G., Kaewpanha, M., Hao, X., Abudula, A., Catalytic steam reforming of biomass tar: Prospects and challenges. *Renewable Sustainable Energy Rev.*, **58**, 450-461 (2016).

Guo, F., Dong, Y., Dong, L., Guo, C., Effect of design and operating parameters on the gasification process of biomass in a downdraft fixed bed: An experimental study. *Int. J. Hydrogen Energy*, **39**, 5625-5633 (2014).

Guo, S., Wei, X., Li, J., Che, D., Liu, H., Sun, B., Wang, Q., Experimental Study on Product Gas and Tar Removal in Air–Steam Gasification of Corn Straw in a Bench-Scale Internally Circulating Fluidized Bed. *Energy Fuels*, **34**, 1908-1917 (2020).

Gupta, A., Thengane, S.K., Mahajani, S., Kinetics of pyrolysis and gasification of cotton stalk in the central parts of India. *Fuel*, **263**, 116752 (2020).

Gusta, E., Dalai, A.K., Uddin, M.A., Sasaoka, E., Catalytic decomposition of biomass tars with dolomites. *Energy Fuels*, **23**, 2264-2272 (2009).

Haddix, M.L., Magrini-Bair, K., Evans, R.J., Conant, R.T., Wallenstein, M.D., Morris, S.J., Calderón, F., Paul, E.A., Progressing towards more quantitative analytical

pyrolysis of soil organic matter using molecular beam mass spectroscopy of whole soils and added standards. *Geoderma*, **283**, 88-100 (2016).

Hafner, M., Raimondi, P.P., Priorities and challenges of the EU energy transition: From the European Green Package to the new Green Deal. *Russ. J. Econ.*, **6**, 374-389 (2021).

Han, Z., Geng, S., Zeng, X., Xu, S., An, P., Cheng, J., Yang, J., Li, F., Zhang, S., Liu, M., Guan, G., Xu, G., Reaction decoupling in thermochemical fuel conversion and technical progress based on decoupling using fluidized bed. *Carbon Resour. Convers.*, **1**, 109-125 (2018).

Hanchate, N., Ramani, S., Mathpati, C.S., Dalvi, V.H., Biomass gasification using dual fluidized bed gasification systems: A review. *J. Clean. Prod.*, **280**, 123148 (2021).

Harb, R., Rivera-Tinoco, R., Nemer, M., Zeghondy, B., Bouallou, C., Towards synthetic fuels production from biomass gasification: Tar content at low temperatures. *Biomass Bioenergy*, **137**, 105540 (2020).

Hattori, H., Takeda, K., Side-outlet spouted bed with inner draft-tube for small-sized solid particles. *J. Chem. Eng. Jpn.*, **11**, 125-129 (1978).

Hattori, H., Tanaka, K., Takeda, K., Minimun spoutable gas flow rate in side-outlet spouted bed with inner draft-tube. *J. Chem. Eng. Jpn.*, **14**, 462-466 (1981).

Heidenreich, S., Nacken, M., Hackel, M., Schaub, G., Catalytic filter elements for combined particle separation and nitrogen oxides removal from gas streams. *Powder Technol.*, **180**, 86-90 (2008).

Heidenreich, S., Foscolo, P.U., New concepts in biomass gasification. *Prog. Energy Combust. Sci.*, **46**, 72-95 (2015).

Hernández, J.J., Aranda-Almansa, G., Bula, A., Gasification of biomass wastes in an entrained flow gasifier: Effect of the particle size and the residence time. *Fuel Process. Technol.*, **91**, 681-692 (2010).

Hernández, J.J., Ballesteros, R., Aranda, G., Characterisation of tars from biomass gasification: Effect of the operating conditions. *Energy*, **50**, 333-342 (2013).

Hoang, A.T., Huang, Z., Nižetić, S., Pandey, A., Nguyen, X.P., Luque, R., Ong, H.C., Said, Z., Le, T.H., Pham, V.V., Characteristics of hydrogen production from steam gasification of plant-originated lignocellulosic biomass and its prospects in Vietnam. *Int. J. Hydrogen Energy*, **47**, 4394-4425 (2022).

Horvat, A., Kwapinska, M., Xue, G., Dooley, S., Kwapinski, W., Leahy, J.J., Detailed Measurement Uncertainty Analysis of Solid-Phase Adsorption-Total Gas Chromatography (GC)-Detectable Tar from Biomass Gasification. *Energy Fuels,* **30**, 2187-2197 (2016a).

Horvat, A., Kwapinska, M., Xue, G., Kwapinski, W., Dooley, S., Leahy, J.J., Study of post sampling treatment of solid phase adsorption method on tar yields and comparison of two methods for volatile tar compounds. *European Biomass Conf. Exhib. Proc.*, **2016**, 929-933 (2016b).

Hu, G., Xu, S., Li, S., Xiao, C., Liu, S., Steam gasification of apricot stones with olivine and dolomite as downstream catalysts. *Fuel Process. Technol.,* **87**, 375-382 (2006).

Huang, J., Schmidt, K.G., Bian, Z., Removal and conversion of tar in Syngas from woody biomass gasification for power utilization using catalytic Hydrocracking. *Energies,* **4**, 1163-1177 (2011).

Hurley, S., Xu, C., Preto, F., Shao, Y., Li, H., Wang, J., Tourigny, G., Catalytic gasification of woody biomass in an air-blown fluidized-bed reactor using Canadian limonite iron ore as the bed material. *Fuel,* **91**, 170-176 (2012).

Huynh, C.V., Kong, S., Performance characteristics of a pilot-scale biomass gasifier using oxygen-enriched air and steam. *Fuel,* **103**, 987-996 (2013).

Ibragimova, O.P., Baimatova, N., Kenessov, B., Low-cost quantitation of multiple volatile organic compounds in air using solid-phase microextraction. *Separations,* **6,** 51 (2019).

IEA, Global Hydrogen Review 2021. (2021).

IEA Bioenergy, Gas analysis in gasification of biomass and waste. Guideline report 1. (2018).

Ishikura, T., Nagashima, H., Ide, M., Hydrodynamics of a spouted bed with a porous draft tube containing a small amount of finer particles. *Powder Technol.,* **131**, 56-65 (2003).

Islam, M.W., A review of dolomite catalyst for biomass gasification tar removal. *Fuel,* **267**, 117095 (2020).

Israelsson, M., Seemann, M., Thunman, H., Assessment of the solid-phase adsorption method for sampling biomass-derived tar in industrial environments. *Energy Fuels,* **27**, 7569-7578 (2013).

Israelsson, M., Larsson, A., Thunman, H., Online measurement of elemental yields, oxygen transport, condensable compounds, and heating values in gasification systems. *Energy Fuels*, **28**, 5892-5901 (2014).

Jaiswal, R., Furuvik, N.C.I.S., Thapa, R.K., Moldestad, B.M.E., A CPFD model to investigate the influence of feeding positions in a gasification reactor. *Int. J. Energy Prod. Manage.,* **5**, 223-233 (2020).

Jand, N., Foscolo, P.U., Decomposition of wood particles in fluidized beds. *Ind. Eng. Chem. Res.,* **44**, 5079-5089 (2005).

Jeremiáš, M., Pohořelý, M., Svoboda, K., Manovic, V., Anthony, E.J., Skoblia, S., Beňo, Z., Šyc, M., Gasification of biomass with CO_2 and H_2O mixtures in a catalytic fluidised bed. *Fuel*, **210**, 605-610 (2017).

Jeremiáš, M., Pohorelý, M., Svoboda, K., Skoblia, S., Beno, Z., Šyc, M., CO_2 gasification of biomass: The effect of lime concentration in a fluidised bed. *Appl. Energy*, **217**, 361-368 (2018).

Kaewluan, S., Pipatmanomai, S., Potential of synthesis gas production from rubber wood chip gasification in a bubbling fluidised bed gasifier. *Energy Convers. Manage.*, **52**, 75-84 (2011a).

Kaewluan, S., Pipatmanomai, S., Gasification of high moisture rubber woodchip with rubber waste in a bubbling fluidized bed. *Fuel Process. Technol.*, **92**, 671-677 (2011b).

Kakoulaki, G., Kougias, I., Taylor, N., Dolci, F., Moya, J., Jäger-Waldau, A., Green hydrogen in Europe – A regional assessment: Substituting existing production with electrolysis powered by renewables. *Energy Convers. Manage.*, **228**, 113649 (2021).

Kállai, M., Veres, Z., Balla, J., Response of flame ionization detectors to different homologous series. *Chromatographia*, **54**, 511-517 (2001).

Kang, M.S., Jeong, H.J., Massoudi Farid, M., Hwang, J., Effect of staged combustion on low NO_x emission from an industrial-scale fuel oil combustor in South Korea. *Fuel*, **210**, 282-289 (2017).

Karl, J., Pröll, T., Steam gasification of biomass in dual fluidized bed gasifiers: A review. *Renewable Sustainable Energy Rev.*, **98**, 64-78 (2018).

Kaufman Rechulski, M.D., Schneebeli, J., Geiger, S., Schildhauer, T.J., Biollaz, S.M.A., Ludwig, C., Liquid-Quench Sampling System for the Analysis of Gas Streams from Biomass Gasification Processes. Part 2: Sampling Condensable Compounds. *Energy Fuels*, **26**, 6358-6365 (2012).

Kaushal, P., Tyagi, R., Steam assisted biomass gasification-an overview. *Canadian J. Chem. Eng.*, **90**, 1043-1058 (2012).

Kern, S., Pfeifer, C., Hofbauer, H., Gasification of lignite in a dual fluidized bed gasifier - Influence of bed material particle size and the amount of steam. *Fuel Process. Technol.*, **111**, 1-13 (2013a).

Kern, S., Pfeifer, C., Hofbauer, H., Gasification of wood in a dual fluidized bed gasifier: Influence of fuel feeding on process performance. *Chem. Eng. Sci.*, **90**, 284-298 (2013b).

Kihedu, J.H., Yoshiie, R., Naruse, I., Performance indicators for air and air–steam auto-thermal updraft gasification of biomass in packed bed reactor. *Fuel Process. Technol.*, **141**, 93-98 (2016).

Kim, S., Prajitno, H., Yoo, J., Kim, S., Chun, D., Lim, J., Choi, H., Lee, S., Im, H., Dispersion behavior of various single metals on carbonaceous coal supports and their reactivity in methanol steam reforming. *J. Ind. Eng. Chem.*, **94**, 317-325 (2021).

Kinoshita, C.M., Wang, Y., Zhou, J., Tar formation under different biomass gasification conditions. *J. Anal. Appl. Pyrolysis*, **29**, 169-181 (1994).

Kirnbauer, F., Wilk, V., Kitzler, H., Kern, S., Hofbauer, H., The positive effects of bed material coating on tar reduction in a dual fluidized bed gasifier. *Fuel*, **95**, 553-562 (2012).

Kirnbauer, F., Wilk, V., Hofbauer, H., Performance improvement of dual fluidized bed gasifiers by temperature reduction: The behavior of tar species in the product gas. *Fuel*, **108**, 534-542 (2013).

Kitzler, H., Pfeifer, C., Hofbauer, H., Pressurized gasification of woody biomass—Variation of parameter. *Fuel Process. Technol.*, **92**, 908-914 (2011).

Knežević, M., Povrenović, D., Influence of fluid-mechanical parameters on volumetric mass transfer coefficient in a spout–fluid bed with a draft tube. *Chem. Eng. Sci.*, **134**, 129-137 (2015).

Kook, J.W., Choi, H.M., Kim, B.H., Ra, H.W., Yoon, S.J., Mun, T.Y., Kim, J.H., Kim, Y.K., Lee, J.G., Seo, M.W., Gasification and tar removal characteristics of rice husk in a bubbling fluidized bed reactor. *Fuel*, **181**, 942-950 (2016).

Koppatz, S., Pfeifer, C., Hofbauer, H., Comparison of the performance behaviour of silica sand and olivine in a dual fluidised bed reactor system for steam gasification of biomass at pilot plant scale. *Chem. Eng. J.*, **175**, 468-483 (2011).

Koppatz, S., Schmid, J.C., Pfeifer, C., Hofbauer, H., The effect of bed particle inventories with different particle sizes in a dual fluidized bed pilot plant for biomass steam gasification. *Ind. Eng. Chem. Res.*, **51**, 10492-10502 (2012).

Kovač, A., Paranos, M., Marciuš, D., Hydrogen in energy transition: A review. *Int. J. Hydrogen Energy*, **46**, 10016-10035 (2021).

Kuba, M., Kirnbauer, F., Hofbauer, H., Influence of coated olivine on the conversion of intermediate products from decomposition of biomass tars during gasification. *Biomass Convers. Biorefin.*, **7**, 11-21 (2017).

Kuba, M., Hofbauer, H., Experimental parametric study on product gas and tar composition in dual fluid bed gasification of woody biomass. *Biomass Bioenergy*, **115**, 35-44 (2018).

Kuba, M., Kraft, S., Kirnbauer, F., Maierhans, F., Hofbauer, H., Influence of controlled handling of solid inorganic materials and design changes on the product gas quality in dual fluid bed gasification of woody biomass. *Appl. Energy*, **210**, 230-240 (2018).

Kuba, M., Benedikt, F., Fürsatz, K., Fuchs, J., Demuth, M., Aichernig, C., Arpa, L., Hofbauer, H., Integration of dual fluidized bed steam gasification into the pulp and paper industry. *Biomass Convers. Biorefin.*, (2021).

Kuhn, J.N., Zhao, Z., Felix, L.G., Slimane, R.B., Choi, C.W., Ozkan, U.S., Olivine catalysts for methane- and tar-steam reforming. *Appl. Catal., B*, **81**, 14-26 (2008a).

Kuhn, J.N., Zhao, Z., Senefeld-Naber, A., Felix, L.G., Slimane, R.B., Choi, C.W., Ozkan, U.S., Ni-olivine catalysts prepared by thermal impregnation: Structure, steam reforming activity, and stability. *Appl. Catal., A*, **341**, 43-49 (2008b).

Kunii, D., Levenspiel, O., Fluidization engineering, Butterworth-Heinemann, (1991).

Kuramoto, K., Matsuoka, K., Murakami, T., Takagi, H., Nanba, T., Suzuki, Y., Hosokai, S., Hayashi, J.I., Cracking and coking behaviors of nascent volatiles derived from flash pyrolysis of woody biomass over mesoporous fluidized-bed material. *Ind. Eng. Chem. Res.*, **48**, 2851-2860 (2009).

Kurkela, E., Kurkela, M., Hiltunen, I., The effects of wood particle size and different process variables on the performance of steam-oxygen blown circulating fluidized-bed gasifier. *Environ. Prog. Sustain. Energy*, **33**, 681-687 (2014).

Kurkela, E., Kurkela, M., Hiltunen, I., Pilot-scale development of pressurized fixed-bed gasification for synthesis gas production from biomass residues. *Biomass Convers. Biorefinery*, (2021).

Lamb, J. J., Hillestad, M., Rytter, E., Bock, R., Nordgård, A. S. R., Lien, K. M., Burheim, O. S., Pollet, B. G., Chapter | three - Traditional Routes for Hydrogen Production and Carbon Conversion. In J. J. Lamb, B. G. Pollet, (Eds.), *Hydrogen, Biomass and Bioenergy*, 21-53, Academic Press, (2020).

Larsson, A., Israelsson, M., Lind, F., Seemann, M., Thunman, H., Using ilmenite to reduce the tar yield in a dual fluidized bed gasification system. *Energy Fuels*, **28**, 2632-2644 (2014).

Larsson, A., Kuba, M., Berdugo Vilches, T., Seemann, M., Hofbauer, H., Thunman, H., Steam gasification of biomass – Typical gas quality and operational strategies derived from industrial-scale plants. *Fuel Process. Technol.*, **212**, 106609 (2021).

Latifi, M., Berruti, F., Briens, C., Jiggle bed reactor for testing catalytic activity of olivine in bio-oil gasification. *Powder Technol.*, **316**, 400-409 (2017).

Lazzari, E., Schena, T., Marcelo, M.C.A., Primaz, C.T., Silva, A.N., Ferrão, M.F., Bjerk, T., Caramão, E.B., Classification of biomass through their pyrolytic bio-oil composition using FTIR and PCA analysis. *Ind. Crops Prod.*, **111**, 856-864 (2018).

Lee, C.S., Conradie, A.V., Lester, E., Review of supercritical water gasification with lignocellulosic real biomass as the feedstocks: Process parameters, biomass composition, catalyst development, reactor design and its challenges. *Chem. Eng. J.*, **415**, 128837 (2021).

Li, B., Magoua Mbeugang, C.F., Huang, Y., Liu, D., Wang, Q., Zhang, S., A review of CaO based catalysts for tar removal during biomass gasification. *Energy*, **244**, 123172 (2022).

Li, C., Suzuki, K., Tar property, analysis, reforming mechanism and model for biomass gasification-An overview. *Renewable Sustainable Energy Rev.*, **13**, 594-604 (2009).

Li, H., Wang, Y., Zhou, N., Dai, L., Deng, W., Liu, C., Cheng, Y., Liu, Y., Cobb, K., Chen, P., Ruan, R., Applications of calcium oxide–based catalysts in biomass pyrolysis/gasification – A review. *J. Cleaner Prod.*, **291,** 125826 (2021a).

Li, J., Liu, J., Liao, S., Yan, R., Hydrogen-rich gas production by air–steam gasification of rice husk using supported nano-NiO/γ-Al_2O_3 catalyst. *Int. J. Hydrogen Energy*, **35**, 7399-7404 (2010).

Li, J., Tao, J., Yan, B., Jiao, L., Chen, G., Hu, J., Review of microwave-based treatments of biomass gasification tar. *Renewable Sustainable Energy Rev.*, **150**, 111510 (2021b).

Li, X.T., Grace, J.R., Lim, C.J., Watkinson, A.P., Chen, H.P., Kim, J.R., Biomass gasification in a circulating fluidized bed. *Biomass Bioenergy*, **26**, 171-193 (2004).

Liu, M., Aravind, P.V., The fate of tars under solid oxide fuel cell conditions: A review. *Appl. Therm. Eng.*, **70**, 687-693 (2014).

Liu, P., Li, Z., Bennett, A., Lin, H., Sarathy, S.M., Roberts, W.L., The site effect on PAHs formation in HACA-based mass growth process. *Combust. Flame*, **199**, 54-68 (2019).

Liu, Q., Yang, S., Liu, Z., Liu, Q., Shi, L., Han, W., Zhang, L., Li, M., Comparison of TG-MS and GC-simulated distillation for determination of the boiling point distribution of various oils. *Fuel*, **301**, 121088 (2021).

Lopez, G., Pirólisis Atmosférica y a Vacío de Neumáticos con Alimentación Continua en un Reactor Spouted Bed Cónico, PhD Thesis, University of the Basque Country, Bilbao. (2008).

López, G., Olazar, M., Aguado, R., Bilbao, J., Continuous pyrolysis of waste tyres in a conical spouted bed reactor. *Fuel*, **89**, 1946-1952 (2010).

Lopez, G., Erkiaga, A., Amutio, M., Bilbao, J., Olazar, M., Effect of polyethylene co-feeding in the steam gasification of biomass in a conical spouted bed reactor. *Fuel*, **153**, 393-401 (2015).

Lopez, G., Alvarez, J., Amutio, M., Arregi, A., Bilbao, J., Olazar, M., Assessment of steam gasification kinetics of the char from lignocellulosic biomass in a conical spouted bed reactor. *Energy*, **107**, 493-501 (2016).

Lopez, G., Cortazar, M., Alvarez, J., Amutio, M., Bilbao, J., Olazar, M., Assessment of a conical spouted with an enhanced fountain bed for biomass gasification. *Fuel*, **203**, 825-831 (2017).

Lopez, G., Artetxe, M., Amutio, M., Alvarez, J., Bilbao, J., Olazar, M., Recent advances in the gasification of waste plastics. A critical overview. *Renewable Sustainable Energy Rev.*, **82**, 576-596 (2018).

Lorente, E., Millan, M., Brandon, N.P., Use of gasification syngas in SOFC: Impact of real tar on anode materials. *Int. J. Hydrogen Energy*, **37**, 7271-7278 (2012).

Lu, Y.J., Guo, L.J., Ji, C.M., Zhang, X.M., Hao, X.H., Yan, Q.H., Hydrogen production by biomass gasification in supercritical water: A parametric study. *Int. J. Hydrogen Energy*, **31**, 822-831 (2006).

Luo, B., Lim, C.J., Freitas, L.A.P., Grace, J.R., Flow Characteristics in Slot-Rectangular Spouted Beds with Draft Plates. *Can. J. Chem. Eng.*, **82**, 83-88 (2004).

Luo, S., Xiao, B., Guo, X., Hu, Z., Liu, S., He, M., Hydrogen-rich gas from catalytic steam gasification of biomass in a fixed bed reactor: Influence of particle size on gasification performance. *Int. J. Hydrogen Energy*, **34**, 1260-1264 (2009).

Luo, X., Wu, T., Shi, K., Song, M., Rao, Y., Biomass Gasification: An Overview of Technological Barriers and Socio-Environmental Impact. (2018).

Lv, P.M., Xiong, Z.H., Chang, J., Wu, C.Z., Chen, Y., Zhu, J.X., An experimental study on biomass air-steam gasification in a fluidized bed. *Bioresour. Technol.*, **95**, 95-101 (2004).

Ma, L., Verelst, H., Baron, G.V., Integrated high temperature gas cleaning: Tar removal in biomass gasification with a catalytic filter. *Catal. Today*, **105**, 729-734 (2005).

Ma, X., Zhao, X., Gu, J., Shi, J., Co-gasification of coal and biomass blends using dolomite and olivine as catalysts. *Renewable Energy*, **132**, 509-514 (2019).

Ma, Z., Zhang, S., Xie, D., Yan, Y., A novel integrated process for hydrogen production from biomass. *Int. J. Hydrogen Energy*, **39**, 1274-1279 (2014).

Machin, E.B., Pedroso, D.T., Proenza, N., Silveira, J.L., Conti, L., Braga, L.B., Machin, A.B., Tar reduction in downdraft biomass gasifier using a primary method. *Renewable Energy*, **78**, 478-483 (2015).

Magrini, K., Follett, R., Kimble, J., Davis, M., Pruessner, E., Using pyrolysis molecular beam mass spectrometry to characterize soil organic carbon in native prairie soils. *Soil Sci.*, **172,** 659-672 (2007).

Mahapatra, S., Dasappa, S., Influence of surface area to volume ratio of fuel particles on gasification process in a fixed bed. *Energy Sustainable Dev.*, **19**, 122-129 (2014).

Mahidhara, G., Burrow, H., Sasikala, C., Ramana, C.V., Biological hydrogen production: molecular and electrolytic perspectives. *World J. Microbiol. Biotechnol.*, **35**(2019).

Mahinpey, N., Gomez, A., Review of gasification fundamentals and new findings: Reactors, feedstock, and kinetic studies. *Chem. Eng. Sci.*, **148**, 14-31 (2016).

Makibar, J., Fernandez-Akarregi, A.R., Alava, I., Cueva, F., Lopez, G., Olazar, M., Investigations on heat transfer and hydrodynamics under pyrolysis conditions of a

pilot-plant draft tube conical spouted bed reactor. *Chem. Eng. Process. Process Intensif.*, **50**, 790-798 (2011).

Makibar, J., Fernandez-Akarregi, A.R., Díaz, L., Lopez, G., Olazar, M., Pilot scale conical spouted bed pyrolysis reactor: Draft tube selection and hydrodynamic performance. *Powder Technol.*, **219**, 49-58 (2012).

Mallick, D., Mahanta, P., Moholkar, V.S., Co-gasification of biomass blends: Performance evaluation in circulating fluidized bed gasifier. *Energy*, **192**, 116682 (2020).

Manyà, J.J., Sánchez, J.L., Gonzalo, A., Arauzo, J., Air gasification of dried sewage sludge in a fluidized bed: Effect of the operating conditions and in-bed use of alumina. *Energy Fuels*, **19**, 629-636 (2005).

Martos, C., Dufour, J., Ruiz, A., Synthesis of Fe_3O_4-based catalysts for the high-temperature water gas shift reaction. *Int. J. Hydrogen Energy*, **34**, 4475-4481 (2009).

Mathur, K.B., Gishler, P.E., A technique for contacting gases with coarse solid particles. *AIChE J.*, **1**, 157-164 (1955).

Matsuoka, K., Shimbori, T., Kuramoto, K., Hatano, H., Suzuki, Y., Steam reforming of woody biomass in a fluidized bed of iron oxide-impregnated porous alumina. *Energy Fuels*, **20**, 2727-2731 (2006).

Matsuoka, K., Kuramoto, K., Murakami, T., Suzuki, Y., Steam gasification of woody biomass in a circulating dual bubbling fluidized bed system. *Energy Fuels*, **22**, 1980-1985 (2008).

Mauerhofer, A.M., Benedikt, F., Schmid, J.C., Fuchs, J., Müller, S., Hofbauer, H., Influence of different bed material mixtures on dual fluidized bed steam gasification. *Energy*, **157**, 957-968 (2018).

Mauerhofer, A.M., Schmid, J.C., Benedikt, F., Fuchs, J., Müller, S., Hofbauer, H., Dual fluidized bed steam gasification: Change of product gas quality along the reactor height. *Energy*, **173**, 1256-1272 (2019).

Mayerhofer, M., Mitsakis, P., Meng, X., De Jong, W., Spliethoff, H., Gaderer, M., Influence of pressure, temperature and steam on tar and gas in allothermal fluidized bed gasification. *Fuel*, **99**, 204-209 (2012).

Mazumder, J., de Lasa, H.I., Catalytic steam gasification of biomass surrogates: Thermodynamics and effect of operating conditions. *Chem. Eng. J.*, **293**, 232-242 (2016).

McMinn, D., Chromatography: gas. Detectors: General (Flame Ionization Detectors and Thermal Conductivity Detectors). In I. D. Wilson, (Ed.), *Encyclopedia of Separation Science*, 443-447, Academic Press, Oxford, (2000).

Meng, J., Zhao, Z., Wang, X., Wu, X., Zheng, A., Huang, Z., Zhao, K., Li, H., Effects of catalyst preparation parameters and reaction operating conditions on the activity and stability of thermally fused Fe-olivine catalyst in the steam reforming of toluene. *Int. J. Hydrogen Energy*, **43**, 127-138 (2018a).

Meng, J., Wang, X., Zhao, Z., Zheng, A., Huang, Z., Wei, G., Lv, K., Li, H., Highly abrasion resistant thermally fused olivine as in-situ catalysts for tar reduction in a circulating fluidized bed biomass gasifier. *Bioresour. Technol.*, **268**, 212-220 (2018b).

Meng, J., Zhao, Z., Wang, X., Zheng, A., Zhang, D., Huang, Z., Zhao, K., Wei, G., Li, H., Comparative study on phenol and naphthalene steam reforming over Ni-Fe alloy catalysts supported on olivine synthesized by different methods. *Energy Convers. Manage.*, **168**, 60-73 (2018c).

Meng, J., Zhao, Z., Wang, X., Chen, J., Zheng, A., Huang, Z., Wei, G., Li, H., Steam reforming and carbon deposition evaluation of phenol and naphthalene used as tar model compounds over Ni and Fe olivine-supported catalysts. *J. Energy Inst.*, **92**, 1765-1778 (2019).

Meng, X., Mitsakis, P., Mayerhofer, M., de Jong, W., Gaderer, M., Verkooijen, A.H.M., Spliethoff, H., Tar formation in a steam-O_2 blown CFB gasifier and a steam blown PBFB gasifier (BabyHPR): Comparison between different on-line measurement techniques and the off-line SPA sampling and analysis method. *Fuel Process. Technol.*, **100**, 16-29 (2012).

Miccio, F., Piriou, B., Ruoppolo, G., Chirone, R., Biomass gasification in a catalytic fluidized reactor with beds of different materials. *Chem. Eng. J.*, **154**, 369-374 (2009).

Miccio, F., Picarelli, A., Ruoppolo, G., Increasing tar and hydrocarbons conversion by catalysis in bubbling fluidized bed gasifiers. *Fuel Process. Technol.*, **141**, 31-37 (2016).

Michel, R., Rapagnà, S., Burg, P., Mazziotti di Celso, G., Courson, C., Zimny, T., Gruber, R., Steam gasification of Miscanthus X Giganteus with olivine as catalyst production of syngas and analysis of tars (IR, NMR and GC/MS). *Biomass Bioenergy*, **35**, 2650-2658 (2011a).

Michel, R., Rapagnà, S., Di Marcello, M., Burg, P., Matt, M., Courson, C., Gruber, R., Catalytic steam gasification of Miscanthus X giganteus in fluidised bed reactor on olivine based catalysts. *Fuel Process. Technol.*, **92**, 1169-1177 (2011b).

Michel, R., Ammar, M.R., Poirier, J., Simon, P., Phase transformation characterization of olivine subjected to high temperature in air. *Ceram. Int.*, **39**, 5287-5294 (2013).

Michel, R., Ammar, M.R., Véron, E., Simon, P., Poirier, J., Investigating the mechanism of phase transformations and migration in olivine at high temperature. *RSC Adv.*, **4**, 26645-26652 (2014).

Migliaccio, R., Brachi, P., Montagnaro, F., Papa, S., Tavano, A., Montesarchio, P., Ruoppolo, G., Urciuolo, M., Sewage Sludge Gasification in a Fluidized Bed: Experimental Investigation and Modeling. *Ind. Eng. Chem. Res.*, **60**, 5034-5047 (2021).

Milne, T. A., Evans, R. J., Abatzaglou, N., Biomass gasifier tars: Their nature, formation, and conversion (1998)

Mishra, S., Upadhyay, R.K., Review on biomass gasification: Gasifiers, gasifying mediums, and operational parameters. *Mater. Sci. Energy Technol.*, **4**, 329-340 (2021).

Mitsakis, P., Mayerhofer, M., Meng, X., Spliethoff, H., Gaderer, M., Optical measurement of tars in a fluidized bed gasifier: influence of fuel type and gasification parameters on their formation. *Biomass Convers. Biorefin.*, **3**, 157-167 (2013).

Moiceanu, G., Paraschiv, G., Voicu, G., Dinca, M., Negoita, O., Chitoiu, M., Tudor, P., Energy consumption at size reduction of lignocellulose biomass for bioenergy. *Sustainability*, **11,** 2477 (2019).

Molino, A., Chianese, S., Musmarra, D., Biomass gasification technology: The state of the art overview. *J. Energy Chem.*, **25**, 10-25 (2016).

Molino, A., Larocca, V., Chianese, S., Musmarra, D., Biofuels production by biomass gasification: A review. *Energies*, **11,** 811 (2018).

Mollick, P.K., Venugopalan, R., Roy, M., Rao, P.T., Sathiyamoorthy, D., Sengupta, P., Sharma, G., Basak, C.B., Chakravartty, J.K., Deposition of diversely textured buffer pyrolytic carbon layer in TRISO coated particle by controlled manipulation of spouted bed hydrodynamics. *Chem. Eng. Sci.*, **128**, 44-53 (2015).

Montiano, M.G., Fernández, A.M., Díaz-Faes, E., Barriocanal, C., Tar from biomass/coal-containing briquettes. Evaluation of PAHs. *Fuel*, **154**, 261-267 (2015).

Morf, P., Hasler, P., Nussbaumer, T., Mechanisms and kinetics of homogeneous secondary reactions of tar from continuous pyrolysis of wood chips. *Fuel*, **81**, 843-853 (2002).

Morin, M., Nitsch, X., Pécate, S., Hémati, M., Tar conversion over olivine and sand in a fluidized bed reactor using toluene as model compound. *Fuel*, **209**, 25-34 (2017).

Motta, I.L., Miranda, N.T., Maciel Filho, R., Wolf Maciel, M.R., Biomass gasification in fluidized beds: A review of biomass moisture content and operating pressure effects. *Renewable Sustainable Energy Rev.*, **94**, 998-1023 (2018).

Nagashima, H., Ishikura, T., Ide, M., Hydrodynamics of a spouted bed with an impermeable draft tube for binary particle systems. *Korean J. Chem. Eng.*, **16**, 688-693 (1999).

Nagashima, H., Ishikura, T., Ide, M., Effect of the tube shape on gas and particle flow in spouted beds with a porous draft tube. *Can. J. Chem. Eng.*, **87**, 228-236 (2009).

Nagashima, H., Suzukawa, K., Ishikura, T., Hydrodynamic performance of spouted beds with different types of draft tubes. *Particuology*, **11**, 475-482 (2013).

Nahil, M.A., Wang, X., Wu, C., Yang, H., Chen, H., Williams, P.T., Novel bi-functional Ni-Mg-Al-CaO catalyst for catalytic gasification of biomass for hydrogen production with in situ CO_2 adsorption. *RSC Adv.*, **3**, 5583-5590 (2013).

Nam, H., Wang, S., Sanjeev, K.C., Seo, M.W., Adhikari, S., Shakya, R., Lee, D., Shanmugam, S.R., Enriched hydrogen production over air and air-steam fluidized bed gasification in a bubbling fluidized bed reactor with CaO: Effects of biomass and bed material catalyst. *Energy Convers. Manage.*, **225**, 113408 (2020).

Nam, S., Park, Y., Yun, Y., Gu, J., Sung, H., Horio, M., Catalytic application of metallic iron from the dyeing sludge ash for benzene steam reforming reaction in tar emitted from biomass gasification. *Korean J. Chem. Eng.*, **33**, 465-472 (2016).

Narnaware, S.L., Panwar, N.L., Catalysts and their role in biomass gasification and tar abetment: a review. *Biomass Convers. Biorefinery*, (2021).

Narváez, I., Orío, A., Aznar, M.P., Corella, J., Biomass gasification with air in an atmospheric bubbling fluidized bed. Effect of six operational variables on the quality of the produced raw gas. *Ind. Eng. Chem. Res.*, **35**, 2110-2120 (1996).

National Research Council, Opportunities and obstacles in large-scale biomass utilization: The role of the chemical sciences and engineering communities: A workshop summary, The National Academies Press, Washington, DC, (2012).

Neeft, J., Knoef, H., Buffinga, G. J., Zielke, U., Sjöström, K., Brage, C., Hasler, P., Smell, P. A., Suomalainen, M., Dorrington, M. A., Greil, C., Guideline for Sampling and Analysis of Tars and Particles in Biomass Producer Gases. 162-175, (2008).

Neto, J.L.V., Duarte, C.R., Murata, V.V., Barrozo, M.A.S., Effect of a Draft Tube on the Fluid Dynamics of a Spouted Bed: Experimental and CFD Studies. *Drying Technol.*, **26**, 299-307 (2008).

Neubauer, Y., Gredinger, A., Borgmeyer, J., Kleinhappl, M., Biollaz, S.M.A., Comparison of two on-line tar-monitoring devices with off-line liquid sample tar-analysis operated on a test gas generation system applying ethene pyrolysis. *Biomass Bioenergy*, **117**, 63-70 (2018).

Neubert, M., Reil, S., Wolff, M., Pöcher, D., Stork, H., Ultsch, C., Meiler, M., Messer, J., Kinzler, L., Dillig, M., Beer, S., Karl, J., Experimental comparison of solid phase adsorption (SPA), activated carbon test tubes and tar protocol (DIN CEN/TS 15439) for tar analysis of biomass derived syngas. *Biomass Bioenergy*, **105**, 443-452 (2017).

Nguyen, H.N.T., Seemann, M., Thunman, H., Fate of Polycyclic Aromatic Hydrocarbons during Tertiary Tar Formation in Steam Gasification of Biomass. *Energy Fuels*, **32**, 3499-3509 (2018).

Nguyen, N.M., Alobaid, F., Epple, B., Chemical looping gasification of torrefied woodchips in a bubbling fluidized bed test rig using iron-based oxygen carriers. *Renewable Energy*, **172**, 34-45 (2021).

Ni, M., Leung, D.Y.C., Leung, M.K.H., Sumathy, K., An overview of hydrogen production from biomass. *Fuel Process. Technol.*, **87**, 461-472 (2006).

Nitsch, X., Commandré, J.M., Clavel, P., Martin, E., Valette, J., Volle, G., Conversion of phenol-based tars over olivine and sand in a biomass gasification atmosphere. *Energy Fuels*, **27**, 5459-5465 (2013).

Niu, M., Huang, Y., Jin, B., Liang, S., Dong, Q., Gu, H., Sun, R., A novel two-stage enriched air biomass gasification for producing low-tar high heating value fuel gas: Pilot verification and performance analysis. *Energy*, **173**, 511-522 (2019).

Niu, Y., Han, F., Chen, Y., Lyu, Y., Wang, L., Experimental study on steam gasification of pine particles for hydrogen-rich gas. *J. Energy Inst.*, **90**, 715-724 (2017).

Nordgreen, T., Liliedahl, T., Sjöström, K., Metallic iron as a tar breakdown catalyst related to atmospheric, fluidised bed gasification of biomass. *Fuel*, **85**, 689-694 (2006).

Nordgreen, T., Nemanova, V., Engvall, K., Sjöström, K., Iron-based materials as tar depletion catalysts in biomass gasification: Dependency on oxygen potential. *Fuel*, **95**, 71-78 (2012).

Ochoa, A., Arregi, A., Amutio, M., Gayubo, A.G., Olazar, M., Bilbao, J., Castaño, P., Coking and sintering progress of a Ni supported catalyst in the steam reforming of biomass pyrolysis volatiles. *Appl. Catal., B,* **233**, 289-300 (2018).

Okolie, J.A., Rana, R., Nanda, S., Dalai, A.K., Kozinski, J.A., Supercritical water gasification of biomass: A state-of-the-art review of process parameters, reaction mechanisms and catalysis. *Sustainable Energy Fuels,* **3**, 578-598 (2019).

Olazar, M., San José, M.J., Aguayo, A.T., Arandes, J.M., Bilbao, J., Stable Operation Conditions for Gas-Solid Contact Regimes in Conical Spouted Beds. *Ind. Eng. Chem. Res.,* **31**, 1784-1792 (1992).

Olazar, M., San José, M.J., Aguayo, A.T., Arandes, J.M., Bilbao, J., Pressure drop in conical spouted beds. *Chem. Eng. J.*, **51**, 53-60 (1993a).

Olazar, M., San José, M.J., Aguayo, A.T., Arandes, J.M., Bilbao, J., Design Factors of Conical Spouted Beds and Jet Spouted Beds. *Ind. Eng. Chem. Res.,* **32**, 1245-1250 (1993b).

Olazar, M., San José, M.J., Peñas, F.J., Aguyo, A.T., Arandes, J.M., Bilbao, J., A model for gas flow in jet spouted beds. *Can. J. Chem. Eng.,* **71**, 189-194 (1993c).

Olazar, M., San José, M.J., LLamosas, R., Bilbao, J., Hydrodynamics of Sawdust and Mixtures of Wood Residues in Conical Spouted Beds. *Ind. Eng. Chem. Res.*, **33**, 993-1000 (1994a).

Olazar, M., San José, M.J., Zabala, G., Bilbao, J., New reactor in jet spouted bed regime for catalytic polymerizations. *Chem. Eng. Sci.*, **49**, 4579-4588 (1994b).

Olazar, M., San José, M.J., Ricardo, L.L., Alvarez, S., Bilbao, J., Study of Local Properties in Conical Spouted Beds Using an Optical Fiber Probe. *Ind. Eng. Chem. Res.,* **34**, 4033-4039 (1995).

Ong, H.C., Chen, W.H., Farooq, A., Gan, Y.Y., Lee, K.T., Ashokkumar, V., Catalytic thermochemical conversion of biomass for biofuel production: A comprehensive review. *Renewable Sustainable Energy Rev.,* **113,** 109266 (2019).

Ordonez-Loza, J., Chejne, F., Jameel, A.G.A., Telalovic, S., Arrieta, A.A., Sarathy, S.M., An investigation into the pyrolysis and oxidation of bio-oil from sugarcane bagasse: Kinetics and evolved gases using TGA-FTIR. *J. Environ. Chem. Eng.,* **9**, 106144 (2021).

Orío, A., Corella, J., Narváez, I., Performance of Different Dolomites on Hot Raw Gas Cleaning from Biomass Gasification with Air. *Ind. Eng. Chem. Res.*, **36**, 3800-3808 (1997).

Osipovs, S., Sampling of benzene in tar matrices from biomass gasification using two different solid-phase sorbents. *Anal. Bioanal. Chem.*, **391**, 1409-1417 (2008).

Osipovs, S., Use of two different adsorbents for sampling tar in gas obtained from peat gasification. *Int. J. Environ. Anal. Chem.*, **89**, 871-880 (2009).

Osipovs, S., Comparison of efficiency of two methods for tar sampling in the syngas. *Fuel*, **103**, 387-392 (2013).

Paasen, S. V., Kiel, J. H. A., Tar formation in a fluidised-bed gasifier, (2004).

Pablos, A., Aguado, R., Tellabide, M., Altzibar, H., Freire, F.B., Bilbao, J., Olazar, M., A new fountain confinement device for fluidizing fine and ultrafine sands in conical spouted beds. *Powder Technol.*, **328**, 38-46 (2018).

Pablos, A., Aguado, R., Vicente, J., Tellabide, M., Bilbao, J., Olazar, M., Elutriation, attrition and segregation in a conical spouted bed with a fountain confiner. *Particuology*, **51**, 35-44 (2020).

Pan, J., Huang, Y., Liu, L., Hu, Y., Li, G., A novel fractionized sampling and stacking strategy for online hyphenation of solid-phase-based extraction to ultra-high performance liquid chromatography for ultrasensitive analysis. *J. Chromatogr. A*, **1316**, 29-36 (2013).

Pan, Y., Abulizi, A., Talifu, D., Tursun, Y., Xu, S., Catalytic gasification of biomass and coal blend with Fe_2O_3/olivine in a decoupled triple bed. *Fuel Process. Technol.*, **194,** 106121 (2019).

Pan, Y.G., Roca, X., Velo, E., Puigjaner, L., Removal of tar by secondary air in fluidised bed gasification of residual biomass and coal. *Fuel*, **78**, 1703-1709 (1999).

Park, S.J., Son, S.H., Kook, J.W., Ra, H.W., Yoon, S.J., Mun, T., Moon, J.H., Yoon, S.M., Kim, J.H., Kim, Y.K., Lee, J.G., Lee, D., Seo, M.W., Gasification operational characteristics of 20-tons-Per-Day rice husk fluidized-bed reactor. *Renew. Energy*, **169**, 788-798 (2021).

Parkinson, D.R., Warren, J.M., Pawliszyn, J., Analysis of ergosterol for the detection of mold in soils by automated on-fiber derivatization headspace extraction-SPME-GC/MS. *Anal. Chim. Acta*, **661**, 181-187 (2010).

Parthasarathy, P., Narayanan, K.S., Hydrogen production from steam gasification of biomass: Influence of process parameters on hydrogen yield - A review. *Renewable Energy*, **66**, 570-579 (2014).

Patuzzi, F., Roveda, D., Mimmo, T., Karl, J., Baratieri, M., A comparison between on-line and off-line tar analysis methods applied to common reed pyrolysis. *Fuel*, **111**, 689-695 (2013).

Patuzzi, F., Prando, D., Vakalis, S., Rizzo, A.M., Chiaramonti, D., Tirler, W., Mimmo, T., Gasparella, A., Baratieri, M., Small-scale biomass gasification CHP systems: Comparative performance assessment and monitoring experiences in South Tyrol (Italy). *Energy*, **112**, 285-293 (2016).

Patuzzi, F., Basso, D., Vakalis, S., Antolini, D., Piazzi, S., Benedetti, V., Cordioli, E., Baratieri, M., State-of-the-art of small-scale biomass gasification systems: An extensive and unique monitoring review. *Energy*, **223**, 120039 (2021).

Pei, H., Wang, X., Dai, X., Jin, B., Huang, Y., A novel two-stage biomass gasification concept: Design and operation of a 1.5 MWth demonstration plant. *Bioresour. Technol.*, **267**, 102-109 (2018).

Peñalver, R., Campillo, N., López-García, I., Hernández-Córdoba, M., Solid-phase microextraction for the determination of iron organic compounds in seawaters and soils by gas chromatography coupled to microwave-induced plasma with atomic emission detection spectrometry. *Microchem. J.*, **154,** 104630 (2020).

Pereira, E. G., Martins, M. A., Gasification Technologies. In M. A. Abraham, (Ed.), *Encyclopedia of Sustainable Technologies*, 315-325, Elsevier, Oxford, (2017).

Pfeifer, C., Rauch, R., Hofbauer, H., In-Bed Catalytic Tar Reduction in a Dual Fluidized Bed Biomass Steam Gasifier. *Ind. Eng. Chem. Res.*, **43**, 1634-1640 (2004).

Pfeifer, C., Koppatz, S., Hofbauer, H., Steam gasification of various feedstocks at a dual fluidised bed gasifier: Impacts of operation conditions and bed materials. *Biomass Convers. Biorefin.*, **1**, 39-53 (2011).

Phuphuakrat, T., Namioka, T., Yoshikawa, K., Tar removal from biomass pyrolysis gas in two-step function of decomposition and adsorption. *Appl. Energy*, **87**, 2203-2211 (2010).

Pietzcker, R.C., Osorio, S., Rodrigues, R., Tightening EU ETS targets in line with the European Green Deal: Impacts on the decarbonization of the EU power sector. *Appl. Energy*, **293**, 116914 (2021).

Pinto, F., André, R.N., Lopes, H., Dias, M., Gulyurtlu, I., Cabrita, I., Effect of experimental conditions on gas quality and solids produced by sewage sludge cogasification. 2. Sewage sludge mixed with biomass. *Energy Fuels*, **22**, 2314-2325 (2008).

Pinto, F., André, R.N., Carolino, C., Miranda, M., Abelha, P., Direito, D., Perdikaris, N., Boukis, I., Gasification improvement of a poor quality solid recovered fuel (SRF). Effect of using natural minerals and biomass wastes blends. *Fuel*, **117**, 1034-1044 (2014).

Pinto, F., André, R.N., Carolino, C., Miranda, M., Abelha, P., Direito, D., Dohrup, J., Sørensen, H.R., Girio, F., Effects of experimental conditions and of addition of natural minerals on syngas production from lignin by oxy-gasification: Comparison of bench- and pilot scale gasification. *Fuel*, **140**, 62-72 (2015).

Pinto, F., André, R., Miranda, M., Neves, D., Varela, F., Santos, J., Effect of gasification agent on co-gasification of rice production wastes mixtures. *Fuel*, **180**, 407-416 (2016).

Pio, D.T., Gomes, H.G.M.F., Tarelho, L.A.C., Ruivo, L.C.M., Matos, M.A.A., Pinto, R.G., Frade, J.R., Lemos, F.M.S., Ilmenite as low-cost catalyst for producer gas quality improvement from a biomass pilot-scale gasifier. *Energy Rep.*, **6**, 325-330 (2020).

Pio, D.T., Ruivo, L.C.M., Tarelho, L.A.C., Frade, J.R., Kantarelis, E., Engvall, K., Tar formation during eucalyptus gasification in a bubbling fluidized bed reactor: Effect of feedstock and reactor bed composition. *Energy Convers. Manage.*, **229**, 113749 (2021).

Pissot, S., Faust, R., Aonsamang, P., Berdugo Vilches, T., Maric, J., Thunman, H., Knutsson, P., Seemann, M., Development of Oxygen Transport Properties by Olivine and Feldspar in Industrial-Scale Dual Fluidized Bed Gasification of Woody Biomass. *Energy Fuels*, **35**, 9424-9436 (2021).

Prando, D., Shivananda Ail, S., Chiaramonti, D., Baratieri, M., Dasappa, S., Characterisation of the producer gas from an open top gasifier: Assessment of different tar analysis approaches. *Fuel*, **181**, 566-572 (2016).

Prasertcharoensuk, P., Bull, S.J., Arpornwichanop, A., Phan, A.N., Sustainable Hydrogen Production from Waste Wood and CO_2. *Ind. Eng. Chem. Res.*, **60**, 12362-12376 (2021).

Pratali Maffei, L., Pelucchi, M., Faravelli, T., Cavallotti, C., Theoretical study of sensitive reactions in phenol decomposition. *React. Chem. Eng.*, **5**, 452-472 (2020).

Pudukudy, M., Yaakob, Z., Mhd Syahri, K., Jia, Q., Shan, S., Production of hydrogen-rich syngas and multiwalled carbon nanotubes by biogas decomposition over zirconia supported iron catalysts. *J. Ind. Eng. Chem.,* **84**, 150-166 (2020).

Pushp, M., Gall, D., Davidsson, K., Seemann, M., Pettersson, J.B.C., Influence of Bed Material, Additives, and Operational Conditions on Alkali Metal and Tar Concentrations in Fluidized Bed Gasification of Biomass. *Energy Fuels,* **32**, 6797-6806 (2018).

Qin, Y., Campen, A., Wiltowski, T., Feng, J., Li, W., The influence of different chemical compositions in biomass on gasification tar formation. *Biomass Bioenergy,* **83**, 77-84 (2015).

Qin, Y., Feng, J., Li, W., Formation of tar and its characterization during air–steam gasification of sawdust in a fluidized bed reactor. *Fuel,* **89**, 1344-1347 (2010).

Qiu, K., Hu, C., Yang, S., Luo, K., Zhang, K., Fan, J., Computational evaluation of depth effect on the hydrodynamics of slot-rectangular spouted bed. *Powder Technol.,* **287**, 51-60 (2016).

Quan, C., Xu, S., Zhou, C., Steam reforming of bio-oil from coconut shell pyrolysis over Fe/olivine catalyst. *Energy Convers. Manage.,* **141**, 40-47 (2017).

Rabou, L.P.L.M., Zwart, R.W.R., Vreugdenhil, B.J., Bos, L., Tar in Biomass Producer Gas, the Energy research Centre of The Netherlands (ECN) Experience: An Enduring Challenge. *Energy Fuels,* **23**, 6189-6198 (2009).

Rahman, M.M., Henriksen, U.B., Ahrenfeldt, J., Arnavat, M.P., Design, construction and operation of a low-tar biomass (LTB) gasifier for power applications. *Energy,* **204**, 117944 (2020).

Rahman, M.M., Aravindakshan, S., Matin, M.A., Design and performance evaluation of an inclined nozzle and combustor of a downdraft moving bed gasifier for tar reduction. *Renewable Energy,* **172**, 239-250 (2021).

Rakesh, N., Dasappa, S., A critical assessment of tar generated during biomass gasification - Formation, evaluation, issues and mitigation strategies. *Renewable Sustainable Energy Rev.,* **91**, 1045-1064 (2018).

Ramadhani, B., Kivevele, T., Kihedu, J.H., Jande, Y.A.C., Catalytic tar conversion and the prospective use of iron-based catalyst in the future development of biomass gasification: a review. *Biomass Convers. Biorefinery,* (2020).

Rapagnà, S., Jand, N., Kiennemann, A., Foscolo, P.U., Steam-gasification of biomass in a fluidised-bed of olivine particles. *Biomass Bioenergy*, **19**, 187-197 (2000).

Rapagnà, S., Mazziotti di Celso, G., Devolatilization of wood particles in a hot fluidized bed: Product yields and conversion rates. *Biomass Bioenergy*, **32**, 1123-1129 (2008).

Rapagnà, S., Gallucci, K., Marcello, M.D., Foscolo, P.U., Nacken, M., Heidenreich, S., In situ catalytic ceramic candle filtration for tar reforming and particulate abatement in a fluidized-bed biomass gasifier. *Energy Fuels*, **23**, 3804-3809 (2009).

Rapagnà, S., Gallucci, K., di Marcello, M., Matt, M., Nacken, M., Heidenreich, S., Foscolo, P.U., Gas cleaning, gas conditioning and tar abatement by means of a catalytic filter candle in a biomass fluidized-bed gasifier. *Bioresour. Technol.*, **101**, 7123-7130 (2010).

Rapagnà, S., Virginie, M., Gallucci, K., Courson, C., Di Marcello, M., Kiennemann, A., Foscolo, P.U., Fe/olivine catalyst for biomass steam gasification: Preparation, characterization and testing at real process conditions. *Catal. Today*, **176**, 163-168 (2011).

Rapagnà, S., Gallucci, K., Di Marcello, M., Foscolo, P.U., Nacken, M., Heidenreich, S., Matt, M., First Al_2O_3 based catalytic filter candles operating in the fluidized bed gasifier freeboard. *Fuel*, **97**, 718-724 (2012).

Rapagnà, S., Gallucci, K., Foscolo, P.U., Olivine, dolomite and ceramic filters in one vessel to produce clean gas from biomass. *Waste Manage.*, **71**, 792-800 (2018).

Ratnasamy, C., Wagner, J., Water gas shift catalysis. *Catal. Rev. Sci. Eng.*, **51**, 325-440 (2009).

Rauch, R., Bosch, K., Hofbauer, H., Świerczyński, D., Courson, C., Kiennemann, A., Comparison of different olivines for biomass steam gasification. *Proceedings of the Conference for Science in Thermal and Chemical Biomass Conversion*, (2004).

Rauch, R., Hrbek, J., Hofbauer, H., Biomass Gasification for Synthesis Gas Production and Applications of the Syngas. *Adv.Bioenerg. Sustainable. Challenge*, **3**, 342-362 (2016).

Reizer, E., Csizmadia, I.G., Palotás, Á,B., Viskolcz, B., Fiser, B., Formation Mechanism of Benzo(a)pyrene: One of the Most Carcinogenic Polycyclic Aromatic Hydrocarbons (PAH). *Molecules*, **24**, 1040 (2019).

Remiro, A., Valle, B., Aguayo, A.T., Bilbao, J., Gayubo, A.G., Operating conditions for attenuating Ni/La_2O_3–αAl_2O_3 catalyst deactivation in the steam reforming of bio-oil aqueous fraction. *Fuel Process. Technol.*, **115**, 222-232 (2013).

Ren, J., Cao, J.P., Zhao, X.Y., Yang, F.L., Wei, X.Y., Recent advances in syngas production from biomass catalytic gasification: A critical review on reactors, catalysts, catalytic mechanisms and mathematical models. *Renewable Sustainable Energy Rev.*, **116,** 109426 (2019a).

Ren, J., Liu, Y.L., Zhao, X.Y., Cao, J.P., Biomass thermochemical conversion: A review on tar elimination from biomass catalytic gasification. *J. Energy Inst.*, **93**, 1083-1098 (2019b).

Ren, Q., Wang, S., Catalytic Gasification of Biomass Over Fe-MgO Catalyst. *Rev. Chim.*, **69**, 2933-2936 (2018).

Robinson, T., Bronson, B., Gogolek, P., Mehrani, P., Comparison of the air-blown bubbling fluidized bed gasification of wood and wood–PET pellets. *Fuel*, **178**, 263-271 (2016).

Roche, E., de Andrés, J.M., Narros, A., Rodríguez, M.E., Air and air-steam gasification of sewage sludge. The influence of dolomite and throughput in tar production and composition. *Fuel*, **115**, 54-61 (2014).

Rodriguez Correa, C., Kruse, A., Supercritical water gasification of biomass for hydrogen production – Review. *J. Supercrit. Fluids*, **133**, 573-590 (2018).

Roets, L., Bunt, J.R., Neomagus, H.W.J.P., Van Niekerk, D., An evaluation of a new automated duplicate-sample Fischer Assay setup according to ISO/ASTM standards and analysis of the tar fraction. *J. Anal. Appl. Pyrolysis,* **106**, 190-196 (2014).

Ruivo, L.C.M., Pio, D.T., Yaremchenko, A.A., Tarelho, L.A.C., Frade, J.R., Kantarelis, E., Engvall, K., Iron-based catalyst ($Fe_{2-x}Ni_xTiO_5$) for tar decomposition in biomass gasification. *Fuel*, **300**, 120859 (2021).

Ruiz-Jimenez, J., Lan, H., Leleev, Y., Hartonen, K., Riekkola, M., Comparison of multiple calibration approaches for the determination of volatile organic compounds in air samples by solid phase microextraction Arrow and in-tube extraction. *J. Chromatogr. A,* **1616,** 460825 (2020).

Ruoppolo, G., Miccio, F., Miccio, M., Brachi, P., Chirone, R., Sewage sludge ashes as a primary catalyst for the abatement of tar in biomass gasification: Bubbling versus spouted-fluidized bed configuration. *Can. J. Chem. Eng.*, **99**, 1706-1714 (2021).

Rupesh, S., Muraleedharan, C., Arun, P., Influence of Residence Time on Syngas Composition in CaO Enhanced Air–Steam Gasification of Biomass. *Environ. Dev. Sustain.,* (2021).

Saidi, M., Basirat Tabrizi, H., Grace, J.R., Lim, C.J., Hydrodynamic investigation of gas-solid flow in rectangular spout-fluid bed using CFD-DEM modeling. *Powder Technol.,* **284**, 355-364 (2015).

San José, M.J., Olazar, M., Aguayo, A.T., Arandes, J.M., Bilbao, J., Expansion of spouted beds in conical contactors. *Chem. Eng. J.,* **51**, 45-52 (1993).

San José, M.J., Olazar, M., Peñas, F.J., Arandes, J.M., Bilbao, J., Correlation for calculation of the gas dispersion coefficient in conical spouted beds. *Chem. Eng. Sci.,* **50**, 2161-2172 (1995).

San José, M.J., Olazar, M., Alvarez, S., Bilbao, J., Local bed voidage in conical spouted beds. *Ind. Eng. Chem. Res.,* **37**, 2553-2558 (1998a).

San José, M.J., Olazar, M., Alvarez, S., Izquierdo, M.A., Bilbao, J., Solid cross-flow into the spout and particle trajectories in conical spouted beds. *Chem. Eng. Sci.,* **53**, 3561-3570 (1998b).

Sansaniwal, S.K., Pal, K., Rosen, M.A., Tyagi, S.K., Recent advances in the development of biomass gasification technology: A comprehensive review. *Renewable Sustainable Energy Rev.,* **72**, 363-384 (2017a).

Sansaniwal, S.K., Rosen, M.A., Tyagi, S.K., Global challenges in the sustainable development of biomass gasification: An overview. *Renewable Sustainable Energy Rev.,* **80**, 23-43 (2017b).

Santamaria, L., Lopez, G., Arregi, A., Amutio, M., Artetxe, M., Bilbao, J., Olazar, M., Influence of the support on Ni catalysts performance in the in-line steam reforming of biomass fast pyrolysis derived volatiles. *Appl. Catal., B,* **229**, 105-113 (2018).

Santamaria, L., Design and performance of Ni-based catalysts for the steam reforming of biomass fast pyrolysis volatiles. PhD Thesis, University of the Basque Country, Bilbao. (2019).

Santamaria, L., Lopez, G., Arregi, A., Artetxe, M., Amutio, M., Bilbao, J., Olazar, M., Catalytic steam reforming of biomass fast pyrolysis volatiles over Ni–Co bimetallic catalysts. *J. Ind. Eng. Chem.,* **91**, 167-181 (2020a).

Santamaria, L., Arregi, A., Lopez, G., Artetxe, M., Amutio, M., Bilbao, J., Olazar, M., Effect of La_2O_3 promotion on a Ni/Al_2O_3 catalyst for H_2 production in the in-line biomass pyrolysis-reforming. *Fuel*, **262**, 116593 (2020b).

Santamaria, L., Lopez, G., Fernandez, E., Cortazar, M., Arregi, A., Olazar, M., Bilbao, J., Progress on Catalyst Development for the Steam Reforming of Biomass and Waste Plastics Pyrolysis Volatiles: A Review. *Energy Fuels*, **35**, 17051-17084 (2021).

Savuto, E., Navarro, R.M., Mota, N., Di Carlo, A., Bocci, E., Carlini, M., Fierro, J.L.G., Steam reforming of tar model compounds over Ni/Mayenite catalysts: effect of Ce addition. *Fuel*, **224**, 676-686 (2018).

Savuto, E., Di Carlo, A., Steele, A., Heidenreich, S., Gallucci, K., Rapagnà, S., Syngas conditioning by ceramic filter candles filled with catalyst pellets and placed inside the freeboard of a fluidized bed steam gasifier. *Fuel Process. Technol.*, **191**, 44-53 (2019).

Schmid, J.C., Wolfesberger, U., Koppatz, S., Pfeifer, C., Hofbauer, H., Variation of feedstock in a dual fluidized bed steam gasifier-influence on product gas, tar content, and composition. *Environ. Progress Sustainable Energy*, **31**, 205-215 (2012).

Schmid, J.C., Benedikt, F., Fuchs, J., Mauerhofer, A.M., Müller, S., Hofbauer, H., Syngas for biorefineries from thermochemical gasification of lignocellulosic fuels and residues—5 years' experience with an advanced dual fluidized bed gasifier design. *Biomass Convers. Biorefinery*, **11**, 2405-2442 (2021a).

Schmid, M., Beirow, M., Schweitzer, D., Waizmann, G., Spörl, R., Scheffknecht, G., Product gas composition for steam-oxygen fluidized bed gasification of dried sewage sludge, straw pellets and wood pellets and the influence of limestone as bed material. *Biomass Bioenergy*, **117**, 71-77 (2018).

Schmid, M., Hafner, S., Biollaz, S., Schneebeli, J., Waizmann, G., Scheffknecht, G., Steam-oxygen gasification of sewage sludge: Reduction of tar, H_2S and COS with limestone as bed additive. *Biomass Bioenergy*, **150**, 106100 (2021b).

Schweitzer, D., Gredinger, A., Schmid, M., Waizmann, G., Beirow, M., Spörl, R., Scheffknecht, G., Steam gasification of wood pellets, sewage sludge and manure: Gasification performance and concentration of impurities. *Biomass Bioenergy*, **111**, 308-319 (2018).

Serrano, D., Kwapinska, M., Horvat, A., Sánchez-Delgado, S., Leahy, J.J., Cynara cardunculus L. gasification in a bubbling fluidized bed: The effect of magnesite and olivine on product gas, tar and gasification performance. *Fuel*, **173**, 247-259 (2016).

Shahbaz, M., Yusup, S., Inayat, A., Patrick, D.O., Ammar, M., The influence of catalysts in biomass steam gasification and catalytic potential of coal bottom ash in

biomass steam gasification: A review. *Renewable Sustainable Energy Rev.*, **73**, 468-476 (2017).

Shayan, E., Zare, V., Mirzaee, I., Hydrogen production from biomass gasification; a theoretical comparison of using different gasification agents. *Energy Convers. Manage.*, **159**, 30-41 (2018).

Shen, Y., Yoshikawa, K., Recent progresses in catalytic tar elimination during biomass gasification or pyrolysis - A review. *Renewable Sustainable Energy Rev.*, **21**, 371-392 (2013).

Shen, Y., Zhao, P., Shao, Q., Ma, D., Takahashi, F., Yoshikawa, K., In-situ catalytic conversion of tar using rice husk char-supported nickel-iron catalysts for biomass pyrolysis/gasification. *Appl. Catal., B*, **152-153**, 140-151 (2014).

Shi, Q., Pan, N., Long, H., Cui, D., Guo, X., Long, Y., Chung, K.H., Zhao, S., Xu, C., Hsu, C.S., Characterization of middle-temperature gasification coal tar. Part 3: Molecular composition of acidic compounds. *Energy Fuels*, **27**, 108-117 (2013).

Shukla, B., Koshi, M., A highly efficient growth mechanism of polycyclic aromatic hydrocarbons. *Phys. Chem. Chem. Phys.*, **12**, 2427-2437 (2010).

Shukla, B., Susa, A., Miyoshi, A., Koshi, M., Role of Phenyl Radicals in the Growth of Polycyclic Aromatic Hydrocarbons. *J. Phys. Chem. A*, **112**, 2362-2369 (2008).

Shukla, B., Miyoshi, A., Koshi, M., Role of Methyl Radicals in the Growth of PAHs. *J. Am. Soc. Mass Spectrom.*, **21**, 534-544 (2010).

Shukla, B., Koshi, M., Comparative study on the growth mechanisms of PAHs. *Combust. Flame*, **158**, 369-375 (2011).

Shukla, B., Koshi, M., A novel route for PAH growth in HACA based mechanisms. *Combust. Flame*, **159**, 3589-3596 (2012).

Shuyan, W., Zhenghua, H., Dan, S., Yikun, L., Lixin, W., Shuai, W., Hydrodynamic simulations of gas–solid spouted bed with a draft tube. *Chem. Engi. Sci.*, **65**, 1322-1333 (2010).

Siedlecki, M., Nieuwstraten, R., Simeone, E., de Jong, W., Verkooijen, A.H.M., Effect of Magnesite as Bed Material in a 100 kWth Steam-Oxygen Blown Circulating Fluidized-Bed Biomass Gasifier on Gas Composition and Tar Formation. *Energy Fuels*, **23**, 5643-5654 (2009).

Siedlecki, M., de Jong, W., Verkooijen, A.H.M., Fluidized bed gasification as a mature and reliable technology for the production of bio-syngas and applied in the production of liquid transportation fuels-a review. *Energies*, **4**, 389-434 (2011).

Sietsma, J.R.A., Jos van Dillen, A., de Jongh, P.E., de Jong, K.P., Application of ordered mesoporous materials as model supports to study catalyst preparation by impregnation and drying. *Stud. Surf. Sci. Catal.*, **162**, 95-102 (2006).

Sikarwar, V.S., Zhao, M., Clough, P., Yao, J., Zhong, X., Memon, M.Z., Shah, N., Anthony, E.J., Fennell, P.S., An overview of advances in biomass gasification. *Energy Environ. Sci.*, **9**, 2939-2977 (2016).

Sikarwar, V. S., Zhao, M., Biomass Gasification. In M. A. Abraham, (Ed.), *Encyclopedia of Sustainable Technologies*, 205-216, Elsevier, Oxford, (2017).

Singh Siwal, S., Zhang, Q., Sun, C., Thakur, S., Kumar Gupta, V., Kumar Thakur, V., Energy production from steam gasification processes and parameters that contemplate in biomass gasifier – A review. *Bioresour. Technol.*, **297**, 122481 (2020).

Situmorang, Y.A., Zhao, Z., Yoshida, A., Abudula, A., Guan, G., Small-scale biomass gasification systems for power generation: A review. *Renewable Sustainable Energy Rev.*, **117**, 109486 (2020).

Skjærseth, J.B., Towards a European Green Deal: The evolution of EU climate and energy policy mixes. *Int. Envir. Agreem. Polit. Law Econ.*, **21**, 25-41 (2021).

Song, T., Wu, J., Shen, L., Xiao, J., Experimental investigation on hydrogen production from biomass gasification in interconnected fluidized beds. *Biomass Bioenergy*, **36**, 258-267 (2012).

Soria-Verdugo, A., Von Berg, L., Serrano, D., Hochenauer, C., Scharler, R., Anca-Couce, A., Effect of bed material density on the performance of steam gasification of biomass in bubbling fluidized beds. *Fuel*, **257**, 116118 (2019).

Sousa, R.C., Ferreira, M.C., Altzibar, H., Freire, F.B., Freire, J.T., Drying of pasty and granular materials in mechanically and conventional spouted beds. *Particuology*, **42**, 176-183 (2019).

Su, G., Huang, G., Li, M., Liu, C., Study on the flow behavior in spout-fluid bed with a draft tube of sub-millimeter grade silicon particles. *Chem. Eng. J.*, **237**, 277-285 (2014).

Sui, M., Li, G., Guan, Y., Li, C., Zhou, R., Zarnegar, A., Hydrogen and syngas production from steam gasification of biomass using cement as catalyst. *Biomass Convers. Biorefinery,* **10**, 119-124 (2020).

Šulc, J., Štojdl, J., Richter, M., Popelka, J., Svoboda, K., Smetana, J., Vacek, J., Skoblja, S., Buryan, P., Biomass waste gasification – Can be the two stage process suitable for tar reduction and power generation? *Waste Manage.,* **32**, 692-700 (2012).

Sun, H., Wang, J., Zhao, J., Shen, B., Shi, J., Huang, J., Wu, C., Dual functional catalytic materials of Ni over Ce-modified CaO sorbents for integrated CO_2 capture and conversion. *Appl. Catal., B,* **244**, 63-75 (2019).

Sun, R., Zobel, N., Neubauer, Y., Cardenas Chavez, C., Behrendt, F., Analysis of gas-phase polycyclic aromatic hydrocarbon mixtures by laser-induced fluorescence. *Opt. Lasers Eng.*, **48**, 1231-1237 (2010).

Sun, Z., Zhang, W., Chemical composition and structure characterization of distillation residues of middle-temperature coal tar. *Chin. J. Chem. Eng.*, **25**, 815-820 (2017).

Suryawanshi, S.J., Shewale, V.C., Thakare, R.S., Yarasu, R.B., Parametric study of different biomass feedstocks used for gasification process of gasifier—a literature review. *Biomass Convers. Bioref.,* (2021).

Susanto, H., Beenackers, A.A.C.M., A moving-bed gasifier with internal recycle of pyrolysis gas. *Fuel,* **75**, 1339-1347 (1996).

Susastriawan, A.A.P., Saptoadi, H., Purnomo, Small-scale downdraft gasifiers for biomass gasification: A review. *Renewable Sustainable Energy Rev.,* **76**, 989-1003 (2017).

Susastriawan, A.A.P., Saptoadi, H., Purnomo, Comparison of the gasification performance in the downdraft fixed-bed gasifier fed by different feedstocks: Rice husk, sawdust, and their mixture. *Sustain. Energy Technol. Assess.,* **34**, 27-34 (2019).

Sutkar, V.S., Deen, N.G., Salikov, V., Antonyuk, S., Heinrich, S., Kuipers, J.A.M., Experimental and numerical investigations of a pseudo-2D spout fluidized bed with draft plates. *Powder Technol.,* **270**, 537-547 (2015).

Sutton, D., Kelleher, B., Ross, J.R.H., Review of literature on catalysts for biomass gasification. *Fuel Process. Technol.,* **73**, 155-173 (2001).

Swasdisevi, T., Tanthapanichakoon, W., Charinpanitkul, T., Kawaguchi, T., Tanaka, T., Tsuji, Y., Prediction of gas-particle dynamics and heat transfer in a two-dimensional spouted bed. *Adv. Powder Technol.,* **16**, 275-293 (2005).

Swierczynski, D., Courson, C., Bedel, L., Kiennemann, A., Vilminot, S., Oxidation reduction behavior of iron-bearing olivines $(Fe_xMg_{1-x})_2SiO_4$ used as catalysts for biomass gasification. *Chem. Mater.*, **18**, 897-905 (2006).

Świerczyński, D., Libs, S., Courson, C., Kiennemann, A., Steam reforming of tar from a biomass gasification process over Ni/olivine catalyst using toluene as a model compound. *Appl. Catal,. B,* **74**, 211-222 (2007).

Sykes, R., Yung, M., Novaes, E., Kirst, M., Peter, G., Davis, M., High-Throughput Screening of Plant Cell-Wall Composition Using Pyrolysis Molecular Beam Mass Spectroscopy. *Methods Mol. Biol.,* **581**, 169-83 (2009).

Szul, M., Głód, K., Iluk, T., Influence of pressure and CO_2 in fluidized bed gasification of waste biomasses. *Biomass Convers. Biorefinery,* **11**, 69-81 (2021).

Tan, R.S., Tuan Abdullah, T.A., Abdul Jalil, A., Md Isa, K., Optimization of hydrogen production from steam reforming of biomass tar over Ni/dolomite/La_2O_3 catalysts. *J. Energy Inst.*, (2020).

Tellabide, M., Estiati, I., Pablos, A., Altzibar, H., Aguado, R., Olazar, M., Minimum spouting velocity of fine particles in fountain confined conical spouted beds. *Powder Technol.*, **374**, 597-608 (2020a).

Tellabide, M., Estiati, I., Pablos, A., Altzibar, H., Aguado, R., Olazar, M., New operation regimes in fountain confined conical spouted beds. *Chem. Eng. Sci.,* **211**, 115255 (2020b).

Tellabide, M., Estiati, I., Atxutegi, A., Altzibar, H., Aguado, R., Olazar, M., Fine particle flow pattern and region delimitation in fountain confined conical spouted beds. *J. Ind. Eng. Chem.*, **95**, 312-324 (2021a).

Tellabide, M., Estiati, I., Atxutegi, A., Altzibar, H., Olazar, M., Effect of operating conditions on the hydrodynamics in fountain confined conical spouted beds. *J. Taiwan Inst. Chem. Eng.*, **123**, 1-10 (2021b).

Thamavithya, M., Jarungthammachote, S., Dutta, A., Basu, P., Experimental study on sawdust gasification in a spout–fluid bed reactor. *Int. J. Energy Res.*, **36**, 204-217 (2012).

Thanit, T., Wiwut, W., Tawatchai, T., Toshihiro, T., Toshitsugu, T., Yutaka, Y., Prediction of gas-particle dynamics and heat transfer in a two-dimensional spouted bed. *Adv. Powder Technol.,* **16**, 275-293 (2005).

Tian, Y., Zhou, X., Lin, S., Ji, X., Bai, J., Xu, M., Syngas production from air-steam gasification of biomass with natural catalysts. *Sci. Total Environ.,* **645**, 518-523 (2018).

Tian, Y., Zhou, X., Yang, Y., Nie, L., Experimental analysis of air-steam gasification of biomass with coal-bottom ash. *J. Energy Inst.,* **93**, 25-30 (2020).

Tsekos, C., del Grosso, M., de Jong, W., Gasification of woody biomass in a novel indirectly heated bubbling fluidized bed steam reformer. *Fuel Process. Technol.,* **224**, 107003 (2021).

Tuomi, S., Kaisalo, N., Simell, P., Kurkela, E., Effect of pressure on tar decomposition activity of different bed materials in biomass gasification conditions. *Fuel,* **158**, 293-305 (2015).

Tursumbayeva, M., Koziel, J.A., Maurer, D.L., Kenessov, B., Rice, S., Development of Time-Weighted Average Sampling of Odorous Volatile Organic Compounds in Air with Solid-Phase Microextraction Fiber Housed inside a GC Glass Liner: Proof of concept. *Molecules*, **24**(2019).

Tursun, Y., Liu, J., Xu, S., Wei, L., Zou, W., Catalytic steam gasification of lignite with olivine as solid heat carrier. *Fuel,* **112**, 641-645 (2013).

Tursun, Y., Xu, S., Abulikemu, A., Dilinuer, T., Biomass gasification for hydrogen rich gas in a decoupled triple bed gasifier with olivine and NiO/olivine. *Bioresour. Technol.*, **272**, 241-248 (2019).

Ud Din, Z., Zainal, Z.A., The fate of SOFC anodes under biomass producer gas contaminants. *Renewable Sustainable Energy Rev.,* **72**, 1050-1066 (2017).

Umeki, K., Yamamoto, K., Namioka, T., Yoshikawa, K., High temperature steam-only gasification of woody biomass. *Appl. Energy,* **87**, 791-798 (2010).

Unterreiner, B.V., Sierka, M., Ahlrichs, R., Reaction pathways for growth of polycyclic aromatic hydrocarbons under combustion conditions, a DFT study. *Phys. Chem. Chem. Phys.,* **6**, 4377-4384 (2004).

Valderrama Rios, M.L., González, A.M., Lora, E.E.S., Almazán del Olmo, O.A., Reduction of tar generated during biomass gasification: A review. *Biomass Bioenergy*, **108**, 345-370 (2018).

Valin, S., Ravel, S., de Vincent, P.P., Thiery, S., Miller, H., Defoort, F., Grateau, M., Fluidised bed gasification of diverse biomass feedstocks and blends — An overall performance study. *Energies*, **13,** 3706 (2020).

Van Der Drift, A., Van Doorn, J., Effect of Fuel Size and Process Temperature on Fuel Gas Quality from CFB Gasification of Biomass. *Prog. Thermochem. Biomass Convers.*, (2008).

Velez, D., Aspectos Básicos de la Tecnología de Pirólisis de Neumáticos en un Reactor Spouted Bed Cónico, PhD Thesis, University of the Basque Country, Bilbao. (2004).

Virginie, M., Courson, C., Niznansky, D., Chaoui, N., Kiennemann, A., Characterization and reactivity in toluene reforming of a Fe/olivine catalyst designed for gas cleanup in biomass gasification. *Appl. Catal., B,* **101**, 90-100 (2010a).

Virginie, M., Adánez, J., Courson, C., De Diego, L.F., García-Labiano, F., Niznansky, D., Kiennemann, A., Gayán, P., Abad, A., Effect of Fe-olivine on the tar content during biomass gasification in a dual fluidized bed. *Appl. Catal., B,* **121-122**, 214-222 (2012).

Virginie, M., Courson, C., Kiennemann, A., Toluene steam reforming as tar model molecule produced during biomass gasification with an iron/olivine catalyst. *C. R. Chim.*, **13**, 1319-1325 (2010b).

Waheed, Q.M.K., Williams, P.T., Hydrogen production from high temperature pyrolysis/steam reforming of waste biomass: Rice husk, sugar cane bagasse, and wheat straw. *Energy Fuels,* **27**, 6695-6704 (2013).

Waheed, Q.M.K., Wu, C., Williams, P.T., Pyrolysis/reforming of rice husks with a Ni–dolomite catalyst: Influence of process conditions on syngas and hydrogen yield. *J. Energy Inst.,* **89**, 657-667 (2016).

Wang, C., Zhang, M., Han, Z., Bai, D., Duo, W., Bi, X., Abudula, A., Guan, G., Xu, G., Pilot verification of a two-stage fluidized bed gasifier with a downer pyrolyzer using oxygen-rich air. *Fuel,* **307**, 121816 (2022).

Wang, D., Liu, Y.Q., Li, W.P., Wei, M.M., Ye, Y.Y., Li, S.R., Wang, M., Study on the gasification of pine sawdust with dolomite catalyst in a pilot-scale fluidized bed gasifier. *Energy Sources Part A,* **42**, 1132-1139 (2020).

Wang, G., Xu, S., Wang, C., Zhang, J., Fang, Z., Desulfurization and tar reforming of biogenous syngas over Ni/olivine in a decoupled dual loop gasifier. *Int. J. Hydrogen Energy*, **42**, 15471-15478 (2017).

Wang, H., Frenklach, M., A detailed kinetic modeling study of aromatics formation in laminar premixed acetylene and ethylene flames. *Combust. Flame*, **110**, 173-221 (1997).

Wang, J., Cheng, G., You, Y., Xiao, B., Liu, S., He, P., Guo, D., Guo, X., Zhang, G., Hydrogen-rich gas production by steam gasification of municipal solid waste (MSW) using NiO supported on modified dolomite. *Int. J. Hydrogen Energy,* **37**, 6503-6510 (2012).

Wang, S., Lin, H., Ru, B., Sun, W., Wang, Y., Luo, Z., Comparison of the pyrolysis behavior of pyrolytic lignin and milled wood lignin by using TG-FTIR analysis. *J. Anal. Appl. Pyrolysis,* **108**, 78-85 (2014).

Wang, T., Chang, J., Lv, P., Zhu, J., Novel catalyst for cracking of biomass tar. *Energy Fuels,* **19**, 22-27 (2005).

Wang, X., Zhu, Z., Wang, K., Yu, K., Lyu, Q., Experimental study of pilot-scale CFB gasification: Effect of gasifying agent and coal feeding modes on the gasification performance. *Fuel,* **251**, 603-610 (2019).

Warguła, Ł, Kukla, M., Wieczorek, B., Krawiec, P., Energy consumption of the wood size reduction processes with employment of a low-power machines with various cutting mechanisms. *Renew. Energy,* **181**, 630-639 (2022).

WBA, Global Bionergy Statistics 2020. (2020).

Wei, L., Xu, S., Liu, J., Lu, C., Liu, S., Liu, C., A novel process of biomass gasification for hydrogen-rich gas with solid heat carrier: Preliminary experimental results. *Energy Fuels,* **20**, 2266-2273 (2006).

Wei, L., Xu, S., Zhang, L., Liu, C., Zhu, H., Liu, S., Steam gasification of biomass for hydrogen-rich gas in a free-fall reactor. *Int. J. Hydrogen Energy,* **32**, 24-31 (2007).

Wilk, V., Hofbauer, H., Influence of fuel particle size on gasification in a dual fluidized bed steam gasifier. *Fuel Process. Technol.,* **115**, 139-151 (2013).

Wilk, V., Schmid, J.C., Hofbauer, H., Influence of fuel feeding positions on gasification in dual fluidized bed gasifiers. *Biomass Bioenergy,* **54**, 46-58 (2013).

Wolfesberger, U., Aigner, I., Hofbauer, H., Tar content and composition in producer gas of fluidized bed gasification of wood-influence of temperature and pressure. *Environ. Prog. Sustainable Energy,* **28**, 372-379 (2009).

Wu, M., Guo, Q., Liu, L., Hydrodynamic performance of a spout-fluid bed with draft tube at different temperatures. *Ind. Eng. Chem. Res.,* **53**, 1999-2010 (2014).

Wu, M., Guo, Q., Xie, H., Liu, L., A new empirical equation for minimum spouting/spout-fluidization velocity in draft tube spout-fluid beds at elevated temperature. *Can. J. Chem. Eng.*, **93**, 1819-1829 (2015).

Xiao, X., Cao, J., Meng, X., Le, D.D., Li, L., Ogawa, Y., Sato, K., Takarada, T., Synthesis gas production from catalytic gasification of waste biomass using nickel-loaded brown coal char. *Fuel*, **103**, 135-140 (2013).

Xiao, Y., Xu, S., Song, Y., Shan, Y., Wang, C., Wang, G., Biomass steam gasification for hydrogen-rich gas production in a decoupled dual loop gasification system. *Fuel Process. Technol.*, **165**, 54-61 (2017a).

Xiao, Y., Xu, S., Tursun, Y., Wang, C., Wang, G., Catalytic steam gasification of lignite for hydrogen-rich gas production in a decoupled triple bed reaction system. *Fuel*, **189**, 57-65 (2017b).

Xiao, Y., Xu, S., Liu, Y., Qiao, C., Catalytic steam co-gasification of biomass and coal in a dual loop gasification system with olivine catalysts. *J. Energy Inst.*, **93**, 1074-1082 (2020).

Xie, Y., Xiao, J., Shen, L., Wang, J., Zhu, J., Hao, J., Effects of Ca-based catalysts on biomass gasification with steam in a circulating spout-fluid bed reactor. *Energy Fuels*, **24**, 3256-3261 (2010).

Xu, T., Xu, F., Moyo, G.G., Sun, Y., Chen, Z., Xiao, B., Wang, X., Hu, Z., Comparative study of M_xO_y (M=Cu, Fe and Ni) supported on dolomite for syngas production via chemical looping reforming with toluene. *Energy Convers. Manage.*, **199**, 111937 (2019).

Yahaya, A.Z., Rao Somalu, M., Muchtar, A., Anwar Sulaiman, S., Ramli Wan Daud, W., Effects of temperature on the chemical composition of tars produced from the gasification of coconut and palm kernel shells using downdraft fixed-bed reactor. *Fuel*, **265**, 116910 (2020).

Yamashita, T., Hayes, P., Analysis of XPS spectra of Fe^{2+} and Fe^{3+} ions in oxide materials. *Appl. Surf. Sci.*, **254**, 2441-2449 (2008).

Ye, B., Lim, C.J., Grace, J.R., Hydrodynamics of spouted and spout-fluidized beds at high temperature. *Can. J. Chem. Eng.*, **70**, 840-847 (1992).

Yu, H., Zhang, Z., Li, Z., Chen, D., Characteristics of tar formation during cellulose, hemicellulose and lignin gasification. *Fuel*, **118**, 250-256 (2014).

Yu, H., Wu, Z., Chen, G., Catalytic gasification characteristics of cellulose, hemicellulose and lignin. *Renewable Energy*, **121**, 559-567 (2018).

Zamboni, I., Courson, C., Kiennemann, A., Fe-Ca interactions in Fe-based/CaO catalyst/sorbent for CO_2 sorption and hydrogen production from toluene steam reforming. *Appl. Catal., B*, **203**, 154-165 (2017).

Zeng, X., Shao, R., Wang, F., Dong, P., Yu, J., Xu, G., Industrial demonstration plant for the gasification of herb residue by fluidized bed two-stage process. *Bioresour. Technol.*, **206**, 93-98 (2016).

Zeng, X., Ueki, Y., Yoshiie, R., Naruse, I., Wang, F., Han, Z., Xu, G., Recent progress in tar removal by char and the applications: A comprehensive analysis. *Carbon Resour. Convers.*, **3**, 1-18 (2020).

Zhang, C., Li, Z., Xu, X., Yang, L., Zhang, R., Catalytic conversion of tar compounds from biomass over modified Ni/olivine catalysts. *Adv. Mater. Res.*, **666**, 67-75 (2013).

Zhang, T., Jiang, D., Zhang, H., Jing, Y., Tahir, N., Zhang, Y., Zhang, Q., Comparative study on bio-hydrogen production from corn stover: Photo-fermentation, dark-fermentation and dark-photo co-fermentation. *Int. J. Hydrogen Energy*, **45**, 3807-3814 (2020).

Zhang, W., Zhang, Z., Meng, J., Zhou, W., Chen, Z., Adsorptive behavior and solid-phase microextraction of bare stainless steel sample loop in high performance liquid chromatography. *J. Chromatogr. A*, **1365**, 19-28 (2014).

Zhang, Z., Pang, S., Experimental investigation of biomass devolatilization in steam gasification in a dual fluidised bed gasifier. *Fuel*, **188**, 628-635 (2017).

Zhang, Z., Pang, S., Experimental investigation of tar formation and producer gas composition in biomass steam gasification in a 100 kW dual fluidised bed gasifier. *Renew. Energy*, **132**, 416-424 (2019).

Zhao, M., Yang, X., Church, T.L., Harris, A.T., Interaction between a bimetallic Ni-Co catalyst and micrometer-sized CaO for enhanced H_2 production during cellulose decomposition. *Int. J. Hydrogen Energy*, **36**, 421-431 (2011).

Zhao, X.L., Yao, Q., Li, S.Q., Effects of draft tubes on particle velocity profiles in spouted beds. *Chem. Eng. Technol.*, **29**, 875-881 (2006).

Zhao, Z., Lakshminarayanan, N., Kuhn, J.N., Senefeld-Naber, A., Felix, L.G., Slimane, R.B., Choi, C.W., Ozkan, U.S., Optimization of thermally impregnated Ni-olivine catalysts for tar removal. *Appl. Catal., A*, **363**, 64-72 (2009).

Zheng, J., Zhu, Y., Zhu, M., Wu, H., Sun, R., Bio-oil gasification using air - Steam as gasifying agents in an entrained flow gasifier. *Energy*, **142**, 426-435 (2018).

Zhou, B., Dichiara, A., Zhang, Y., Zhang, Q., Zhou, J., Tar formation and evolution during biomass gasification: An experimental and theoretical study. *Fuel*, **234**, 944-953 (2018).

Zhou, H., Wu, C., Onwudili, J.A., Meng, A., Zhang, Y., Williams, P.T., Polycyclic aromatic hydrocarbon formation from the pyrolysis/gasification of lignin at different reaction conditions. *Energy Fuels*, **28**, 6371-6379 (2014).

Zore, U.K., Yedire, S.G., Pandi, N., Manickam, S., Sonawane, S.H., A review on recent advances in hydrogen energy, fuel cell, biofuel and fuel refining via ultrasound process intensification. *Ultrason. Sonochem.*, **73**, 105536 (2021).

Zou, X., Chen, T., Zhang, P., Chen, D., He, J., Dang, Y., Ma, Z., Chen, Y., Toloueinia, P., Zhu, C., Xie, J., Liu, H., Suib, S.L., High catalytic performance of Fe-Ni/Palygorskite in the steam reforming of toluene for hydrogen production. *Appl. Energy*, **226**, 827-837 (2018).

12

DISSEMINATION OF RESULTS

12.1. PUBLICATIONS DERIVED FROM THE THESIS

Cortazar, M., Santamaria, L., Lopez, G., Alvarez, J., Amutio, M., Bilbao, J., Olazar, M.

Fe/olivine as primary catalyst in the biomass steam gasification in a fountain confined spouted bed reactor

J. Ind. Eng. Chem., **99**, 364-379 (2021)

Impact factor (2020): 6.064

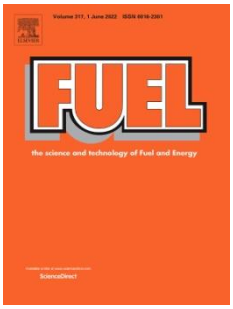

Cortazar, M., Alvarez, J., Lopez, G., Amutio, M., Bilbao, J., Olazar, M.

Behaviour of primary catalysts in the biomass steam gasification in a fountain confined spouted bed

Fuel, **253**, 1446-1456 (2019)

Impact factor (2019): 5.578

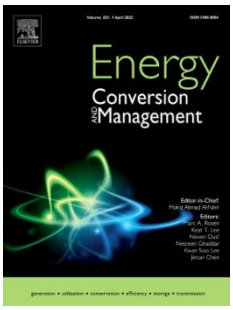

Cortazar, M., Alvarez, J., Lopez, G., Amutio, M., Santamaria, L., Bilbao, J., Olazar, M.

Role of temperature on gasification performance and tar composition in a fountain enhanced conical spouted bed reactor.

Energy Convers. Manage., **171**, 1589-1597 (2018)

Impact factor (2018): 7.181

Cortazar, M., Alvarez, J., Lopez, G., Amutio, M., Bilbao, J., Olazar, M.

Advantages of confining the fountain in a conical spouted bed reactor for biomass steam gasification

Energy, **153**, 455-463 (2018)

Impact factor (2018): 5.537

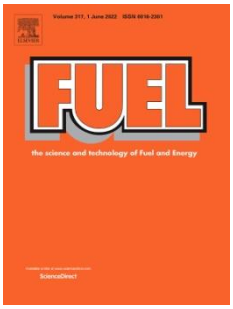

Lopez, G., Cortazar, M., Alvarez, J., Amutio, M., Bilbao, J., Olazar, M.

Assessment of a conical spouted with an enhanced fountain bed for biomass gasification

Fuel, **203**, 825-831 (2017)

Impact factor (2017): 4.908

12.2. OTHER PUBLICATIONS

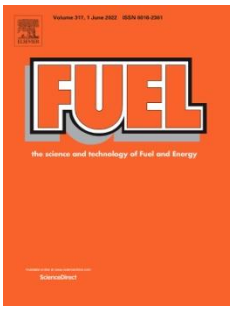

Cortazar M., Alvarez, J., Olazar, L., Santamaria, L., Lopez, G., Villafan-Vidales, H.I., Asueta, A., Olazar M.

Activity and stability of different Fe loaded primary catalysts for tar elimination

Fuel, **317**, 123457 (2022)

Impact factor (2020): 6.609

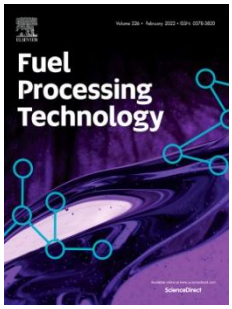

Cortazar, M., Gao, N., Quan, C., Suarez, M.A., Orozco, S., Santamaria, L., Amutio, M., Olazar, M.

Analysis of hydrogen production potential from waste plastics by pyrolysis and in-line oxidative steam reforming

Fuel Process. Techonol., **225**, 107044 (2022)

Impact factor (2020): 7.033

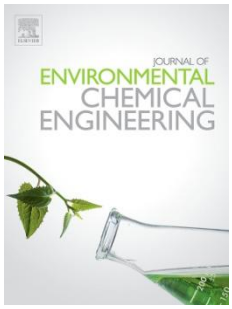

Cortazar, M., Sun, S., Wu, C., Santamaria, L., Olazar, L., Fernandez, E., Artetxe, M., Lopez, G., Olazar, M.

Sorption enhanced ethanol steam reforming on a bifunctional Ni/CaO catalyst for H_2 production

J. Environ. Chem. Eng., **9** (6), 106725 (2021)

Impact factor (2020): 5.909

Bensidhom, G., Arabiourrutia, M., Ben Hassen, A., Cortazar, M., Ceylan, S., Olazar, M.

Fast pyrolysis of date palm biomass using Py-GCMS

J. Energy Inst., **99**, 229-239 (2021)

Impact factor (2020): 6.186

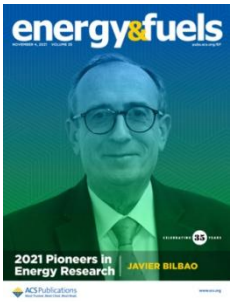

Santamaria, L., Lopez, G., Fernandez, E., Cortazar, M., Arregi, A., Olazar, M., Bilbao, J.

Progress on catalyst development for the steam reforming of biomass and waste plastics pyrolysis volatiles: a review.

Energy Fuels, **35** (21), 17051-17084 (2021)

Impact factor (2020): 3.605

Cortazar, M., Lopez, G., Alvarez, J., Arregi, A., Amutio, M., Bilbao, J., Olazar, M.

Experimental study and modelling of biomass char gasification kinetics in a thermogravimetric flow reactor

Chem. Eng. J., **396**, 125200 (2020)

Impact factor (2020): 13.273

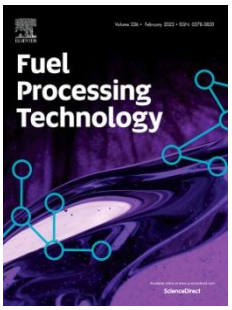

Santamaria, L., Artetxe, M., Lopez, G., Cortazar, M., Amutio, M., Bilbao, J., Olazar, M.

Effect of CeO_2 and MgO promoters on the performance of Ni/Al_2O_3 catalyst in the steam reforming of biomass pyrolysis volatiles

Fuel Process.Techonol., **198**, 106233 (2020)

Impact factor (2020): 7.033

Kinetic modelling and experimental validation of biomass fast pyrolysis in a conical spouted bed reactor

Lopez, G., Alvarez, J., Amutio, M., Hooshdaran, B., Cortazar, M., Haghshenasfard, M., Hosseini, S.H., Olazar, M.

Chem. Eng. J., **373**,677-686 (2019)

Impact factor (2019): 10.652

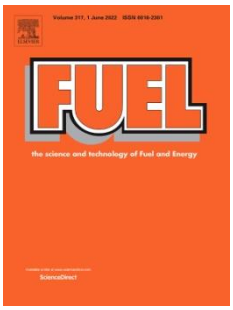

Valorization of citrus wastes by fast pyrolysis in a conical spouted bed reactor

Alvarez, J., Hooshdaran, B., Cortazar, M., Amutio, M., Lopez, G., Freire, F.B., M., Haghshenasfard, M., Hosseini, S.H., Olazar, M.

Fuel, **224**, 111-120 (2018)

Impact factor (2018): 5.128